STRENGTHENING OF BRICK INFILLED RC FRAMES WITH CFRP REINFORCEMENT-GENERAL PRINCIPLES

A THESIS SUBMITTED TO
THE GRADUATE SCHOOL OF NATURAL AND APPLIED SCIENCES
OF
MIDDLE EAST TECHNICAL UNIVERSITY

BY

EMRE AKIN

IN PARTIAL FULFILLMENT OF THE REQUIREMENTS
FOR
THE DEGREE OF DOCTOR OF PHILOSOPHY
IN
CIVIL ENGINEERING

APRIL 2011

Approval of the thesis:

STRENGTHENING OF BRICK INFILLED RC FRAMES WITH CFRP REINFORCEMENT-GENERAL PRINCIPLES

submitted by **EMRE AKIN** in partial fulfillment of the requirements for the degree of **Doctor of Philosophy in Civil Engineering Department, Middle East Technical University** by,

Prof. Dr. Canan Özgen ______________________
Dean, Graduate School of **Natural and Applied Sciences**

Prof. Dr. Güney Özcebe ______________________
Head of Department, **Civil Engineering**

Prof. Dr. Güney Özcebe ______________________
Supervisor, **Civil Engineering Dept., METU**

Examining Committee Members:

Assoc. Prof. Dr. Barış Binici ______________________
Civil Engineering Dept., METU

Prof. Dr. Güney Özcebe ______________________
Civil Engineering Dept., METU

Prof. Dr. Alper İlki ______________________
Civil Engineering Dept., ITU

Assoc. Prof. Dr. Erdem Canbay ______________________
Civil Engineering Dept., METU

Asst. Prof. Dr. Burcu Burak ______________________
Civil Engineering Dept., METU

Date: 11.04.2011

I hereby declare that all information in this document has been obtained and presented in accordance with academic rules and ethical conduct. I also declare that, as required by these rules and conduct, I have fully cited and referenced all material and results that are not original to this work.

Name, Last Name : Emre AKIN

Signature :

ABSTRACT

STRENGTHENING OF BRICK INFILLED RC FRAMES WITH CFRP REINFORCEMENT-GENERAL PRINCIPLES

Akın, Emre
Ph.D., Department of Civil Engineering
Supervisor : Prof. Dr. Güney Özcebe

April 2011, 232 pages

There is an excessive demand for the rehabilitation of frame type reinforced concrete (RC) buildings which do not satisfy current earthquake code provisions. Therefore, it is imperative to develop user-friendly seismic strengthening methodologies which do not necessitate the evacuation of building during rehabilitation period.

In this study, it was aimed to strengthen the brick infill walls by means of diagonal Carbon Fiber-Reinforced Polymer (CFRP) fabrics and to integrate them with the existing structural frame in order to form a new lateral load resisting system. The possible effects of height to width (aspect) ratio of the infill walls and scale of the frame test specimens on the overall behavior attained by the developed rehabilitation methodology were investigated.

The experimental part of the study was carried out in two steps. In the first step, ten individual panel specimens were tested in order to understand the behavior of strengthened/non-strengthened masonry walls under diagonal earthquake loads. And in the second step, the tests of eight 1/3 and four 1/2 scaled one-bay, two-story RC frames having two different aspect ratios were performed to determine design details. The experimental results were revealed in terms of lateral stiffness, strength, drift and energy dissipation characteristics of the specimens.

In the analytical part, an equivalent strut and tie approach was used for modeling the strengthened/non-strengthened infill walls of the frames. The predicted pushover responses of the frame models were compared with the test results. The design criteria required for the aforementioned strengthening methodology was developed referring these analytical results.

Keywords: Reinforced concrete frame, infill wall, seismic strengthening, carbon fiber reinforced polimer, aspect ratio, scale effects

ÖZ

BOŞLUKLU TUĞLA DOLGU DUVARLI BETONARME ÇERÇEVELERİN CFRP ŞERİTLERLE GÜÇLENDİRİLMESİ-GENEL PRENSİPLER

Akın, Emre
Doktora, İnşaat Mühendisliği Bölümü
Tez Yöneticisi : Prof. Dr. Güney Özcebe

Nisan 2011, 232 sayfa

Mevcut deprem yönetmeliklerine uygun olmayan betonarme binaların güçlendirilmesine yönelik büyük ölçekte bir talep bulunmakta. Bu nedenle, binaların boşaltılmalarına gerek kalmadan, kolaylıkla uygulanabilecek sismik güçlendirme metotlarının geliştirilmesi gerekiyor.

Bu çalışmada, karbon fiber lifli polimerler kullanılarak tuğla dolgu duvarların güçlendirilmesi ve yeni bir yanal taşıyıcı sistem oluşturmak amacıyla bunların mevcut yapıya entegre edilmesi amaçlanmıştır. Dolgu duvarların yüksekliğinin genişliğine oranı ve deney elemanlarının ölçeği, rehabilitasyon yöntemiyle sağlanan genel davranışa muhtemel etkileri bakımından incelenmiştir.

Çalışmanın deneysel kısmı iki aşamada yürütülmüştür. Birinci aşamada, güçlendirilmiş/güçlendirilmemiş duvarların diyagonal deprem yükleri altındaki davranışını anlayabilmek için on adet bağımsız panel test edilmiştir. İkinci aşamada

ise, dizayn detaylarının belirlenmesi amacıyla, iki farklı boy-en oranına sahip sekiz adet 1/3 ve dört adet 1/2 ölçekli tek açıklıklı, iki katlı betonarme çerçeve deneyleri gerçekleştirilmiştir. Deneysel sonuçlar, deney elemanlarına ait yanal rijitlik, dayanım, ötelenme ve enerji sönüm karakteristikleri yardımıyla açıklanmıştır.

Analitik kısımda, güçlendirilmiş/güçlendirilmemiş çerçeve dolgu duvarlarının modellenmesi için eşdeğer gergi yaklaşımı kullanılmıştır. Çerçeve eleman modelleri için hesaplanan statik itme analiz sonuçları, deney sonuçlarıyla karşılaştırılmıştır. Bu analitik sonuçlara dayanarak, bahsi geçen güçlendirme yöntemi için gerekli dizayn kriterleri geliştirilmiştir.

Anahtar Kelimeler: Betonarme çerçeve, dolgu duvar, sismik güçlendirme, karbon fiber lifli polimer, boy-en oranı, ölçek etkileri

To my family

ACKNOWLEDGEMENTS

I would like to express my endless gratitude to Prof. Dr. Güney Özcebe, who supervised this thesis, for his guidance and support through my entire graduate study. It was an honor for me to have the opportunity to study with him.

I appreciate the valuable supports and guidance of Assoc. Prof. Dr. Erdem Canbay, Assoc. Prof. Dr. Barış Binici and Asst. Prof. Dr. Burcu Burak. I would also like to thank to Prof. Dr. Alper İlki for his constructive comments. It is a pleasure to thank to Prof. Dr. Uğur Ersoy for his valued contributions. It was a great chance for me to be able to take his lesson and learn from him not only scientifically but also personally. I am also grateful to Prof. Dr. Tuğrul Tankut for his support in some tough times during this study.

I would like to express my appreciation to the staff of Structural Mechanics Laboratory, but especially to Hasan Metin, Barış Esen and Osman Keskin, for their help while working in the laboratory. Sincere thanks are extended to all METU Civil Engineering Department staff who helped me in many different ways.

It is precious for me to have the lifelong brotherhood and support of Bora Acun. He leaded me while walking on this path.

I should thank to Özgür Avşar for not only his suggestions for this study but also his friendship. I am indebted to my colleagues Beyhan Bayhan, Ali Şahin Taşlıgedik, Dilek Okuyucu, Hakan Erdoğan, Okan Özcan Gökhan Özdemir, Abdullah Dilsiz, and many others from Structural Mechanics Laboratory for their help, collaboration and great friendship. Barış Erdil and Gözde Paksoy Özerkan deserve special thanks for always being there whenever I need accompany and support.

Erman-Funda Uçal and Serkan-Zeynep Güvey require many thanks for always being next to me, not only during this study but also in a larger stage of my life. Many appreciations go to Işıl Işık who pushed me forward whenever it became hard to continue.

Also thanks to "Construction Materials" group for letting me forget the stress of this study with their friendship. I owe a special acknowledgment to Tümay Çelikkol for being my destined friend and giving so much insight during this journey.

Cheers to Franziska Fischer, Roberto Riovanto and Simon O'Dowd who made me feel supported continuously while writing this thesis. An additional thank to Simon for introducing me some of the software tools that were used in this study.

This study would be nothing without unconditional support, encouragement and love of my mother Huriye Akın, my father Hüseyin Akın and my sister Esin Akın. They deserve my deepest gratitude for everything. And thanks to my nephew, our "little monster" Akın Mete for giving me the joy when I feel exhausted.

TABLE OF CONTENTS

LIST OF TABLES

TABLES

LIST OF FIGURES

FIGURES

CHAPTER 1

INTRODUCTION

1.1. GENERAL

The reinforced concrete (RC) frame type buildings with masonry infill partitions and claddings have been commonly practiced worldwide. A considerable amount of these buildings are in high seismic hazard regions, as in Turkey (Murty et al., 2006; Özcebe et al., 2006-a). The current seismic code regulations assure a certain structural performance under defined level of seismic actions by provided strength, stiffness and ductility. However, a considerable number of buildings that are still in use were not designed and constructed according to the current codes (Canbay et al., 2003). Besides, the issues and problems related to the possible renovation, and usage of the buildings for purposes other than design objectives constitute another phase of the problem. In some other cases, the lack of supervision during the construction period might have lead to disparities from the design specifications and substandard quality in terms of seismic resistance (Yakut, 2004).

The structural deficiencies engendered by at least one of the aforementioned reasons have been observed to cause catastrophic destruction and loss of life in highly populated urban regions in the past earthquakes (Jirsa, 2006). Some of these crucial deficiencies of the RC buildings as particularly observed in Turkey and elsewhere may be listed as follows (Üzümeri et al., 1999; Ersoy and Özcebe, 2002; Canbay et al., 2003; Özcebe et al., 2004; Sonuvar et al., 2004; Ersoy, 2009):

- irregularities in the horizontal plan and/or elevation,
- lack of sufficient lateral stiffness,
- soft stories,
- short columns,
- frames constituted by weak columns and strong beams,
- insufficient (i.e. excessive spacing of ties) and improper (i.e. 90 degree hooks of the ties) confinement of both beams and columns, especially at the member ends,
- inappropriate detailing of column longitudinal reinforcement (i.e. inadequate lap-splice length provided above the floor level where bar slip actions are most critical due to high level of moments),
- inadequate anchorage length of beam bottom reinforcement,
- lack of transverse reinforcement at beam-column joints,
- poor concrete quality and workmanship at the construction phase.

In addition to these deficiencies, even properly designed/constructed existing buildings might have experienced different extent of damage in the past earthquakes, precluding their service. The seismic assessment studies performed in the regions of high seismicity revealed the colossal number of buildings that are vulnerable to the ground motions (Özcebe et al., 2004). Therefore, it is inevitable to improve the seismic performance of these buildings by rehabilitation, if economy compared to demolition and re-construction costs is assured. Since there are numerous retrofitting techniques, the proper application should be decided after an evaluation process with deduced objectives. The selection of rehabilitation objectives may require consideration of various performance and seismic hazard levels (FEMA 356, 2000).

The rehabilitation of the structures can be achieved by either strengthening individual structural components or system improvement with insertion of additional members (Ersoy and Özcebe, 2002; Ersoy, 2007). It is possible to increase ductility, and hence the energy dissipation capacity of the structure by the rehabilitation of individual members. On the other hand, lateral capacity of the structure may be improved with/without decreasing the drift demand through system improvement (El-Sokkary and Galal, 2009). When large amount of individual components are involved in the rehabilitation process and/or lateral rigidity of the overall system is deficient, system improvement of the building may become a necessity (Ersoy, 2009). RC infill wall application to the selected bays of the building has been the most esteemed system improvement technique in the last few decades (Altın and Ersoy, 1992; Canbay et al., 2003; Sonuvar et al., 2004). The method attested its efficiency in the past earthquakes by the superior performance of the buildings having shear walls. However, this technique requires substantial amount of time and evacuation of the building during the construction period. Therefore, it may not be convenient for the rehabilitation of excessive number of buildings that require urgent treatment. In order to manage this issue, practical solutions should be developed for the rehabilitation of seismically deficient buildings (Özcebe et al., 2004; Özcebe et al., 2006-b).

In the last two decades, fiber-reinforced polymers (FRP's) have been brought to the use of construction technology with the advantages of high tensile strength to weight ratio, corrosion resistance, overall durability and ease of application. Different types of FRP's, as usually being made of glass (GFRP), aramid (AFRP) or carbon (CFRP) have been used for various rehabilitation applications. One of many applications of this material has been the strengthening of masonry walls for both improving the in-plane and out-of-plane behavior (Triantafillou, 1998; Bakis et al., 2002; Van Den Einde et al., 2003).

The masonry infill walls of RC frames have generally been recognized as non-structural members and their effect on the overall structural response has been ignored. However, numerous experimental investigations on the behavior of infilled frames revealed significant effects of infill walls on the overall response, especially in the case of lateral loading. These effects, although they may be unfavorable in certain cases, generally defined as beneficial since strength and stiffness characteristics of the frame are improved considerably (CEB, 1996). But the brittle nature of masonry hinder further contribution of infill walls in the inelastic range, with the damage experienced in an early stage under lateral actions (Mohyeddin-Kermani et al., 2008). Moreover, this early damage of the infill may lead to unfavorable distribution of demands within the frame members (i.e. short column formations after crushing of the upper corners of masonry). A retrofit strategy with the aim of improving the mechanical properties of existing infill walls, integrating them with the existing structural system and thereby, constituting a new lateral load resisting mechanism would offer an alternative for the RC infill wall application. A joint research project, the details of which will be presented in the next chapter, was initiated for this purpose at METU Structural Mechanics Laboratory (SML) in 2001. In that research, which was the predecessor of the current study, carbon fiber reinforced polymer (CFRP) fabrics were used for strengthening the infill walls having a constant aspect ratio (Ersoy et al., 2003; Özden and Akgüzel, 2003; Özcebe et al., 2004; Özcebe et al., 2006-b; Erol et al., 2006; Yüksel et al., 2006).

1.2. OBJECTIVE AND SCOPE

This study is performed with an objective of bringing a better interpretation on the CFRP strengthening methodology developed for infilled RC frames in the former studies. To this end, the influence of different parameters on the efficiency of this methodology is emphasized with a bipartite research having experimental and analytical phases. The main test parameter is the height/width (aspect) ratio of infill walls, which was not considered as a variable in the previous studies. The effects of insufficient development length of the lapped longitudinal column bars and scale of the specimens on the applied retrofitting are also considered. A total of twelve RC frames were tested in different sets reflecting the test parameters and corresponding in-plane response results are evaluated. In the analytical part of the study, the key objective was to obtain an enhanced numerical model of the specimens. The aspect ratio of the infill walls are further investigated through a parametric study, with an aim of attaining optimum range of this ratio in terms of strengthening efficiency. The drift limitations of Turkish Earthquake Code (TEC) (The Ministry of Public Works and Settlement, 2007) for reinforced infill walls are also assessed through a comparison with the experimental and analytical results.

Other than frame tests, a panel test program was conducted in order to understand the individual in-plane shear response of masonry panels under diagonal loading with/without different forms of CFRP application. The panel specimens, test setup and test results are presented thoroughly in Appendix A.

The content of the study as submitted in the following chapters are outlined as:

- In Chapter 2, the literature review of the previous studies on the behavior of infilled frames and FRP strengthening of infill walls is presented. A summary of the pioneer research efforts at METU SML on system improvement is also given in this section; since these efforts constituted a basis for the following studies including this one.

- In Chapter 3, the test program is explained with the details of material properties, specifications of test specimens, manufacturing/strengthening process, test setup and instrumentation.

- In Chapter 4, test results are presented in the light of observed behavior with a consideration of the notes and pictures taken during the experiments. The monitored response parameters and damage patterns are illustrated through hysteretic curves and pictures of the test specimens, respectively.

- In Chapter 5, the frame test results are evaluated in terms of strength, stiffness, ductility, energy dissipation and drift characteristics.

- In Chapter 6, the implemented numerical model of the specimens is depicted with all constituents of the model and the analytical results are presented in comparison with the experimental curves. The parametric study is also explained briefly in this chapter.

- In Chapter 7, the overall study is summarized, and the conclusions and recommendations are given.

CHAPTER 2

LITERATURE REVIEW

2.1. GENERAL

The previous experimental research projects related to system improvement of RC frames may be regarded as the pioneer efforts for other rehabilitation studies performed at METU SML. Therefore, a brief summary of these studies conducted at METU is depicted in Section 2.2 separately. The review of other studies related to masonry infilled RC frames and FRP strengthening of masonry infill walls are presented in Sections 2.3 and 2.4, respectively.

2.2. SYSTEM IMPROVEMENT STUDIES AT METU

At METU SML, the studies related to system improvement of RC frame type buildings initiated at early seventies. A study was conducted by Ersoy and Uzsoy (1971), in which nine 1/2-scale, one-story and one-bay RC frames that were strengthened with RC infills were tested under monotonic loading. The test results of strengthened specimens pointed out an approximately 700% and 500% increments in lateral strength and stiffness, respectively. Besides, the deflections at failure were decreased by nearly 65%. Also, an analytical study was performed where the infill walls were modeled as struts and the results were compared with the experimental findings.

Altın and Ersoy (1990) performed a study with an aim of assessing the hysteretic response of frames having cast-in-place RC infills. The study was composed of experimental and analytical parts. In the experimental phase, fourteen two-story and one-bay RC frames were tested under reversed cyclic loading. All of the specimens, except one reference bare frame, were strengthened by the application of infills with different reinforcement details. According to the test results, the authors concluded that a significant lateral strength and stiffness increase could be provided by RC infills which were properly connected to the frame. In the analytical study, the numerical calculations of the lateral load capacity using different models were evaluated in comparison with the test results. Furthermore, the change in the dynamic properties of the frames as a result of RC infill application was investigated. It was stated that gain in the lateral capacity was much higher than the demand increase induced by the reduction of fundamental period. However, a generalized conclusion about this phenomenon was avoided by the researchers.

In an experimental study conducted by Sonuvar (2001), different rehabilitation alternatives were investigated through reversed cyclic testing of five RC frame specimens. The 1/3 scale, two-story and one-bay nonductile bare frames were loaded for moderate damage and consequently rehabilitated by the addition of RC infills. Three different local strengthening techniques were also utilized to eliminate the inadequate lap-splice problem of the column bars. The results indicated significant increase in the ultimate strength, initial stiffness and energy dissipation capacity with the addition of RC infills. However, it was reported that optimal improvement could be attained only by the local strengthening applied for lap-splice regions.

Canbay (2001) carried out an experimental and analytical research to investigate the contribution of RC infill walls to the overall lateral frame response. A two-story and three-bay RC bare frame was tested as a reference specimen under reversed cyclic loading up to 1.6% roof drift. It should be noted that columns of the frame had lap-splices at floor levels with an insufficient development length. RC infill walls were applied only to middle bay of the damaged frame at both stories without any additional rehabilitation. The specimen was re-tested cyclically up to the same drift level. During both tests, the internal forces at the base of the first story exterior columns were monitored through specially produced force transducers (Canbay et al., 2004). The initial stiffness and ultimate strength were increased by 15 and 4 folds, respectively, with the addition of RC infill. The results showed the superior contribution of infill to the total base shear capacity of the frame, which was stated as 90% even after yielding of the wall reinforcement. The unfavorable effect of insufficient column lap-splice and the need for a local rehabilitation at these regions were emphasized. In the last stage, the results of a numerical model were verified by comparing them with the test results.

In 2001, a joint research project started at METU SML with an objective of developing a strengthening methodology applicable in case of nonductile RC frames with minimum disturbance to the occupants. This was intended to be achieved by upgrading masonry infill walls with externally bonded CFRP fabrics and employing these members as structural walls. The initial part of the study was conducted in three phases which were carried out by Mertol (2002), Keskin (2002) and Erduran (2002), respectively. A total of seven 1/3 scale, two-story and one-bay RC frames were tested with different CFRP reinforcement configurations. The aspect ratio of the infill walls were 0.58 at both stories. The optimal configuration was investigated considering both economy (i.e. less CFRP) and efficiency. Although covering the infill surface with CFRP which were extended to the frame members and anchored both to the frame and infill was reported to be the most efficient configuration, a close efficiency could be attained with properly anchored diagonal cross-overlay CFRP strips in a more economical way. The initial stiffness was indicated not to be altered by any of the CFRP configurations. It was stated that strengthened infill walls did not experience damage even at a drift ratio of 1.0 percent. The applied methodology was concluded not to be as effective as RC infill wall addition. However, the advantage of applying this method with far less disturbance to the occupants makes it attractive. It should be mentioned once again that this joint research project was the main motivation for the current study with further test parameters.

Erdem (2003) conducted an experimental study in which two 1/3-scale, two-story and three-bay nonductile RC frames were subjected to reversed cyclic lateral loading. The two strengthening methods (i.e. addition of RC infills and upgrading existing masonry infills through diagonal CFRP sheets) were compared. Both strengthening techniques were applied only in the middle bay of each frame for this purpose. The frame specimens were the same as the one used by Canbay (2001). Therefore, the bare frame tested by Canbay was regarded as the reference specimen for comparison. According to the results, the ultimate strength and initial stiffness of the bare frames were increased considerably by both strengthening methods. However, the anchorage failure reported for CFRP strengthened specimen resulted in a more abrupt strength and stiffness decay after the ultimate point compared to the frame having RC infills.

Duvarcı (2003), Süsoy (2004), Baran (2005) and Okuyucu (2009) performed studies related to the strengthening of existing infill walls by applying high strength precast concrete panels sufficiently connected to each other and anchored to the frame members. Duvarcı tested two one-bay and two-story strengthened frames in addition to a reference specimen. Süsoy carried out a test program on eight single-bay and single-story RC frames. Baran performed tests of fourteen RC frames which were similar to those tested by Duvarcı. Two of these were reference bare frames. Okuyucu reported test results of five single-bay and single-story RC frames, one of which is a reference frame. All specimens were 1/3-scale of a nonductile frame and tested under reversed cyclic quasi-static lateral loading. The researchers mainly studied various types of precast concrete panels with varying geometry and connection details. A substantial amount of increase in strength, initial stiffness and energy dissipation capacity was concluded to be achieved by the applied strengthening in all three studies. The considerable role of the precast concrete panels in controlling the excessive drifts was also reported. Besides, the limit for the inter-story drift ratio of the strengthened specimens was recommended to be 1.0 percent by Baran (2005).

2.3. EVALUATION OF THE HCT INFILLED FRAME BEHAVIOR

One of the earliest attempts to understand the effect of infill walls on the overall frame response was carried out by Smith (1967). In this study, eighteen scaled two-story steel frames infilled with mortar, which was supposed to imitate the masonry response, were tested monotonically in four series. The effects of the beam and column dimensions and varying length/height ratios of the infills were considered as the basic test parameters. The stiffness and strength characteristics of the infilled frames were described with respect to these parameters. The results revealed that the infill walls could be represented by pin-jointed equivalent members with a defined effective width. The effective width of the infill was defined to be highly dependent on the relative infill/column stiffness and length/height ratio.

Bertero and Brokken (1983) conducted an experimental and analytical study which investigated the effects of masonry and lightweight concrete infills on seismic response of RC frame buildings. They performed eighteen tests on 1/3-scale model of the 3-1/2 story and 1-1/2 bay subassemblage of an eleven-story and three-bay RC frame. Four different types of infills were considered. Both monotonic and quasi-static cyclic test procedures were applied for different infill types. It was concluded that addition of infills not only increased the initial stiffness and strength considerably, but also altered the dynamic characteristics of the buildings significantly. The resultant effect of increased mass and stiffness due to infills was stated to be a decrease in the natural period, which was mainly influenced by stiffness. Subsequently modified (i.e. increased) demand was estimated through linear elastic response spectra analyses for selected ground motions. The comparison of the increased capacity and demand values, considering different cases of varying number of infilled frames in a building and infill type, designated that the increase in capacity highly exceeded demand increment for most of the cases. The decreased displacement demands provided by the infill walls were also highlighted by the researchers.

Zarnic and Tomazevic (1984) tested a total of 28 one-bay and one-story frames in four series in order to investigate the effect of different types of infill walls, openings in the infills and two different rehabilitation techniques. The applied rehabilitation methods were epoxy-grouting and reinforced-cement coating on both faces of the infill walls. The specimens were tested under reversed cyclic loading with repeated load reversals so as to determine the change in the hysteretic behavior of infilled frames (i.e. strength deterioration and decrease in the energy absorption capacity). The results showed a significant increase in both lateral strength and stiffness, and decrease in the displacement demand of the frames for all infill types. Besides, repair of the damaged frames by epoxy-grouting was reported to improve the behavior only moderately. However, a repair through both epoxy-grouting and reinforced-cement coating resulted in significant improvement in the lateral response. The researchers also proposed equations governing the lateral resistance and deformability of the infilled frames through an observation of test results in the small and large deformation ranges.

Mehrabi et al. (1996) performed an experimental study in which twelve 1/2-scale, single-story and single-bay infiled RC frames were tested. The frames were subjected to either monotonic or reversed cyclic lateral and constant vertical loading. The test parameters were the relative strength of the infill panel (i.e. weak or strong infill) and bounding frame (i.e. weak or strong frame), panel aspect ratio, distribution of vertical loads and lateral load history. The varying stiffness and strength increments and failure mechanisms were defined with respect to different combinations of infill and frame strength. Since a small range of aspect ratios were considered, no significant effect of this parameter was observed. Different distributions of vertical loads between columns and beam were also reported to be inefficient on the overall response. The faster load degradation engendered by cyclic in comparison to monotonic loading was indicated. All in all, the beneficial influence of masonry walls on the seismic performance of RC frames was emphasized with further recommendation on the possible advantages of strengthening the infill walls.

Negro and Verzeletti (1996) conducted three pseudo-dynamic tests on a full-scale, four-story and two-bay (in both directions) RC building. The same building was tested without infills, with infill walls in the two exterior frames and lastly, same as the latter one but with no infill in the first story (i.e. soft story). The building was designed to have a high level of ductility. Based on time histories of the total absorbed energy at each story, they stated on variations in the energy dissipation due to different infill wall distributions. They concluded that a regular infill wall distribution lead to a decreased energy dissipation demand of the frame; however irregularities of this distribution may cause unacceptable damage of the frame members. They suggested using the relative energy demand of an infilled frame with respect to corresponding bare frame, which was calculated by a SDOF system assumption, as an indicator for the presence of infill walls. The use of such a parameter was indicated to be beneficial in the simplified design of infilled RC frames (i.e. modified design forces according to the differences in SDOF energy demands).

In order to investigate the seismic behavior of infilled frames, Marjani (1997) tested six 1/3-scale, one-bay and two-story RC frames; two of which were reference bare frames. The other frames had hollow clay tile masonry infill walls. Plaster was applied on both faces of three specimens, whereas the remaining infilled frame had no plaster. Reversed cyclic lateral and constant axial load was applied on the specimens. Also, the tests of isolated infill panels were conducted so as to have an idea on the behavior and characteristics of infills alone. These panel specimens were loaded monotonically in the diagonal direction. The test results indicated that the infill walls improved strength and stiffness of the frames, considerably. Further increment could be attained by plaster application together with a more ductile response compared to non-plastered specimen. In the analytical part of the study, the lateral strength and stiffness of the infilled frames were calculated by using strut method proposed by Smith and Carter. It was stated that the strength of the specimens were overestimated by this method, whereas the stiffness values were underestimated. Also, linear and nonlinear finite element methods were utilized to estimate the lateral response of infilled frames.

Hashemi and Mosalam (2006) carried out a shake table test of a one-story RC structure, as part of a larger-scale research project. The 3/4-scale structure had two bays in one direction and one bay in the orthogonal one. The interior frame was filled with unreinforced masonry wall. The structure was subjected to a series of shake table tests, performed in three stages. In the first stage, the infill wall was damaged to a point which terminated its contribution to the overall response. In the second stage, the bare structure was tested in order to understand the effect of infill. And in the last stage, the structure was tested up to failure. In each stage, the structure was subjected to a series of selected and scaled ground motions. At each applied ground motion level, the sequence of damage was depicted so as to express the effect of infill wall in detail. The change in the demands and distribution of internal forces after the failure of infill wall were also evaluated.

2.4. FRP STRENGTHENING OF INFILL WALLS

FRP materials have been employed for both in-plane and out-of-plane retrofitting of masonry walls. The research and application field may either be masonry-work structures or masonry infill walls of frame-type structures. As being the main subject of this study, only the research efforts related to the in-plane behavior of FRP strengthened infill walls are considered herein. Accordingly, the studies in this particular subject, other than those summarized in Chapter 2.1 that were performed at METU SML, are reviewed as follows in the chronological order.

In the study performed by Akgüzel (2003), five 1/3-scale, one-bay and two-story nonductile RC frames were tested. The first two specimens were reference frames, namely a bare and an infilled frame. The other three frames were strengthened with an advancing retrofitting scheme, each taking measures of the deficiencies observed in the previous specimen. But in general, the strengthening was provided by means of constant-width CFRP strips applied along the diagonals of infill walls (i.e. cross-overlay CFRP sheets). These CFRP strips were extended over the frame members and anchored to the RC frame with varying type and number of dowels. All of the specimens were subjected to reversed cyclic lateral and constant axial (i.e. ten percent of the axial capacity of columns) loading. The applied retrofit method was concluded to be beneficial in terms of increasing the lateral load (around 1.5~2.0 times) and energy dissipation capacity (approximately 3.0 times). On the other hand, the initial stiffness increment was reported to be low. The stiffness degradation of all specimens was indicated to be stabilized beyond a drift ratio of 1.0%.

Garevski et al. (2004) carried out an experimental joint research with the contributions of “Institute of Earthquake Engineering and Engineering Seismology-University of “Ss. Cyril and Methodius”” in Skopje, Republic of Macedonia and “METU Civil Engineering Department” in Ankara, Turkey. They performed dynamic shaking table tests of two 1/3-scale models of a four-story prototype RC building. The specimens were designed and constructed to reflect the common structural deficiencies observed in practice. The two-story model specimens had three bays in the longitudinal and one bay in the transverse direction. The hollow clay tile infill walls were constructed only in the middle spans of the specimens along the longitudinal directions. The second specimen was retrofitted by means of CFRP fabrics with the same methodology as developed in the previous studies at METU SML (Mertol, 2002; Keskin, 2002; Erduran, 2002; Erdem, 2003). The model specimens were subjected to a series of input motions simulating the scaled Izmit Earthquake record (east-west direction). The authors indicated that the roof displacement demand decreased from 168 mm to 87 mm by the applied retrofitting.

They also stated that the overall seismic response of the test specimen could be improved considerably (i.e. increased lateral load capacity) with the implemented CFRP strengthening methodology.

Although steel frames were considered instead of RC, the experimental study performed by El-Dakhakhni et al. (2004) is also included herein. In their study, they intended to upgrade the mechanical properties of infill walls by FRP's as a retrofitting procedure. To this end, six full scale, one-bay and one-story steel frames were tested with the generated reversed cyclic displacement protocols. One bare frame and two infilled frames were used as reference specimens. The first reference frame with walls was fully infilled, whereas the other one had a symmetrical door opening. Two of the frames, again one fully infilled and one with an opening, were strengthened by covering the entire wall with two orthogonal layers of GFRP on both faces. The last strengthened specimen was a fully infilled frame where two orthogonal layers of GFRP were applied only on one face of the wall. The GFRP fabrics were only bonded on the masonry without extending on the frame and no anchorage was implemented on the infill. It was stated that the ultimate strength, initial stiffness and energy dissipation capacity of the specimens were increased in all the specimens by virtue of applied strengthening. The authors also concluded that, in addition to the supplied shear strength, retrofitted walls experienced less damage, contributed to the in-plane frame response for a longer period and resulted in "a gradual prolonged failure".

Saatçioğlu et al. (2005) carried out an experimental study with an objective of developing a retrofit strategy for infilled RC frames through utilization of CFRP fabrics. In this study, the test results of two 1/2-scale, one-bay and one-story RC frames were presented. The first specimen was a reference frame with non-strengthened infill walls, whereas the other frame was strengthened by means of CFRP. In this strengthened frame, two layers of CFRP was bonded on both faces of infill, such that the fibers of each layer correspond to one diagonal direction, covering the whole infill surface. Later on, in a subsequent study presented by

Saatçioğlu (2006), another strengthened specimen was included and the results of these three frames were evaluated together. In the latter strengthened frame, one-layer of CFRP fabric with a constant width was bonded along each diagonal direction of the infill on both faces. In both retrofitted specimens, CFRP sheets were extended and anchored to the RC frame members, however no anchorage was reported to be provided on the masonry. All of the frames were designed according to pre-1970 design codes and had an infill height/width ratio of 1.0. They were tested under constant gravity and reversed cyclic lateral loading with repeated load reversals at the same displacement level. According to the test results, the applied strengthening controlled cracking that led to a stiffness deterioration in unreinforced infill walls. The strengthening resulted in a significant increase in the lateral load capacity (i.e. by a factor of three). However, along with the failure of CFRP layers, a rapid strength degradation was observed which hindered an improvement in terms of ductility. The importance of the anchor dowels in providing a more efficient frame-infill interaction during seismic response was emphasized. The hysteretic curves showed that the behavior could not be improved beyond 0.5% lateral drift. Therefore, it was suggested that the proposed retrofit technique should be based on elastic force limits rather than ductility and energy dissipation concepts.

In a study presented by Yüksel et al. (2006), the test results of six 1/2-scale, one-bay and two-story nonductile RC frames (i.e. two bare, two infilled and two strengthened specimens) were evaluated. One of each different types of frame had lapped longitudinal column bars at the floor level with insufficient development lengths. The strengthening was implemented by one-layer of CFRP cross-overlay sheets bonded on both faces of the infill and extended over the surrounding frame. Similar to the previous studies, constant axial (i.e. 23 percent of the axial capacity of columns) and reversed cyclic lateral loading was applied for testing. The results indicated significant improvement in the lateral load capacity and energy dissipation capacity attained by retrofitting in either types of frame, having lap-spliced or continuous column reinforcements. Although presented envelope curves of the specimens demonstrate a close behavior at small drift levels, a stiffness increment was also reported by the authors. It was stated that the load carrying capacity of specimens decreased rapidly after the rupture of diagonal CFRP sheets. Subsequently, in another study (Erol et al., 2006) presented by the same research group, one additional strengthened frame was included. In this specimen, as distinct from the previous ones, two layers of cross-overlay sheets were applied along the diagonal directions only on one face. The cyclic response of the frame revealed that this method was also very efficient. This is important for cases where application of CFRP is not possible on both faces of the walls, i.e. adjacent buildings.

Binici et al. (2007) carried out an analytical study with the aim of developing a design oriented structural model for FRP strengthened hollow clay tile infill walls. On the bases of the previous experimental results and principles of mechanics, diagonal tri-linear strut and tie models were proposed, so as to represent the inelastic compressive and tensile responses of FRP-infill composites, respectively. The generated models were implemented in the modeling of previously tested RC frames having infills that were strengthened by means of CFRP. The nonlinear static pushover response curves of the analytical models were compared with the load-deformation envelopes of the corresponding test specimens. The comparative results revealed a good agreement in terms of stiffness, strength and deformation capacity. Moreover, simplified versions of the proposed models were presented for displacement based design purposes. Lastly, the analyses of a real case deficient RC frame type building with/without CFRP retrofitted infill walls were performed in order to assess the performance of retrofit scheme. As a result, it was concluded that CFRP retrofit of the existing infill walls provided drift control with decreased deformation demands.

Kobayashi (2007) investigated a more unique application of FRP’s for retrofitting of RC frames with masonry partitions. The method, namely “sewing bands” was provided by inserting epoxy resin impregnated “FRP strands” through the holes drilled at the junction points of the mortar lines in a continuous zigzag form, as in sewing. Lastly, the ends of strands meeting the frame were attached to the columns by binding. An experimental program was conducted in two test groups in order to investigate effectiveness of the method with different test parameters. All specimens were scaled one-bay and one-story RC frames, which were subjected to reverse cyclic loading. In both groups, the main test parameter for the strengthened frames was the amount of strand used on the wall (i.e. “fiber volume fraction of sewing bands”). In the first group, four specimens, one of which was a frame with non-strengthened infills, were tested. No axial load was applied during testing. In the other group, a bare, a non-strengthened infilled and three strengthened frames were tested. The transverse and longitudinal reinforcement ratios of the columns were lower in this group; however an axial force of 20 kN was applied on each column. The sewing bands were stated not to provide any confinement to the hollow bricks. The effectiveness of the sewing bands for two different failure modes, namely horizontal joint interface and diagonal compression failure modes, were defined regarding the experimental observations. The improved deformability in case of horizontal joint slip could not be supported by the same amount of strength increment. It was also noted by the author that there was an optimum amount of fiber volume required for increased deformability.

Binici and Kobayashi (2008) investigated the same strengthening method suggested by Kobayashi (2007) in a different test program with a complementary analytic study. The “sewing bands” method was applied on four single-bay and single-story frames with differing number of FRP strands. The specimens were tested under compressive cyclic loading where the load was applied along the diagonal direction. Referring to the test results, the authors indicated that the sewing bands postponed crack formation along the mortar bed joints and assured a monolithic response with considerable residual capacity. A simple design-oriented numerical model of the retrofitted infill walls, which was based on test observations, was developed by the authors. The analytical and experimental results were compared and it was concluded that the inelastic static response of the specimens strengthened by this method could be estimated reasonably well by the proposed model.

Erol et al. (2008) carried out an experimental research including both frame and masonry panel tests. A total number of 28 panel specimens having in plane dimensions of 755 mm x 755 mm were loaded in the diagonal direction monotonically. A number of test parameters; such as thickness of panel, existence of plaster, surface area of CFRP, width of diagonal CFRP sheets, anchorage through masonry, CFRP and epoxy type were investigated. Moreover, five 1/2-scale, one-story and one-bay RC frames were tested under reversed cyclic lateral and constant axial (i.e. 20 percent of the axial capacity of columns) loading. A bare and an infilled frame were used as reference. The other three specimens were strengthened by one layer of CFRP cross-overlay sheets applied on both faces of the infill. These sheets were connected to the surrounding frame and anchored to each other through masonry by means of anchor dowels. First two retrofitted frames differ in terms of anchorage details. However, the last strengthened frame was challenging. The cross-overlay sheets were bonded to the infill only at the corners by use of additional CFRP fabrics which were typically utilized for confinement of these corner regions. The frame test results indicated that the ultimate capacity and stiffness could be increased considerably by the applied strengthening in all frames. Though, this improvement was designated to be lower in case of the last strengthened frame. The CFRP, in addition to its benefit under tensile stresses, was featured to be conducive in keeping the masonry in place and spreading the compressive stress over a larger area. The failure of strengthened specimens was reported to be eventuated by rupturing of diagonal CFRP at about 1% drift ratio.

Altın et al. (2008) investigated the effect of width and arrangement of diagonal CFRP sheets on the efficiency of applied strengthening through tests of ten 1/3-scale, one-story and one-bay nonductile RC frames. The first specimen, which was a frame with non-retrofitted infill was regarded as reference. Three different configurations of diagonal CFRP fabrics was used; as applied on both faces, on the interior face and exterior face. Also varying diagonal CFRP widths; 200, 300 and 400 mm were utilized for each different configuration. All of the frames were subjected to reversed cyclic lateral and constant axial (i.e. 10 percent of the axial capacity of columns) loading. Regarding the experimental results, the authors indicated that the ultimate strength and initial stiffness were increased by 2.18~2.61 and 4.00~6.00 times, respectively, for specimens where CFRP was applied on both faces. In the case where CFRP was bonded only on one face, these ratios remained in the level of 1.57~1.85 and 3.81~5.70 times for strength and stiffness, respectively. The utilization of CFRP on the interior or exterior face did not result any significant difference in terms of response. The strength and stiffness of specimens further improved with increasing CFRP width; however this improvement was stated to be limited.

Nateghi-Elahi and Dehghani (2008) conducted an experimental study in which four 1/2-scale, one-bay and one-story nonductile RC frames were tested under reversed cyclic lateral loading. The infill walls were constructed by use of solid bricks. Three of the frames were strengthened with slight differences in the retrofit scheme, whereas one frame was tested to serve as a reference specimen. The retrofitting was provided by CFRP sheets having a width of 300 mm bonded along the diagonals of the infill on both sides and anchored both to the frame and infill wall. Also the lap-splice regions of the columns at the base level and beam-column joints were confined by CFRP. In the last specimen, the upper column ends were also confined distinctively. According to the results, it was concluded that the strength of frames was increased by around 2.5 folds; however the initial stiffness was not altered by the applied strengthening. The lateral confinement applied at the bottom of the columns were reported to be beneficial in terms of hindering severe damage at these regions, yet changed the failure mechanism and lead to shear failure of the upper regions of the columns. The confinement of upper parts in the last frame was reported to prevent this brittle type of failure mechanism.

In a recent study performed by Yüksel et al. (2009), six 1/3-scale, one-story and one-bay RC frames were tested. The efficiency of different CFRP retrofitting schemes was investigated. Two specimens, bare and infilled frames tested as reference. The other four frames were strengthened by varying CFRP configurations. The specimens were subjected to lateral displacement cycles under constant axial load (i.e. 20 percent of the axial capacity of columns). The test results of different retrofitting schemes were compared in terms of lateral strength, stiffness, energy dissipation capacity, cumulative damage and post-peak behavior. In general, a significant strength and stiffness improvement was reported to be obtained by all retrofit schemes. The specimen which was named as cross diamond-braced frame, was denoted to display the best response with regard to attained strength, cumulative damage and resulting post-peak behavior. The strengthening of this frame was also provided by CFRP cross-overlay sheets along the diagonals of the infill. However, these sheets were not connected to the beam-column joints, instead linked to the supplementary CFRP reinforcement on the columns and beams. In this way, imposing additional loads on the weak beam-column joints was prevented.

CHAPTER 3

EXPERIMENTAL PROGRAM

3.1 GENERAL

It was mentioned previously that in a former comprehensive study conducted in METU (Mertol, 2002; Keskin, 2002; and Erduran, 2002) in collaboration with other universities (Özden and Akgüzel, 2003; Erol et al., 2006; Yüksel et al., 2006), a rehabilitation methodology had been developed for nonductile RC frames. The main idea of this methodology was to improve the mechanical properties of existing hollow clay tile (HCT) infill walls by the application of CFRP sheets and integrate these walls with the existing structural system in order to constitute a new lateral load resisting system. In the experimental part of the current study, it was aimed to carry the efforts of previous project forward with additional test parameters. Therefore, it can be regarded as sequential of the aforementioned study where a similar strengthening scheme was applied with diagonal CFRP sheets. The principal objective was to investigate the possible effect of the aspect ratio of infill walls on the performance of this strengthening methodology. Besides, the influence of insufficient lap length at the bottom of the columns and scale of the frames were also evaluated. In this chapter, the RC frame test program is described. The dimensions and details of the frame specimens are introduced in Section 3.2.2. In Section 3.2.3, the properties of materials used for the construction and strengthening of specimens are presented. The construction and strengthening of the frames are described in Sections 3.2.4 and 3.2.5, respectively. Lastly, the testing facility is explained Sections 3.2.6, 3.2.7 and 3.2.8.

3.2 FRAME TESTS

3.2.1 General

Since early seventies, many studies, as reviewed in Section 2.2, have been performed at METU SML regarding the rehabilitation of reinforced concrete frame type structures. In most of the studies which were performed before 2002, the frame tests were performed in the horizontal position (Altın, 1990; Sonuvar, 2001; Mertol, 2002; Keskin, 2002; and Erduran, 2002). The total load was used to be applied on the strong foundation beam that was in between the twin frames. The reaction forces thus created at the floor level of these twin frames were used as applied lateral loads. In the absence of a reaction wall, this kind of test setup was a necessity. Although valuable results could be accomplished in these studies, it was rather impractical compared to the current test method in the vertical position. After the construction of a reaction wall, a new test setup was built which allows testing of the RC frame specimens in the vertical position (Duvarcı, 2003; Erdem, 2003; Süsoy, 2004; and Baran, 2005). In the latter case, the frames were cast monolithically with a rigid footing which was fixed to a universal base. Majority of the test program in the current study was conducted using this test setup. In 2005, a new and larger reaction wall was constructed in the laboratory, where a similar test setup was also constructed in front of this reaction wall. The last group of frame specimens was tested using the latest test setup.

The basis of the current study was constituted by an experimental program which involves testing of the scaled one-bay, two-story RC frames with different aspect ratios. Since more than one parameter was investigated, the specimens were assembled in different groups and further subgroups. The two main test groups, namely Group-I and Group-II were constituted by the specimens which were designed to be 1/3 and 1/2 scale models of a non-ductile frame, respectively. In each group, specimens having two different aspect ratios were tested, which were named as Series-N and Series-L, referring to narrow (i.e. slender) and large (i.e. squat) RC frames. The properties of the frame specimens are shown in Table 3.1.

The first letter used for the designation of the specimens refers to Series-N and Series-L. The remaining letters before the dash represents whether the specimen is a reference (REF) or a strengthened (STR) frame. The first and the second 1/3-scale reference specimens which were indicated with “REF1” and “REF2”, were the bare frame and frame with non-strengthened infill walls, respectively. The letters “L”, “C” and “W” used after the dash in the strengthened frames refer to the lap-spliced, continuous and partially welded longitudinal column bars, respectively. The partial welding process is explained in the following sections. Lastly, the scale ratios of the test frames were indicated with “1/3” and “1/2”.

The test specimens were designed and constructed so as to include the common structural deficiencies which had been observed to cause catastrophic damage in the previous earthquakes. The frames were designed to be scaled models of a non-ductile frame having strong beams and weak columns. The spacing of the transverse reinforcement was far from satisfying the provisions of TEC (The Ministry of Public Works and Settlement, 2007), especially at the potential plastic hinge regions. Besides, the free ends of the ties were anchored to the cover with 90^0 hooks, not into the core concrete. Ties were not provided at the beam-column joints. The beam reinforcement was detailed considering only the gravity loads; therefore the anchorage of beam bottom reinforcement was inadequate. Concrete used for the construction of specimens was poor in quality considering the recent concrete technology. Plain bars were used both as longitudinal and transverse reinforcement of all members, instead of deformed bars. In majority of the specimens, column longitudinal bars were lapped over a length of twenty times the bar diameter ($20d_b$) at both story levels. This lap length corresponds only to 50 percent of what is required by TEC. Only two exceptions for lap-splice application were the specimens NSTR-W-1/3 and LSTR-C-1/3. These frames were tested in order to conceive the possible changes in the behavior due to lap-splice.

3.2.2 Dimensions and Details of the Test Specimens

3.2.2.1 Group-I Specimens

In Group-I, four specimens were tested in each series (Table 3.1). The first and second specimens, which were bare and infilled frames respectively, were regarded as the reference specimens. The differences in the behavior of these two reference specimens were supposed to show the contribution of infill walls to the bare frame response and the interaction between them. The third and fourth specimens were strengthened by the rapid and user-friendly rehabilitation method which is explained in Section 3.2.5.

Table 3. 1 RC Frame Test Specimens

Main Groups	Subgroups	Aspect Ratio	Specimen	Type	Long. Reinf.
Group-I 1/3 scaled	Series-N	1.54 (1st story) 1.15 (2nd story)	NREF1-1/3	Bare	Lap-Splice
			NREF2-1/3	Infilled	Lap-Splice
			NSTR-L-1/3	Strengthened	Lap-Splice
			NSTR-W-1/3	Strengthened	Welded
	Series-L	0.40 (both stories)	LREF1-1/3	Bare	Lap-Splice
			LREF2-1/3	Infilled	Lap-Splice
			LSTR-L-1/3	Strengthened	Lap-Splice
			LSTR-C-1/3	Strengthened	Continuous
Group -II 1/2 scaled	Series-N	2.30 (1st story) 1.72 (2nd story)	LREF-1/2	Infilled	Lap-Splice
			LSTR-1/2	Strengthened	Lap-Splice
	Series-L	0.60 (both stories)	NREF-1/2	Infilled	Lap-Splice
			NSTR-1/2	Strengthened	Lap-Splice

As shown in Figure 3.1, the clear spans of the 1/3-scale Series-N and Series-L specimens were 650 mm and 1930 mm, respectively. In Series-N, the clear heights of the first and second story columns were 1000 mm and 750 mm, respectively. The elevated column length in the first story was designed to introduce a soft story in the system. On the other hand, the clear height of all the columns was 750 mm in Series-L. The dimensions of the footings in Series-N were 1250x450x400 mm (corresponding to length, width and height, respectively). These measures were 2530x450x400 mm for the footings in Series-L. A total number of fourteen cylindrical holes with a diameter of 50 mm were left as voids during the casting of footings. These holes were used for fixing the footings to the universal base.

The columns and beams of all Group-I specimens were identical. The column and beam cross-sectional dimensions were 100x150 mm and 150x150 mm, respectively. Approximately 15 mm clear cover was provided in all RC members. The columns were reinforced with symmetrically situated four ϕ8 plain bars in the longitudinal direction which corresponds to a reinforcement ratio (ρ_l) of 1.3 % (Figure 3.2). As explained previously, only specimen LSTR-C-1/3 had continuous column longitudinal bars. The reinforcement details of this specimen are shown in Figure 3.3. In specimen NSTR-W-1/3, the lapped longitudinal bars at the two exterior corners of the first story columns were welded. The remaining six specimens had lap-splice regions at the floor levels. At these regions, longitudinal bars were lapped over a length of $20d_b$, which corresponds to 160 mm for this group of specimens. The reinforcement details of 1/3-scale specimens with lap-splices are indicated in Figure 3.4 for the two series. The column longitudinal bars were anchored properly into the rigid footing with 135^0 hooked ends bent in the opposite directions. The beams had 6ϕ8 plain bars as the longitudinal reinforcement, which were equally distributed at the bottom and top of the cross-section (Figure 3.2). This results in an identical longitudinal reinforcement ratio as the columns, i.e. ρ_l = 1.3%. These bars were extended into the columns and bent in the perpendicular direction. The top reinforcements were terminated with 135^0 hooks having a length of 90 mm; whereas no hook was provided at the end of the bottom bars (Figures 3.3 and 3.4). 4-mm diameter plain bars were used for manufacturing lateral stirrups of the columns and beams, which were spaced at 100 mm (i.e. ϕ4/100 mm).

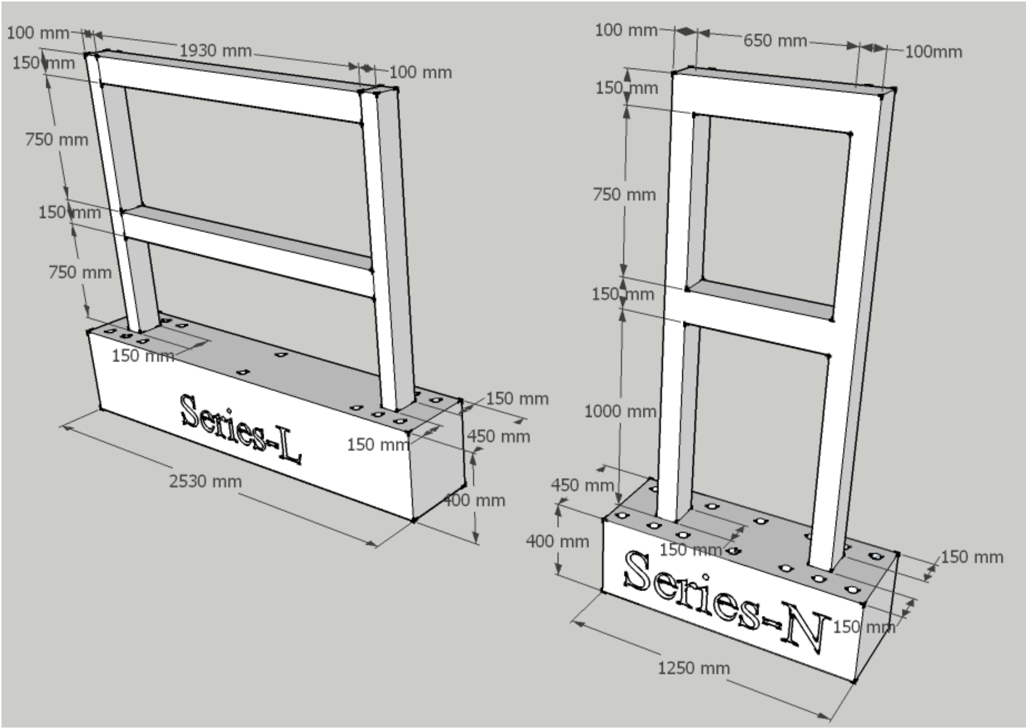

Figure 3. 1 Dimensions of Group-I specimens

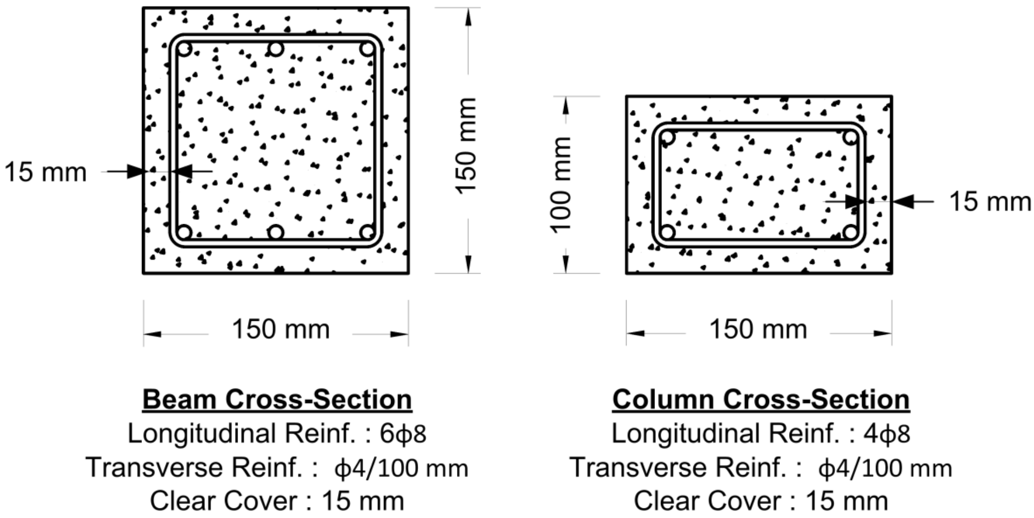

Figure 3. 2 Reinforcement layout of beam and column cross-sections in Group-I

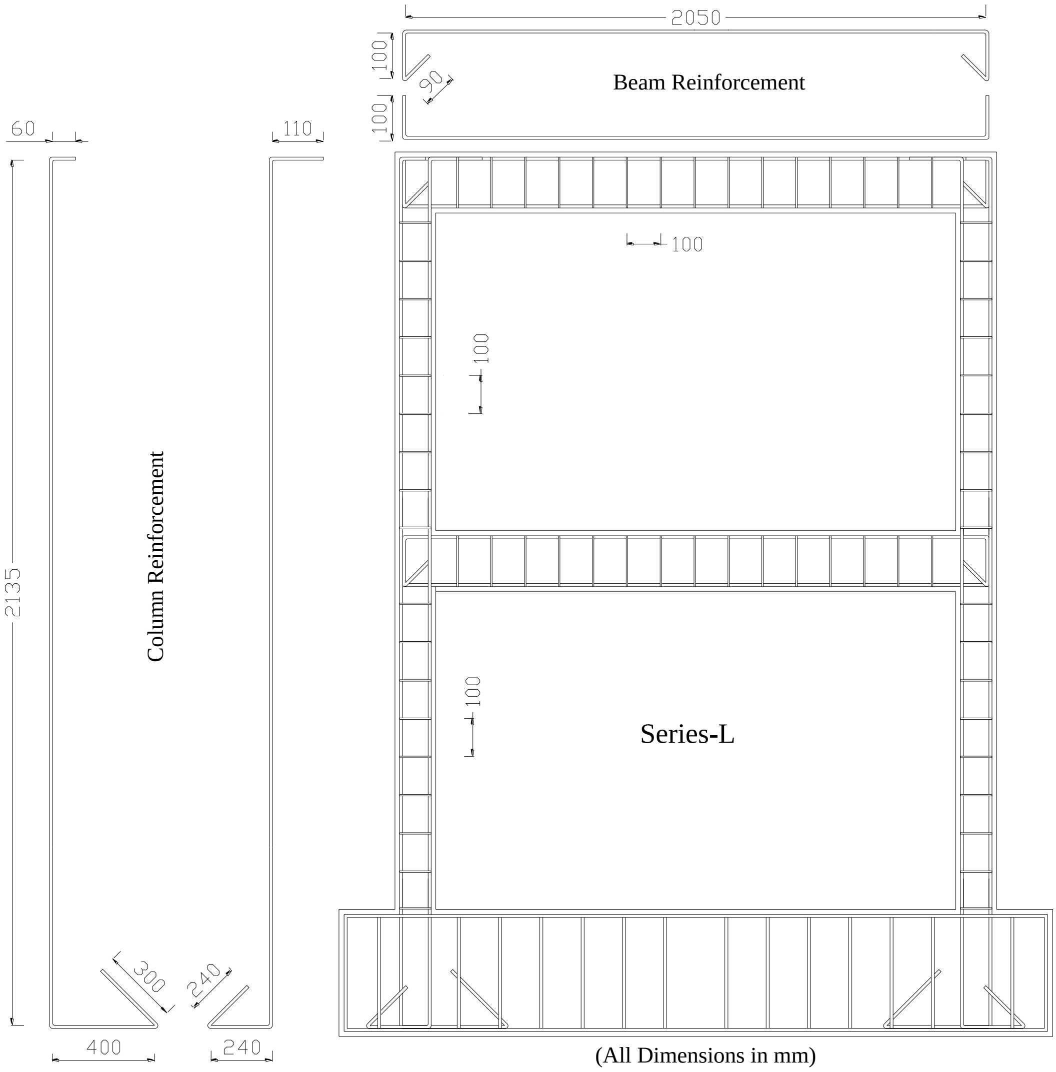

Figure 3. 3 Reinforcement detailing of specimen LSTR-C-1/3

3.2.2.2 Group-II Specimens

A total number of four 1/2-scale Group-II specimens; two from each series, were tested (Table 3.1). In each series, the first specimens constituted the reference specimens with infill walls. The second specimens, on the other hand, were strengthened with CFRP, as described in Section 3.2.5.

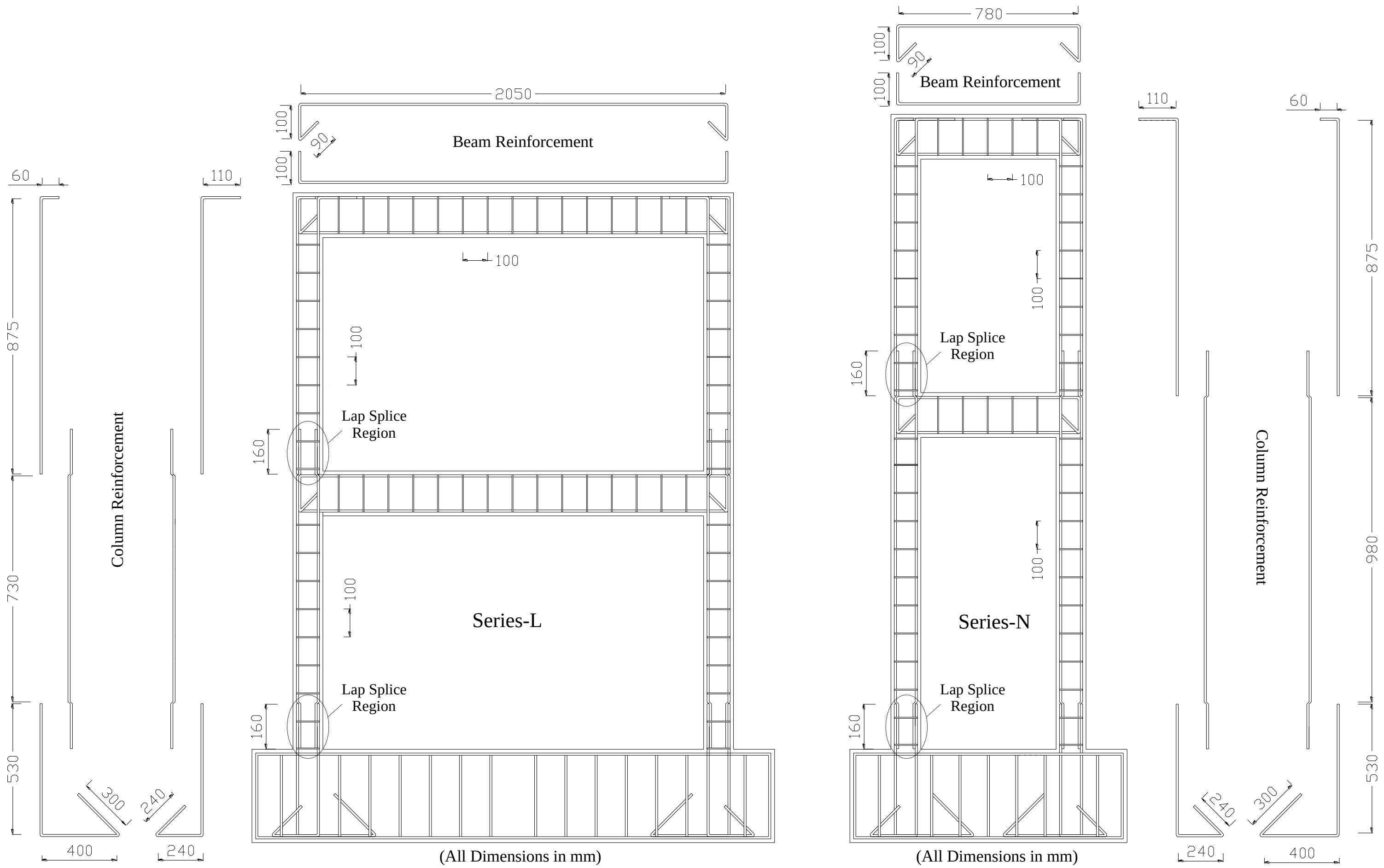

Figure 3. 4 Reinforcement detailing of Group-I specimens having lapped longitudinal column bars

The dimensions of Group-II specimens were arranged so as to be compatible with some other research programs performed parallel to this study in different institutions (Yüksel et al., 2006). The dimensions of 1/2-scale Series-L frames of the current study were set equal to the dimensions of specimens tested in the study given as a reference. Consequently, the aspect ratio of Group-II Series-L frames became to be 50 % higher than the 1/3-scale companions (Table 3.1). The final dimensions of Series-L specimens are shown in Figure 3.5. The clear span of the beams and height of the columns were 2040 mm and 1250 mm, respectively. The same amount of increase in the aspect ratio was also applied in both stories of Series-N specimens (Table 3.1). While doing this, the clear height of the second story columns of Series-N were set equal to those of Series-L specimens (i.e. 1250 mm), in the same way as in the previous group, Group-I. Considering this, in Group-II Series-N frames, the clear span was calculated to be 720 mm. By referring to these values, the clear height of the first story columns was estimated to be 1670 mm. The procedure followed in order to determine these dimensions is also explained in Figure 3.6.

In Group-II specimens, the sizes of the footings were increased considering the available dimensions of the universal base. The dimensions of the footings in Series-N and Series-L specimens were 1460x640x500 mm and 2800x640x500 mm, respectively. The cross-sectional dimensions of the columns and beams were 160x240 mm and 240x240 mm, respectively. The 12 mm diameter plain bars were used for the longitudinal reinforcement of the columns and beams. Other than the sizes of the bars and dimensions, the reinforcement layout and details of the members were the same as that of 1/3-scale frames. The longitudinal bars of all columns in Group-II specimens were lapped over a length of 240 mm (which corresponds to $20d_b$) at floor levels. The use of $4\phi12$ and $6\phi12$ bars for the columns and the beams, respectively, corresponds to a longitudinal reinforcement ratio of 1.2% for both members. The lateral confinement of all members was provided by 6 mm diameter stirrups which were spaced at 130 mm. The reinforcement detailing and cross-sectional layout of 1/2-scale Series-L and Series-N specimens can be seen in Figures 3.7 and 3.8, respectively.

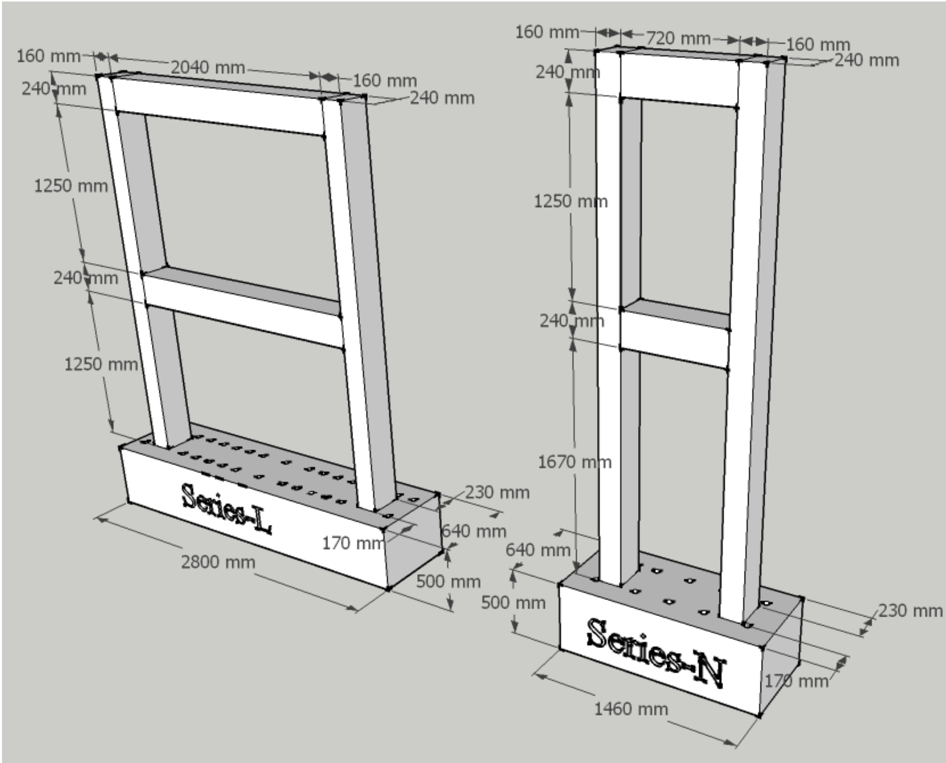

Figure 3. 5 Dimensions of Group-II specimens

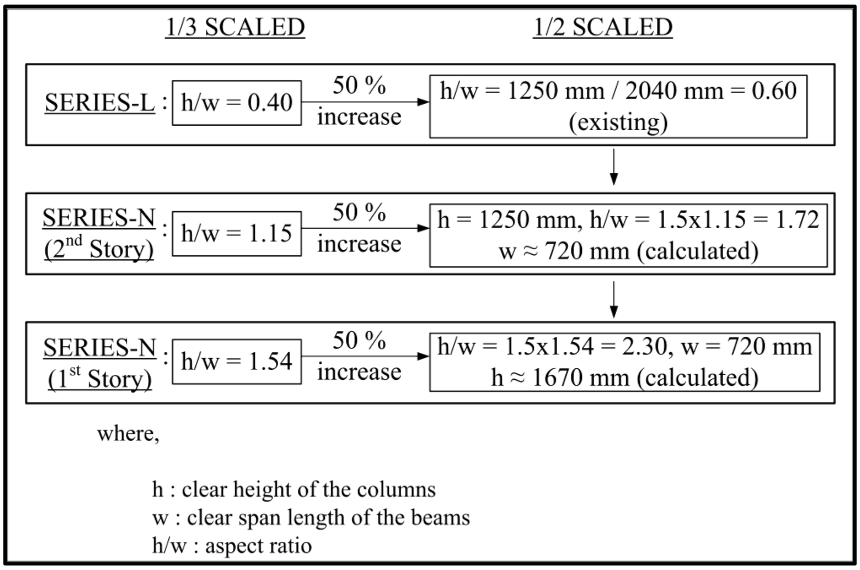

Figure 3. 6 The procedure for determining the dimensions of Group-II fames

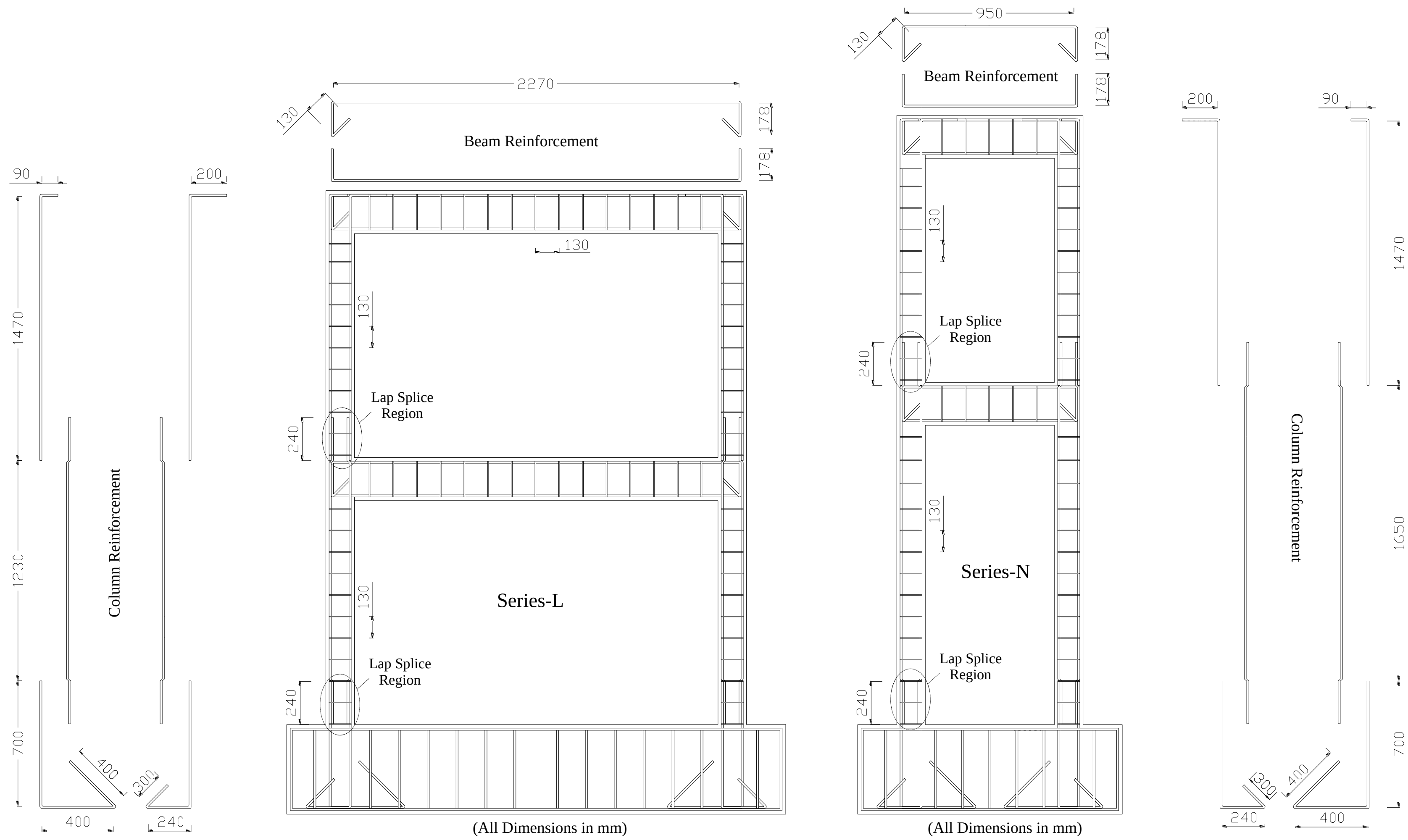

Figure 3. 7 Reinforcement detailing of Group-II specimens

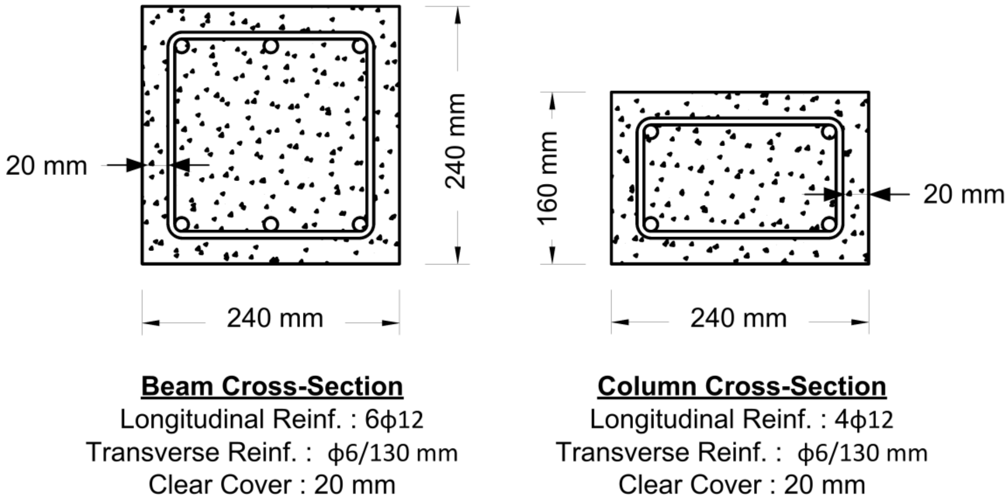

Figure 3. 8 Reinforcement layout of beam and column cross-sections in Group-II

3.2.3 Material Properties

The materials used during the construction of frame specimens are given in the following sections with their certain properties. These properties for the concrete, steel and HCT units were determined by the laboratory tests. However, those related to the CFRP material were introduced as supplied by the manufacturer.

3.2.3.1 Concrete

The concrete used for the frames in Group-I was manufactured in the laboratory. The concrete mix design is shown in Table 3.2. An approximate concrete compressive strength of 15 MPa was aimed with the values presented in terms of the weight proportions of aggregate, cement and water. In order to obtain the average compressive strength, sample concrete cylinders were cast during casting of the frames. Approximately ten cylinders having a diameter of 150 mm and a height of 300 mm were taken for each frame. These cylinders had the same curing conditions as for the frames and tested under monotonic compressive loads up to failure on the date of frame testing. The resulting average concrete strengths for each frame are shown in Table 3.3.

Table 3. 2 Concrete mix design proportions for Group-I frames

Material	0-3 mm Aggregate	3-7 mm Aggregate	7-15 mm Aggregate	Cement	Water	Total
Weight Proportions (%)	18.9	38.0	20.0	12.1	11.0	100

In Group-II, it was not convenient to prepare the required amount of concrete considering the capacity of existing mixer in the laboratory. Accordingly, ready-mixed concrete was used in this group. C12/15 was the minimum class of ready-mixed concrete that could be supplied; hence it was used in casting of Group-II specimens. The water to cement ratio of this type of concrete was 0.88 and the maximum aggregate size was 22.4 mm. For each concrete casting, twelve sample concrete cylinders were taken and tested similar to Group-I specimens. The concrete compressive strengths of Group-II specimens are also summarized in Table 3.3.

3.2.3.2 Reinforcing Steel

As mentioned in Section 3.2.2, the longitudinal reinforcements used in Group-I and Group-II frames were $\phi 8$ and $\phi 12$ plain bars, respectively. These steel bars were supplied in 12 m long batches and cut in the required lengths. On the other hand, $\phi 4$ and $\phi 6$ plain bars were used for the preparation of lateral stirrups. The latter steel bars were provided as ring-shaped batches and used after straightening. Three coupons were taken from each different size of steel bars and tested in tension. The resulting average stress-strain diagrams are shown in Figure 3.9 for each different size of steel bar. Besides, the tensile strengths of steel reinforcements are presented in Table 3.3.

Table 3. 3 Material properties of the specimens

Specimen		***Compressive Strength (MPa)***			***Tensile Yield Strength (MPa)***		**Ultimate Tensile Strength (MPa)**	
		Concrete, f'_{co}	**Mortar, f'_{m}**	**HCT, f'_{in}**	**Longitudinal Steel, f'_{y}**	**Transverse Steel, f'_{yw}**	**Longitudinal Steel, f'_{u}**	**Transverse Steel, f'_{uw}**
Group-I 1/3 scaled	NREF1-1/3	13.0	N/A	N/A	405 (ϕ8)	268 (ϕ4)	605 (ϕ8)	398 (ϕ4)
	NREF2-1/3	17.1	3.9	10.5				
	NSTR-L-1/3	19.4	4.0	10.5				
	NSTR-W-1/3	17.1	3.9	10.5				
	LREF1-1/3	16.1	N/A	N/A				
	LREF2-1/3	16.3	3.9	10.5				
	LSTR-L-1/3	16.7	3.9	10.5				
	LSTR-C-1/3	21.0	4.0	10.5				
Group-II 1/2 scaled	NREF-1/2	19.3	5.3	15.3	380 (ϕ12)	340 (ϕ6)	510 (ϕ12)	474 (ϕ6)
	NSTR-1/2	20.4	5.6	15.3				
	LREF-1/2	19.8	5.3	15.3				
	LSTR-1/2	20.7	5.6	15.3				

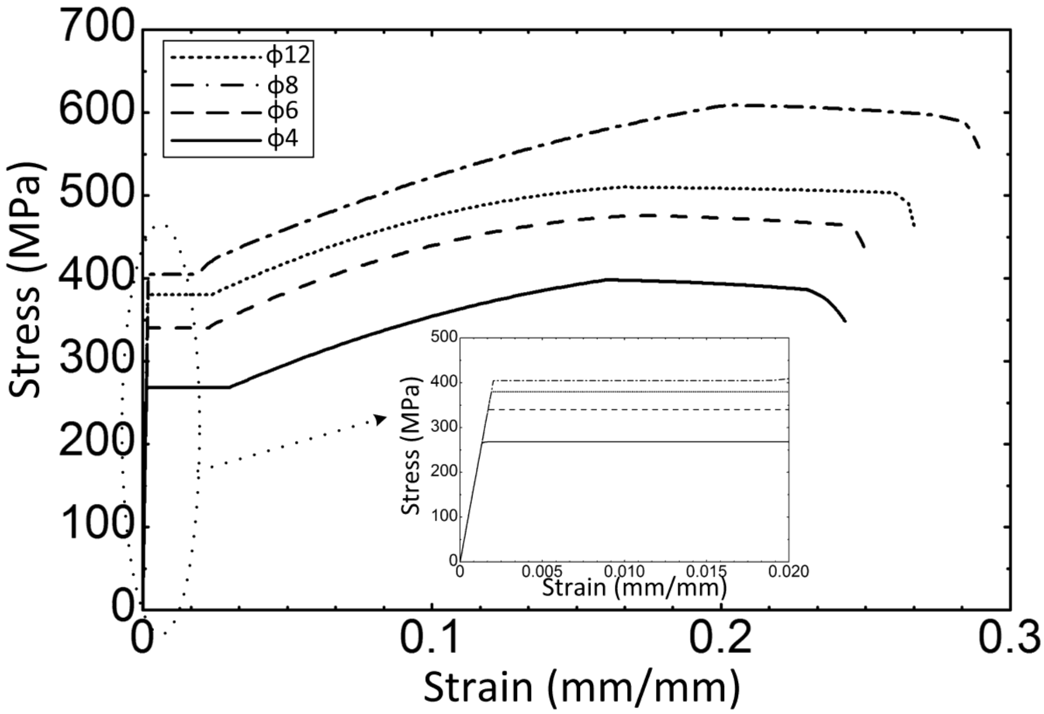

Figure 3. 9 The tensile stress-strain diagrams of steel reinforcements

3.2.3.3 Hollow Clay Tile

The hollow clay tiles used for the construction of the infill walls in Group-I frames were produced specially as one-third scale of the conventional tiles used in practice. They were designed and produced as part of an experimental study initiated previously at METU SML (Baran, 2005). The tiles used in Group-I had the dimensions given in Figure 3.10 and had a void ratio (i.e. the ratio of the void area to the total area over the cross-section) of 52%.

The infill units of Group-II frames were produced by cutting the conventional HCT's into two pieces, such that they had a void ratio of 59%. The dimensions of the cut HCT's used for the infill walls are shown in Figure 3.11.

The compressive strength of the individual HCT units was determined through compressive testing where the loads were applied parallel to the holes. Before testing, mortar cap was applied at the top and bottom faces of the HCT's in order to obtain an even surface for uniform stress distribution. The resulting compressive strengths of the HCT units are given in Table 3.4 for both test groups. The average of the net compressive strengths of HCT tiles are also presented in Table 3.3.

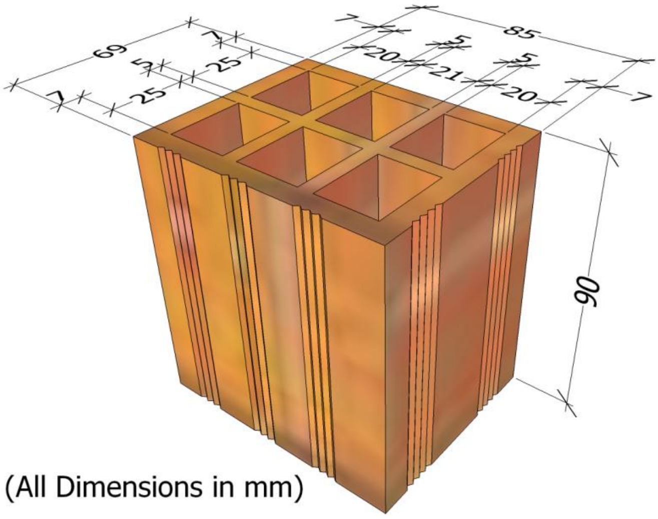

Figure 3. 10 The dimensions of the 1/3 scaled tiles

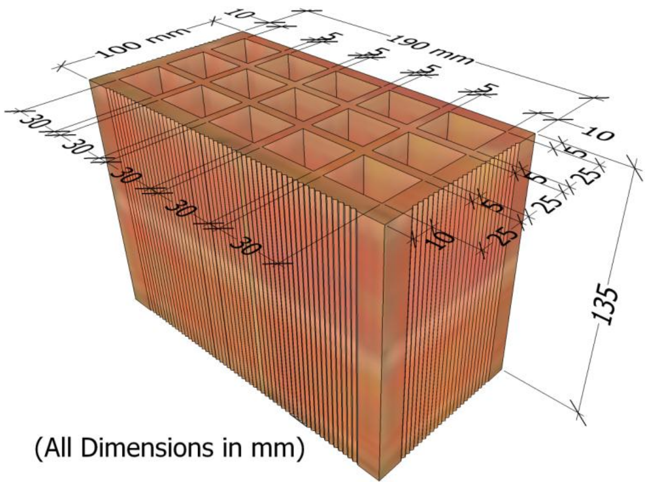

Figure 3. 11 The dimensions of the HCT used in Group-II specimens

The infill walls were built-up by a professional mason. These walls were placed such that they are on the same horizontal plane on one side of the RC frame members and recessed on the other side. As an example, the placement of the infill walls in Group-I Series-N specimens is shown in Figure 3.12. Plaster was applied on both faces of the HCT walls with an approximate thickness of 10 mm. The final thickness of the HCT walls was approximately 90 mm and 120 mm in Group-I and -II, respectively.

Table 3. 4 Compressive strength of the HCT units

	HCT Specimen	Net Compressive Strength (MPa)	Gross Compressive Strength (MPa)
Group-I	#1	10.9	5.2
	#2	8.5	4.1
	#3	11.3	5.4
	#4	11.1	5.3
	Average	10.5	5.0
Group-II	#1	14.8	6.0
	#2	15.8	6.4
	Average	15.3	6.2

During the construction of infill walls, sample cylinders of the mortar and plaster were taken. The compressive strength of the mortar and plaster was determined through testing of these cylinders. The test results of mortar, plaster and HCT are shown in Table 3.3.

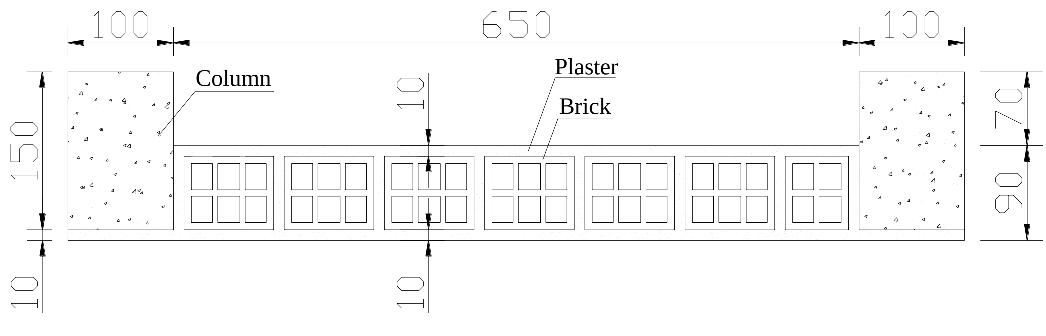

Figure 3. 12 The horizontal cross-sectional view of the frame-HCT infill wall assemblage (for specimen NREF2-1/3)

3.2.3.4 CFRP and Other Chemical Substances

Carbon fiber-reinforced polymer, CFRP, which was used for rehabilitation purposes in the content of this study, is a unidirectional (i.e. has its tensile strength in one direction) composite material. The mechanical and physical properties of CFRP are shown in Table 3.5, as provided by the manufacturer. During the application of the wet lay-up procedure which is explained in Section 3.2.5, MBT-MBrace® Primer, Concressive® 1406 (putty) and MBT-MBrace® Adesivo Saturant (adhesive) were used for the purposes mentioned in the same section. These chemicals were prepared through mixing two components, namely components A and B. The mechanical and physical properties and, mixing proportions of the putty and adhesive are given in Table 3.6, again as provided by the manufacturer.

Table 3. 5 Mechanical and physical properties of CFRP

Properties	
Characteristic Tensile Modulus of Elasticity, E_f (MPa)	230000
Characteristic Tensile Strength, f_f (MPa)	3430
Ultimate Tensile Strain, ε_{fu} (%)	1.5
Effective Thickness, t_f (mm)	0.166
Weight per Unit Area (kg/m^2)	0.3
Width of the Roll (mm)	500

The properties of adhesive impregnated CFRP composite become to be more crucial rather than individual properties of both materials, due to combined utilization. In order to determine the tensile strength of CFRP composite, coupon tests were carried out in a previous study at METU Construction Materials Laboratory (Çamlı, 2005). In this study, three coupons were prepared with the dimensions of 450 mm x 25 mm. The thicknesses of the coupons were 1.00, 1.05 and 1.00 mm, respectively. These coupons were tested under direct tension. The ultimate tensile strengths were obtained as 431.64, 541.51 and 384.55 MPa for the three coupons, respectively. The maximum measured strain was 0.0085. The average modulus of elasticity of the CFRP composite was calculated to be 61000 MPa.

Table 3. 6 The Properties of Concressive® 1406 and MBT-MBrace® Adesivo Saturant

Properties	MBT-MBrace® Adesivo Saturant	Concressive® 1406
Mixing Proportions • Component A (kg) • Component B (kg)	 3.73 1.27	 3.75 1.25
Density of the Mixture (kg/lt)	1.02±0.024	1.70±0.05
Compressive Strength (on 7th day) (MPa)	>60	75
Flexural Strength (on 7th day) (MPa)	>50	25
Bond Strength for concrete (MPa)	>3 (on 7th day)	3 (on 28th day)
Hardening Time (days)	7	7

3.2.4 Construction of the Specimens

The RC frame specimens were prepared at METU SML. The reinforcement cages of the frames were prepared in the first step. The steel bars were cut in the required dimensions and possible warps on these bars were straightened through slight hammering. The straight bars were bent to form the required shape as may be seen in Figures 3.3, 3.4 and 3.7. The ready longitudinal bars were tied up around the stirrups by using construction wires. The reinforcement of RC frame members were manufactured in this way separately and assembled afterwards as can be seen in Figure 3.13.

Figure 3. 13 The assemblage of the reinforcement cage

3.2.4.1 Formwork

The modular steel formworks were used for concrete casting of the frame specimens. These formworks were designed and manufactured to be a set of sixteen pieces made of 2 mm thick galvanized steel. Different sets of formworks were prepared for different types of frames. At the edges of formwork pieces, there were bolt holes matching their counterparts, which help to assemble these pieces by threading. The formwork was set up in the horizontal position. The assemblage of the formwork is illustrated in Figure 3.14. After the formwork was assembled, silicone sealant was applied at the connection regions between the joining pieces. The reinforcement cage was placed in the formwork by leaving space between the reinforcement and the formwork to provide the clear cover. The steel tubes were placed which would be used to leave cylindrical holes in the footings. The absolute horizontal position of these tubes and also the formwork was assured by checking with a water level. In the last step, the formwork was supported with braces so as to prevent possible deformations which might be caused during concrete casting.

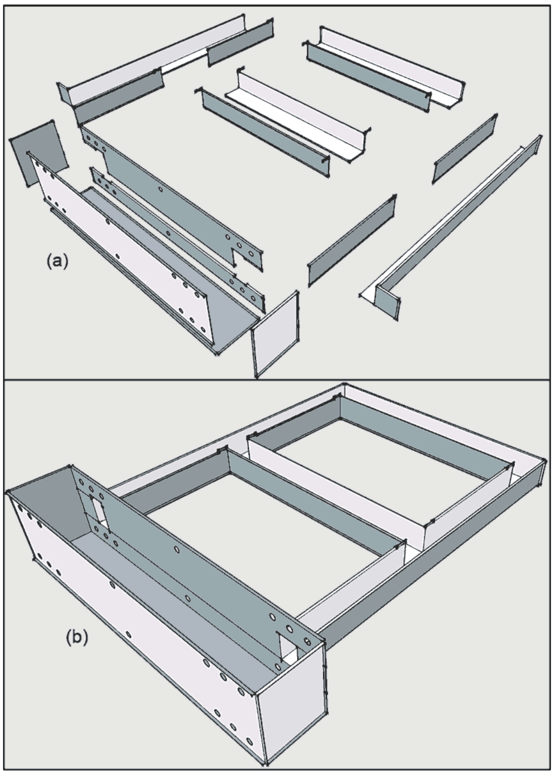

Figure 3. 14 Formwork for the frame specimens (a) before, and (b) after assembling the pieces

3.2.4.2 Concrete Casting

The quality of the concrete used for the frames should be lower than the minimum requirement of the Turkish Earthquake Code (i.e. 20 MPa). Therefore, an approximate concrete strength of 15 MPa was aimed in all tests. However, this was not always possible to maintain. The concrete for Group-I specimens was prepared in the laboratory with a concrete mixer. Since the capacity of the mixer did not allow the preparation of the volume of concrete required for one specimen at once, this was carried out in at least three steps depending on the frame type. But special attention was given to use the same mixture proportions in each concrete batch. Sample concrete cylinders were taken from every single batch. In Group-II, the size of the specimens made it inconvenient to cast the concrete using the concrete mixer as in the former case. Therefore, concrete for the Group-II frames was supplied from a ready-mixed concrete company.

In all frame specimens, the inner faces of the formwork were coated with oil to avoid the bond between formwork and concrete. Concrete was placed manually and compacted insufficiently in order to mimic the poor concrete quality in many existing buildings. The concrete casting was carried out such that the specimens were formed in the horizontal position. The curing of concrete was performed by covering the surfaces with wet burlaps (Figure 3.15). After about three weeks of wet curing, the specimens were raised to the vertical position at which they will be tested. The raising up of the specimens was achieved by an apparatus specially produced for this purpose and with the help of a crane without causing any damage on the frame.

Figure 3. 15 The specimens after concrete casting and curing of the concrete with wet burlaps

3.2.5 Strengthening of Frame Specimens

The strengthening scheme of the frames was detailed on the basis of a former study as mentioned previously (Mertol, 2002; Keskin, 2002; and Erduran, 2002). The strengthening applied in each series of the two test groups are illustrated in Figures 3.16 to 3.19.

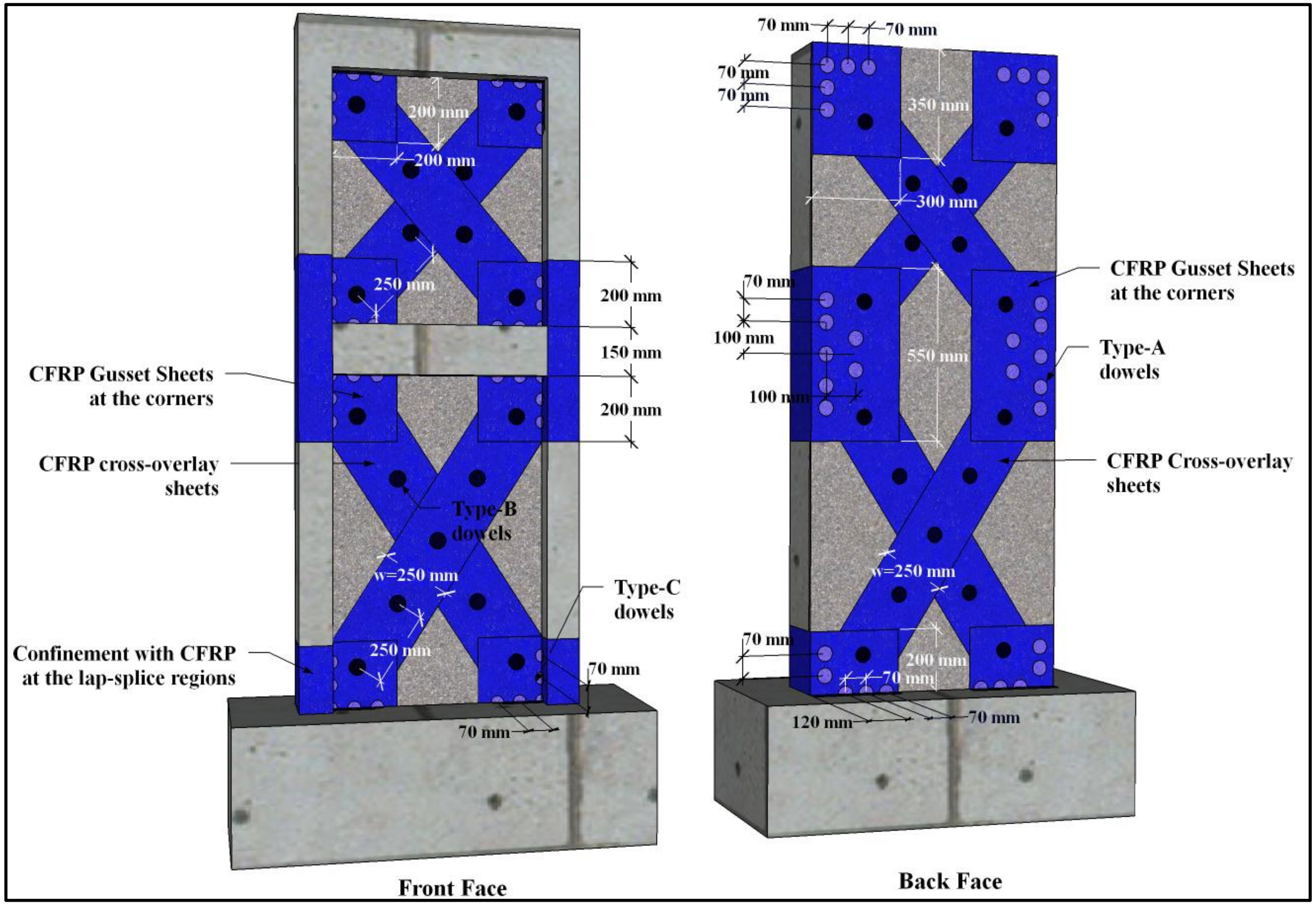

Figure 3. 16 The CFRP strengthening scheme of Series-N specimens in Group-I

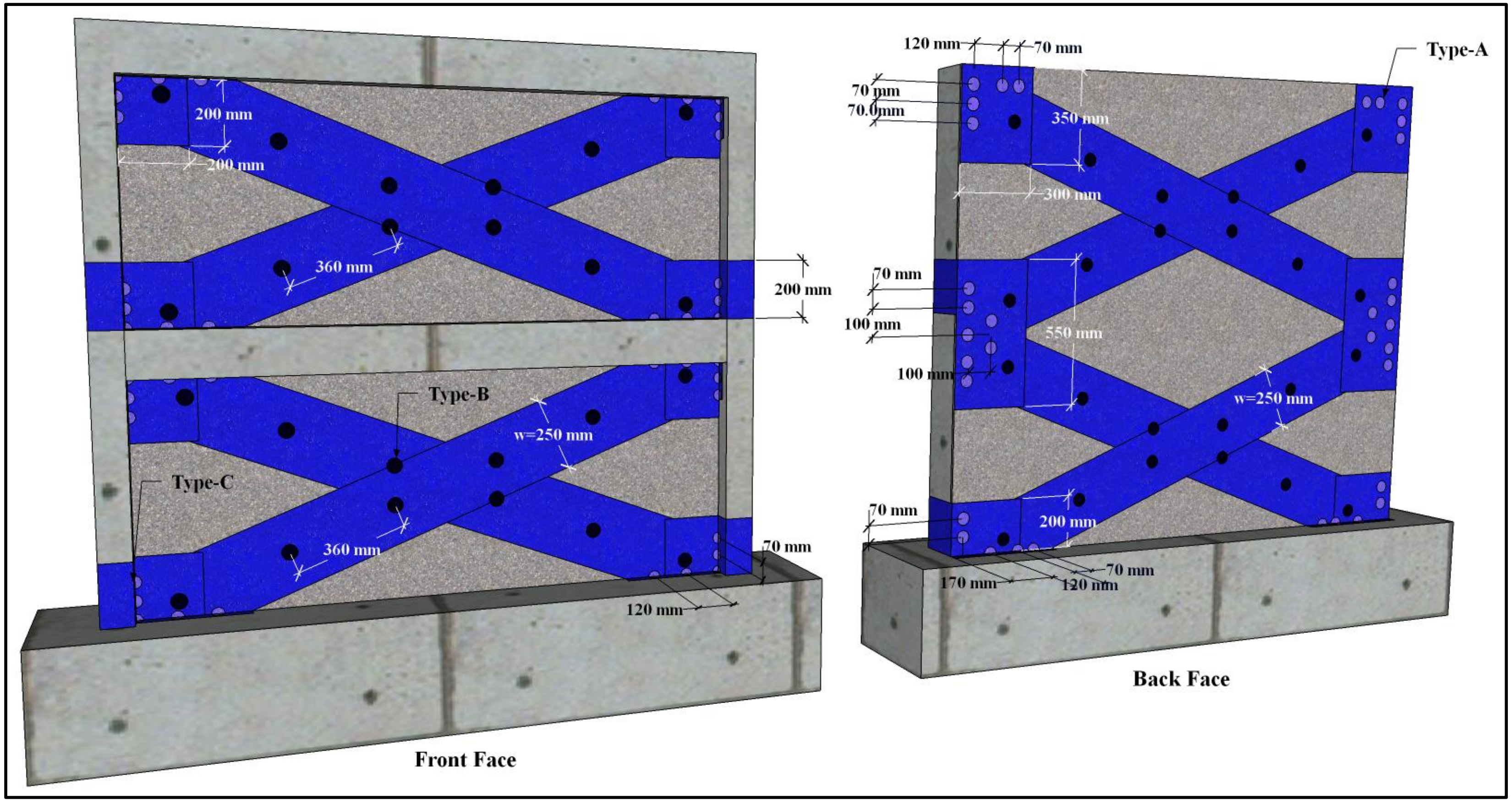

Figure 3. 17 The CFRP strengthening scheme of Series-L specimens in Group-I

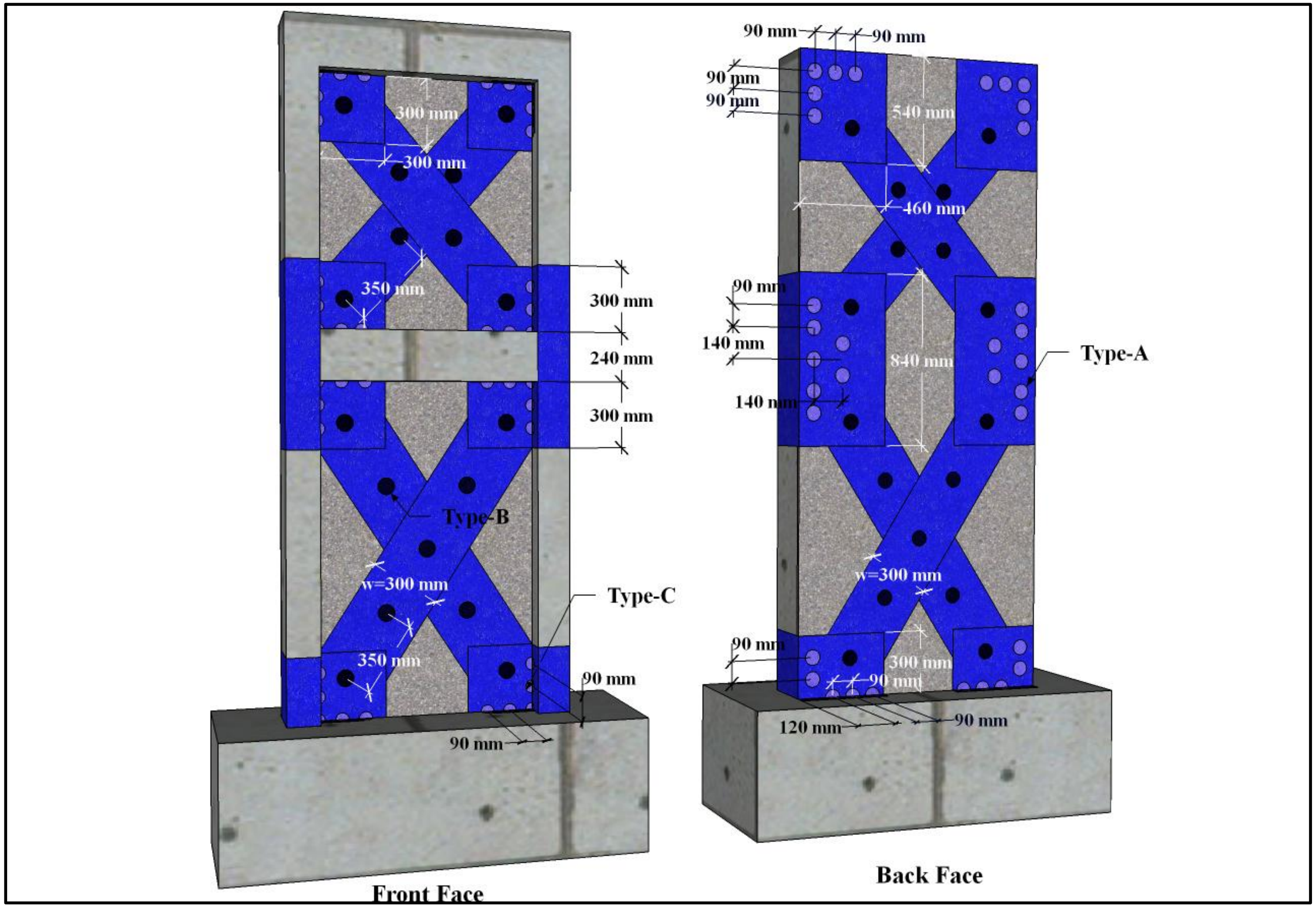

Figure 3. 18 The CFRP strengthening scheme of Series-N specimen in Group-II

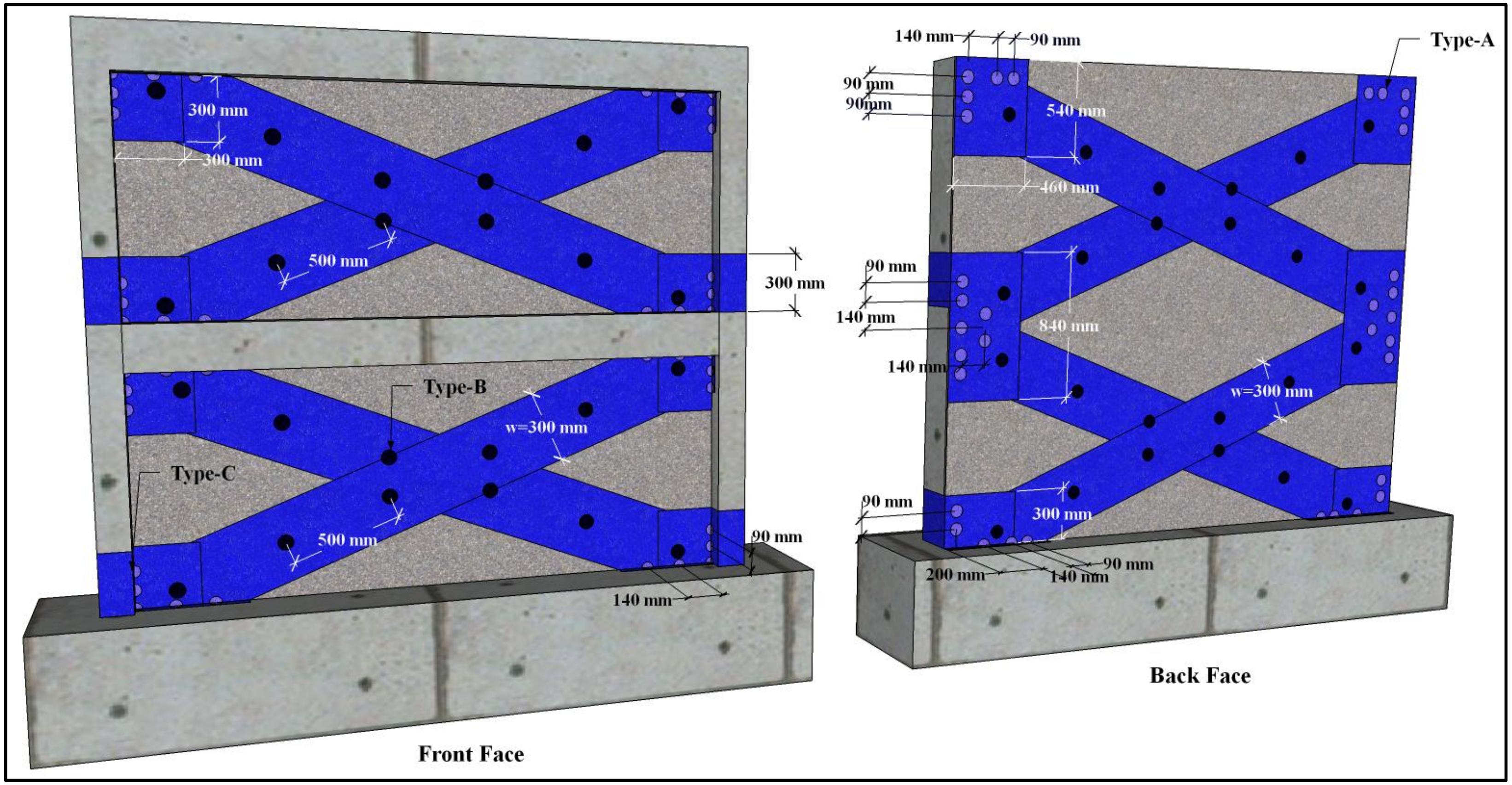

Figure 3. 19 The CFRP strengthening scheme of Series-L specimen in Group-II

The anchor dowels, which were made of rectangular CFRP strips, were employed for the anchorage of CFRP reinforcement to the RC frame and HCT infill walls. The rectangular CFRP strips were rolled tightly around wires which would guide the dowels along the holes, and tied up using strings. The CFRP strips and guide wires used for the preparation of anchor dowels together with the made-up form are shown in Figure 3.20.a. The dowels inserted to the HCT walls and RC columns are also illustrated in Figures 3.20.b and 3.20.c, respectively. Different types of dowels used in Group-I and Group-II are shown in Figure 3.21.a. and 3.21.b, respectively. In these figures, Type-A represents the dowels used to connect CFRP sheets to the beams and columns at the back face of the frames. Type-B stands for the dowels implemented throughout the HCT walls. The dowels used to anchor the CFRP sheets to the RC members at the front face were called as Type-C dowels. The whole strengthening process which is explained in the following paragraphs sequentially was also illustrated in Figure 3.22.

The specimens were prepared before the implementation of CFRP reinforcement. The locations of all the CFRP laminates and anchorages were marked on the frames and the infill walls. The corners of columns at the lap-splice regions which would be confined with CFRP were rounded to a radius of about 10 mm. The aim of this was to prevent the stress concentrations at the sharp edges. The holes were drilled at the predetermined locations of the anchorages with a depth and diameter as given in Table 3.7 for the two groups of specimens. The width of the CFRP used for manufacture of the anchor dowels were also presented in the same table. The holes were cleaned out of dust by using an air-compressor. A thin layer of undercoat material (MBT-MBrace® Primer), which would clean-up the dust on the surface, was applied at regions where CFRP would be installed (Figure 3.22.a). After one day of curing, the surface was flattened by the application of an epoxy-based chemical mortar, Concressive® 1406 in order to obtain a perfect bond between the CFRP and infill surface. (Figure 3.22.b). The CFRP sheets for different components of the applied strengthening scheme were cut in appropriate dimensions as determined for each frame (Figure 3.22.d).

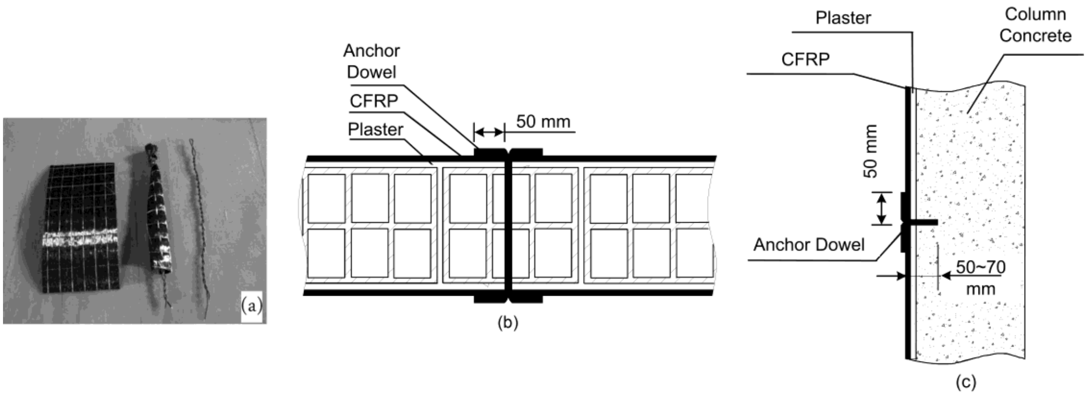

Figure 3. 20 (a) Made-up anchor dowels and application of anchor dowels to the (b) HCT infill walls and (c) RC members

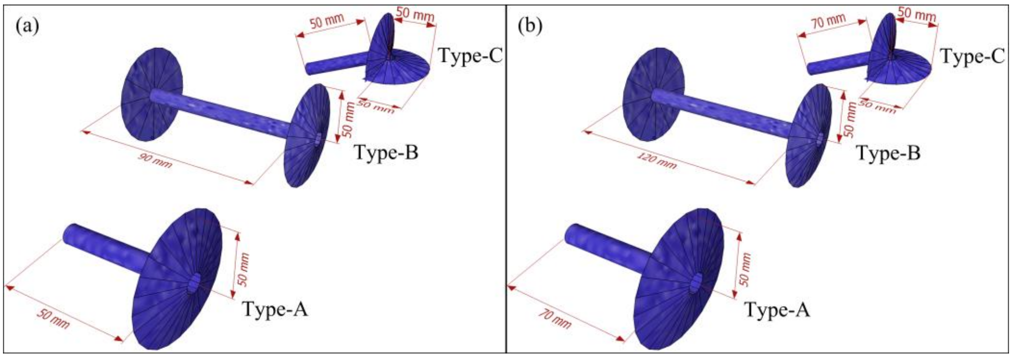

Figure 3. 21 The three different types of anchor dowels used in (a) Group-I, and (b) Group-II specimens

Table 3. 7 Properties of the anchor dowels

Test Groups	Anchor Type	Embedment Depth (mm)	Diameter of Anchor Hole (mm)	Strip Width (mm)
Group-I	Type-A and -C	50	10	80
	Type-B	90	10	80
Group-II	Type-A and -C	70	12	100
	Type-B	120	12	100

The main component in the strengthening process was fastening one-layer of CFRP sheet along the two main diagonals of the infill walls at both stories (cross-overlay sheets). A wet-lay-up process was implemented for bonding CFRP by using a two-component epoxy resin recommended by the manufacturer as adhesive (MBT-MBrace® Adesivo Saturant). The adhesive was coated over the chemical mortar (Figure 3.22.c). Afterwards, the epoxy resin impregnated CFRP sheets were placed on these regions (Figures 3.22.e, and 3.22.f). The widths of the cross-overlay sheets were 250 mm and 300 mm in Group-I and Group-II specimens, respectively. The CFRP width used on both faces and at both stories of the HTC infill walls was constant in each frame. The cross-overlay sheets were also extended to the frame members.

The lap-splice regions of the columns at the base of each story were confined with one-layer of CFRP where the fibers were oriented horizontally. The confinement was implemented with the wet-lay-up process just after placement of the cross-overlay sheets. The length of the confined region was 200 mm in Group-I and 300 mm in Group-II frames. The confinement at the second story columns of the flexure-dominant Series-N frames were also extended to the upper ends of the first story columns.

The corners of cross-overlay sheets were further covered with square, adhesive impregnated CFRP gusset sheets (Figures 3.16 to 3.19). The main reason of using gusset sheets was to provide a uniform stress transfer between the RC frame members and cross-overlay reinforcement. Another function of the gusset sheets was to confine the corners of the HCT walls where significant crushing had been observed in the reference frames. The gusset sheets which were applied at the front face were also applied on the opposite face of the HCT infills, extending over the corners of the columns and beams.

Figure 3. 22 Different phases of the implementation of CFRP reinforcement

The next step in the strengthening process was placing the anchor dowels (Figure 3.22.g). The anchor hole locations under the laminates were determined and made much evident by opening up the longitudinal fibers of CFRP over these holes, without damaging the fibers. Previously prepared CFRP anchor dowels were impregnated with adhesive and inserted in the holes. The free end fibers of the dowels were arranged to have an approximate length of 50 mm outside the holes. These free end fibers were spread over the underlying CFRP laminates and glued with adhesive. The guide wires were taken out carefully. The final view of these anchor dowels can be seen in Figures 3.20 and 3.21. In both groups of Series-N specimens, the numbers of Type-B anchor dowels were five and four in the first and second stories, respectively. A number of six dowels were used on the HCT walls of all Series-L specimens. In order to provide the structural integrity between the strengthened walls and RC frame, the sheets were also anchored to the RC members using CFRP dowels at the back (Type-A) and front faces (Type-C). In all strengthened specimens, five Type-A and Type-C anchor dowels were used at each corner. The concern about any possible damage that would be caused by the drilling of socket holes was an issue while determining the depth, interval and number of anchorages. The intervals of anchor dowels, as denoted in Figures 3.16 to 3.19, were arranged so as to ensure an equal distribution over the sheets which were connected to the RC members or HCT walls. In a previous study (Özdemir, 2005), it was stated that CFRP anchor dowels with embedment depths up to 50 mm experience cone failure. However, further increase in the embedment depth results bond slip failure beyond 50 mm, which has slight contribution to the resistance against pull out actions. Considering this, together with the concern about the damage created as a result of drilling for the dowels, a 50 mm embedment depth (i.e. one third of the width of the RC members) was chosen for Type-A and -C dowels in Group-I. In the next group of specimens, this embedment depth was increased to 70 mm in consideration of the increased member dimensions.

In the last step of strengthening, more adhesive was coated over the CFRP material and the voids between the fabrics and specimen were removed by the help of a steel-roller.

3.2.6 Test Setup

The frames in Group-I were tested using the setup which was established previously and have been used in many different experimental studies (Duvarcı, 2003; Erdem, 2003; Süsoy, 2004; and Baran, 2005). The pioneer reaction wall which had been constructed in 2002 was used for this purpose. After a renovation held at the laboratory and consequently, the construction of a larger scale reaction wall in 2005, a new similar setup was established for testing specimens in Group-II. This new setup was analogous to the previous one. The strong floor of the laboratory which was also renovated in 2005, allows fixing the test specimens by use of holes distributed along one meter distances in the two horizontal directions.

A universal base was used in order to function as an adaptor between the footing of the specimens and the strong floor. For Group-II tests, a new universal base which was identical to the previous one was constructed. The dimensions of the universal base were 2950x1500x400 mm as shown in Figure 3.23. The base was heavily reinforced by using deformed steel bars in both directions. A number of six holes having a diameter of 60 mm were provided in two rows. These holes were used to fix the universal base to the strong floor by use of “Dywidag bars” having a diameter of 50 mm. Thirty four steel nuts with a diameter of 38 mm were embedded into the universal base in two rows with the intervals indicated in Figure 3.23. The reinforcing cage of the universal base and installed nuts during the construction are shown in Figure 3.24. These nuts were utilized with post-tensioned “Dywidag bars” for fixing different specimen footings in varying dimensions.

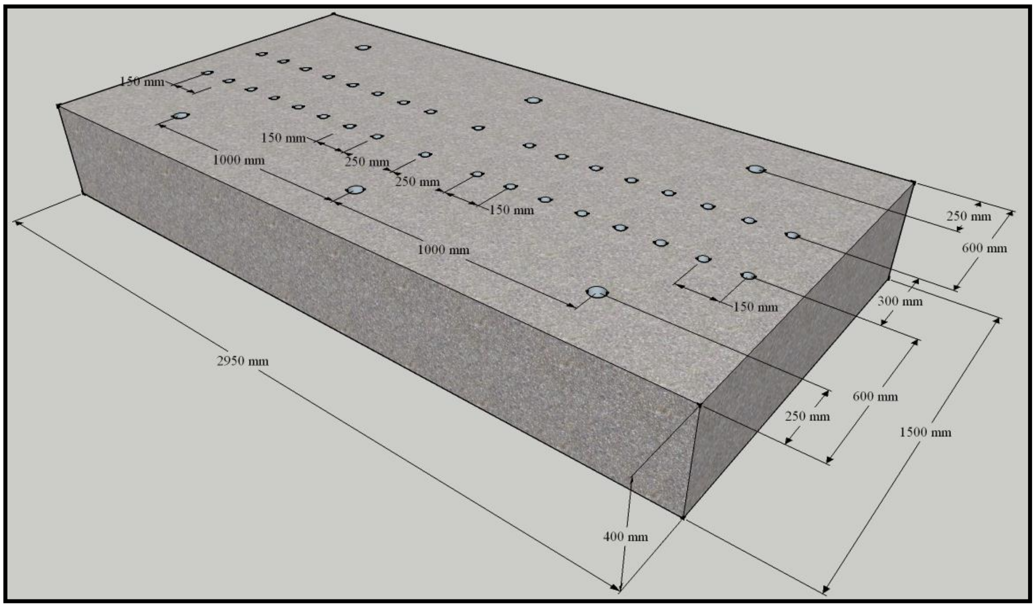

Figure 3. 23 The dimensions of the universal base

Figure 3. 24 The reinforcing cage, installed steel nuts and pipes of the universal base before concrete casting

Two different types of loading equipments were used for each reversed cyclic lateral and constant axial loading. These equipments had slight differences in both setups for the two test groups. The loading systems and the general test setups for Group-I and -II specimens are illustrated with the drawings in Figures 3.25 and 3.27, respectively. Also, two sample frame specimens from each test group are shown in Figures 3.26 and 3.28, as they were fixed on the corresponding test setups.

In the first group, the lateral load was applied by means of a double acting hydraulic actuator (i.e. Enerpac-RR 5020) which has a capacity of 600 kN in compression and 420 kN in tension (Baran, 2005). The hydraulic actuator was connected to the reaction wall through a steel frame. The steel frame was adjustable in the vertical direction so as to level the lateral loading equipment for different specimen heights. The attachments of hydraulic actuator to the specimen and to the adjustable steel frame were provided by pin connection at both ends. A load cell, which detects the magnitude of lateral loads, was connected to the actuator by using an adaptor. The load cell was capable of measuring 600 kN in compression and 300 kN in tension. The load was transferred to the specimen through a steel spreader beam placed between the actuator-load cell assemblage and the specimen. The main role of spreader beam was to distribute the applied lateral load, such that two thirds of the total lateral load is applied to the second floor and the rest to the first floor. In the forward loading direction, the spreader beam was leaning to the specimen only at the beam levels by means of two steel plates (i.e. pushing). The loading in the backward direction was provided by tensioning steel tie rods connected to the other two plates that were placed on the reverse side (i.e. pulling). All plates covered the projection of beam cross-sections at the floor levels. Four tie-rods were used at each floor level, i.e. two on both sides of the beams. The tie-rods were connected loosely to the plates.

In Group-II, the lateral load was applied in the same manner. However, servo-controlled hydraulic actuator (i.e. Moog L085-752 with a capacity of 500 kN) was used instead of the previous one (Figure 3.27). This new actuator was supplied as part of a new “Pseudo Dynamic Test” (PSD) facility established in the laboratory after 2005. Although the system was also capable of and mainly used for simulation of dynamic earthquake forces, in order to be compatible with the previous test group, it was used for reversed cyclic loading.

There was a load cell already mounted on these actuators for measurement of the applied loads. This was connected to the computer of the PSD system for data collection. However, another load cell (i.e. CAS LSU-50T) was also mounted on the actuator by an adaptor to collect the same data in a separate data acquisition system. The reliability of PSD system was also assured in this way, since this was the first experimental study in which the system was used. The transfer of load to the frame was performed in the same way as the previous group (i.e. the lateral load applied to the second floor was two times the magnitude of the load applied to the first floor). A new steel spreader beam, steel plates and tie-rods were manufactured considering the sizes compatible with the dimensions of Group-II specimens. Since heights of the footings were different in each group, a new set of steel bolts and nuts, which were also used to fix specimens to the universal base, were produced for Group-II.

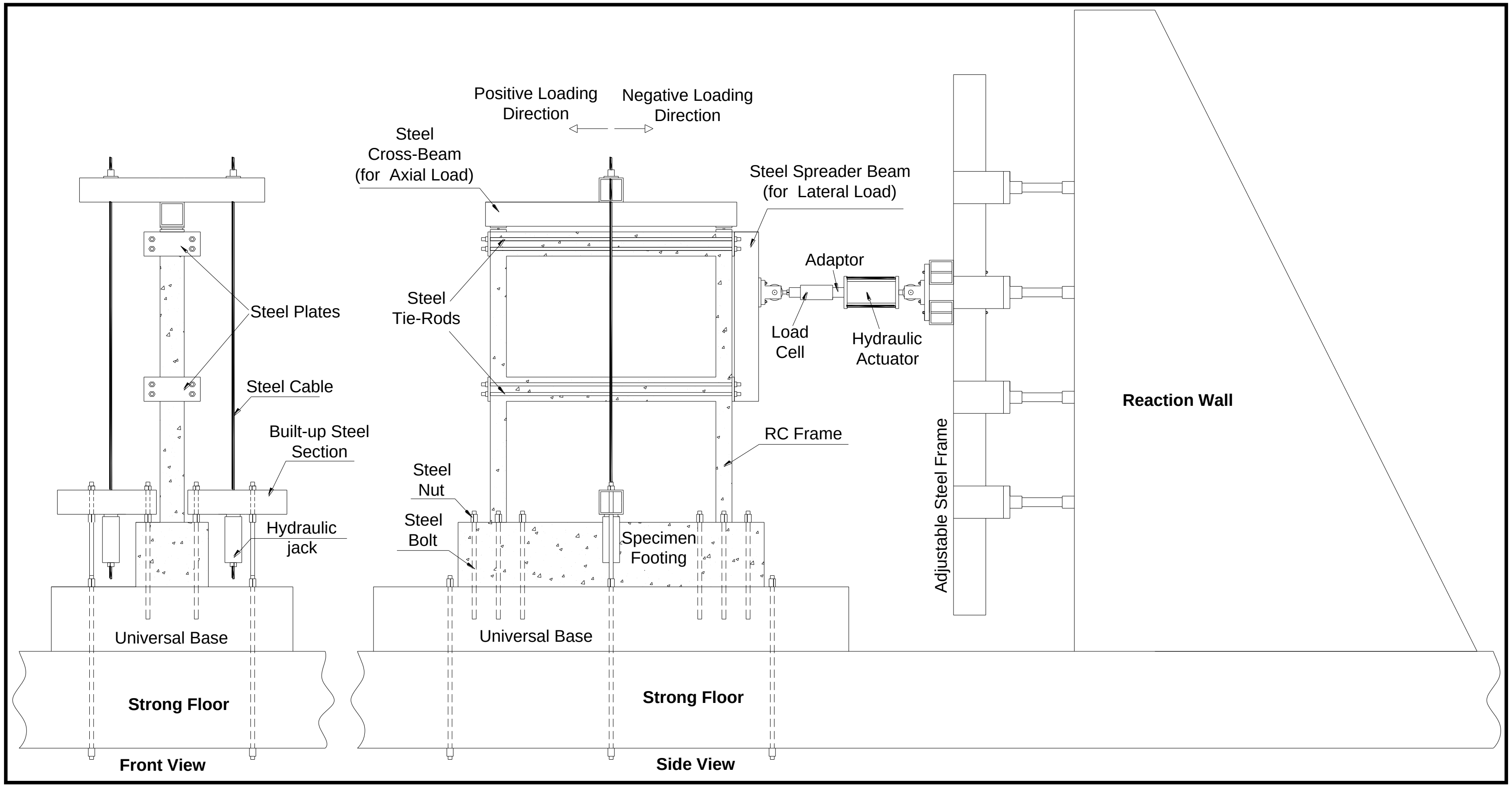

Figure 3. 25 The test setup for Group-I frames

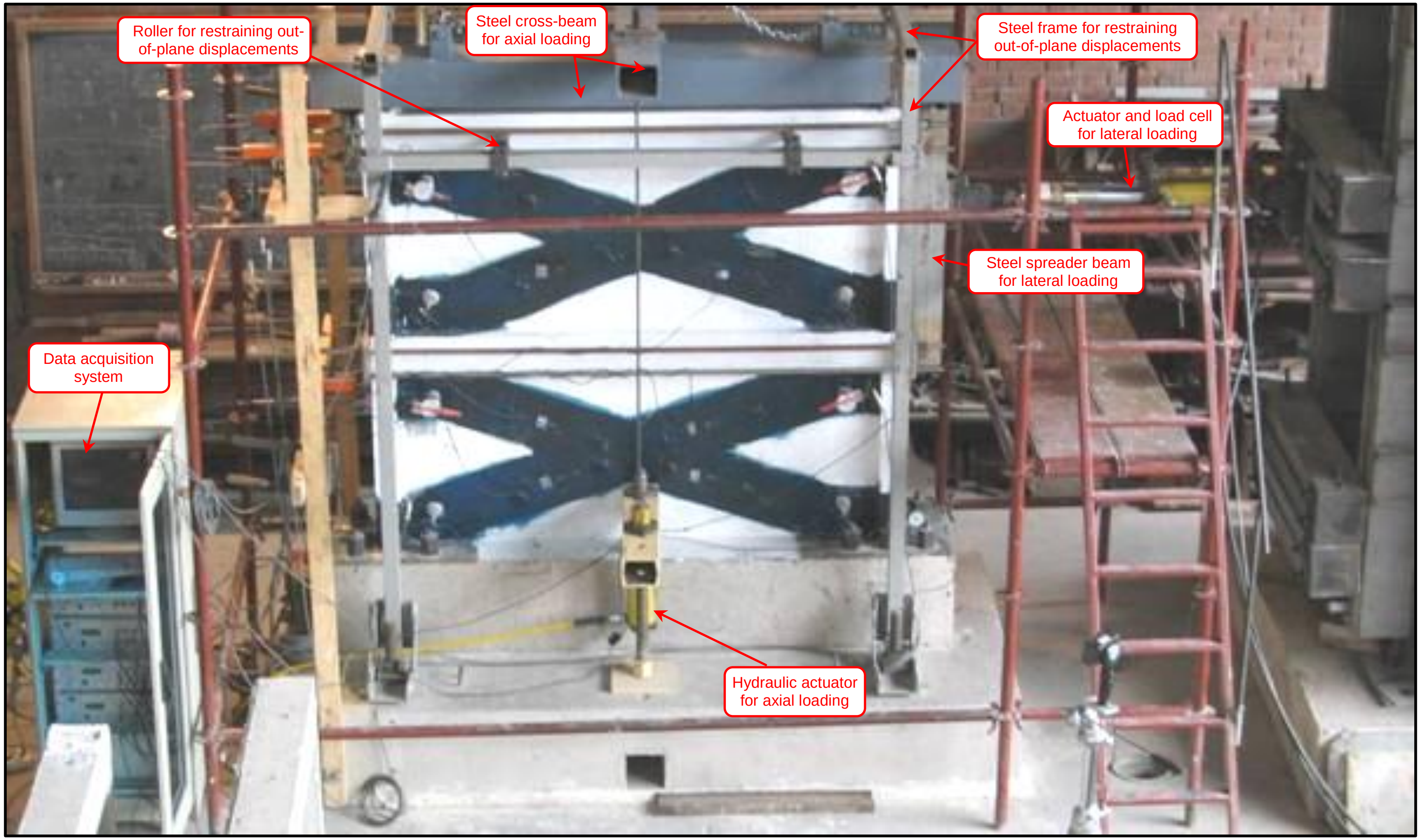

Figure 3. 26 The general view of a Group-I frame on the test setup

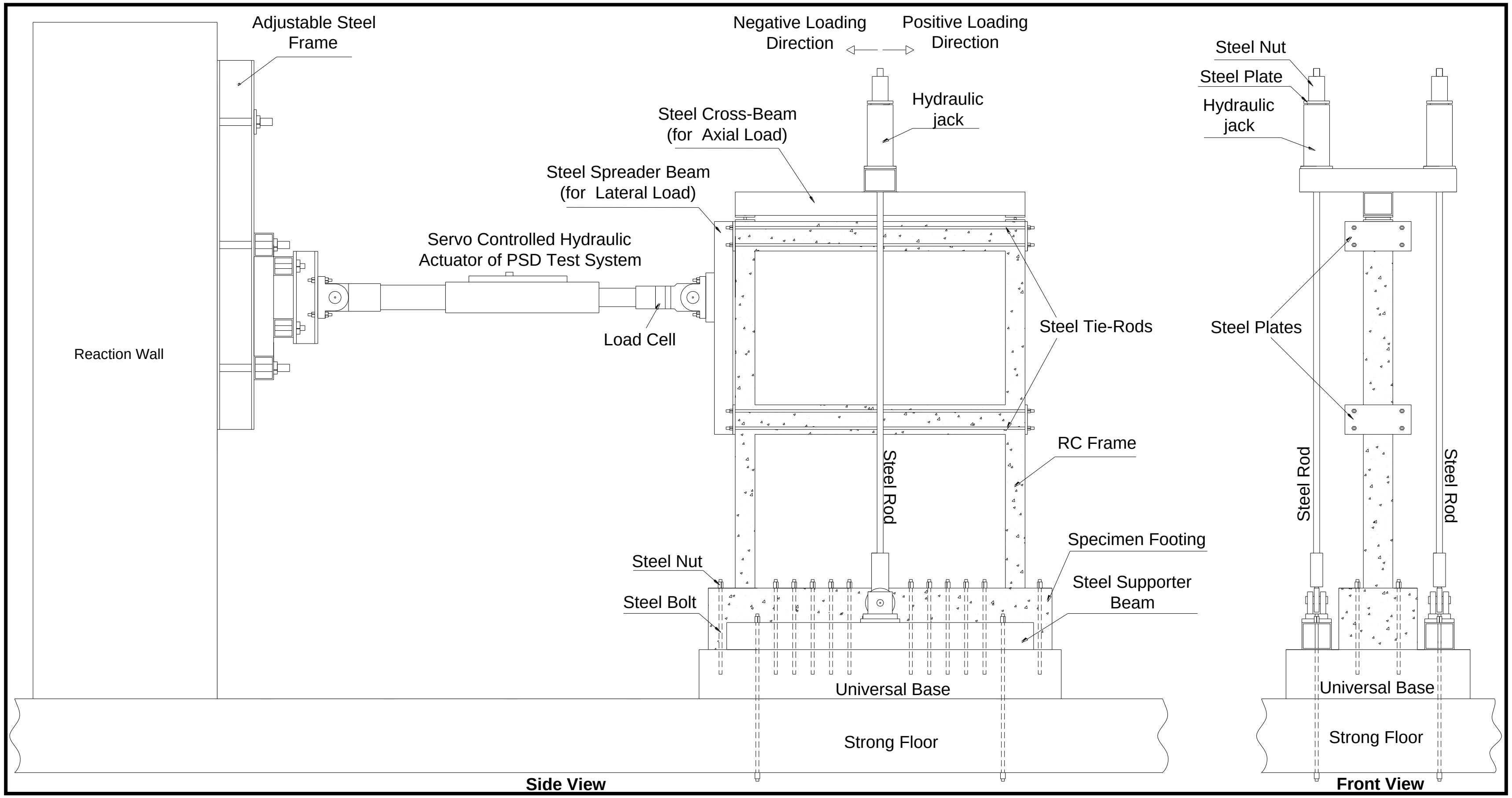

Figure 3. 27 The test setup for Group-II frames

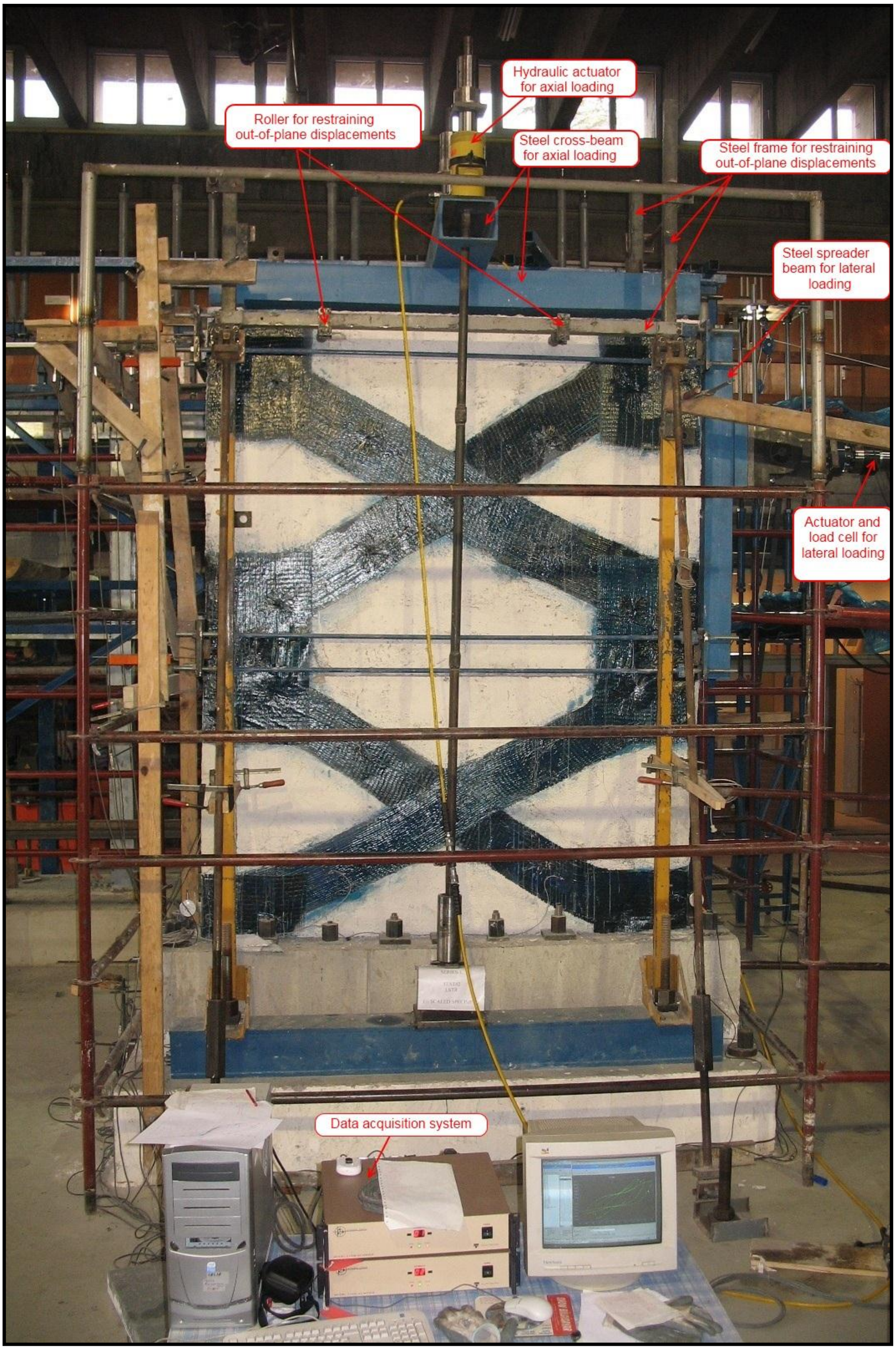

Figure 3. 28 The general view of a Group-II frame on the test setup

A constant axial load (i.e. 30 kN in Group-I and 75 kN in Group-II), which corresponds to approximately 10% of the axial load carrying capacity, was applied on the columns during the tests. In Group-I, the axial load was originated by post-tensioning of the steel cables through hydraulic jacks which were placed at the footing level of the specimens as shown in Figure 3.25. The hydraulic jacks were supported by the built-up steel sections which were fixed using the bolts present at the middle of the specimen footing and universal base. The post-tensioned cables passing through the holes in these steel sections were clamped to the steel cross-beam situated at the top of the frames. The cross beam was simply supported on the RC columns, in order to evenly distribute the total axial load which was conveyed by the cables to the columns.

In Group-II, again the cross-beams, which were simply supported on the RC columns, were used to transfer the axial loads on the columns. New cross-beams were manufactured considering the dimensions of new specimens. Two high strength steel rods on two sides of the setup were used instead of steel cables utilized in the previous group. At the bottom, the steel rods were connected to the steel supporter beams as shown in Figure 3.27. The steel supporter beams were situated parallel to the specimen footing on both sides and fixed by means of the bolts used for anchoring the universal base to the strong floor. The connections of the rods were hinge type at the bottom so as to allow the rotational movements, reflecting the lateral displacements experienced by the specimen. The steel rods were passing through holes on the cross-beams at the top of the frames. The hydraulic jacks were connected to these rods on top of the cross beams and fixed by nuts placed at the very top of the rods. The jacks post-tensioned the steel rods and the resultant reaction forces were transferred as axial loads equally on the RC columns.

Since the main interest was the in-plane response of the frames to the reversed cyclic actions, the out-of-plane movements should be prevented. In order to restrain these possible out-of-plane displacements, a rigid steel frame was constituted around the test specimen in both test groups. The main structure was similar in both test setups; however support conditions of the steel frames had slight differences. On both sides of the test setups, two columns made up of steel box sections were fixed through the bolts used for the anchorage of the universal base to the strong floor. These columns were connected to a steel beam at the level of the second story beam of the RC frames. On each side of the specimen, two rollers which were fixed to the steel beams were placed such that they were slightly meeting the RC beams. Therefore, the in-plane movements of the specimens were not disturbed while the out-of-plane movements were restrained. The steel frames were fixed to the wall of the laboratory in Group-I tests by means of another steel beam. However, in Group-II, inclined steel struts, which were fixed to the laboratory floor at one end, were used to support the steel frames. Moreover, in the latter case, the steel frames on both sides of the specimen were clamped to each other by using post-tensioned steel bars. The rigid steel frames can be seen in Figures 3.26 and 3.28.

3.2.7 Instrumentation

Different types of instruments were installed on the frame specimens in order to monitor the structural response continuously during the tests. Linear variable differential transformers (LVDT's), dial gauges, strain gauges (only in strengthened frames), load cell and pressure gauge were used for this purpose. A data acquisition system was used to collect the data transmitted from these instruments; which was further connected to a computer to record and monitor the gathered data. The instrumentation was basically same for Group-I and -II specimens as shown in Figure 3.29.

The lateral displacements of the frame at story levels were recorded by LVDT's. Three LVDT's with 200 mm stroke capacity were used at the second story level, whereas only one LVDT with 100 mm stroke was installed at the first story level. In Group-II, exceeding 100 mm top story displacement was probable, considering the global drift ratios reached in Group-I specimens. Therefore, an LVDT with 500 mm stroke was used instead of one of the existing devices at the top story of Group-II frames. And the LVDT used at the first story level was replaced by the LVDT with 200 mm stroke. The displacements were measured with respect to the universal base (i.e. the transducers were installed on a timber framing supported on the universal base). However, after experiencing a problem related to the movement of the universal base during the test of specimen LSTR-1/2, another framing was formed around the test setup which was supported on the strong floor instead of the universal base. The LVDT's were installed on this framing and the lateral displacement measurements were performed with respect to the strong floor during the last two tests in Group-II.

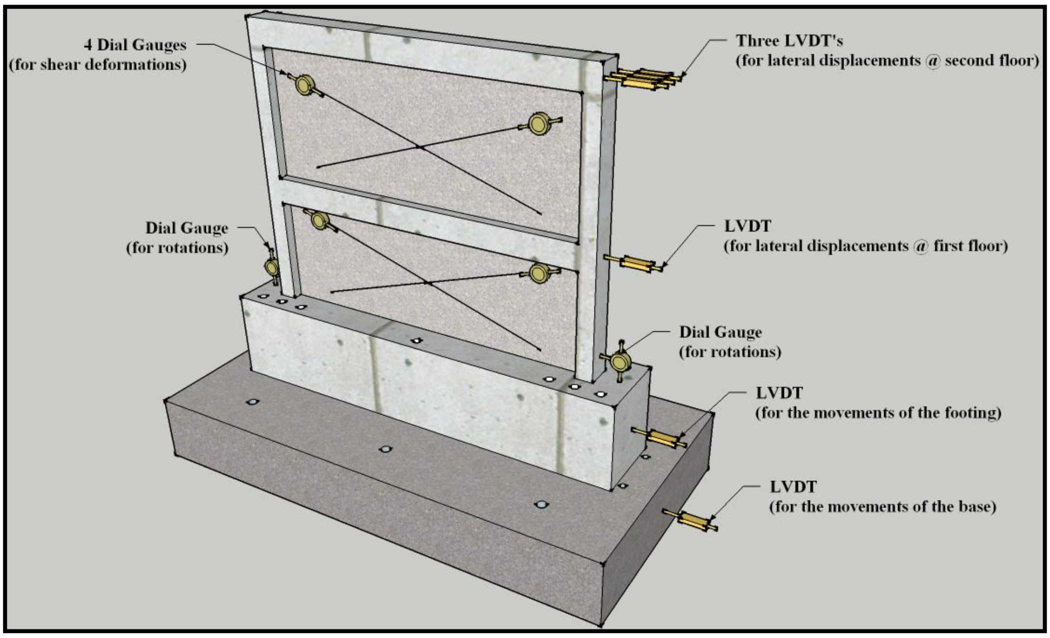

Figure 3. 29 Instrumentation of the frame specimens

Two dial gauges with 50 mm stroke were installed on the front face of each story infill walls in order to measure the shear deformations. The dial gauges were inclined in the diagonal directions and installed 130 mm away from the corners of the infill so as not to be affected by the local damage of the HCT walls at these regions. The dial gauges were attached at the predetermined locations on the HCT walls by the use of epoxy mortar.

The rotations at the column bases were measured by dial gauges located at the bottom exterior faces of the columns. The stroke capacity of these transducers was 20 mm. The possible movements of the universal base and the specimen footing were checked by means of two LVDT's with 100 mm stroke capacity.

Unidirectional strain gauges with a gauge length of 10 mm were also installed on the diagonal CFRP reinforcements of the strengthened frames in order to measure the strains developing on CFRP fibers. In Appendix B, these measurements are presented in the form of hysteretic CFRP strain vs. base shear curves for the most critical location of each frame specimen.

A calibrated load cell was used as mentioned in Section 3.2.6 to record the applied lateral loads. The possible deviations in the axial load level were monitored by the help of a pressure gauge installed on the exit of the hydraulic jack.

In Group-II tests, the PSD test system and two different data acquisition systems were used as indicated in the last section. The load cell which was already situated on the servo-controlled hydraulic actuator was connected to the data acquisition device of the PSD system. Besides, the displacement transducer of this system which was connected to the same device was also used for the measurement of top story displacements. This transducer, namely "Heidenhain" had a 500 mm stroke capacity. All other instruments, same as used in Group-I, were connected to the pre-existing data acquisition system for the collection of data.

3.2.8 Test Procedure

The specimens were whitewashed with limewater before placing on the setup in order to enable the observation of minor crack patterns. The specimens were placed on the test setup, such that the holes used for their anchorage face with the corresponding holes on the universal base. The Dywidag bars were used for fixing the specimens to the universal base through these holes. The axial and lateral loading equipments and the rollers to prevent the out-of-plane displacements were mounted. The instruments were installed and cabled to the data acquisition system. Before the tests, the calibrations of all the instruments were checked. The sample concrete cylinders were tested and the compressive strength of concrete was determined.

The axial load was applied in the first step; corresponding to approximately 10 percent of the nominal axial capacity of columns. During the test, the level of axial load was monitored continuously and kept constant through the use of valves at the gate of hydraulic pump.

All of the frames were tested under reversed cyclic lateral loading. In Group-I, a load-controlled loading scheme was adopted until the peak resistance was reached. The displacement-controlled loading scheme was applied after this point. A displacement-controlled loading was applied throughout the tests of Group-II frames by using the PSD system. The tests were paused for short periods at the end of each half cycle in order to mark the cracks and take pictures of the observed cracks and damages. Also notes were taken about the observed damages indicating location, type and related loading cycle. The tests were terminated after failure of the frames in conjunction with a significant reduction of the ultimate lateral load level.

CHAPTER 4

EXPERIMENTAL RESULTS

4.1 GENERAL

The results of RC frame tests are presented by means of the observed behavior at different phases of loading and related curves showing the response of specimens. The loading histories of the frame specimens are also presented in a tabular form. The failure states of all specimens are shown through the pictures taken during the tests. Besides, the damage pattern of each frame specimen is illustrated by means of the drawings presented in Appendix E.

The frame test results are presented in Sections 4.2 and 4.3, for the specimens in Group-I and -II, respectively. While describing the observed behavior of each frame, the columns are termed as “north” and “south”. In Group-I tests, the column close to the reaction wall was the north column. However, in Group-II, the south column was on the same side with the reaction wall. This is due to the use of new test setup in Group-II, which was constructed in mirror-symmetric position of the previous one. The applied shear vs. inter-story displacement/drift ratio curves are shown for both story levels. The shear deformation response of both first and second story infill walls under the action of applied lateral forces are also presented for the infilled frames. The rotations at the frame bases were calculated by using the data obtained from the dial gauges at the column ends. These rotations were related with the frame base moments and corresponding curves are shown for each frame.

The details for the estimations of infill shear deformations and frame base rotations are explained in Appendices C and D, respectively.

It should be noted that the total lateral load may be affected by the horizontal component of the constant axial load, especially in high drift levels. This alteration of applied lateral load was checked in frame specimens. However, even for specimen NREF1-1/3, which experienced the minimum strength and highest drift, the alteration of the lateral load at the ultimate drift level remained at most ten percent of the ultimate load, that is to say, about 1.0 kN. Therefore, the influence of axial load on the applied lateral load was ignored in the presented response curves.

4.2 GROUP-I: 1/3 SCALED RC FRAMES

4.2.1 Series-N

4.2.1.1 NREF1-1/3

This was a bare frame without infill walls which would provide the results as a reference specimen. The average concrete compressive strength of the specimen was about 13.0 MPa on the day of testing. The constant axial load applied on each column was 30 kN, the same as all other specimens in Group-I. The lateral loading history and test results of specimen NREF1-1/3 are summarized in Table 4.1 in terms of total applied load, first story and roof displacements, and corresponding drift ratios. After the tenth cycle, the first story displacements of this specimen could not be measured, since capacity of the LVDT at this story level was exceeded.

The forward and backward lateral load capacities of the frame were 9.8 and -10.6 kN, respectively. This corresponds to a roof drift ratio of 1.50% in both loading directions. The applied shear force vs. lateral inter-story displacement graphs of the first and second stories are given in Figures 4.1 and 4. 2, respectively. The frame base moment-rotation curve is also presented in Figure 4.3.

Table 4. 1 The load and displacement history of specimen NREF1-1/3

Cycle No.	*Base Shear (kN)*	*Roof Displ. (mm)*	*First Story Displ. (mm)*	*Roof Drift Ratio (%)*	*First Story Drift Ratio (%)*
+1	+4.5	+2.20	+1.17	0.11	0.11
-1	-3.8	-1.10	-1.10	-0.06	-0.10
+2	+7.4	+4.32	+2.68	0.22	0.25
-2	-5.6	-3.27	-2.74	-0.17	-0.25
+3	+9.2	+7.55	+4.83	0.38	0.45
-3	-7.4	-5.90	-4.64	-0.30	-0.43
+4	+9.8	+15.02	+9.81	0.76	0.91
-4	-9.9	-15.53	-10.65	-0.79	-0.99
+5	+9.2	+19.41	+12.60	0.98	1.17
-5	-10.3	-20.05	-14.02	-1.02	-1.30
+6	+9.8	+29.71	+20.31	1.50	1.89
-6	-10.6	-30.42	-22.17	-1.54	-2.06
+7	+9.8	+39.53	+29.10	2.00	2.71
-7	-10.0	-40.19	-30.72	-2.03	-2.86
+8	+9.2	+50.00	+39.60	2.53	3.68
-8	-10.0	-50.71	-40.04	-2.57	-3.72
+9	+8.6	+59.50	+49.07	3.01	4.56
-9	-8.8	-60.60	-49.37	-3.07	-4.59
+10	+7.7	+61.40	-	3.11	-
-10	-7.9	-70.71	-	-3.58	-
+11	+5.6	+61.40	-	3.11	-
-11	-7.1	-80.20	-	-4.06	-
+12	+5.1	+61.40	-	3.11	-
-12	-6.8	-90.60	-	-4.59	-

Initially, hairline flexural cracks formed at the footing interface of the north column at a lateral load of 3.0 kN during the second forward half cycle. In the following half cycle, the symmetric crack was observed at the bottom of the south column. In the next two cycles, the flexural cracks spread over the lap-splice regions of the first story columns. During the fifth cycle, first shear cracks formed at the first story beam-column joints; which further propagated at the joints in the latter cycles.

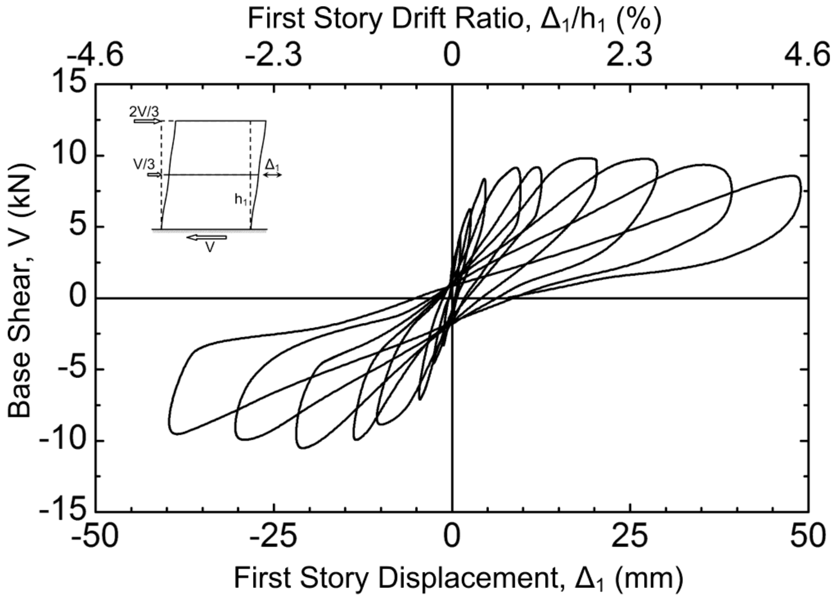

Figure 4. 1 First story shear force vs. displacement / drift ratio curve of specimen NREF1-1/3

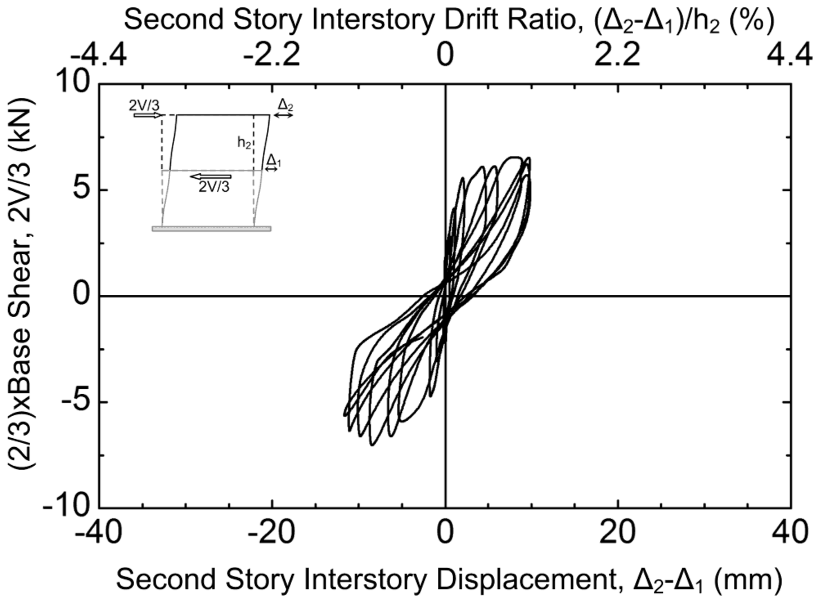

Figure 4. 2 Second story shear force vs. inter-story displacement / drift ratio curve of specimen NREF1-1/3

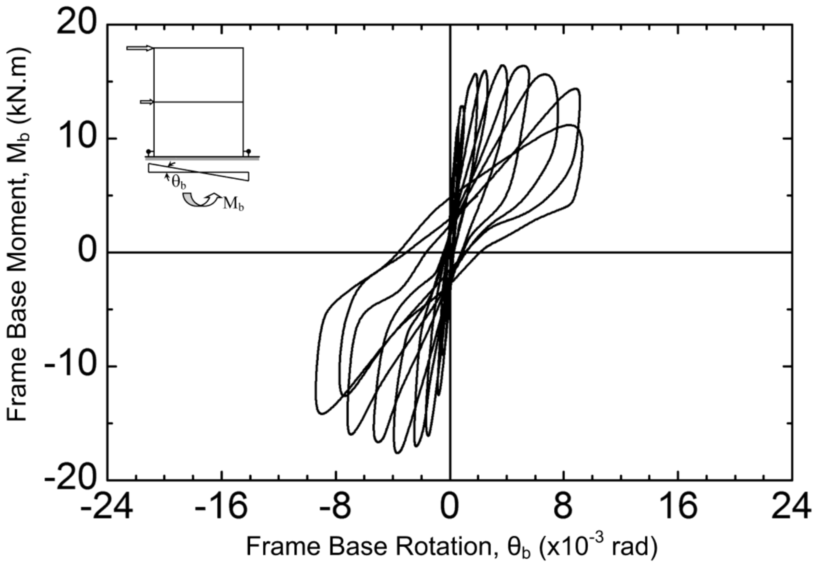

Figure 4. 3 Frame base moment vs. rotation curve of specimen NREF1-1/3

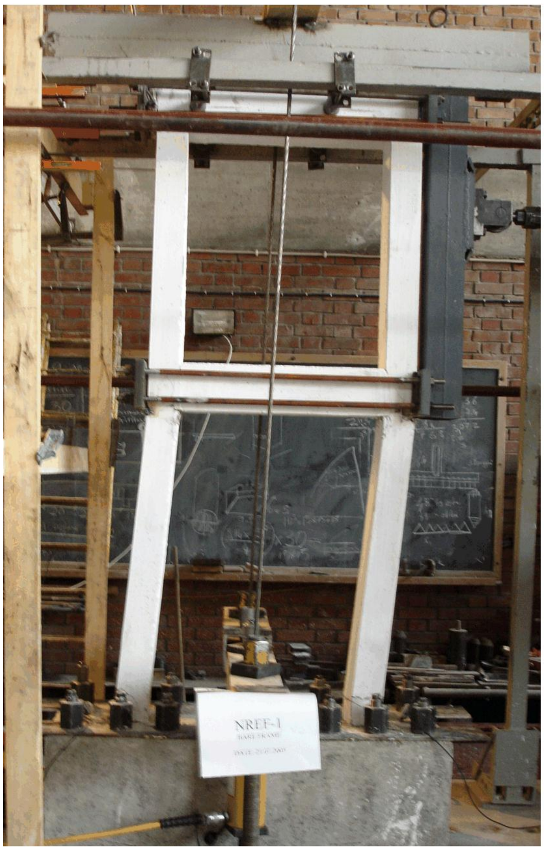

(a) general view after the test

(b) crushing of cover concrete

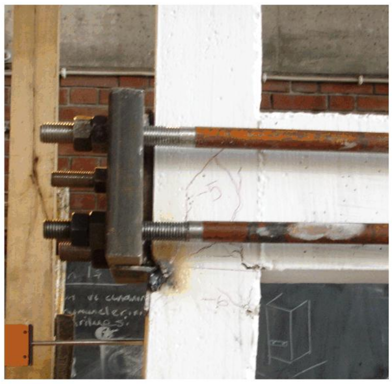

(c) shear cracks at the beam-column joint

Figure 4. 4 Failure pattern of specimen NREF1-1/3

After seventh cycle, local crushing of concrete was observed at the bottom of the first story columns on the compression side. This initiated spalling of the cover concrete towards the end of test. During the eighth cycle, the width of flexural crack on the tension side of the column-footing interface increased suddenly. This sudden increase, which further caused widening of the crack in the next cycles, may be related to the bond-slip of lapped plain bars. Eventually, the bare frame turned into a mechanism due to the formation of plastic hinges at both ends of the first story columns. The general failure pattern of specimen NREF1-1/3 which was described above is shown in Figure 4.4.

4.2.1.2 NREF2-1/3

The second reference specimen in this series was the frame with hollow clay tile infill walls, which was covered with plaster on both faces. The average compressive strength of concrete was around 17.1 MPa on the day of testing. The applied lateral loads and corresponding displacement responses of specimen NREF2-1/3 are given in Table 4.2.

The applied maximum lateral loads were 26.0 and -26.6 kN which were attained in the third forward and backward half cycles, respectively. The roof drift ratio of the frame was around 0.50% at these load levels. The graphs relating applied shear forces with the lateral inter-story displacements of the first and second stories are shown in Figures 4.5 and 4.6, respectively. The shear displacements experienced by the first and second story infill walls were plotted against corresponding shear forces and presented in Figures 4.7 and 4.8, respectively. It is worth noting that an acquisition error occurred during the test lead to shifted shear displacements in Figure 4.7. Lastly, the base moment vs. base rotation response of the frame is shown in Figure 4.9.

The early flexural cracks were observed just above the lap-splice region of the first story columns at a load of 9.4 kN in the second loading cycle. During this cycle, crack formations were also observed between the first story frame-infill intersections.

Table 4. 2 The load and displacement history of specimen NREF2-1/3

Cycle No.	*Base Shear (kN)*	*Roof Displ. (mm)*	*First Story Displ. (mm)*	*Roof Drift Ratio (%)*	*First Story Drift Ratio (%)*
+1	+10.0	+0.79	+0.37	+0.04	+0.03
-1	-10.0	-0.54	-0.34	-0.03	-0.03
+2	+19.2	+2.22	+1.27	+0.11	+0.12
-2	-20.0	-1.90	-1.12	-0.10	-0.10
+3	+26.0	+10.30	+5.76	+0.52	+0.54
-3	-26.6	-9.86	-5.61	-0.50	-0.52
+4	+25.1	+15.34	+8.60	+0.78	+0.80
-4	-24.5	-15.33	-8.50	-0.78	-0.79
+5	+24.8	+20.27	+11.82	+1.03	+1.10
-5	-25.1	-20.58	-10.84	-1.04	-1.01
+6	+25.1	+25.59	+15.19	+1.30	+1.41
-6	-25.7	-25.20	-13.08	-1.28	-1.22
+7	+21.8	+30.23	+21.24	+1.53	+1.98
-7	-26.1	-30.54	-15.92	-1.55	-1.48
+8	+18.0	+35.40	+29.15	+1.79	+2.71
-8	-24.5	-35.40	-19.72	-1.79	-1.83
+9	+14.5	+40.40	+34.52	+2.05	+3.21
-9	-21.3	-40.10	-26.70	-2.03	-2.48
+10	+14.8	+45.14	+39.11	+2.29	+3.64
-10	-18.0	-45.24	-34.86	-2.29	-3.24
+11	+15.7	+50.17	+43.46	+2.54	+4.04
-11	-14.8	-50.37	-40.43	-2.55	-3.76
+12	+19.2	+59.55	-	+3.02	-
-12	-15.1	-60.57	-	-3.07	-

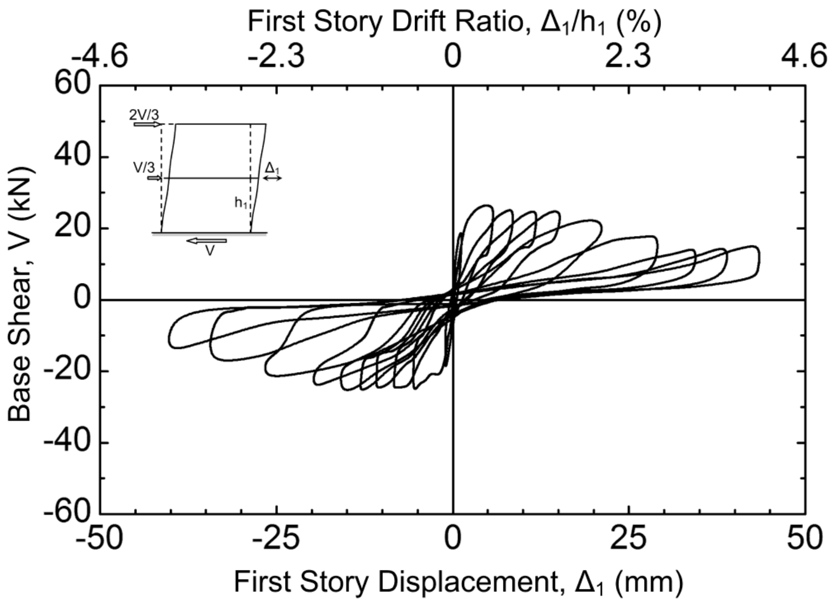

Figure 4. 5 First story shear force vs. displacement / drift ratio curve of specimen NREF2-1/3

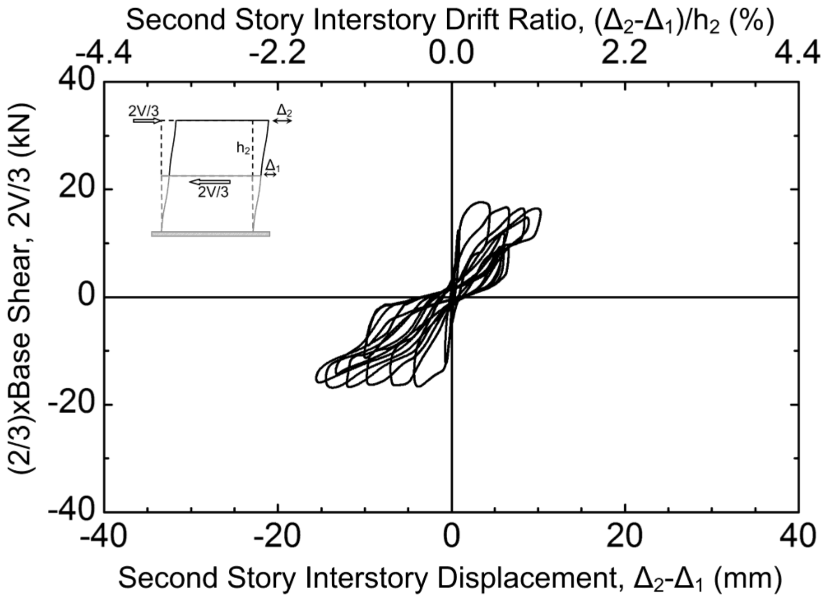

Figure 4. 6 Second story shear force vs. inter-story displacement / drift ratio curve of specimen NREF2-1/3

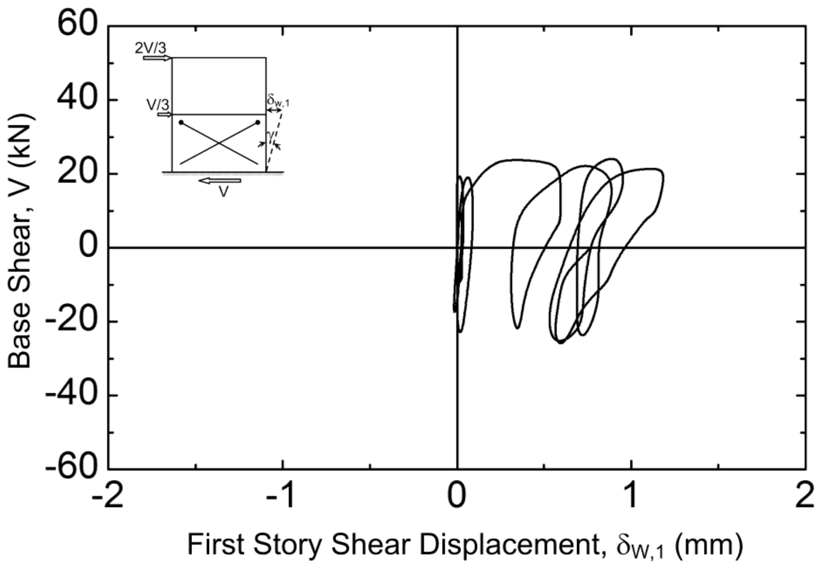

Figure 4. 7 Shear force vs. shear displacement curve for the first story infill of specimen NREF2-1/3

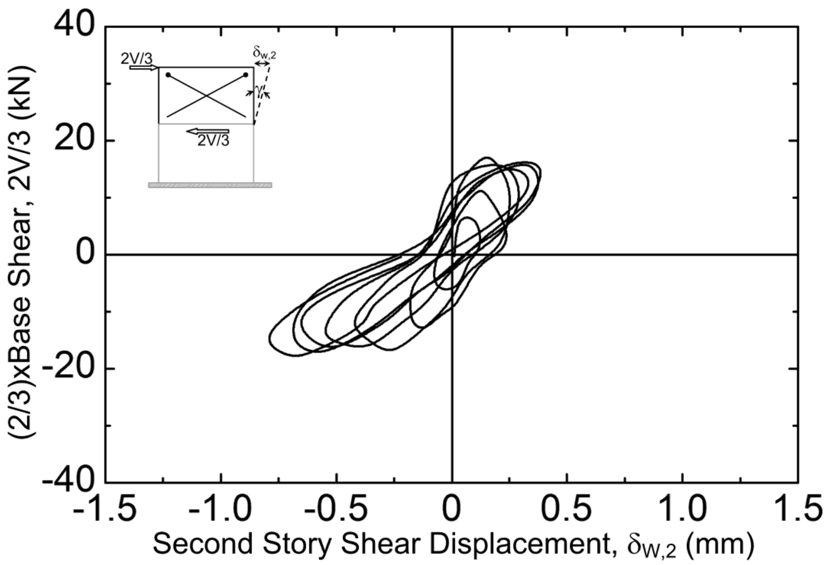

Figure 4. 8 Shear force vs. shear displacement curve for the second story infill of specimen NREF2-1/3

After the frame reached its ultimate lateral load capacity in the third cycle, the lateral stiffness started to decrease rapidly as can be seen in Figures 4.5 and 4.6.

New flexural cracks were observed along the first story columns up to the fourth cycle, when separation between the first story infill and frame foundation initiated.

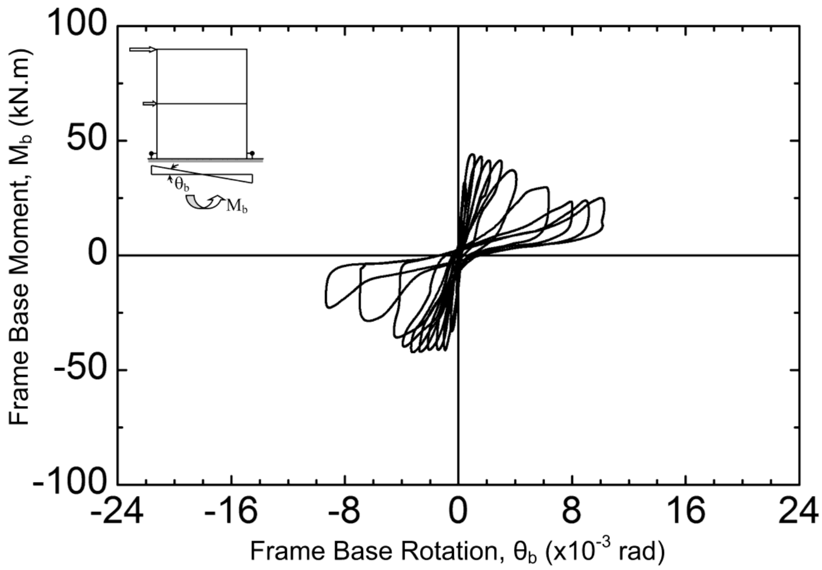

Figure 4. 9 Frame base moment vs. rotation curve of specimen NREF2-1/3

During the positive fifth cycle, the plaster at the corners of the first story infill at the top right corner of the first story wall fell down and the HCT wall started crushing hereafter. At the same cycle, the flexural cracks over the lap-splice region widened considerably, so as to make the longitudinal column bars visible. This was further followed by spalling off of the cover concrete of the columns at the same regions during the sixth cycle. The flexural damage at the lap-splice regions, together with the bond-slip deformations of the lapped bars, may be the reason of sudden rotation increments observed in Figure 4.9 after the sixth cycle. First shear cracks at the beam-column joints and flexural cracks on the first story beam formed during the seventh cycle. After significant separation of the infill walls from the neighboring frame members took place, the system response approached the bare frame response. The local damages and final view of the specimen are shown in Figure 4.10.

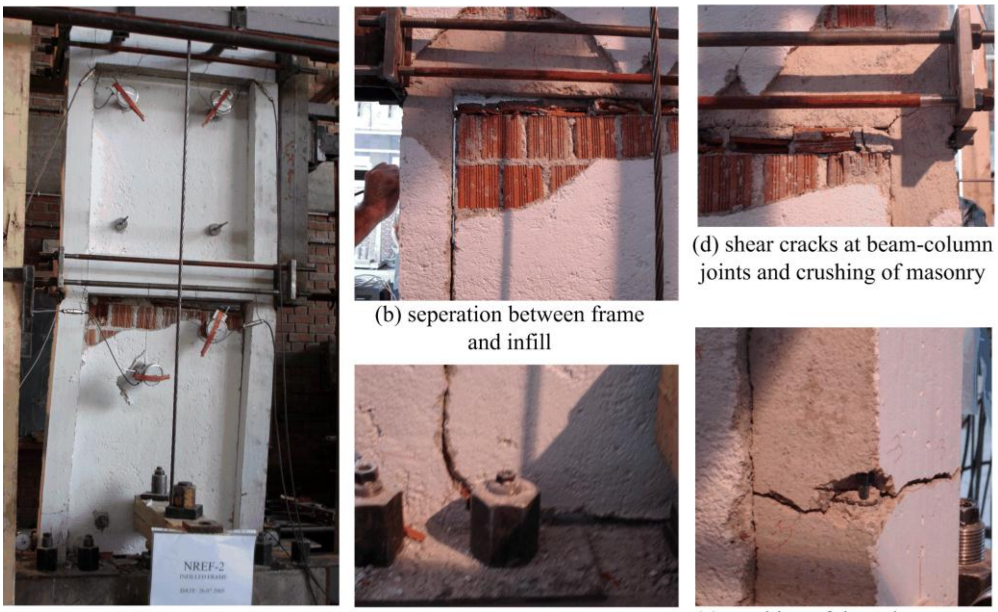

(a) general view after the test

(b) seperation between frame and infill

(c) seperation between footing and infill

(d) shear cracks at beam-column joints and crushing of masonry

(e) crushing of the column cover concrete

Figure 4. 10 Failure pattern of specimen NREF2-1/3

4.2.1.3 NSTR-L-1/3

NSTR-L-1/3 was the last specimen in this series which had lapped column bars at both story levels. The frame was strengthened using the methodology explained in Section 3.2.5. The average concrete compressive strength of the specimen was 19.4 MPa. The applied loading and corresponding response values are presented in Table 4.3.

In the forward and backward directions, the maximum lateral load capacities of the frame were 36.2 and -35.8 kN, respectively. These load levels were attained during the fourth cycle at a roof drift ratio of around 0.45%.

The relationship of the applied shear vs. inter-story displacements of the first and second stories is shown in Figures 4.11 and 4.12, respectively. The shear displacement response of the first and second story infill walls are presented in Figures 4.13 and 4.14, respectively. Moreover, the frame base moment and corresponding base rotation relationship is given in Figure 4.15.

Table 4. 3 The load and displacement history of specimen NSTR-L-1/3

Cycle No.	*Base Shear (kN)*	*Roof Displ. (mm)*	*First Story Displ. (mm)*	*Roof Drift Ratio (%)*	*First Story Drift Ratio (%)*
+1	+10.0	+0.29	+0.07	+0.01	+0.01
-1	-10.1	-0.39	-0.11	-0.02	-0.01
+2	+20.2	+0.76	+0.19	+0.04	+0.02
-2	-20.0	-0.93	-0.27	-0.05	-0.03
+3	+29.8	+2.04	+0.62	+0.10	+0.06
-3	-29.7	-2.10	-0.67	-0.11	-0.06
+4	+36.2	+8.34	+2.98	+0.42	+0.28
-4	-35.8	-9.20	-3.27	-0.47	-0.30
+5	+27.8	+10.30	+3.69	+0.52	+0.34
-5	-29.8	-10.61	-3.70	-0.54	-0.34
+6	+25.8	+15.40	+5.52	+0.78	+0.51
-6	-28.8	-15.90	-5.73	-0.81	-0.53
+7	+23.5	+20.70	+7.16	+1.05	+0.67
-7	-26.6	-21.60	-7.86	-1.09	-0.73
+8	+23.3	+25.80	+9.82	+1.31	+0.91
-8	-25.9	-25.54	-9.40	-1.29	-0.87
+9	+23.3	+30.00	+11.50	+1.52	+1.07
-9	-25.0	-30.30	-11.20	-1.53	-1.04
+10	+23.4	+35.40	+13.80	+1.79	+1.28
-10	-24.3	-35.55	-13.70	-1.80	-1.27
+11	+22.6	+40.56	+15.60	+2.05	+1.45
-11	-24.5	-40.93	-16.10	-2.07	-1.50
+12	+22.4	+45.60	+18.15	+2.31	+1.69
-12	-23.8	-45.62	-17.20	-2.31	-1.60
+13	+22.0	+51.66	+20.10	+2.62	+1.87
-13	-24.4	-51.72	-19.23	-2.62	-1.79
+14	+22.8	+55.70	+21.92	+2.82	+2.04
-14	-24.9	-56.70	-21.90	-2.87	-2.04

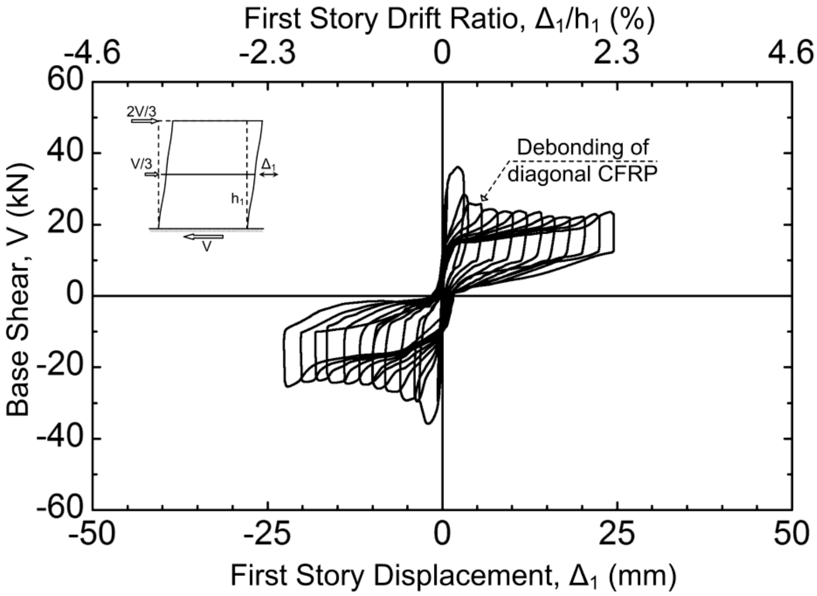

Figure 4. 11 First story shear force vs. displacement / drift ratio curve of specimen NSTR-L-1/3

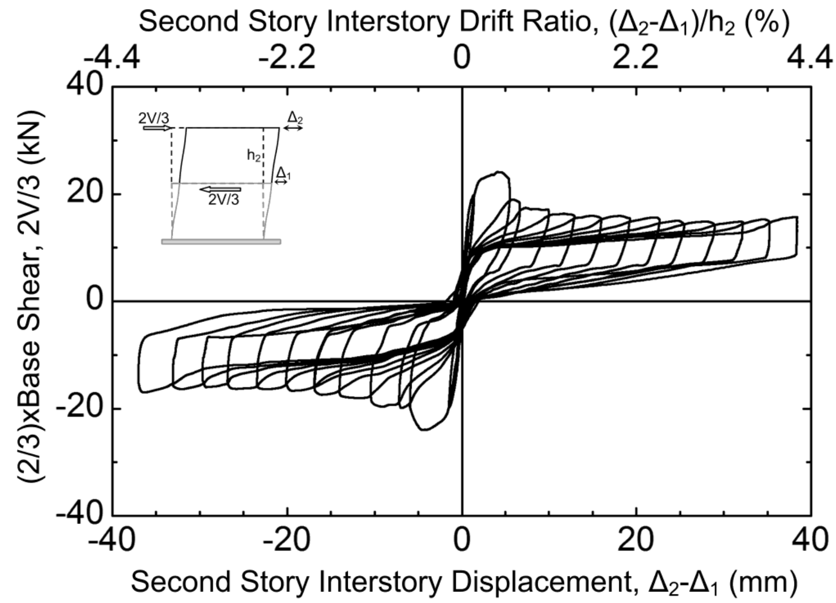

Figure 4. 12 Second story shear force vs. inter-story displacement / drift ratio curve of specimen NSTR-L-1/3

The first flexural cracks were detected at about 200 mm above the lateral CFRP reinforcement of the first story columns when the lateral load was 23.0 kN during the third cycle. Further flexural cracks were observed on the first story columns in the fourth cycle when the specimen reached its ultimate lateral load capacity at 36 kN. The separation between the frame and footing on the tension side initiated during the same cycle. Furthermore, some diagonal shear cracks formed over the plaster at both faces of the first story infill. Also, some popping noises were heard from the CFRP reinforcement. As it can be seen in Figures 4.11 and 4.12, there was a sudden decrease in the lateral load capacity after the fourth cycle which may be related to the heavy damage experienced at this level of loading. New flexural crack formations at different heights of the first story columns were observed in the following two cycles. Also the lateral CFRP reinforcements on the first story columns debonded in patches.

Beyond a drift level of 1 percent, the damage totally concentrated at the infill wall-footing and column-footing interfaces, i.e. widening of cracks at the bottom of the frame due to flexural actions. This can also be noticed in Figure 4.15 with the high level of base rotations. The width of crack at the column-footing interface was around 8~10 mm during the eighth cycle which further increased in the following cycles. The test was terminated when the crack width reached 30 mm at the column-footing interface due to rocking. At this stage the lateral roof drift ratio was almost 3%. The damage pattern, together with a final view of the specimen is shown in Figure 4.16.

It should be noted that, despite some small cracks observed on the first story infill during the early phases of loading, the strengthened infill walls remained almost intact during the test. This may also be associated with the behavior observed in Figures 4.13 and 4.14. The ultimate shear deformation in Figure 4.13 happened to be in the fourth cycle when the only diagonal cracks were observed on the first story infill.

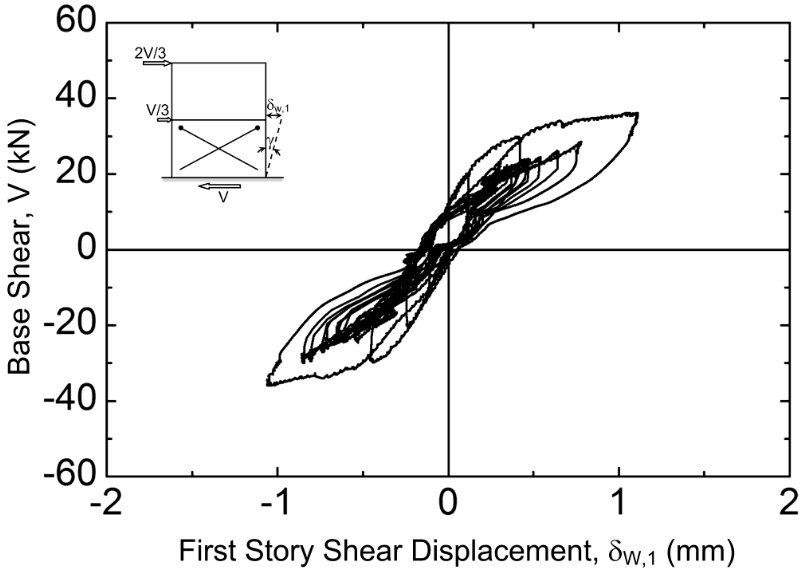

Figure 4. 13 Shear force vs. shear displacement curve for the first story infill of specimen NSTR-L-1/3

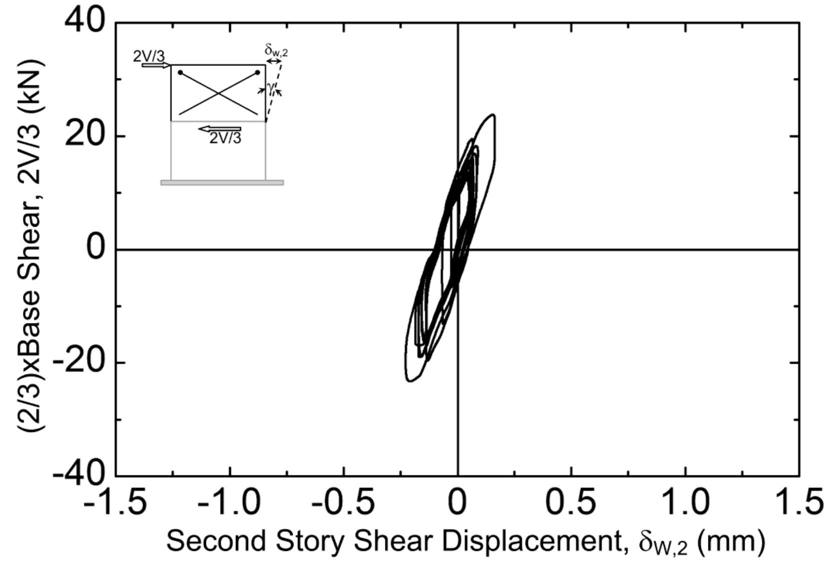

Figure 4. 14 Shear force vs. shear displacement curve for the second story infill of specimen NSTR-L-1/3

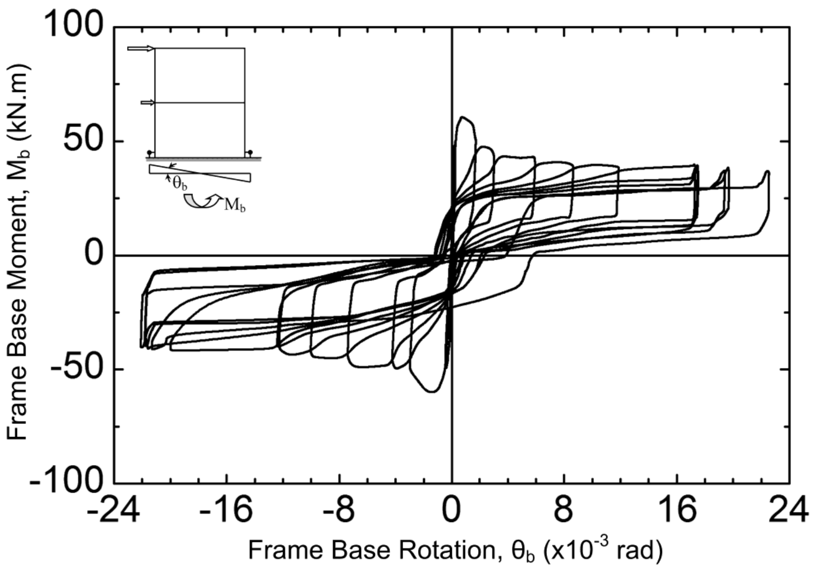

Figure 4. 15 Frame base moment vs. rotation curve of specimen NSTR-L-1/3

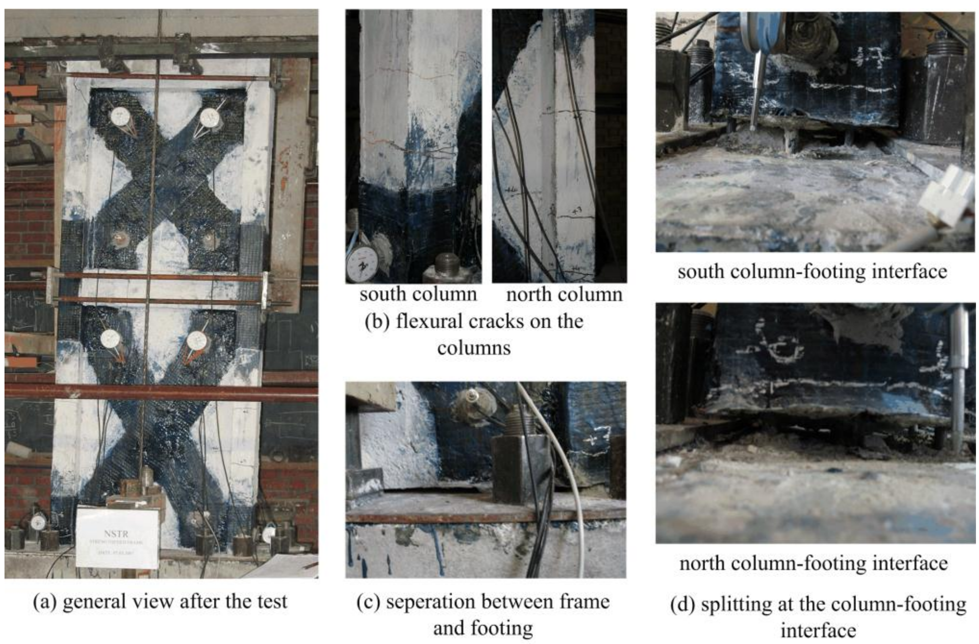

Figure 4. 16 Failure pattern of specimen NSTR-L-1/3

4.2.1.4 NSTR-W-1/3

A premature failure was observed in testing of the first strengthened specimen of this series, which had lap-spliced column longitudinal bars formerly. Due to the bond-slip of the lapped column longitudinal bars at the footing level during the early phases of loading, it was not possible to increase the load when the specimen started to rock on its base. As there was no considerable damage, the test was stopped at this stage and the specimen was rehabilitated by removing the cover concrete and welding the lapped longitudinal reinforcements at the exterior corners of both columns. This region was then filled up with repair mortar and wrapped by one-layer CFRP, over a height of 200 mm. This specimen was renamed as NSTR-W-1/3 and tested following the load and displacement history given in Table 4.4.

The forward and backward lateral load capacities of the frame were 51.2 and -51.6 kN, respectively. The roof drift ratio corresponding to the maximum lateral load was around 0.80%.

The applied shear force vs. inter-story displacement hysteresis curves of the first and second stories are shown in Figures 4.17 and 4.18, respectively. The shear force vs. shear displacement relationships of the first and second story infill walls are presented in Figures 4.19 and 4.20, respectively. The frame base moment vs. base rotation curve is given in Figure 4.21.

During the test of specimen NSTR-W-1/3, the first visible cracks were the diagonal crack on the first story infill wall and flexural crack just above the confined lap-splice region of columns. These cracks formed simultaneously during the fourth cycle. In the next cycle, previously formed flexural cracks propagated and additional cracks, which were close to the confined region, formed on the columns. Although new diagonal cracks were observed on the first story infill during the sixth cycle, these cracks did not widen afterwards. In both forward and backward seventh cycle, new cracks developed on the tension side of the frame-footing interface. These cracks on both sides of the frame propagated and widened in the next cycle. After the ninth cycle, the diagonal CFRP sheets at the lower corners of the first story infill started to debond under compression. During the tenth cycle, the flexural cracks just above the confined lap-splice region widened considerably on the tension side and the column concrete on the symmetric side crushed under compression. After the eleventh cycle, the separation at the frame-footing interface increased significantly under tension.

Table 4. 4 The load and displacement history of specimen NSTR-W-1/3

Cycle No.	*Base Shear (kN)*	*Roof Displ. (mm)*	*First Story Displ. (mm)*	*Roof Drift Ratio (%)*	*First Story Drift Ratio (%)*
+1	+10.5	+0.30	+0.05	+0.02	0.00
-1	-10.0	-0.27	-0.05	-0.01	0.00
+2	+19.5	+0.61	+0.20	+0.03	+0.02
-2	-19.7	-0.76	-0.24	-0.04	-0.02
+3	+29.0	+1.71	+0.60	+0.09	+0.06
-3	-30.1	-1.08	-0.34	-0.05	-0.03
+4	+39.9	+2.88	+1.22	+0.15	+0.11
-4	-39.8	-2.00	-0.58	-0.10	-0.05
+5	+48.5	+7.82	+3.76	+0.40	+0.35
-5	-50.2	-8.60	-3.61	-0.44	-0.34
+6	+50.3	+10.28	+4.93	+0.52	+0.46
-6	-50.5	-10.04	-4.34	-0.51	-0.40
+7	+51.2	+15.73	+7.23	+0.80	+0.67
-7	-51.6	-14.89	-6.25	-0.75	-0.58
+8	+51.2	+20.29	+10.11	+1.03	+0.94
-8	-49.5	-20.21	-8.88	-1.02	-0.83
+9	+50.3	+25.27	+12.21	+1.28	+1.14
-9	-50.5	-24.42	-10.89	-1.24	-1.01
+10	+49.4	+30.11	+13.82	+1.52	+1.29
-10	-52.5	-29.40	-13.13	-1.49	-1.22
+11	+50.0	+35.11	+16.70	+1.78	+1.55
-11	-51.6	-34.70	-16.01	-1.76	-1.49
+12	+50.0	+40.02	+19.48	+2.03	+1.81
-12	-52.2	-40.26	-18.65	-2.04	-1.73
+13	+48.8	+45.00	+21.83	+2.28	+2.03
-13	-51.3	-44.83	-20.85	-2.27	-1.94
+14	+48.2	+50.54	+24.17	+2.56	+2.25
-14	-51.1	-50.51	-23.34	-2.56	-2.17
+15	+48.5	+54.91	+26.08	+2.78	+2.43
-15	-46.6	-55.32	-26.12	-2.80	-2.43
+16	+49.1	+60.35	+28.22	+3.06	+2.63
-16	-19.4	-61.21	-27.83	-3.10	-2.59

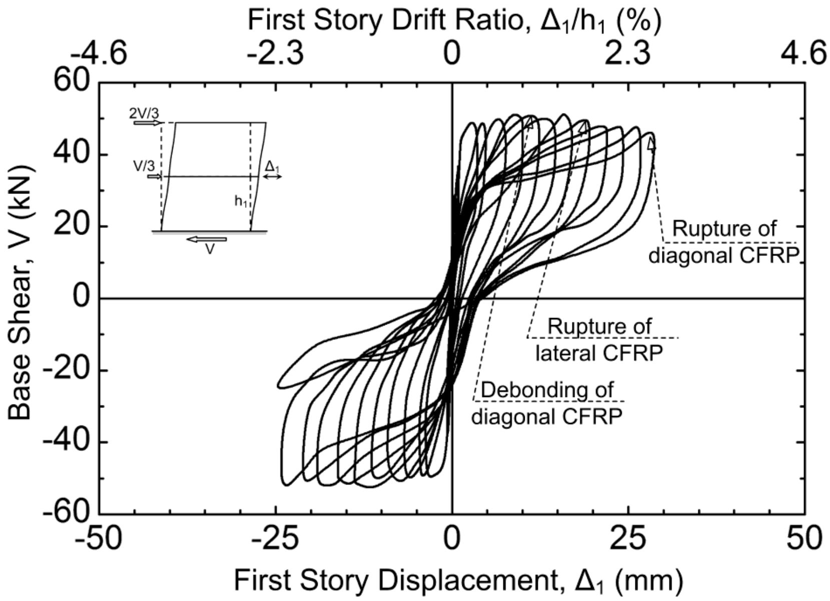

Figure 4. 17 First story shear force vs. displacement / drift ratio curve of specimen NSTR-W-1/3

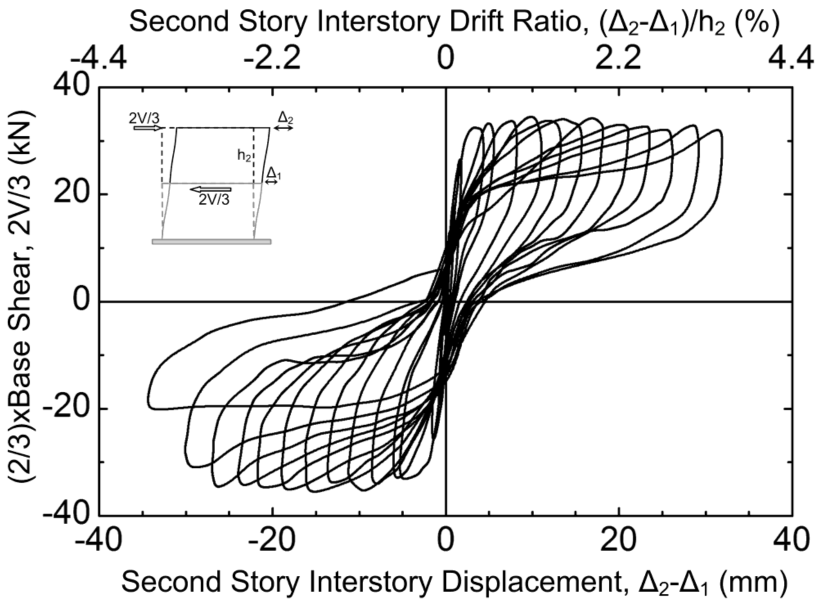

Figure 4. 18 Second story shear force vs. inter-story displacement / drift ratio curve of specimen NSTR-W-1/3

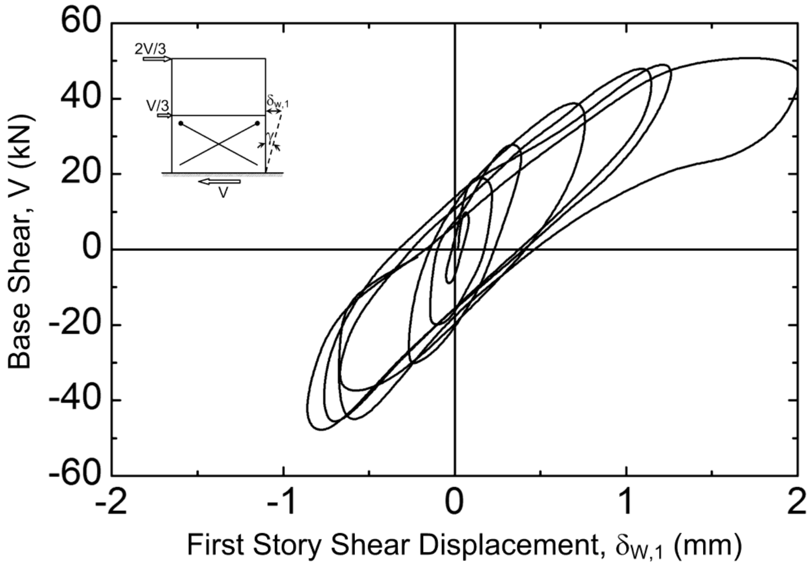

Figure 4. 19 Shear force vs. shear displacement curve for the first story infill of specimen NSTR-W-1/3

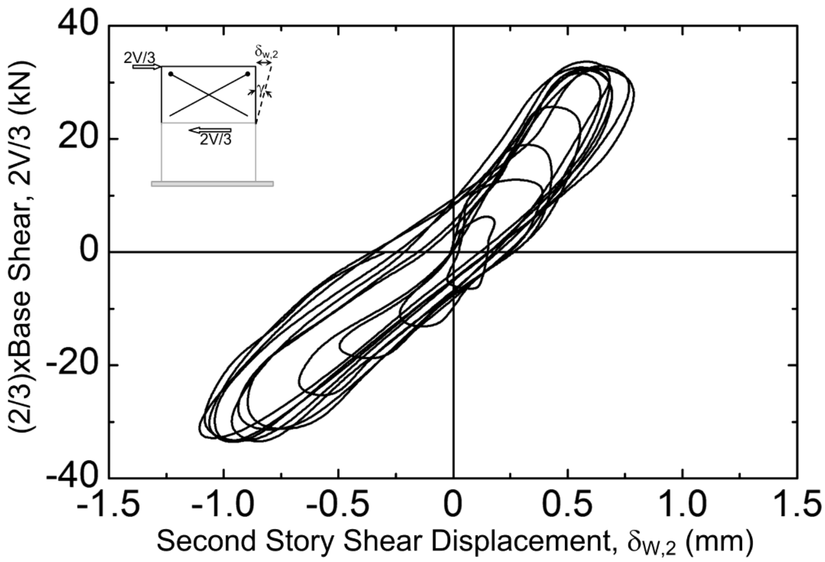

Figure 4. 20 Shear force vs. shear displacement curve for the second story infill of specimen NSTR-W-1/3

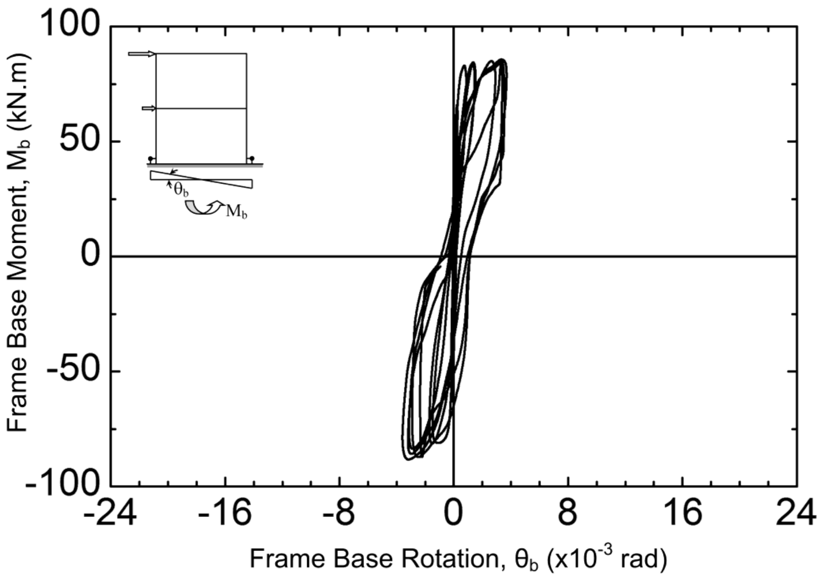

Figure 4. 21 Frame base moment vs. rotation curve of specimen NSTR-W-1/3

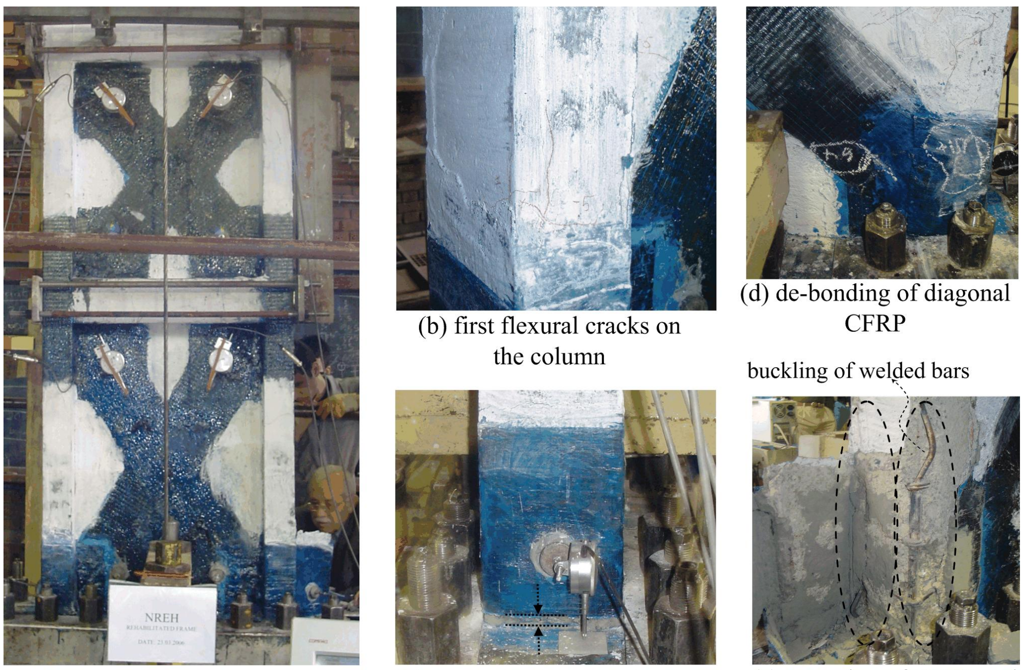

(a) general view after the test

(b) first flexural cracks on the column

(c) seperation between footing and infill

(d) de-bonding of diagonal CFRP

(e) rupturing of CFRP and crushing of cover concrete

Figure 4. 22 Failure pattern of specimen NSTR-W-1/3

During the twelfth cycle, the CFRP sheet used for column confinement started to rupture. The same damage pattern was also observed on the symmetric column, but with less severity. After overall rupture of this CFRP laminate, the underlying cover concrete crushed and the welded longitudinal reinforcements buckled in this region in the following cycles. In the last cycle, diagonal CFRP sheet at the lower corner of the first story HCT infill wall, which was formerly debonded, ruptured under tension. The sudden decrease in the lateral load capacity in this cycle determined the end of test. The failure pattern of this specimen is shown in Figure 4.22.

4.2.2 Series-L

4.2.2.1 LREF1-1/3

LREF1-1/3 was a bare frame which was regarded as the first reference specimen in Series-L. The average compressive strength of concrete used for casting of the frame was around 16.1 MPa. The loading scheme applied on the specimen, which was load-controlled in the first five cycles and displacement based in the rest of the test, was given in Table 4.5. Due to exceeding capacity of the LVDT, the first story lateral displacements could not be measured in the last two cycles.

The maximum lateral loads that could be applied in the forward and backward directions were 12.5 and -12.4 kN, respectively. The roof drift ratio was approximately 2.00 % at the ultimate lateral load level. The applied shear force vs. lateral inter-story displacement response curves of the first and second stories are presented in Figures 4.23 and 4.24, respectively. The frame base moment vs. base rotation curve is shown in Figure 4.25.

The first visible cracks were observed in the form of flexural cracks at the lap-splice region of the first story columns and shear cracks at first story beam-column joints during the second cycle. These cracks on the south and north columns which developed in the forward and backward cycles, respectively, were symmetric. At this point, it should be noted that this crack symmetry was valid for almost all observed damage throughout the test. Additional flexural cracks at the bottom of the first story columns and shear cracks at first story beam-column joints formed during the next three cycles. Also a shear crack was observed at the second story beam-column joint during the third cycle.

Table 4. 5 The load and displacement history of specimen LREF1-1/3

Cycle No.	*Base Shear (kN)*	*Roof Displ. (mm)*	*First Story Displ. (mm)*	*Roof Drift Ratio (%)*	*First Story Drift Ratio (%)*
+1	+5.7	+4.60	+2.10	+0.27	+0.25
-1	-6.2	-5.10	-2.60	-0.30	-0.32
+2	+7.7	+7.80	+3.80	+0.45	+0.46
-2	-7.6	-8.40	-4.20	-0.49	-0.51
+3	+9.5	+12.60	+6.25	+0.73	+0.76
-3	-9.7	-15.00	-7.43	-0.87	-0.90
+4	+10.7	+19.50	+10.15	+1.13	+1.23
-4	-10.9	-21.20	-10.75	-1.23	-1.30
+5	+12.5	+38.20	+17.60	+2.21	+2.13
-5	-12.4	-40.20	-22.50	-2.33	-2.73
+6	+12.2	+45.10	+25.78	+2.61	+3.12
-6	-12.0	-44.50	-22.95	-2.58	-2.78
+7	+11.9	+50.20	+30.00	+2.91	+3.64
-7	-11.2	-50.00	-32.00	-2.90	-3.88
+8	+11.9	+55.40	+38.60	+3.21	+4.68
-8	-10.9	-55.40	-36.14	-3.21	-4.38
+9	+11.6	+59.10	+43.10	+3.43	+5.22
-9	-10.3	-60.50	-42.40	-3.51	-5.14
+10	+11.0	+69.60	-	+4.03	-
-10	-9.1	-70.40	-	-4.08	-
+11	+8.9	+74.10	-	+4.30	-
-11	-7.3	-80.50	-	-4.67	-

After the sixth cycle, cover concrete crushed at the bottom of the first story columns on the compression side. New shear cracks were observed at the first story beam-column joint during the seventh cycle. The existing cracks propagated and widened in the next loading cycles. At a roof drift ratio of about 4.5 percent, failure was observed with crushing of the cover concrete in columns just above the footing level and wide shear cracks at beam-column joints. The applied base shear was approximately 65 percent of the ultimate lateral load capacity at this level. The damage state of the frame at the end of the test is shown in Figure 4.26.

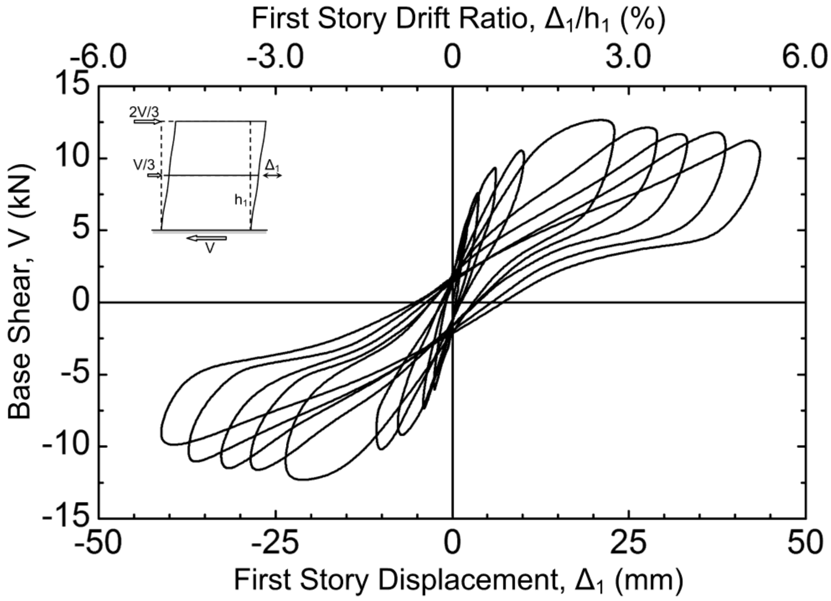

Figure 4. 23 First story shear force vs. displacement / drift ratio curve of specimen LREF1-1/3

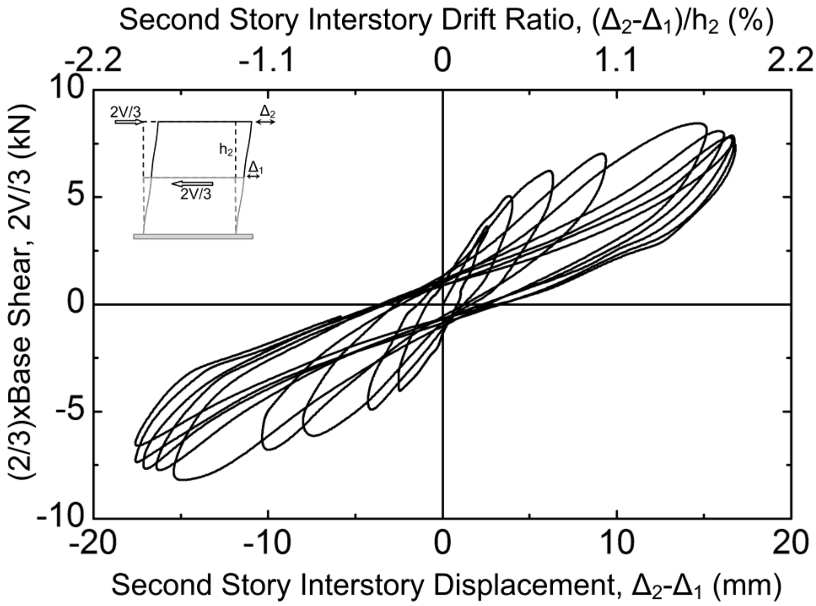

Figure 4. 24 Second story shear force vs. inter-story displacement / drift ratio curve of specimen LREF1-1/3

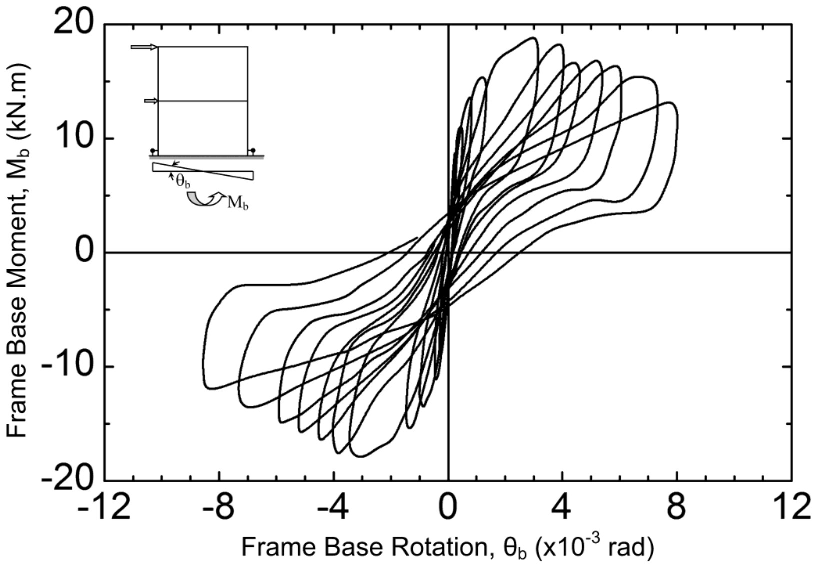

Figure 4. 25 Frame base moment vs. rotation curve of specimen LREF1-1/3

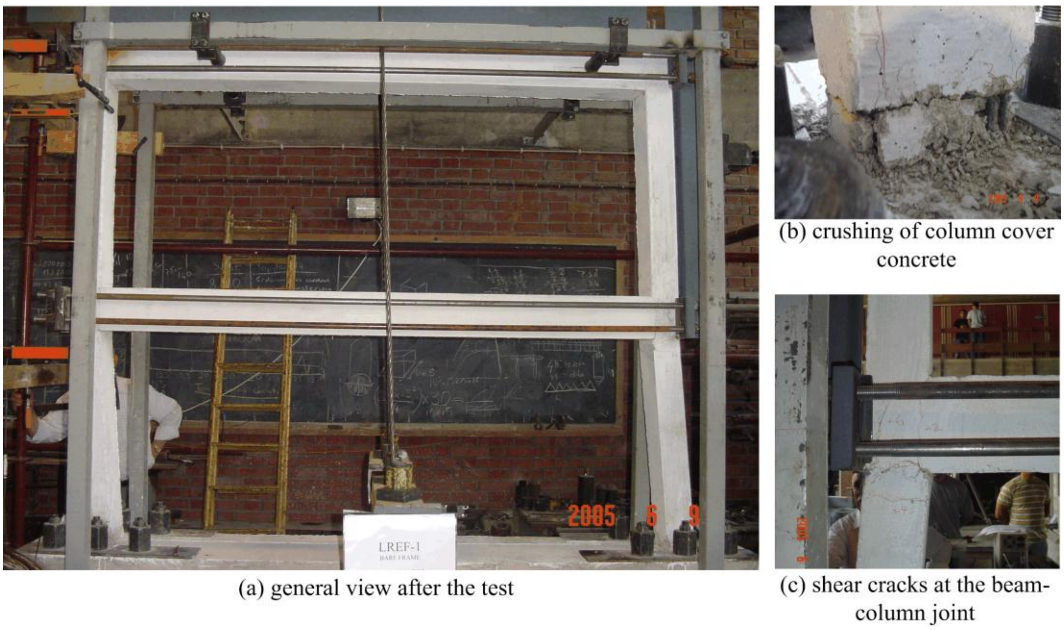

(a) general view after the test

(b) crushing of column cover concrete

(c) shear cracks at the beam-column joint

Figure 4. 26 Failure pattern of specimen LREF1-1/3

4.2.2.2 LREF2-1/3

The second reference specimen of this series was the non-strengthened HTC infill frame, LREF2-1/3. The average concrete compressive strength of the specimen was

16.3 MPa. The applied load and displacement history of the specimen throughout the test was as given in Table 4.6.

The lateral load capacity of the frame was almost 70.0 kN in both loading directions. This lateral load level was reached during the sixth cycle when the roof drift ratios were 0.13% and -0.24%, in the forward and backward directions.

The base shear vs. roof and first story displacement hysteresis curves of LREF2-1/3 are presented in Figures 4.27 and 4.28, respectively. The base shear and infill wall shear displacement relationships are given in Figures 4.29 and 4.30 for the first and second stories, respectively. The base moment vs. base rotation response curve of the frame is shown in Figure 4.31.

During the third cycle, initial cracks were observed at the first story frame-wall intersections at a lateral load level of 29.2 kN. These cracks were on the opposite sides of the zones, where the RC frame was bearing against the HCT infill wall. This indicates a separation between the frame and infill due to a diagonal compression strut formation on the opposite side. These cracks propagated along the frame-infill boundary in the following cycles; decreasing the contact length between the two and increasing the stresses on the HTC infill. The result of this was the formation of diagonal cracks on the HCT walls after the sixth cycle. In the same cycle, the first flexural cracks were observed at the base of the first story columns.

During the seventh cycle, the widths of the cracks at the frame-infill interface and diagonal cracks on the HCT wall increased significantly. Following this, new flexural cracks were observed at different heights of the first story columns. Furthermore, a shear crack formed at the beam-column joint during the forward cycle.

After the eighth cycle, the plaster at the back face started to separate from the infill and spall off at regions where diagonal cracks accumulated. During the ninth cycle, the first story infill started to crush at the top corners under high compressive stresses transferred from the frame. The plaster also spalled off at these regions, rendering the underneath HCT's visible. Additional shear cracks formed at the first story beam-column joints in this cycle.

Table 4. 6 The load and displacement history of specimen LREF2-1/3

Cycle No.	*Base Shear (kN)*	*Roof Displ. (mm)*	*First Story Displ. (mm)*	*Roof Drift Ratio (%)*	*First Story Drift Ratio (%)*
+1	20.7	0.19	0.00	0.01	0.00
-1	-21.2	-0.03	0.00	0.00	0.00
+2	29.3	0.24	0.00	0.01	0.00
-2	-29.2	-0.10	0.00	-0.01	0.00
+3	39.9	0.46	0.25	0.03	0.03
-3	-40.1	-0.35	-0.48	-0.02	-0.06
+4	50.3	0.95	0.64	0.06	0.08
-4	-49.0	-0.93	-0.97	-0.05	-0.12
+5	59.1	1.40	1.13	0.08	0.14
-5	-58.4	-1.62	-1.31	-0.09	-0.16
+6	69.8	2.17	1.62	0.13	0.20
-6	-69.7	-4.15	-2.29	-0.24	-0.28
+7	69.5	5.90	2.89	0.34	0.35
-7	-58.4	-11.10	-4.63	-0.64	-0.56
+8	50.6	14.97	8.79	0.87	1.07
-8	-52.0	-14.34	-5.71	-0.83	-0.69
+9	35.8	20.63	14.60	1.20	1.77
-9	-36.3	-20.78	-7.56	-1.20	-0.92
+10	26.3	25.75	20.41	1.49	2.47
-10	-28.3	-25.10	-11.37	-1.46	-1.38
+11	21.6	30.35	25.98	1.76	3.15
-11	-23.3	-30.62	-15.47	-1.78	-1.88
+12	19.8	35.23	30.96	2.04	3.75
-12	-19.7	-35.45	-19.77	-2.06	-2.40

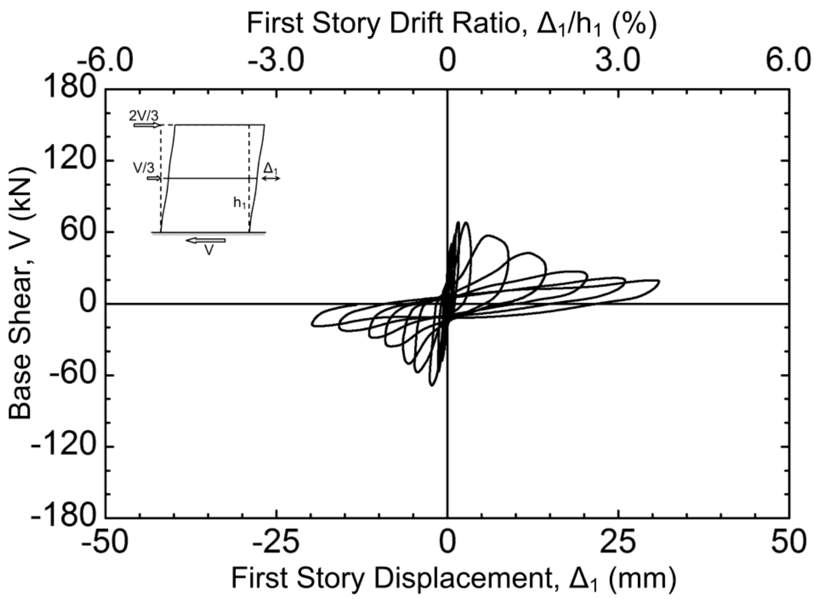

Figure 4. 27 First story shear force vs. displacement / drift ratio curve of specimen LREF2-1/3

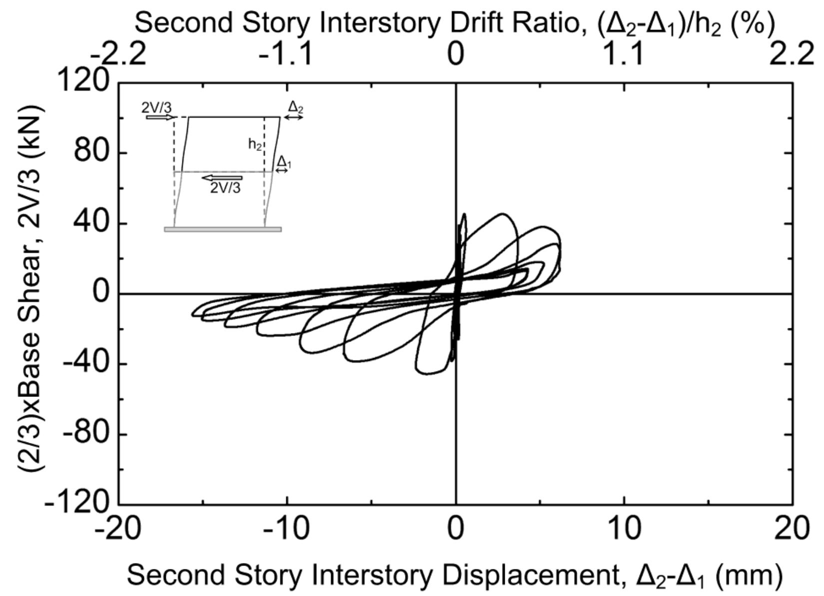

Figure 4. 28 Second story shear force vs. inter-story displacement / drift ratio curve of specimen LREF2-1/3

In the next cycle, the HCT's at the top corners of the infill wall crushed in compression. Since the ratio of shear carried by the infill decreased considerably, shear cracks developed on the first story columns between the mid-height and top of the column at this cycle. Besides, crushing of the upper corners of HCT infill lead to a short column effect at these regions. After total crushing of the first story infill walls at the top corners, the damage concentrated fully at the beam-column joints as wide shear cracks.

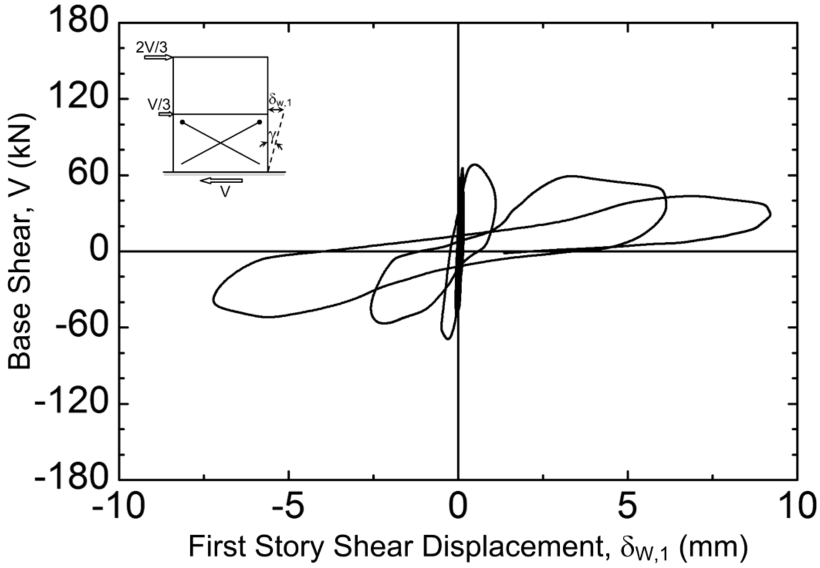

Figure 4. 29 Shear force vs. shear displacement curve for the first story infill of specimen LREF2-1/3

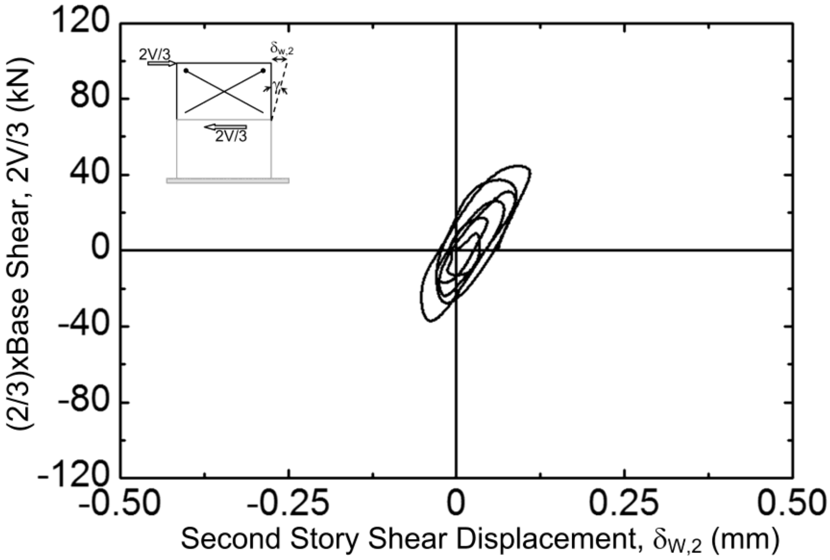

Figure 4. 30 Shear force vs. shear displacement curve for the second story infill of specimen LREF2-1/3

During the last cycle, the cover concrete at the inner corners of the beam-column joints crushed in compression which exposed the longitudinal reinforcement. At this stage, the response of specimen had already deteriorated noticeably, and approached the response displayed by the bare frame. The damage pattern and the view of LREF2-1/3 after the test are shown in Figure 4.32.

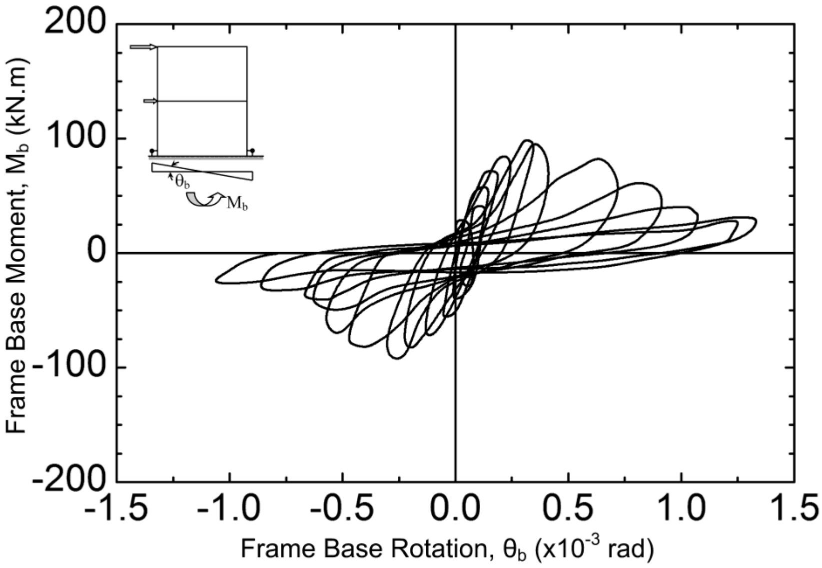

Figure 4. 31 Frame base moment vs. rotation curve of specimen LREF2-1/3

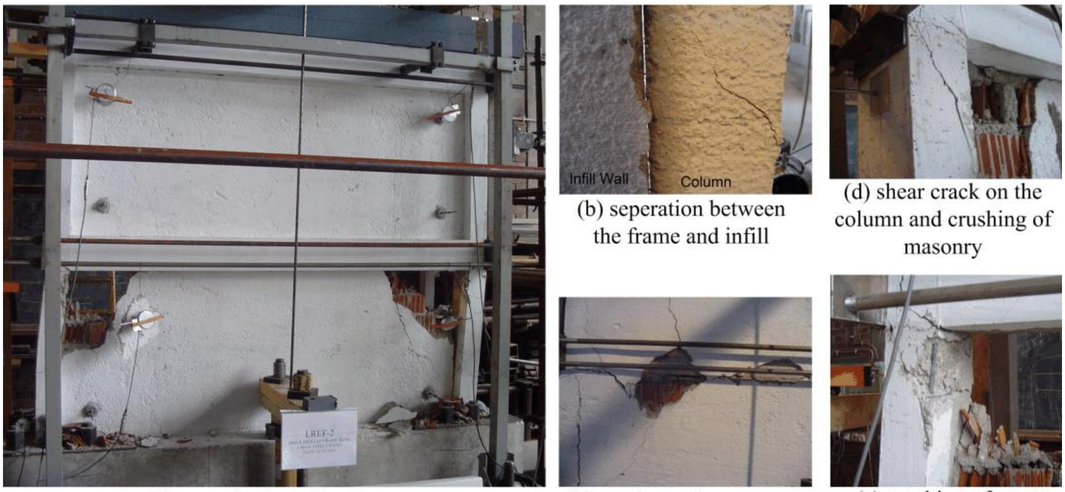

(a) general view after the test

(b) seperation between the frame and infill

(c) cracks on the masonry at the back face

(d) shear crack on the column and crushing of masonry

(e) crushing of cover concrete at the beam-column joints

Figure 4. 32 Failure pattern of specimen LREF2-1/3

4.2.2.3 LSTR-L-1/3

This was the first specimen in Series-L that was strengthened by means of CFRP reinforcement as explained in Section 3.2.5. The column longitudinal bars were lapped at both story levels. The concrete compressive strength of the specimen was 16.7 MPa. LSTR-L-1/3 was tested according to the load and displacement history as indicated in Table 4.7.

The maximum lateral loads which were attained during the forward and backward tenth cycle were 122.0 and -124.0 kN, respectively. The lateral roof drift ratio was around 0.5% at that level.

The hysteretic response curves relating applied shear force with the lateral inter-story displacements at the first and second stories are given in Figures 4.33 and 4.34, respectively. The shear force vs. first and second story infill wall shear deformation curves are shown in Figures 4.35 and 4.36, respectively. The relationship between the imposed base moments and corresponding base rotation responses is presented in Figure 4.37.

The first crack was observed during the fifth cycle at the onset of separation between the first story infill and footing. In the next cycle, the first visible flexural crack developed just above the lap-splice region which was wrapped with CFRP sheet. Also minor diagonal cracks were observed on the first story infill at the same cycle. The first shear cracks formed at the beam-column joints during the eighth cycle. On the tension side of the first story infill-column intersection, some new cracks developed which denotes the formation of a compression strut on the opposite side. However, these cracks remained as hairline cracks until significant damage (debonding and rupturing) of the diagonal CFRP fabrics. This may show the effect of diagonal CFRP acting as a tension tie and restraining the separation of infill from the surrounding frame. Additional diagonal crack formations were observed on the first story infill in the next two cycles. Some popping noises were noticed from the lateral CFRP sheets of the first story column during the tenth cycle.

Table 4. 7 The load and displacement history of specimen LSTR-L-1/3

Cycle No.	*Base Shear (kN)*	*Roof Displ. (mm)*	*First Story Displ. (mm)*	*Roof Drift Ratio (%)*	*First Story Drift Ratio (%)*
+1	40.5	0.35	0.21	0.02	0.03
-1	-40.4	-0.16	-0.11	-0.01	-0.01
+2	50.1	0.60	0.33	0.03	0.04
-2	-50.1	-0.29	-0.18	-0.02	-0.02
+3	60.4	0.91	0.50	0.05	0.06
-3	-60.1	-0.57	-0.31	-0.03	-0.04
+4	70.4	1.18	0.66	0.07	0.08
-4	-70.1	-0.81	-0.45	-0.05	-0.05
+5	80.3	1.60	0.90	0.09	0.11
-5	-80.4	-1.16	-0.65	-0.07	-0.08
+6	90.0	2.10	1.20	0.12	0.15
-6	-90.0	-1.52	-0.85	-0.09	-0.10
+7	100.4	2.71	1.60	0.16	0.19
-7	-100.3	-2.10	-1.20	-0.12	-0.15
+8	110.4	3.90	2.20	0.23	0.27
-8	-110.0	-3.20	-1.73	-0.19	-0.21
+9	118.8	6.10	3.45	0.35	0.42
-9	-119.1	-4.60	-2.43	-0.27	-0.29
+10	122.0	8.63	4.80	0.50	0.58
-10	-124.0	-7.30	-4.00	-0.42	-0.48
+11	118.6	10.56	5.90	0.61	0.72
-11	-115.7	-10.31	-6.47	-0.60	-0.78
+12	109.4	14.80	8.52	0.86	1.03
-12	-100.0	-14.90	-10.30	-0.86	-1.25
+13	94.0	18.10	12.20	1.05	1.48
-13	-76.6	-20.00	-16.43	-1.16	-1.99
+14	67.2	22.10	17.10	1.28	2.07
-14	-56.6	-25.50	-22.84	-1.48	-2.77
+15	51.2	26.60	21.23	1.54	2.57
-15	-50.0	-31.10	-28.50	-1.80	-3.45
+16	32.6	35.20	26.81	2.04	3.25
-16	-36.5	-39.30	-37.80	-2.28	-4.58

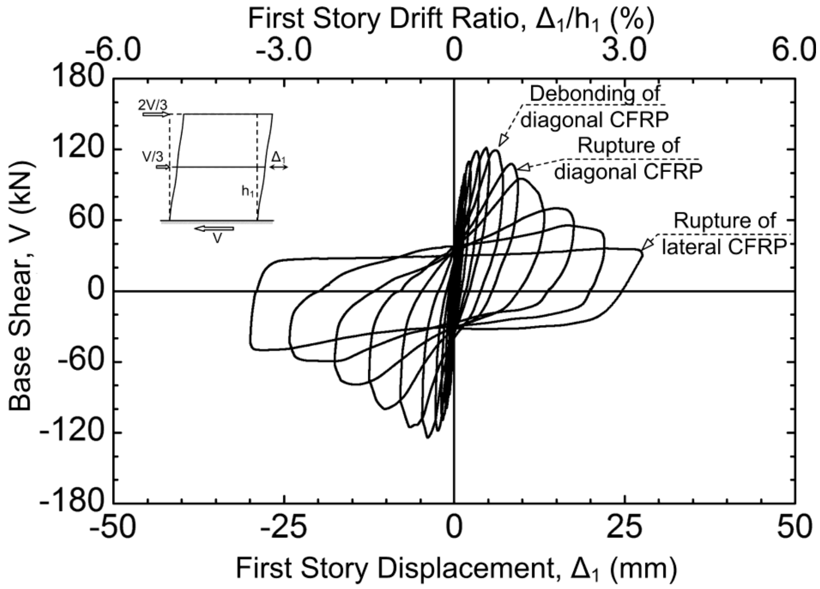

Figure 4. 33 First story shear force vs. displacement / drift ratio curve of specimen LSTR-L-1/3

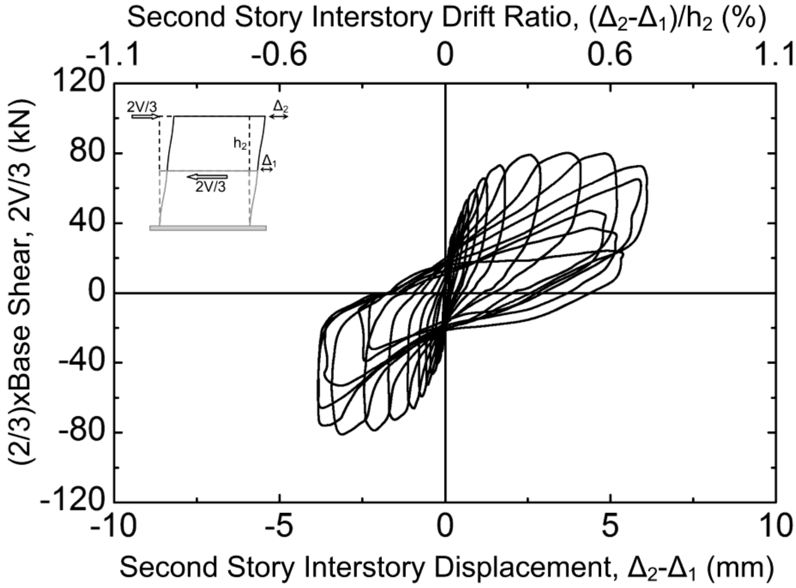

Figure 4. 34 Second story shear force vs. inter-story displacement / drift ratio curve of specimen LSTR-L-1/3

During the eleventh cycle, the diagonal CFRP layers on the lower part of the first story infill started to debond under compression. In the next forward cycle, this propagated to the upper portions of the diagonal CFRP layers. The debonded CFRP sheets which were subjected to tensile strains started to rupture in the following half cycle. This was followed by cracking of the lateral CFRP reinforcement at the column-footing interface. After further debonding and rupturing of the diagonal CFRP reinforcement in the following cycles, the underlying HCT infill started to crush near the region where wide diagonal cracks had developed formerly.

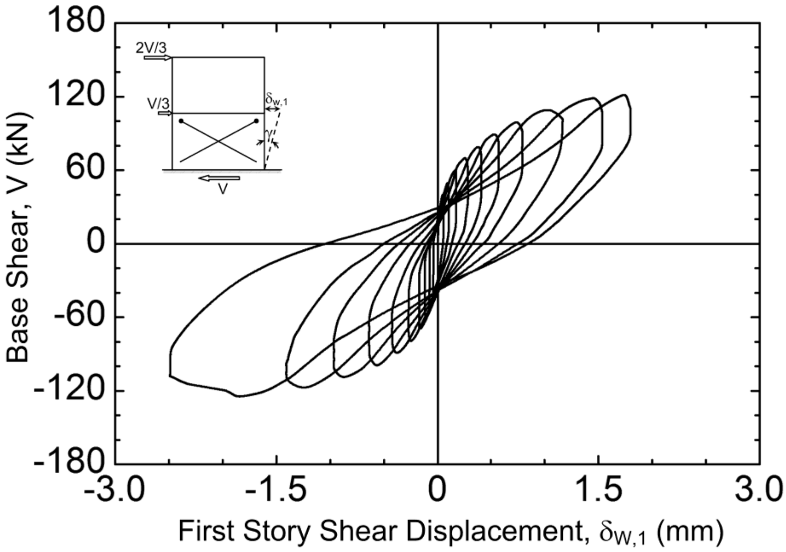

Figure 4. 35 Shear force vs. shear displacement curve for the first story infill of specimen LSTR-L-1/3

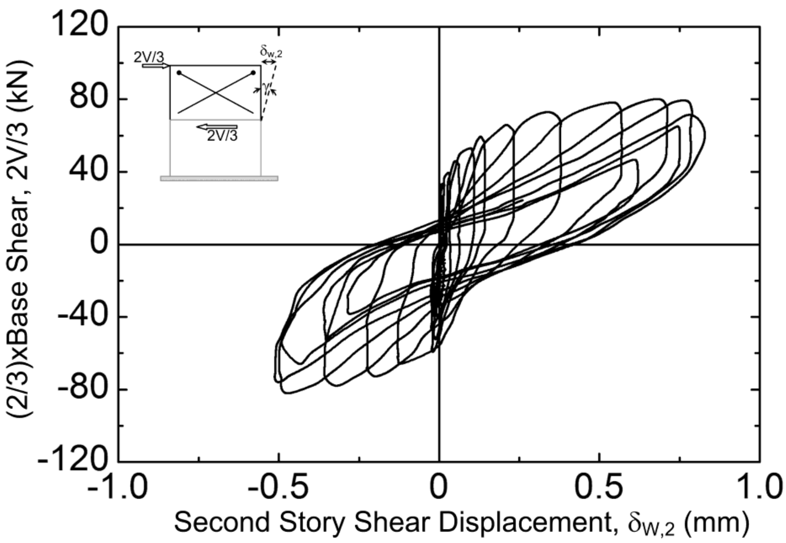

Figure 4. 36 Shear force vs. shear displacement curve for the second story infill of specimen LSTR-L-1/3

At the end of the test, the lateral CFRP reinforcement on the first story columns ruptured and the underlying cover concrete crushed. Wide shear cracks were also observed on the first story columns. The damage pattern that leads to the failure of specimen is presented in Figure 4.38.

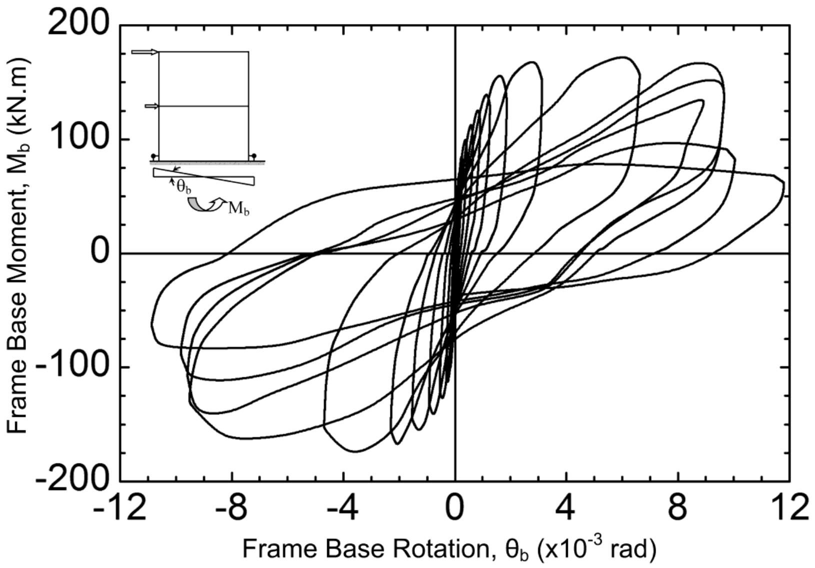

Figure 4. 37 Frame base moment vs. rotation curve of specimen LSTR-L-1/3

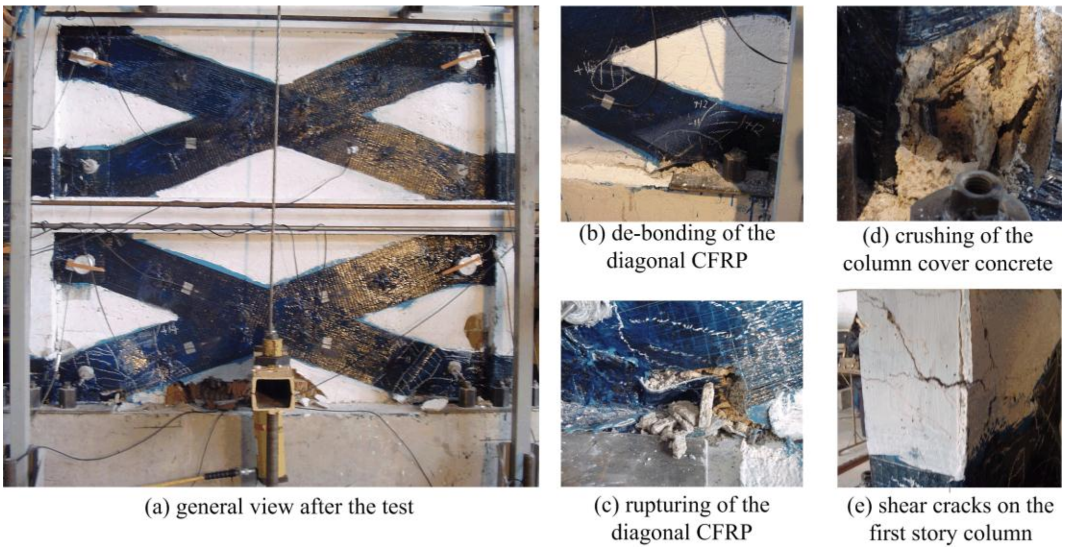

Figure 4. 38 Failure pattern of specimen LSTR-L-1/3

4.2.2.4 LSTR-C-1/3

LSTR-C-1/3 was the second strengthened frame in Series-L which had continuous column longitudinal reinforcement as different from the previous specimen. The concrete compressive strength of the frame was 21.0 MPa. The loading was performed according to the load and displacement history shown in Table 4.8.

The lateral load kept on increasing steadily until the thirteenth cycle, where the maximum lateral load in the forward direction, 159.9 kN was attained at a roof drift ratio of 0.45%. In this cycle, the load in the backward direction was -160.9 kN. However, in the following backward cycle, a higher lateral load level, -176.6 kN could be achieved.

The hysteretic shear force vs. inter-story displacement curves of the first and second stories are shown in Figures 4.39 and 4.40, respectively. Because there was a acquisition error in dial gauge measurements of this specimen, base shear-shear displacement curves for the infill walls and base moment-base rotation response of the frame could not be presented herein.

The first hairline cracks developed as flexural cracks on the tension side of the first story columns during the first cycle. On both columns, the locations of these cracks were just above the CFRP sheets used for the lateral confinement and at the mid-height of the column. In the first four cycles, these flexural cracks propagated but not widened considerably; and no other damage was observed on the frame during this period.

The first diagonal shear cracks on both faces of the first story infill were observed during the fifth cycle. As a possible indicator of the compression strut formation, the separation between the frame and infill started in this cycle. Also, the first snapping sounds of CFRP reinforcement were noticed at this stage.

Table 4. 8 The load and displacement history of specimen LSTR-C-1/3

Cycle No.	*Base Shear (kN)*	*Roof Displ. (mm)*	*First Story Displ. (mm)*	*Roof Drift Ratio (%)*	*First Story Drift Ratio (%)*
+1	40.4	0.15	0.00	0.01	0.00
-1	-40.9	-0.39	0.00	-0.02	0.00
+2	50.6	0.36	0.00	0.02	0.00
-2	-50.9	-0.73	0.00	-0.04	0.00
+3	65.3	0.52	0.47	0.03	0.06
-3	-60.0	-0.82	-0.28	-0.05	-0.03
+4	69.7	0.64	0.52	0.04	0.06
-4	-70.4	-1.03	-0.33	-0.06	-0.04
+5	79.9	0.73	0.58	0.04	0.07
-5	-80.2	-1.36	-0.37	-0.08	-0.04
+6	90.9	0.87	0.64	0.05	0.08
-6	-88.6	-1.82	-0.43	-0.11	-0.05
+7	100.2	1.49	1.10	0.09	0.13
-7	-99.2	-2.17	-0.47	-0.13	-0.06
+8	110.5	2.12	1.51	0.12	0.18
-8	-110.0	-2.70	-0.53	-0.16	-0.06
+9	120.6	2.88	2.06	0.17	0.25
-9	-120.5	-3.20	-0.74	-0.19	-0.09
+10	130.3	3.17	2.26	0.18	0.27
-10	-130.3	-3.67	-1.23	-0.21	-0.15
+11	140.3	3.85	2.75	0.22	0.33
-11	-140.6	-4.30	-1.41	-0.25	-0.17
+12	150.4	5.85	4.30	0.34	0.52
-12	-154.7	-5.03	-1.56	-0.29	-0.19
+13	159.9	7.76	5.47	0.45	0.66
-13	-160.9	-6.10	-1.84	-0.35	-0.22
+14	158.2	10.01	6.37	0.58	0.77
-14	-176.6	-10.00	-4.29	-0.58	-0.52
+15	131.3	14.97	10.05	0.87	1.22
-15	-141.0	-15.00	-8.12	-0.87	-0.98
+16	89.3	20.35	17.89	1.18	2.17
-16	-90.7	-20.11	-14.50	-1.17	-1.76
+17	68.1	24.76	22.74	1.44	2.76
-17	-66.4	-24.98	-20.03	-1.45	-2.43
+18	70.3	30.31	28.69	1.76	3.48
-18	-59.0	-30.01	-25.10	-1.74	-3.04

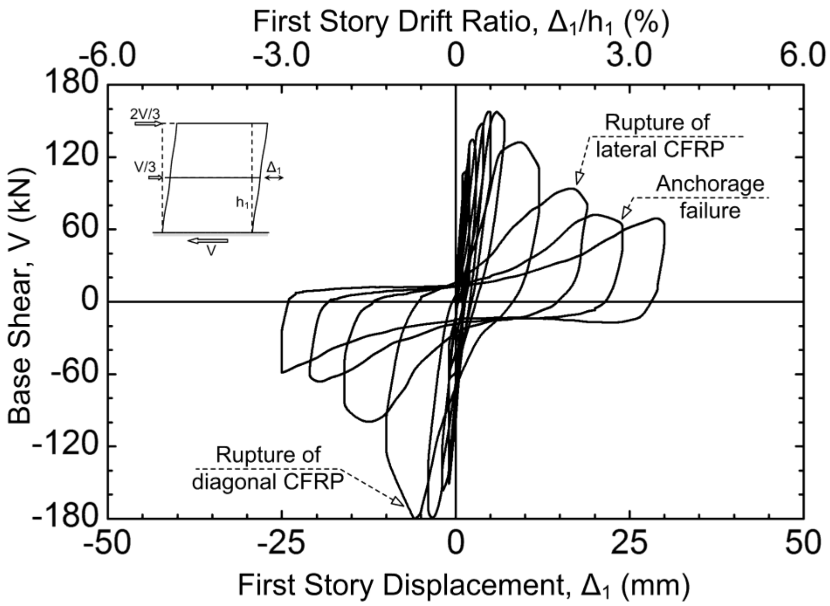

Figure 4. 39 First story shear force vs. displacement / drift ratio curve of specimen LSTR-C-1/3

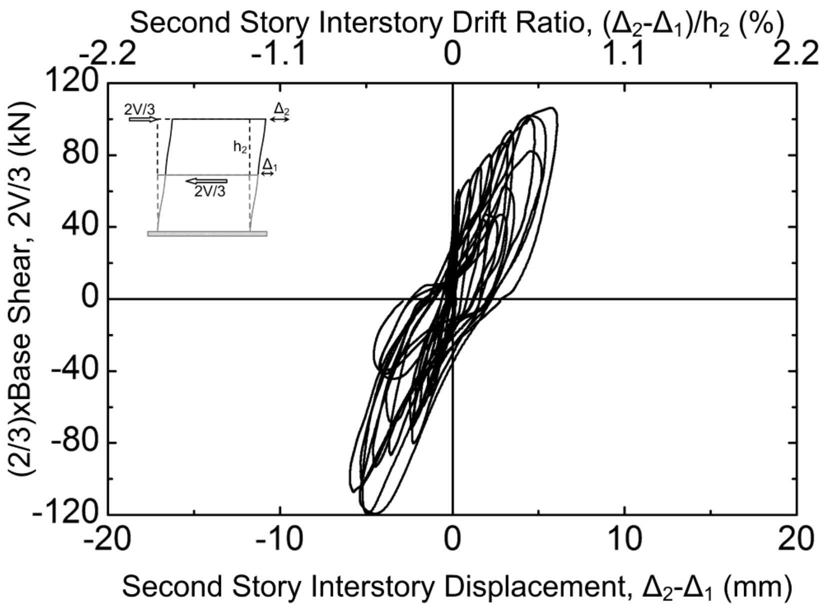

Figure 4. 40 Second story shear force vs. inter-story displacement / drift ratio curve of specimen LSTR-C-1/3

New flexural cracks on the first story columns and diagonal cracks on the first story infill were observed in the tenth cycle. Also the separation between the first story column and infill wall increased in this period. During the tenth cycle, a new crack formed at the infill-footing interface. In the next cycle, the CFRP reinforcement used for the lateral confinement started to crack above the column-footing interface. The separation at the column-footing and infill-footing boundaries increased until the negative fourteenth cycle. At this half-cycle, a wide horizontal crack formed on the first story wall and the diagonal CFRP ruptured at the lower corner close to this crack. This was followed by rupturing of the lateral CFRP sheets at the bottom of the first story columns in the next two cycles. The shear cracks were observed on the first story columns during this period. The cover concrete under the ruptured CFRP at the lap-splice regions crushed under compression.

At the end of the test, some of the anchor dowels of the diagonal CFRP layers failed, the plaster spalled in patches at the back face of the first story infill and the underlying HCT infill crushed in compression. The described failure pattern of the specimen is shown in Figure 4.41.

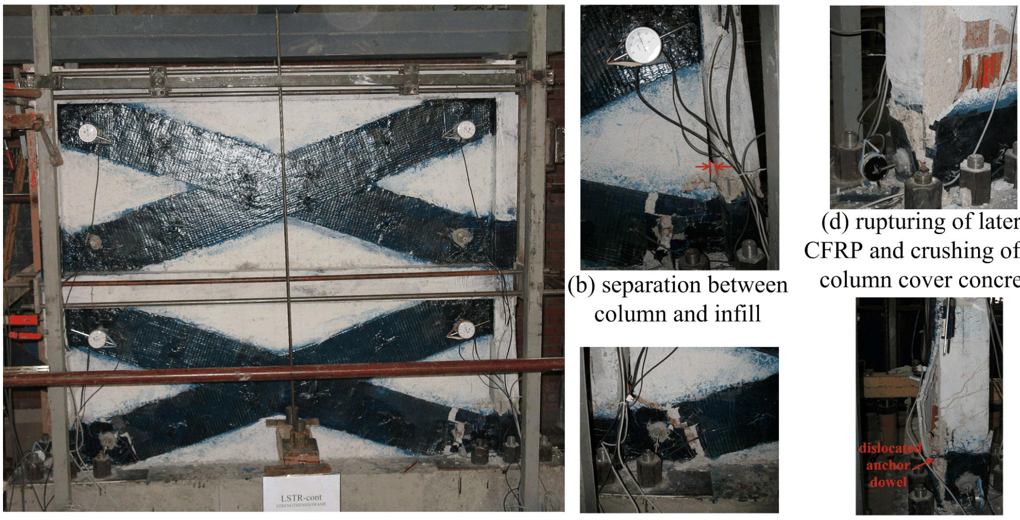

(a) general view after the test

(b) separation between column and infill

(c) rupturing of the diagonal CFRP

(d) rupturing of lateral CFRP and crushing of the column cover concrete

(e) Failure of anchor dowel

Figure 4. 41 Failure pattern of specimen LSTR-C-1/3

4.3 GROUP-II: 1/2 SCALED RC FRAMES

4.3.1 Series-N

4.3.1.1 NREF-1/2

In Group-II, the only reference specimen of Series-N was NREF-1/2 which had HCT infill walls at both stories. Testing of the sample concrete cylinders on the day of testing provided an average concrete compressive strength of 19.3 MPa. Similar to all other Group-II frames, the column longitudinal bars of NREF-1/2 were lapped at both story levels as explained in Section 3.2.2.2. The test was performed according to the displacement history presented in Table 4.9.

The forward and backward lateral load capacities of the specimen were 66.3 kN and -69.1 kN which were attained at approximate roof drift ratios of 0.45% and 0.75%, respectively. The hysteretic first and second story shear force vs. inter-story displacement response curves of the frame are shown in Figures 4.42 and 4.43, respectively. The applied shear vs. shear displacement curves for the first and second story infill walls are presented in Figures 4.44 and 4.45, respectively. In Figure 4.46, the base moment vs. base rotation relationship is given.

During the positive third cycle, the first cracks were observed on the tension side of the first story north column (i.e. flexural cracks). The roof displacement was 6 mm at that moment. Sequentially, a horizontal crack formed on the tension side of the first story infill at about 300 mm above the foundation level. On the consecutive half cycle, symmetric cracks were monitored on the south column and the south side of the first story infill. The horizontal crack on the south side of HCT wall was around 150 mm above the foundation level. Besides, the plaster on the infill started to swell at the back face and first shear crack formed at the south beam-column joint. During the fourth cycle, an inclined crack formed over the lap-splice region of the north column. The first diagonal crack was also observed on the first story infill during the same cycle.

Table 4. 9 The load and displacement history of specimen NREF-1/2

Cycle No.	*Base Shear (kN)*	*Roof Displ. (mm)*	*First Story Displ. (mm)*	*Roof Drift Ratio (%)*	*First Story Drift Ratio (%)*
+1	+21.6	+1.02	+0.56	+0.03	+0.03
-1	-15.1	-1.02	-0.76	-0.03	-0.04
+2	+48.0	+4.07	+2.37	+0.12	+0.13
-2	-46.0	-3.92	-2.56	-0.12	-0.14
+3	+66.3	+15.01	+10.67	+0.46	+0.60
-3	-68.3	-15.06	-10.33	-0.46	-0.58
+4	+64.6	+24.90	+19.94	+0.76	+1.11
-4	-69.1	-25.02	-16.53	-0.76	-0.92
+5	+54.1	+34.86	+29.82	+1.06	+1.67
-5	-67.6	-35.08	-23.10	-1.07	-1.29
+6	+47.6	+40.11	+35.35	+1.22	+1.97
-6	-61.0	-39.35	-27.95	-1.20	-1.56
+7	+44.8	+49.94	+44.97	+1.52	+2.51
-7	-55.9	-49.29	-38.76	-1.50	-2.17
+8	+40.5	+60.06	+55.35	+1.83	+3.09
-8	-42.5	-60.03	-53.65	-1.83	-3.00
+9	+31.8	+69.11	+65.17	+2.11	+3.64
-9	-30.9	-70.00	-64.73	-2.13	-3.62
+10	+26.4	+79.85	+75.11	+2.43	+4.20
-10	-27.4	-80.04	-74.59	-2.44	-4.17
+11	+24.1	+89.86	+79.38	+2.74	+4.43
-11	-25.9	-89.90	-84.49	-2.74	-4.72

In the following cycles, the horizontal cracks at both sides of the first story infill widened, and the separation between the infill and columns started above this horizontal crack. This indicated a diagonal strut formation. However, the diagonal strut starting from the upper corner of the infill could not reach the bottom corner, and met the frame at a higher level (i.e. wide horizontal cracks on the lower portion of first story infill, Figure 4.47 and Figure E.9).

The new flexural cracks on the first story columns and shear cracks at the beam-column joints were observed during the fifth and sixth cycles. Besides, existing column cracks widened considerably (approximately 3 mm at the column base).

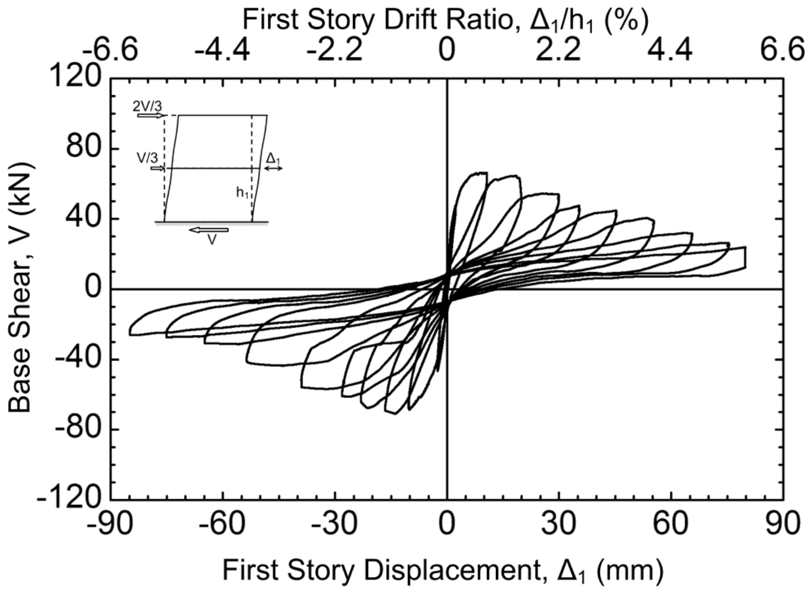

Figure 4. 42 First story shear force vs. displacement / drift ratio curve of specimen NREF-1/2

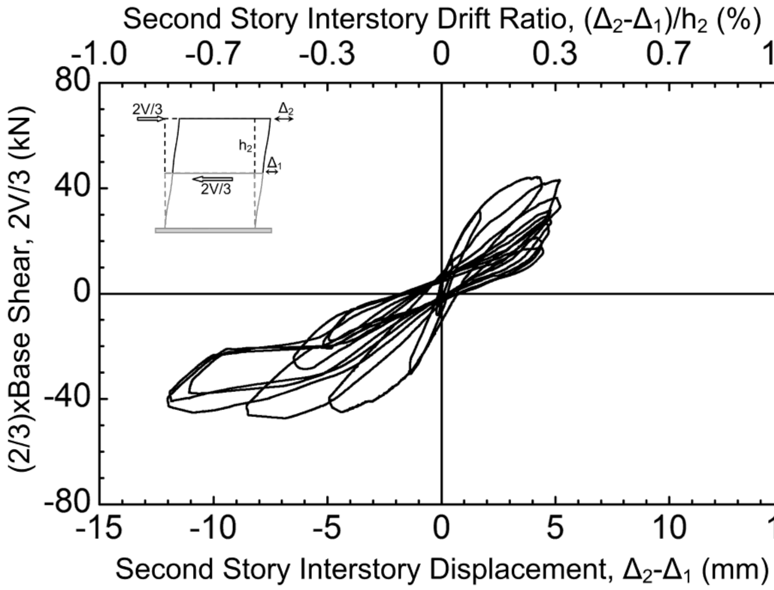

Figure 4. 43 Second story shear force vs. inter-story displacement / drift ratio curve of specimen NREF-1/2

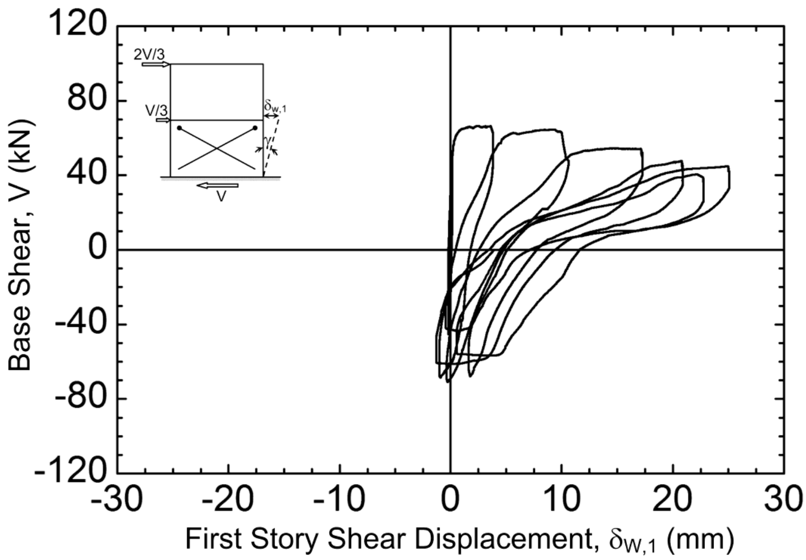

Figure 4. 44 Shear force vs. shear displacement curve for the first story infill of specimen NREF-1/2

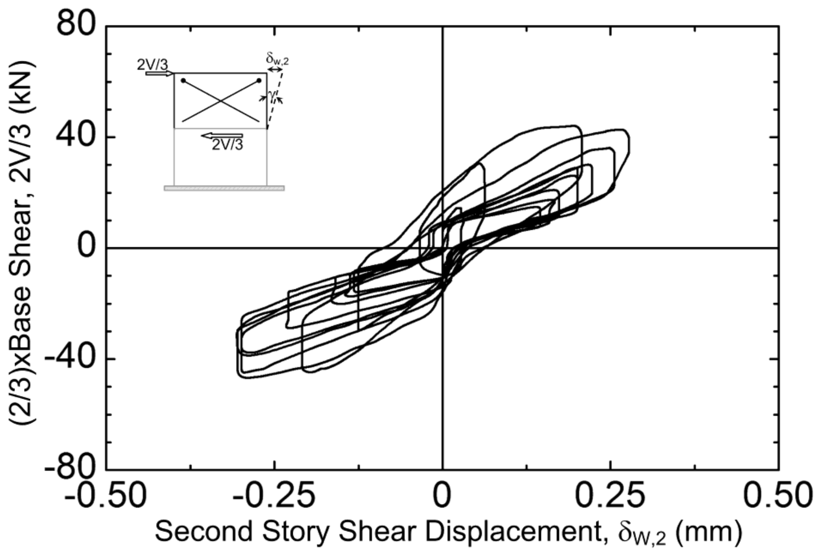

Figure 4. 45 Shear force vs. shear displacement curve for the second story infill of specimen NREF-1/2

After the sixth cycle, damage concentrated at the lap-splice regions of the first story columns. The concrete at the lap-splice regions started to crush under compression, which lead to spalling off of cover concrete and exposed the column bars. The first story infill also crushed at the upper corners and around the horizontal crack at the lower region. As a result of the damage, the lateral load capacity of the frame decreased to about 35% of its ultimate capacity, which corresponds to a roof drift ratio of 2.75%. The damages leading to the failure of the specimen is shown in Figure 4.47.

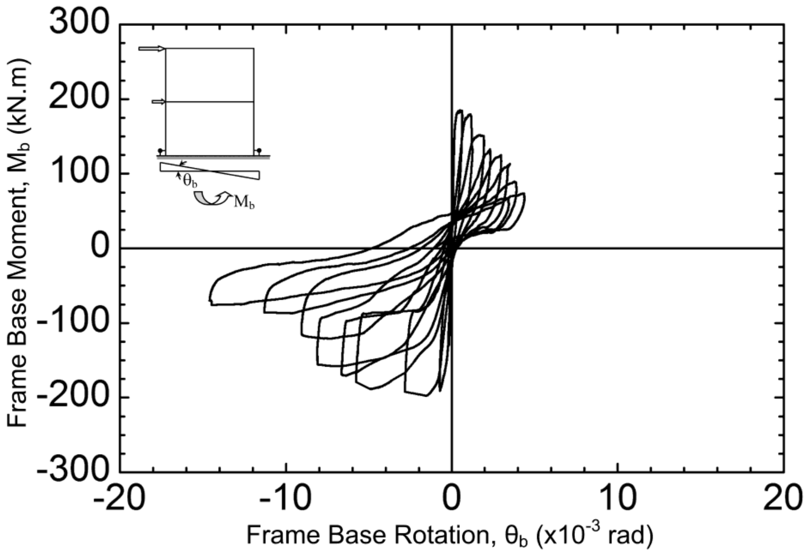

Figure 4. 46 Frame base moment vs. rotation curve of specimen NREF-1/2

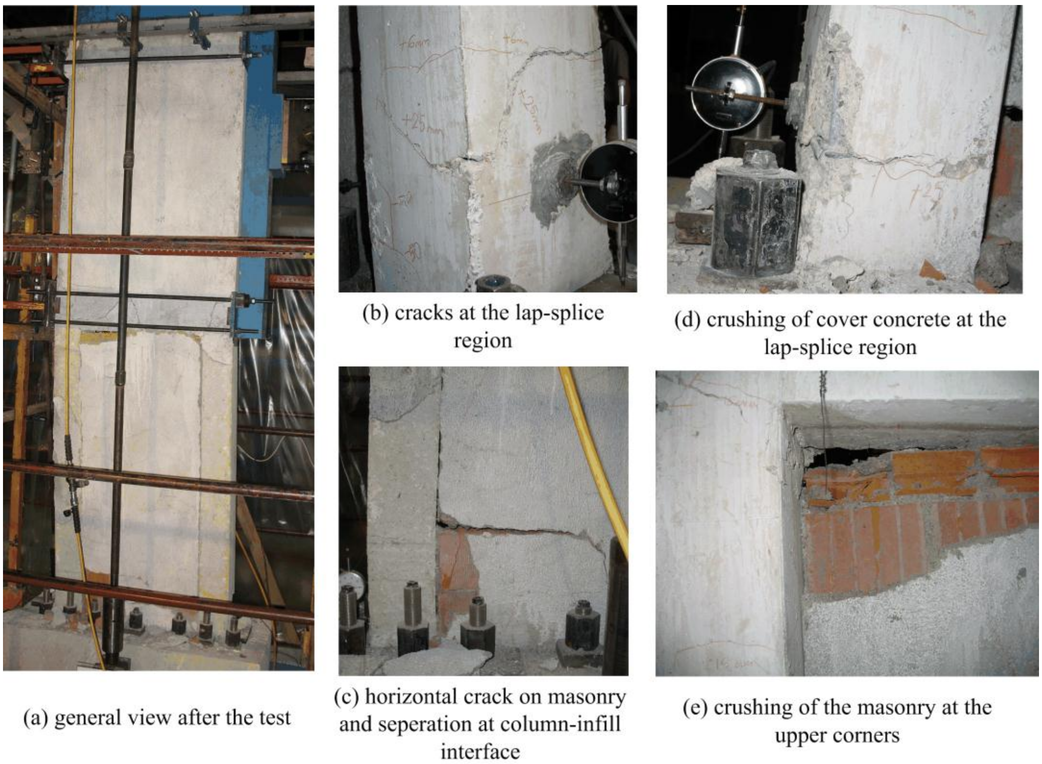

Figure 4. 47 Failure pattern of specimen NREF-1/2

4.3.1.2 NSTR-1/2

NSTR-1/2 was the strengthened specimen of this series. The concrete compressive strength of the frame was 20.4 MPa. The loading of specimen was performed according to the roof displacement values presented in Table 4.10. The corresponding base shear, first story displacement and drift ratios are also given in the same table.

The ultimate lateral load capacity of the frame was reached in the fourth cycle, where the maximum loads in the forward and backward directions were 94.0 kN and -101.9 kN, respectively. The roof drift ratio was around 0.75% at the ultimate load level. It should be noted that some slight increments of the load capacity were noticed in the following backward cycles until failure of the specimen.

The first and second story shear force vs. inter-story displacement response curves of the frame are presented in Figures 4.48 and 4.49, respectively. The shear deformations experienced by the first and second story infill walls are shown in Figures 4.50 and 4.51, respectively, in relation with the applied shear force. The base moment vs. base rotation relationship of the frame is presented in Figure 4.52.

During the positive third cycle, at about 7 mm roof displacement level, the first crack formed at the mid-height of the first story north column. Six more flexural cracks were observed in the same cycle on this column. Symmetric flexural cracks formed on the south column in the consecutive half cycle. Besides, diagonal cracks developed on the first story infill at the back face, where also separation of the plaster on the columns initiated.

In the fifth cycle, the separation between the columns and infill became visible. The plaster at the back face, which had previously separated from the columns, fell off in pieces. New flexural cracks were observed on the first story columns together with the one at the column-footing interface. During the sixth cycle, the separation at the first story column-footing and infill-column boundaries increased significantly. Also some popping voices were heard from the CFRP reinforcement along the diagonals of the first story infill, showing that the diagonal CFRP's were being stressed in tension (i.e. tension tie).

Table 4. 10 The load and displacement history of specimen NSTR-1/2

Cycle No.	*Base Shear (kN)*	*Roof Displ. (mm)*	*First Story Displ. (mm)*	*Roof Drift Ratio (%)*	*First Story Drift Ratio (%)*
+1	+19.1	+1.28	+0.89	+0.04	+0.05
-1	-21.4	-1.34	-0.80	-0.04	-0.04
+2	+46.9	+4.43	+3.05	+0.14	+0.17
-2	-51.4	-4.46	-2.54	-0.14	-0.14
+3	+85.1	+15.54	+9.98	+0.47	+0.56
-3	-90.7	-15.21	-8.82	-0.46	-0.49
+4	+94.0	+25.55	+15.91	+0.78	+0.89
-4	-101.9	-25.25	-15.22	-0.77	-0.85
+5	+91.7	+35.45	+21.85	+1.08	+1.22
-5	-103.1	-35.69	-21.54	-1.09	-1.20
+6	+91.4	+40.38	+25.18	+1.23	+1.41
-6	-100.3	-40.64	-25.04	-1.24	-1.40
+7	+92.7	+50.51	+31.32	+1.54	+1.75
-7	-103.7	-50.91	-31.37	-1.55	-1.75
+8	+90.2	+60.03	+36.87	+1.83	+2.06
-8	-103.1	-61.20	-37.41	-1.87	-2.09
+9	+90.9	+70.29	+43.18	+2.14	+2.41
-9	-104.4	-71.06	-43.57	-2.17	-2.43
+10	+90.9	+80.03	+48.98	+2.44	+2.74
-10	-104.9	-81.68	-50.23	-2.49	-2.81
+11	+90.5	+89.88	+55.27	+2.74	+3.09
-11	-104.1	-91.83	-56.94	-2.80	-3.18
+12	+89.2	+99.81	+61.64	+3.04	+3.44
-12	-104.5	-101.76	-64.48	-3.10	-3.60
+13	+91.9	+109.35	+69.06	+3.33	+3.86
-13	-101.1	-112.11	-74.15	-3.42	-4.14
+14	+86.4	+119.04	+79.40	+3.63	+4.44
-14	-67.1	-99.95	-86.51	-3.05	-4.83

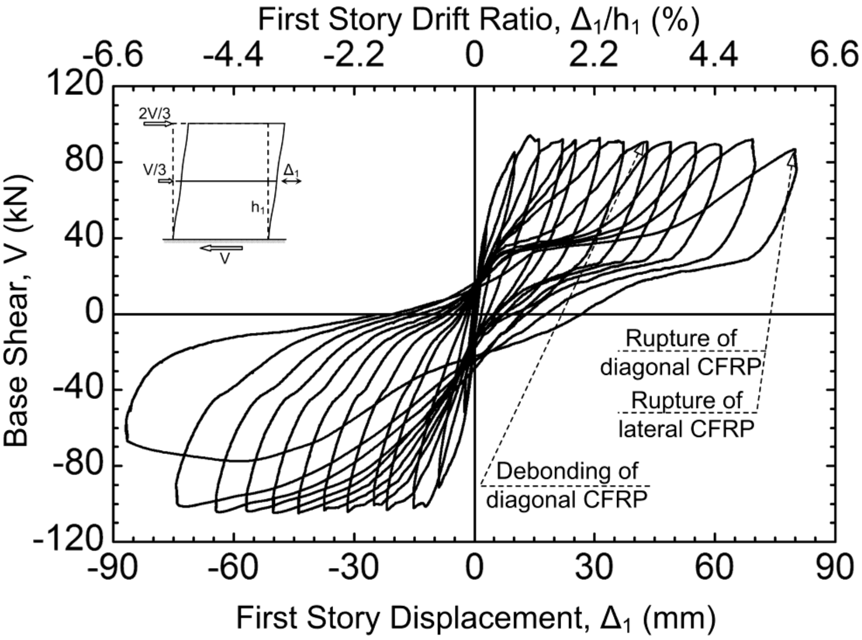

Figure 4. 48 First story shear force vs. displacement / drift ratio curve of specimen NSTR-1/2

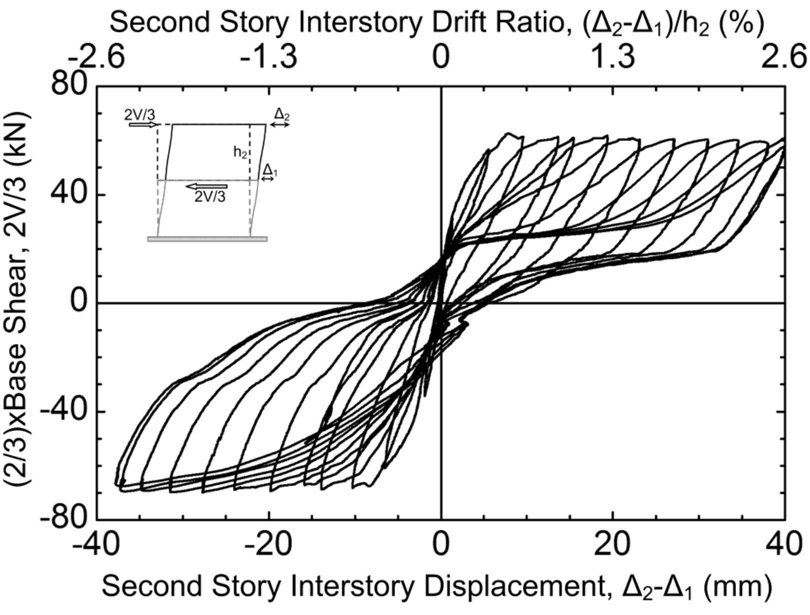

Figure 4. 49 Second story shear force vs. inter-story displacement / drift ratio curve of specimen NSTR-1/2

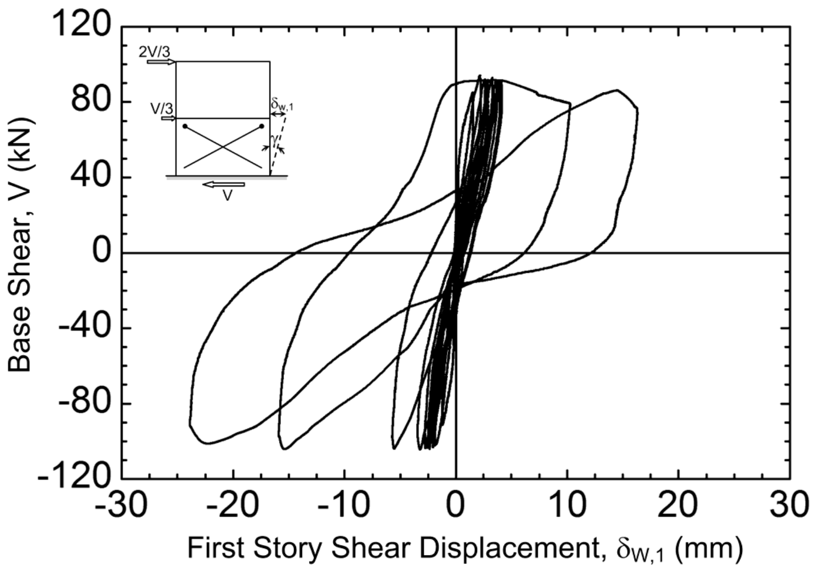

Figure 4. 50 Shear force vs. shear displacement curve for the first story infill of specimen NSTR-1/2

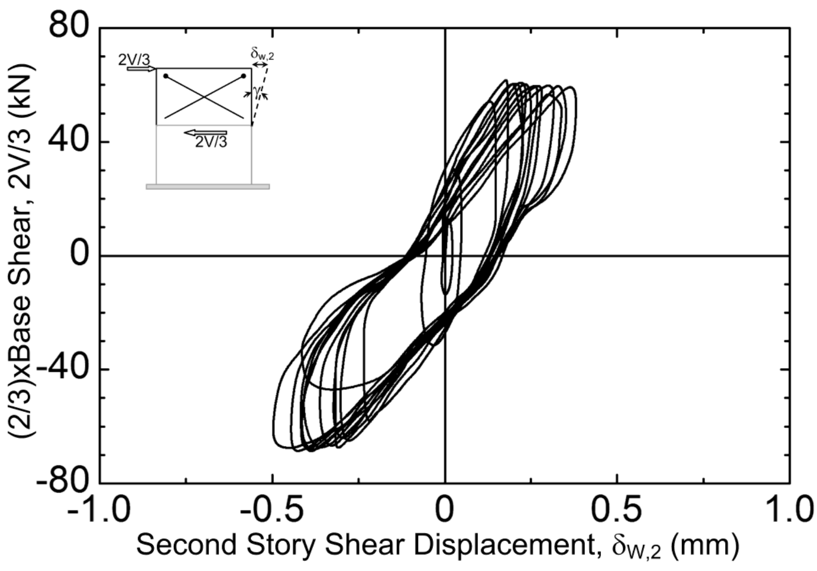

Figure 4. 51 Shear force vs. shear displacement curve for the second story infill of specimen NSTR-1/2

In the next two cycles, the damage concentrated at the separation between the column and footing, which extended to a width of around 20 mm at the end of eighth cycle. During these two cycles, debonding initiated under compression in the lateral CFRP reinforcement at the lap-splice region and diagonal CFRP layers on the first story infill. During the ninth and tenth cycles, debonding of the CFRP layer increased significantly, especially at the lap-splice regions. Besides, the separation at the column-footing interface continued to increase critically.

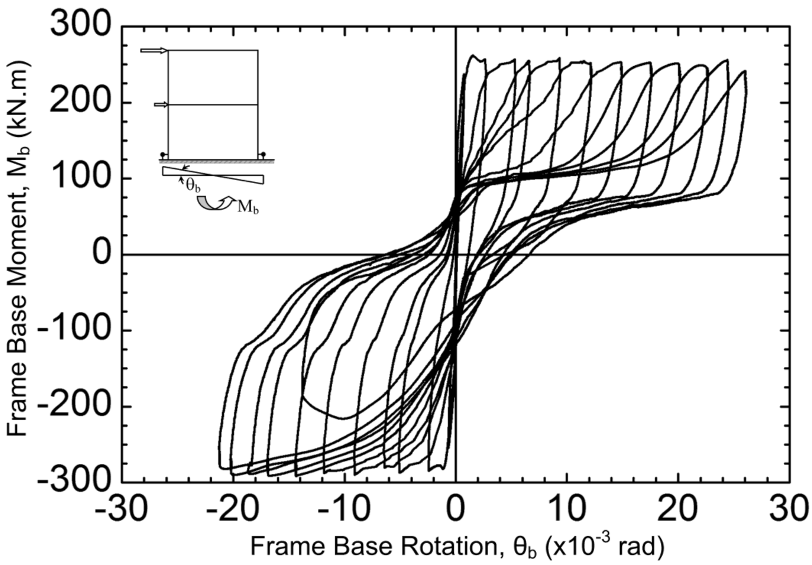

Figure 4. 52 Frame base moment vs. rotation curve of specimen NSTR-1/2

The anchor dowels connecting the upper corners of the diagonal CFRP sheets at both faces through the first story HCT infill failed during the twelfth cycle. This caused bulging of the diagonal CFRP at these locations together with the plaster underneath. Meanwhile, the longitudinal column bars at the bottom of the first story columns became visible due to the wide separation of the columns from the footing (Figure 4.53.c). The frame continued to carry the same level of load until the negative fourteenth cycle. At this level, diagonal CFRP layers on the infill and lateral CFRP on the columns ruptured at different locations (Figures 4.53.d and 4.53.e), which terminated the contribution of CFRP reinforcement on the overall response and lead to a significant decrease in the lateral load capacity. The failure pattern of the specimen described above is shown in Figure 4.53.

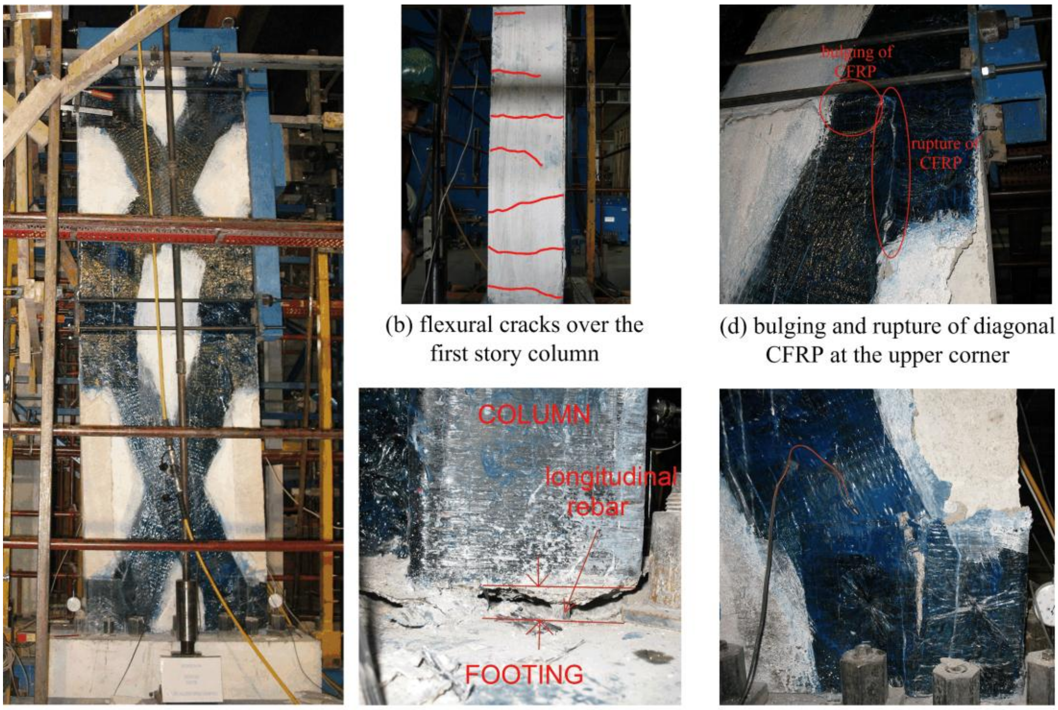

(b) flexural cracks over the first story column

(d) bulging and rupture of diagonal CFRP at the upper corner

(a) general view after the test

(c) seperation at the column-footing interface

(e) rupture of diagonal CFRP at the lower corner

Figure 4. 53 Failure pattern of specimen NSTR-1/2

4.3.2 Series-L

4.3.2.1 LREF-1/2

LREF-1/2 was the non-strengthened reference specimen of Series-L in this group. Similar to NREF-1/2, this frame also had plastered HCT infill partitions at both stories. Average compressive strength of the concrete was approximately 19.8 MPa. The lateral loading of the frame was performed so as to achieve the target displacement values shown in Table 4.11, where some important response values are presented as well.

The forward and backward maximum lateral load capacities of the frame were 152.4 kN and -140.0 kN, respectively. This level of load was reached during seventh cycle at a roof drift ratio of about 0.35%.

The first and second story hysteretic shear force vs. inter-story displacement relationships of specimen LREF-1/2 are presented in Figures 4.54 and 4.55, respectively. In Figures 4.56 and 4.57, the applied shear-shear displacement response curves for the first and second story infill walls are shown, respectively. The frame base moment-base rotation curve is presented in Figure 4.58.

Table 4. 11 The load and displacement history of specimen LREF-1/2

Cycle No.	*Base Shear (kN)*	*Roof Displ. (mm)*	*First Story Displ. (mm)*	*Roof Drift Ratio (%)*	*First Story Drift Ratio (%)*
+1	+24.7	+0.35	0.00	+0.01	0.00
-1	-32.4	-0.47	0.00	-0.02	0.00
+2	+44.2	+1.00	0.00	+0.03	0.00
-2	-74.9	-1.14	-1.09	-0.04	-0.08
+3	+87.4	+2.02	+0.34	+0.07	+0.02
-3	-98.7	-1.99	-1.87	-0.07	-0.14
+4	+111.0	+3.11	+0.74	+0.11	+0.05
-4	-105.2	-2.89	-2.72	-0.10	-0.20
+5	+121.7	+3.78	+1.15	+0.13	+0.08
-5	-120.3	-3.81	-3.23	-0.13	-0.24
+6	+126.2	+4.81	+1.56	+0.17	+0.11
-6	-128.4	-4.79	-3.85	-0.17	-0.28
+7	+152.2	+9.81	+4.92	+0.34	+0.36
-7	-140.3	-9.89	-7.15	-0.35	-0.52
+8	+149.4	+14.87	+8.19	+0.52	+0.60
-8	-137.9	-14.89	-9.74	-0.52	-0.71
+9	+142.0	+29.87	+20.21	+1.04	+1.48
-9	-119.8	-29.84	-24.37	-1.04	-1.78
+10	+110.3	+39.35	+30.32	+1.38	+2.21
-10	-56.4	-39.85	-36.24	-1.39	-2.65
+11	+84.7	+49.42	+40.98	+1.73	+2.99
-11	-50	-49.5	-46.26	-1.73	-3.38
+12	+72.1	+59.8	+51.55	+2.09	+3.76
-12	-46.4	-59.7	-56.02	-2.09	-4.09

First flexural cracks were observed on the first story south column during the negative sixth cycle. One of these cracks was at the column base and the other was about 200 mm above the footing level (i.e. within lap-splice region). A shear crack at the south beam-column joint and diagonal cracks on the first story infill also formed during the same cycle.

During the seventh positive cycle, symmetric flexural cracks on the first story north column and a shear crack at the north beam-column joint were monitored. Besides, separation was observed between the RC frame members and HCT infill walls on the opposite side of the compression strut formation. Distinctively, this separation occurred at both story levels in this group. In the negative seventh cycle, additional flexural cracks on the south column and diagonal cracks on the HCT infill were observed.

During the eighth cycle, plaster at the upper corners of the first story infill started to spall off, which indicates crushing of these regions. New shear cracks at the beam-column joints and a flexural crack on the first story beam also formed in this cycle.

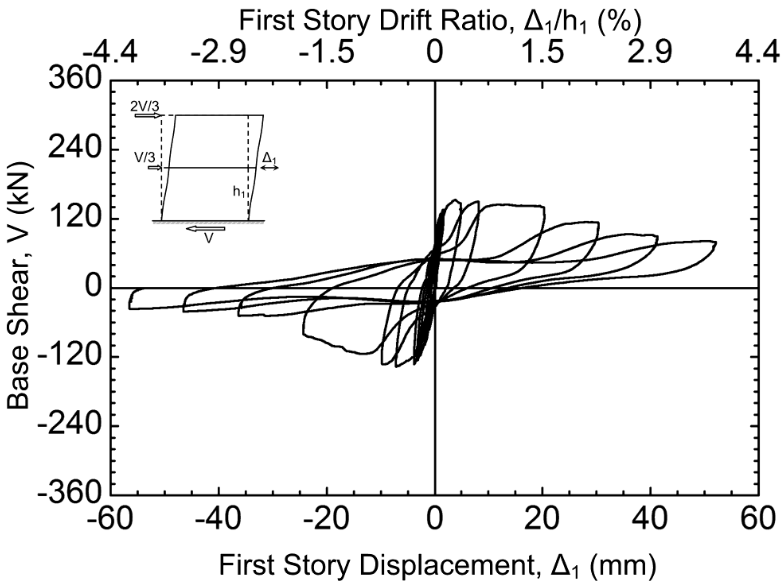

Figure 4. 54 First story shear force vs. displacement / drift ratio curve of specimen LREF-1/2

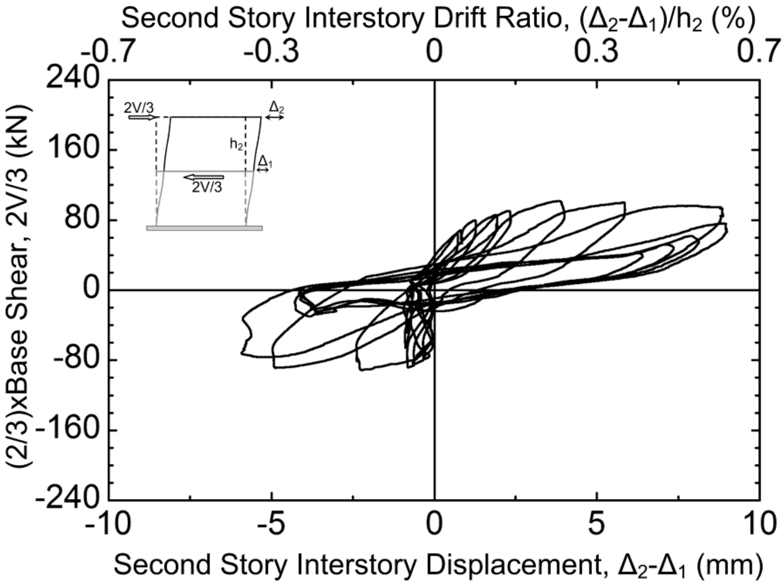

Figure 4. 55 Second story shear force vs. inter-story displacement / drift ratio curve of specimen LREF-1/2

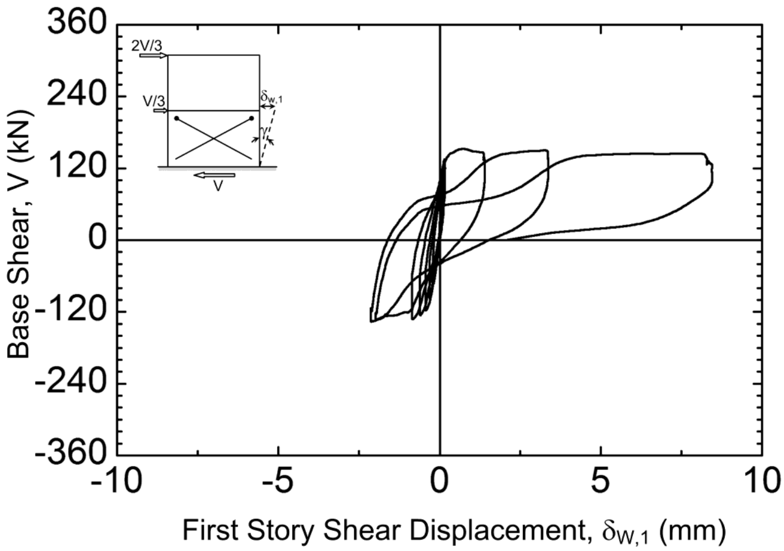

Figure 4. 56 Shear force vs. shear displacement curve for the first story infill of specimen LREF-1/2

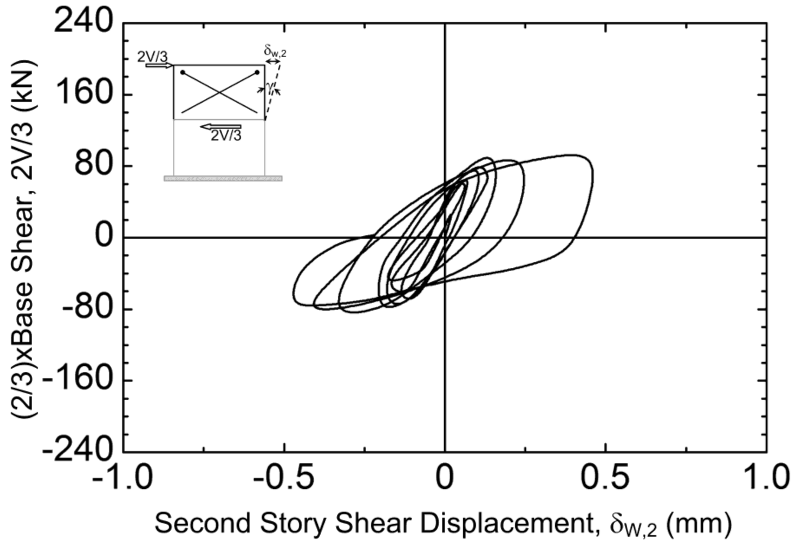

Figure 4. 57 Shear force vs. shear displacement curve for the second story infill of specimen LREF-1/2

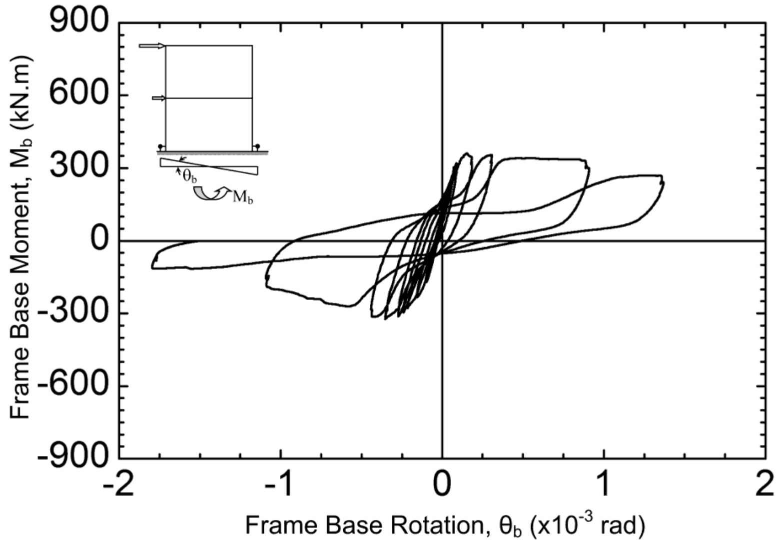

Figure 4. 58 Frame base moment vs. rotation curve of specimen LREF-1/2

In the next cycle, damage intensified on the RC frame members as new flexural cracks on the columns and shear cracks at beam-column joints. Furthermore the infill started to crush at the upper corners when separation from the RC frame members became significant on the opposite side. After total crushing of HCT infill at the corners, beneficial contribution of infill walls to the overall response ended. Subsequently, the shear cracks at the beam-column joints propagated over the upper ends of the first story columns, widened critically and lead to crushing of cover concrete at these regions under compression. The described damage pattern of the specimen is shown in Figure 4.59.

(a) general view after the test

(b) seperation of the second story infill

(c) flexural cracks on the column

(d) shear cracks at the beam-column joint

(e) shear crack propagated on the column

Figure 4. 59 Failure pattern of specimen LREF-1/2

4.3.2.2 LSTR-1/2

LSTR-1/2 was the strengthened specimen of this series. The concrete compressive strength of the frame members was around 20.7 MPa. During the ninth cycle of the test, an error occurred related to the test set-up, which hindered proceeding the test. The specimen was unloaded at that point. Although at that stage the frame was just about to devolve from the elastic to the plastic zone, it was yet in a different position than the original zero point. Therefore, the permanent displacement of the specimen was determined at each story level by using both the recorded data and total station readings. The test was continued thereby repeating the last cycle. The displacement history applied in this second part of the test was determined by considering the permanent roof displacement. The resulting (i.e. corrected) displacement history of the specimen is given in Table 4.12 where all applied load and displacement values are summarized.

The ultimate lateral load capacity of the frame was attained during the repeated ninth cycle. At this stage of the test, the applied maximum lateral loads were 339.8 kN and -317.8 kN in the forward and backward directions, respectively. The roof drift ratio corresponding to the ultimate load capacity was around 1.10%.

The applied shear force vs. inter-story displacement curves of the first and second stories were constructed by joining two parts of the test. This was done by shifting the second part displacement values by the determined permanent displacements. These curves are presented in Figures 4.60 and 4.61, for the first and second floor inter-story displacements, respectively. The applied shear force-shear displacement response curves for the first and second story infill walls are shown in Figures 4.62 and 4.63. And lastly, the base moment vs. base rotation relationship of the frame is given in Figure 4.64.

Although popping noises were coming from the CFRP in the previous cycles, the first visible cracks monitored during the sixth cycle. These cracks were in the form of diagonal cracks on the first story infill walls and flexural cracks at the mid-height of the first story columns. In the next two cycles, existing cracks propagated in addition to the newly developed diagonal wall and flexural column cracks.

During the ninth cycle, separation between the first story infill and the surrounding frame members became visible, showing a compression strut formation on the opposite side. The diagonal cracks spread on the first story infill in the vicinity of the diagonal CFRP sheets. In the negative ninth cycle, south column started to split at the footing interface on the tension side and shear cracks were observed just below the south beam-column joint. Furthermore, popping noises were heard from the lateral CFRP at the lap-splice region of the first story column.

Table 4. 12 The load and displacement history of specimen LSTR-1/2

Cycle No.	*Base Shear (kN)*	*Roof Displ. (mm)*	*First Story Displ. (mm)*	*Roof Drift Ratio (%)*	*First Story Drift Ratio (%)*
+1	+26.9	+0.32	+0.31	+0.01	+0.02
-1	-28.4	-0.36	-0.28	-0.01	-0.02
+2	+82.5	+1.22	+1.10	+0.04	+0.08
-2	-74.7	-1.10	-0.70	-0.04	-0.05
+3	+109.0	+1.96	+1.90	+0.07	+0.14
-3	-117.0	-2.01	-0.83	-0.07	-0.06
+4	+139.0	+3.02	+2.43	+0.11	+0.18
-4	-147.0	-2.86	-1.24	-0.10	-0.09
+5	+160.0	+3.86	+2.87	+0.13	+0.21
-5	-166.0	-3.84	-1.86	-0.13	-0.14
+6	+177.0	+4.99	+3.39	+0.17	+0.25
-6	-159.0	-4.77	-2.14	-0.17	-0.16
+7	+247.0	+9.72	+5.78	+0.34	+0.42
-7	-222.0	-9.79	-5.18	-0.34	-0.38
+8	+264.1	+15.81	+8.49	+0.55	+0.62
-8	-270.6	-15.32	-8.04	-0.54	-0.59
+9	+339.8	+30.50	+18.91	+1.07	+1.38
-9	-317.8	-31.02	-17.91	-1.08	-1.31
+10	+291.4	+40.49	+30.71	+1.42	+2.24
-10	-280.8	-40.60	-27.84	-1.42	-2.03
+11	+209.2	+50.51	+40.60	+1.77	+2.96
-11	-248.3	-51.22	-39.30	-1.79	-2.87
+12	+181.4	+60.56	+50.16	+2.12	+3.66
-12	-186.7	-61.44	-51.35	-2.15	-3.75
+13	+110.0	+70.31	+61.51	+2.46	+4.49
-13	-	-	-	-	-

Similar to the previous half-cycle, popping noises were heard from the stretching lateral CFRP reinforcement of the north column in the positive tenth cycle. Inclined cracks were monitored at the mid-height of the first story columns at this stage. The rectangular CFRP reinforcement at the lower south corner of the first story infill started to debond under compressive stresses.

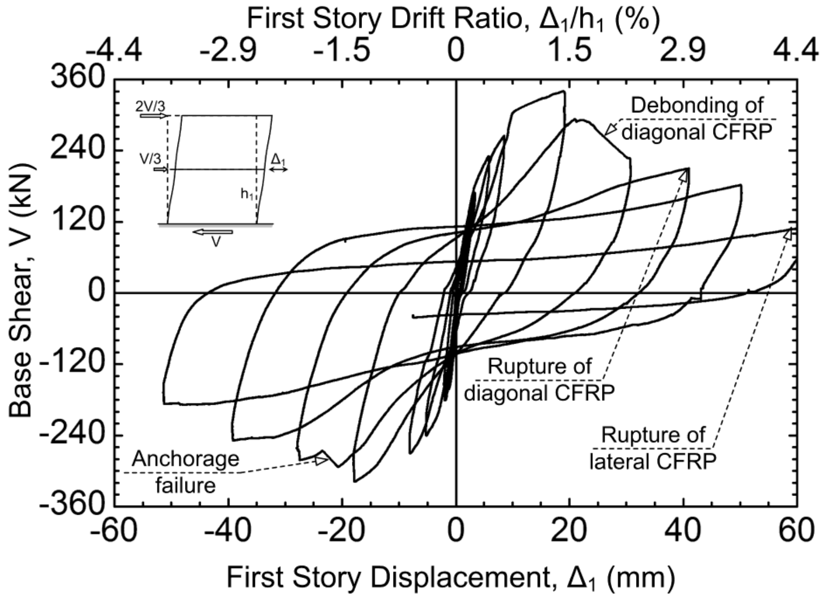

Figure 4. 60 First story shear force vs. displacement / drift ratio curve of specimen LSTR-1/2

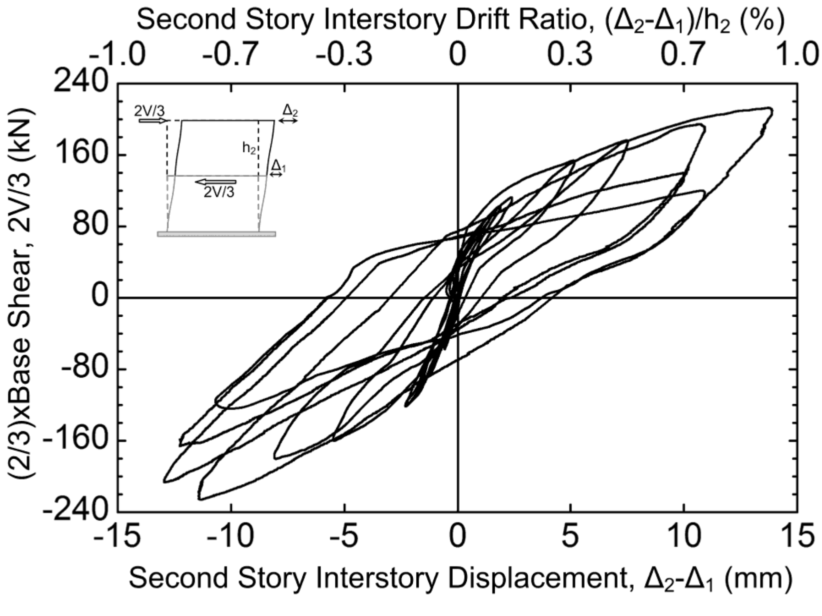

Figure 4. 61 Second story shear force vs. inter-story displacement / drift ratio curve of specimen LSTR-1/2

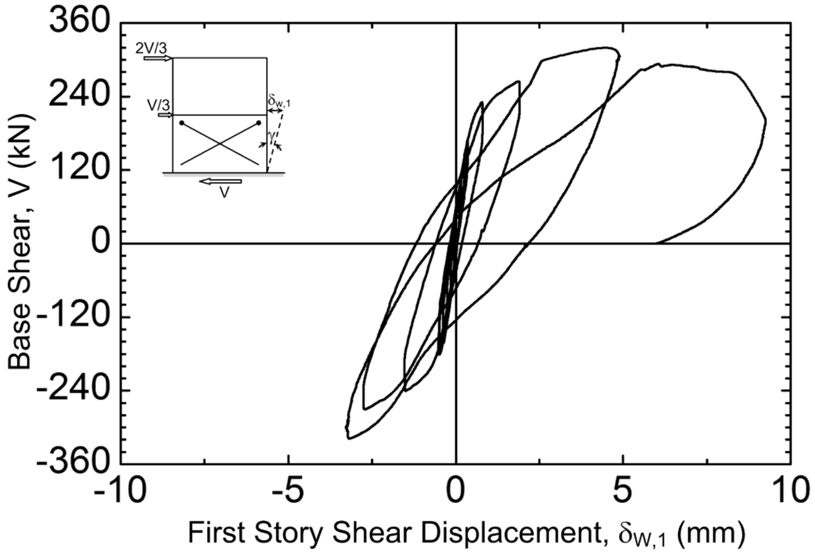

Figure 4. 62 Shear force vs. shear displacement curve for the first story infill of specimen LSTR-1/2

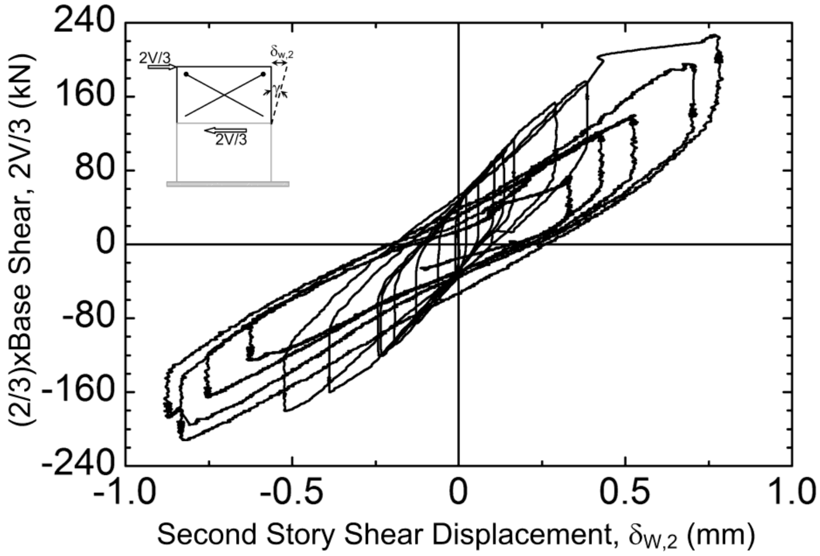

Figure 4. 63 Shear force vs. shear displacement curve for the second story infill of specimen LSTR-1/2

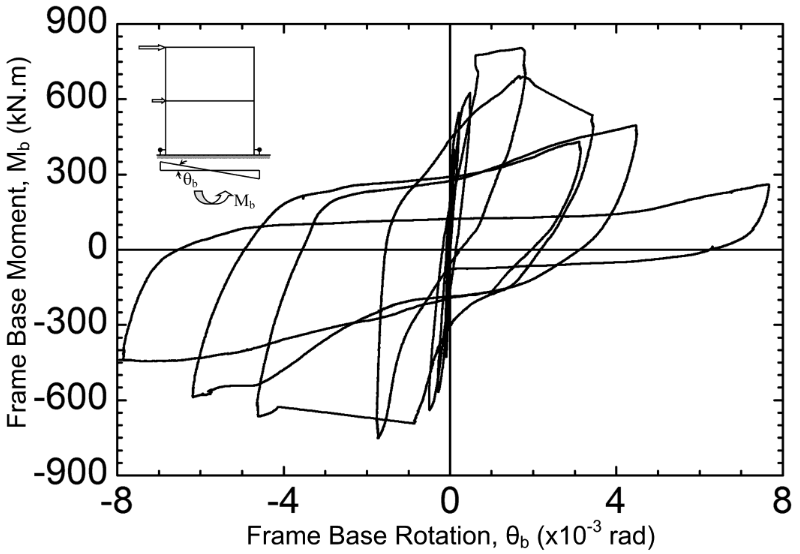

Figure 4. 64 Frame base moment vs. rotation curve of specimen LSTR-1/2

During the negative tenth cycle, some of the anchor dowels failed with a popping noise. These dowels had been connecting the diagonal CFRP reinforcement of the first story infill to the RC frame members on the upper north side. Following this, CFRP in the lap-splice region of the second story of the specimen at the back face ruptured along the first story north column-HCT wall boundary. It should also be noted that one of the dial gages on the first story infill fell off during the tenth cycle, terminating further recording of the shear displacements for this wall (Figure 4.62).

After the failure of the anchor dowels and rupture of the diagonal CFRP at the back face, the separation between the first story infill and column became critical in the next negative cycle. Some of the anchor dowels connecting the diagonal CFRP to RC frame members at the back face of the frame also failed in the eleventh cycle. Furthermore, both diagonal CFRP layers debonded under compression at the lower corners of the first story infill where the HCT wall crushed afterwards. This event, which occurred at both faces of the frame, totally ceased the contribution of the diagonal CFRP layers to the lateral capacity of the frame.

Towards the end of the test, the damage concentrated on the first story columns as shear cracks. The cover concrete at the upper corner of the south column crushed and the column bar buckled in the negative twelfth cycle under compression. In the last cycle, the lateral CFRP reinforcement of the first story north column ruptured and the cover concrete crushed. The test was terminated after the positive thirteenth cycle, when the maximum lateral load was about 30% of the ultimate capacity. The damage pattern leading to failure of the specimen is presented in Figure 4.65.

(a) general view after the test

(b) failure of the anchor dowels at the back face

(c) de-bonded diagonal CFRP and shear crack on the column

(d) shear crack on the column

(e) buckling of the rebars below the beam-colum joint

Figure 4. 65 Failure pattern of specimen LSTR-1/2

4.4 SUMMARY OF FRAME TEST RESULTS

In general, first cracks were observed in the form flexural cracks at different heights of the first story columns; mostly at lap-splice regions in frames having lapped bars. These were accompanied with the diagonal cracks on the first story infill in Series-L frames in both groups. In case of reference frames having non-strengthened infill walls, corner crushing started immediately after attaining the ultimate capacity. Towards the end of the test, this led to severe crushing at the corners of HCT infill in reference specimens of Series-L; however this crushing was not very significant in Series-N reference frames. It may be stated that this difference demonstrates a more superior contribution of infill in squat frames through a strut mechanism. A comparison of the base moment vs. base rotation curves presented for bare and infilled reference frames in both series of Group-I (Figure 4.3 vs. 4.9, and Figure 4.25 vs. 4.31) points out a considerable reduction in the base rotations with the application of infill walls in Series-L. However, such a reduction, which might be caused by the restraining effect of infill walls, could not be observed in Series-N. The crushing of the corner regions did not only terminate the contribution of infill walls, but also evoked wide shear cracks at the upper regions of first story columns and beam-column joints. This may be explained with re-distribution of the shear force between frame and infill after corner crushing. Formation of a short column phenomena at these regions is also believed to stimulate these shear cracks in Series-L.

The strengthening of frames successfully limited the damage on the walls. Again especially in Series-L, this resulted in prolonged contribution of infill walls together with a considerable amount of lateral shear carried by diagonal CFRP sheets connected to the frame. In case of squat frames, this continued up to debonding and consequent rupturing of diagonal CFRP fabrics, after which the same damage pattern as in reference frames was observed by demonstrating considerable strength and stiffness decay. The effectiveness of diagonal CFRP sheets in Series-L specimens may also be observed through CFRP strains provided in Appendix B. As presented in Figures B.2, B.3 and B.5, the ultimate CFRP strain experienced at critical locations of Series-L specimens reached approximately 0.3 percent. In specimen LSTR-L-1/3, which did not experience any anchorage failure, higher CFRP strain levels could be attained, compared to LSTR-C-1/3 and LSTR-1/2. On the other hand, in slender (Series-N) frames, the ultimate CFRP strain remained below 0.1 percent, as shown in Figures B.1 and B.4. This is another observation indicating less effective contribution of the diagonal CFRP sheets in narrow frames. Moreover, the applied strengthening altered the damage pattern in slender specimens, which resulted in accumulated damage at the bottom of the first story columns. Therefore, the specimens NSTR-L-1/3 and NSTR-1/2 which had lapped longitudinal bars at these regions experienced extreme bond-slip deformations. This was also obvious in Figures 4.15 and 4.52 with increased base rotations compared to their reference frames with infill walls. It should also be noted that the CFRP wrapping did not provide the required confinement effect for reducing the bar slip deformations of plain bars and therefore, it is not suitable for the confinement of lap-splice regions where plain bars are used (Özcan et al., 2008). On the other hand, in specimen NSTR-W-1/3, the applied welding restrained bond-slip deformations and corresponding base rotations significantly (Figure 4.21).

CHAPTER 5

DISCUSSION OF TEST RESULTS

5.1 GENERAL

The results of RC frame tests are discussed in this chapter. In Section 5.2, the frame test results are evaluated in terms of strength, stiffness, drift, ductility and energy dissipation characteristics; so as to assess the seismic response of these frames. Besides, the strength and stiffness degradation of the frame specimens as a result of cyclic load reversals are discussed in this chapter. Lastly, the scale effect is investigated by a comparison of the companion specimens in both test groups in terms of ultimate lateral strength and energy dissipation characteristics.

5.2. EVALUATION OF FRAME TEST RESULTS

The basic characteristics of RC frames considered in this section are obtained through analysis of the hysteretic base shear-top displacement graphs and the backbone envelope curves derived from these graphs. These graphs are presented in Figure 5.1 for comparison purposes. The curves that belong to different sub-groups are shown with close load and displacement scales, insofar as they are possible. The high level of discrepancies between ultimate load and displacement levels of frames having various scale and aspect ratios precluded using one common scale for all specimens. The envelope curves are generated by connecting the peak points of the former hysteresis curves and shown in Figure 5.2 for each sub-group of specimens.

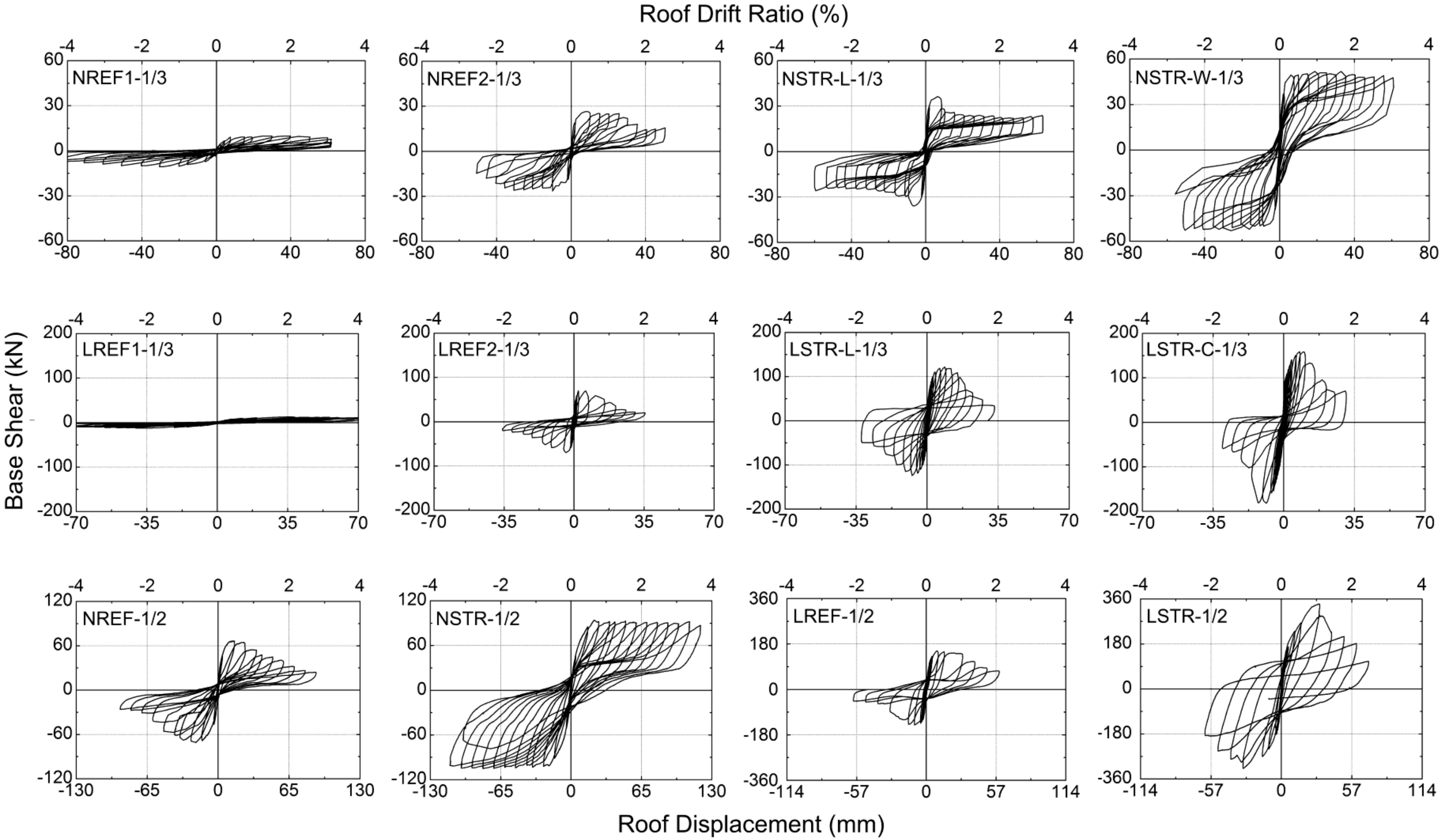

Figure 5. 1 Base shear-roof displacement hysteretic curves of all RC frames

5.2.1 Strength

In order to evaluate the efficiency of strengthening applied in different types of frames, primarily the strength characteristics of the frames at different stages of loading are considered in this section. The ultimate lateral loads and the post-peak strength deterioration of specimens are intended to be compared for this purpose. The maximum lateral loads that could be resisted by the specimens during forward and backward loading cycles, together with the corresponding roof displacements are given in Table 5.1. Besides, the ratio of ultimate capacity of the specimens relative to that of reference frames with non-strengthened infill walls in each sub-group are provided in the same table.

In Group-I, as may also be observed in Figures 5.2.a and 5.2.b, the comparison of the first and second reference specimens in both series points out a significant increase in the lateral load (V_{max}) by contribution of the plastered HCT infill walls. This increase was 2.7 folds in Series-N and 5.6 folds in the case of Series-L. Furthermore, the maximum capacity was attained at considerably lower displacements (Δ_{max}) in the second reference specimens; emphasizing the significant increment in lateral rigidity provided by infill walls (Table 5.1).

In both test groups, the applied CFRP strengthening resulted in further increase in the ultimate lateral load capacity of frames having lap-splices. In Group-I, the ultimate load capacities of NSTR-L-1/3 and LSTR-L-1/3 were 1.35 and 1.74 times greater than NREF2-1/3 and LREF2-1/3, respectively.

In Group-II, the ratio between the ultimate load capacities of strengthened and reference frame specimens were 1.42 and 2.23 in Series-N and Series-L, respectively. It should again be noted that all frames in Group-II had lap-splices and the reference frames had non-strengthened infill walls.

Table 5. 1 Characteristic lateral strength values of RC frame specimens

Specimen			Forward Loading			Backward Loading		
			Ultimate Lateral Load, V_{max}^{+} (kN)	Change in $V_{max,i}^{+}$ compared to that of ref. frame with infills (kN/kN)	Roof Displ. at Ult. Load, Δ_{max}^{+} (mm)	Ultimate Lateral Load, V_{max}^{-} (kN)	Change in $V_{max,i}^{-}$ compared to that of ref. frame with infills (kN/kN)	Roof Displ. at Ult. Load, Δ_{max}^{-} (mm)
Group-I	Series-N	NREF1-1/3	9.8	0.37	29.7	-10.6	0.40	-30.4
		NREF2-1/3	26.6	1.00	10.3	-26.6	1.00	-9.9
		NSTR-L-1/3	36.0	1.35	8.3	-35.8	1.35	-9.2
		NSTR-W-1/3	51.8	1.95	15.7	-51.6	1.94	-14.9
	Series-L	LREF1-1/3	12.8	0.18	38.2	-12.3	0.18	-40.2
		LREF2-1/3	70.0	1.00	2.2	-69.7	1.00	-4.2
		LSTR-L-1/3	122.0	1.74	8.6	-124.0	1.78	-7.3
		LSTR-C-1/3	160.0	2.29	7.8	-176.6	2.53	-10.0
Group-II	Series-N	NREF-1/2	66.3	1.00	15.0	-70.4	1.00	-25.0
		NSTR-1/2	94.0	1.42	25.6	-101.9	1.45	-25.3
	Series-L	LREF-1/2	152.4	1.00	9.8	-140.0	1.00	-9.9
		LSTR-1/2	339.8	2.23	30.5	-317.8	2.27	-31.0

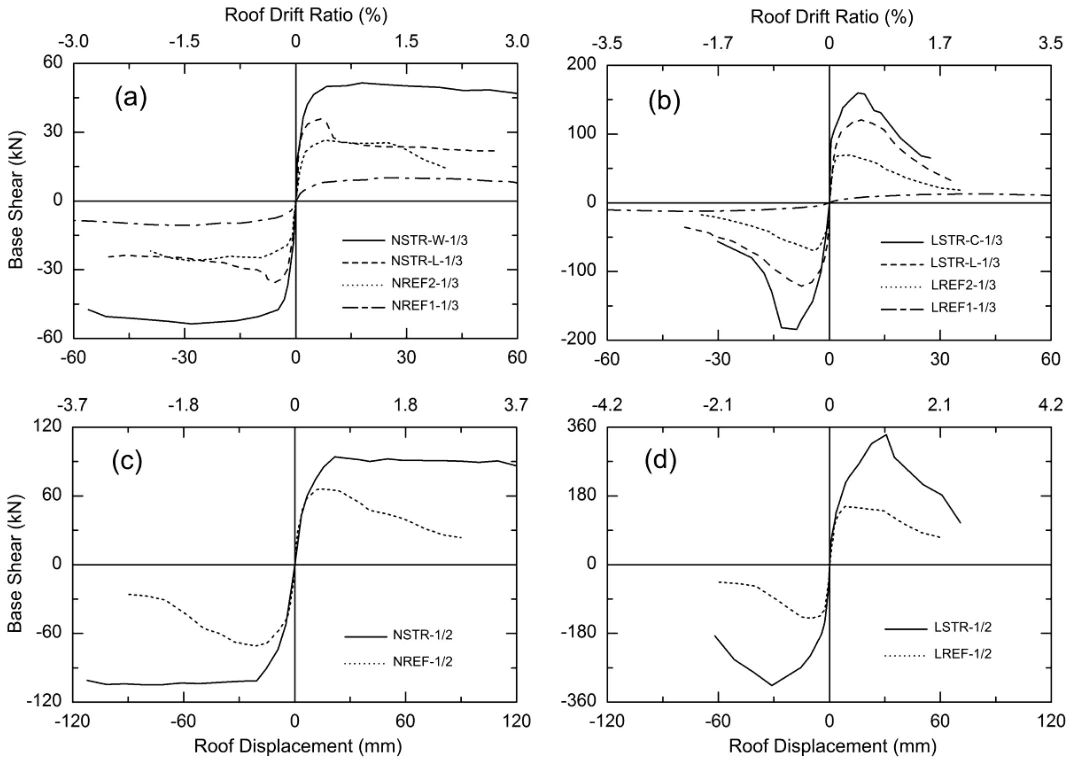

Figure 5. 2 Response envelope curves of (a) Group-I, Series-N; (b) Group-I, Series-L; (c) Group-II, Series-N; (d) Group-II, Series-L specimens

In Group-II, the ratio between the ultimate load capacities of strengthened and reference frame specimens were 1.42 and 2.23 in Series-N and Series-L, respectively. It should again be noted that all frames in Group-II had lap-splices and the reference frames had non-strengthened infill walls.

As a result, it can be deduced that the proposed rehabilitation technique increases the base shear capacity of the frames considerably irrespective of the aspect and scale ratio; however this increase is more remarkable in Series-L.

The test results of Group-I specimens shown in Table 5.1 indicate that lap splices of the column bars had an unfavorable influence on the ultimate load capacity of the specimens. The increase in the capacity attributed to the welding of lapped bars at the two exterior faces of the first story columns in specimen NSTR-W-1/3 was more than 40 percent, compared to specimen NSTR-L-1/3. The superior behavior of

NSTR-W-1/3 relative to other specimens in this series is also obvious in Figures 5.1 and 5.2.a. On the other hand, in Series-L of Group-I, the use of continuous column longitudinal bars in specimen LSTR-C-1/3 resulted in a capacity increase of 30 percent with respect to LSTR-L-1/3.

The post-peak behavior of slender and squat frames (i.e. specimens in Series-N and Series-L, respectively) had some major differences in terms of strength degradation. As seen in Figures 5.1 and 5.2, in each group, Series-L frames displayed significant strength deterioration after the ultimate load level. In this series, the contribution of strengthened/non-strengthened HCT infill walls through strut and tie actions were considerable in terms of ultimate strength. However, substantial damage on the HCT infill (i.e. corner crushing and wide diagonal cracks) yielded a decrease in strength after the ultimate capacity point of reference specimens with infill walls. The applied strengthening in squat frames shifted the onset of strength deterioration (Δ_{max} values in Table 5.1). Nevertheless, the degradation in strength occurred in the strengthened specimens along with the rupture of diagonal CFRP fabrics.

On the other hand, in Series-N, the contribution of infill walls to the lateral resistance of the frame was not as efficient as in squat walls. Therefore, majority of the specimens in Series-N did not experience strength deterioration after the peak point due to damaging of the walls (Figures 5.1 and 5.2). Particularly, the strengthening applied in slender frames engendered a concentration of damage at the lap-splice regions of the first story columns through increased flexural demands.

5.2.2 Stiffness

The initial stiffness values of frames, as an indicator of resistance against applied lateral loads in the elastic range, are appraised herein. Besides, the lateral stiffness degradation of the specimens, as a result of cyclic loading and consequent progressive damage formations, are compared.

The initial stiffness values of the specimens are estimated from the forward envelope curves shown in Figure 5.2 by means of two different approaches. In the first one, slope of the line which is tangent to the initial elastic portion is calculated (i.e. tangential stiffness, $K_{ini,1}^{+}$). In the latter case, the initial stiffness is assumed to be the slope of the line which connects the point corresponding to 60 percent of the ultimate load on the ascending part of the curve to the origin (i.e. secant stiffness, $K_{ini,2}^{+}$). These two approaches are illustrated in Figure 5.3. The resulting initial stiffness values are shown in Table 5.2. The ratio of initial stiffness of each specimen in different sub-groups to that of reference specimen with infill walls in that sub-group are also presented in the same table.

In general, the results obtained using the two approaches are close (slightly higher for the first approach). However, in some strengthened specimens, remarkable cracking up to 60 percent of the ultimate capacity lead to lower initial stiffness values obtained by the second approach. The secant stiffness values of the specimens (i.e. second approach) are mainly considered for comparison purposes. Yet, the results of first approach are utilized as supplementary information in order to avoid any possible misleading evaluation.

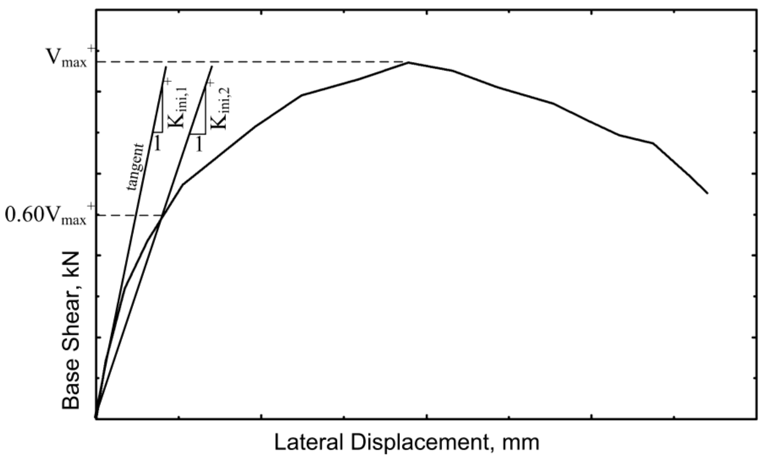

Figure 5. 3 Illustration for the estimation of initial stiffness

In Group-I, the addition of plastered infill walls resulted in an extreme amount of increase in initial stiffness, which was more prominent in Series-L as seen in Table

5.2. In the same group, strengthening applied in Series-L (specimen LSTR-L-1/3) did not alter the initial stiffness of the frame. On the other hand, a significant increase in initial stiffness was observed due to the use of continuous column longitudinal reinforcement in LSTR-C-1/3 compared to LSTR-L-1/3 (i.e. around 92 percent increase). In Series-N of Group-I, the initial stiffness increased nearly 65 percent due to the strengthening of the frame having lap splices (NSTR-L-1/3). This increase was at a level of 93 percent in the case of specimen NSTR-W-1/3. It should be noted that the stiffness increases in specimens NSTR-W-1/3 and LSTR-C-1/3 were most likely due to the elimination of the loss of lateral stiffness resulting from column plain bar slip deformations.

Table 5. 2 Initial stiffness values of specimens

Specimen	First Approach		Second Approach	
	Initial stiffness, $K_{ini,1}^{+}$ (kN/mm)	Change in $K_{ini,1}^{+}$ compared to that of ref. frame with infills	Initial stiffness, $K_{ini,2}^{+}$ (kN/mm)	Change in $K_{ini,2}^{+}$ compared to that of ref. frame with infills
NREF1-1/3	2.4	0.16	1.5	0.14
NREF2-1/3	14.0	1.00	10.9	1.00
NSTR-L-1/3	20.0	1.43	18.0	1.65
NSTR-W-1/3	31.6	2.26	21.0	1.93
LREF1-1/3	1.4	0.03	0.9	0.02
LREF2-1/3	49.5	1.00	49.5	1.00
LSTR-L-1/3	52.0	1.05	52.5	1.06
LSTR-C-1/3	162.0	3.27	95.0	1.92
NREF-1/2	12.8	1.00	12.8	1.00
NSTR-1/2	11.8	0.92	9.4	0.74
LREF-1/2	40.0	1.00	32.0	1.00
LSTR-1/2	47.0	1.18	27.2	0.85

In Group-II, a higher nonlinearity was observed at about 60 percent of the ultimate capacity of strengthened frames due to pre-mentioned reasons. Therefore, the secant stiffness values of these specimens resulted to be lower than those of the corresponding reference frames in each series. However, the same comparison in terms of tangential stiffness leads to a conclusion designating an insignificant change in the initial stiffness. For Series-L, this further supports the former result which asserts that the strengthening alone did not change the initial stiffness in Series-L. This observation indicated that the CFRP intervention on squat HCT infill walls increased the base shear capacity of the system without increasing the seismic demand, as the stiffness characteristics of the building remain almost unchanged.

As the frames which are subjected to cyclic loading devolve into inelastic range along with the experienced damage, the stiffness at each loading cycle degrades. In this study, the stiffness at each cycle is defined as the slope of line connecting the positive and negative peak points of that loading cycle as illustrated in Figure 5.4 (i.e. peak-to-peak stiffness). The stiffness degradation of the frames represented by the normalized peak-to-peak stiffness vs. roof drift ratio curves is presented in Figure 5.5. The normalization was provided by dividing peak-to-peak stiffness values to the one obtained in the first cycle.

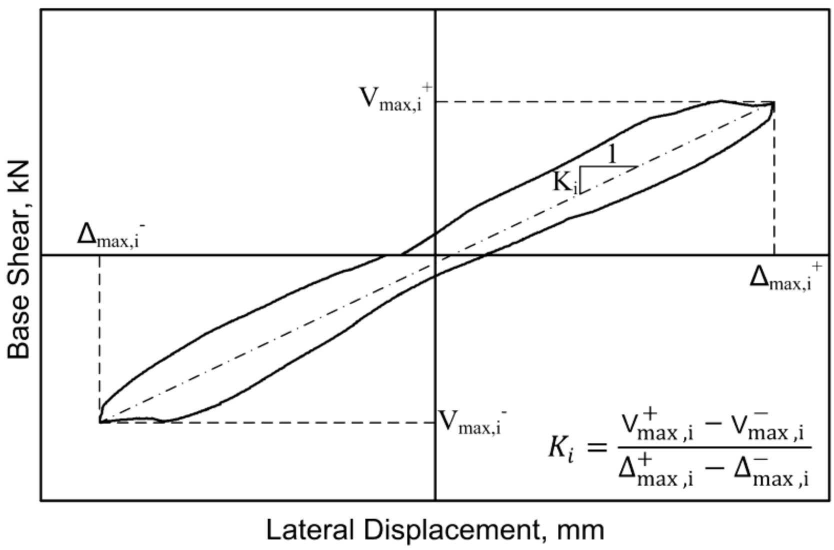

Figure 5. 4 Illustration for the calculation of stiffness in each loading cycle

As a general observation, it may be stated that sudden stiffness degradation was observed up to a drift ratio corresponding to approximately ultimate lateral load capacity of all frames. After this point, the degradation curves tend to stabilize with increasing drift levels.

By a comparison of the degradation curves of bare and infilled frames in Group-I, one may state that the additional rigidity provided by infill walls also yielded a steeper degradation of stiffness through damage on the walls. This difference is more obvious in case of Series-L, where the infill wall contribution was much more significant. In strengthened frames, diagonal CFRP reinforcement prevailed excessive damaging of the infill. Thus, in both groups, degradation of stiffness was more gradual in strengthened specimens in comparison with the companion reference frames with infill walls. The only exception for this observation was specimen NSTR-L-1/3. It should be remembered that this frame experienced extreme bond-slip deformations at the first story lap-splice regions as a result of altered damage pattern after strengthening.

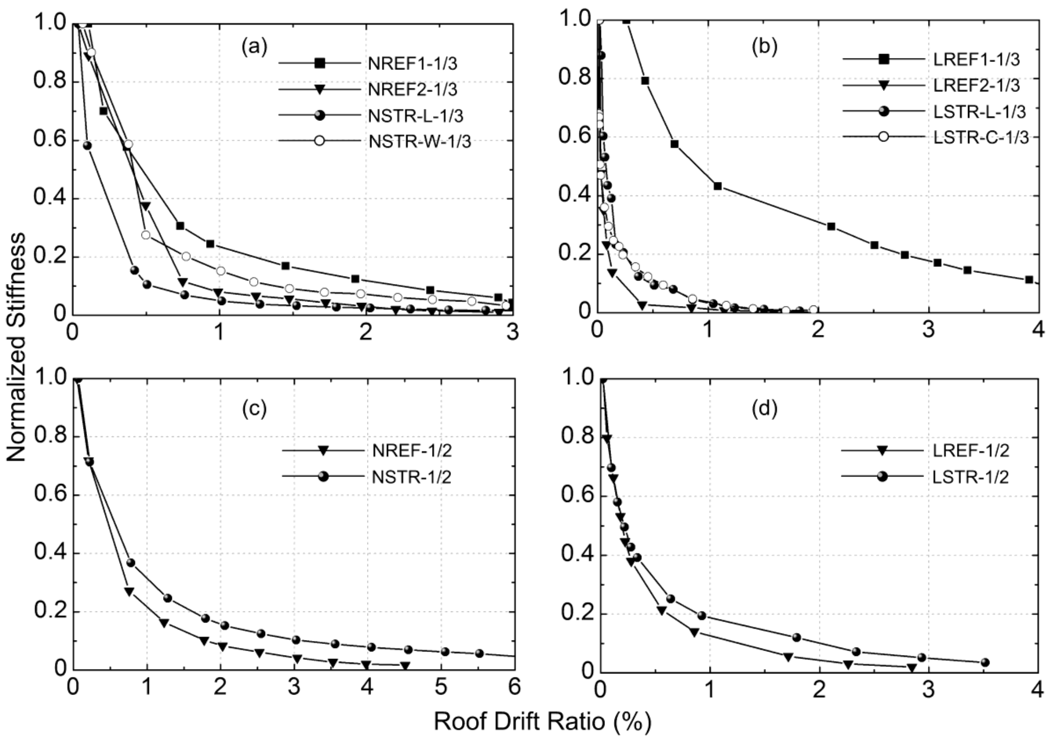

Figure 5. 5 Stiffness degradation curves for (a) Group-I, Series-N; (b) Group-I, Series-L; (c) Group-II, Series-N; (d) Group-II, Series-L specimens

In Group-I, the strengthened Series-L specimens (LSTR-L-1/3 and LSTR-C-1/3), which displayed a similar behavior in terms of damage pattern at approximately similar drift levels, also exhibited a close degradation in stiffness (Figure 5.5.b).

5.2.3 Energy Dissipation

The amount of energy dissipated by a structure through inelastic actions under dynamic excitations is of prime importance in terms of its response to these excitations. Therefore, the energy dissipation capacity of the frame specimens under lateral cyclic loading are compared to evaluate the efficiency of the applied strengthening method. As illustrated in Figure 5.6, the energy dissipated by the frame during each hysteresis loop is assumed and calculated to be the area enclosed by that loop. The resulting cumulative dissipated energy vs. roof drift ratio relationships of specimens are presented in Figure 5.7. The total amounts of energy dissipated by the frames are shown in Table 5.3. Besides, the ratio of these values with respect to that of reference frame having non-strengthened infill walls in each sub-group are also provided in Table 5.3. It is worth noting that the energy values presented below are in units of "kN.m" or "kilojoules".

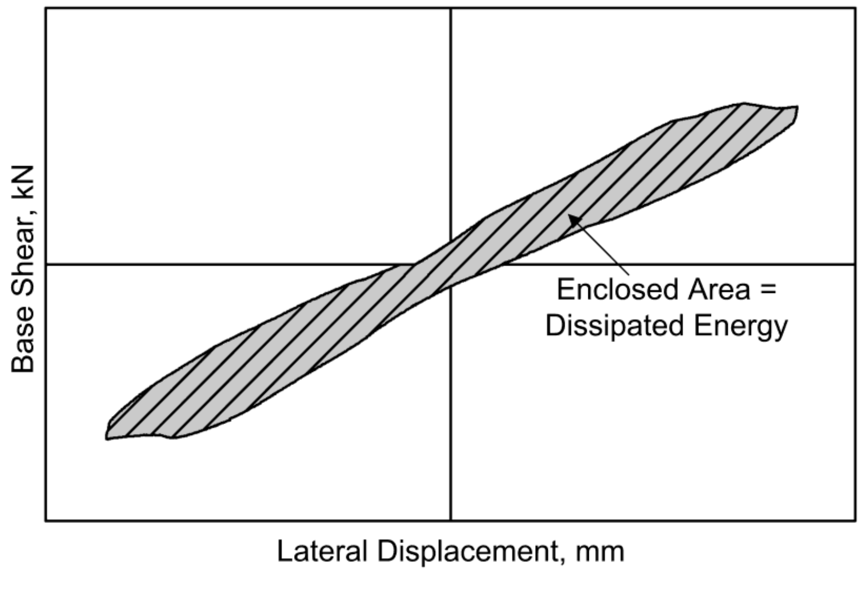

Figure 5. 6 The energy dissipated by the frame in one cycle

In both series of Group-I, the addition of plaster applied HCT infill walls alone increased the energy dissipation considerably. The total energy dissipated by the reference frames with non-strengthened infill walls are nearly twice compared to bare frames (Table 5.3). A major amount of this increment may be attributed to the energy absorbed by the HCT walls through diagonal cracks and crushing at the corner regions.

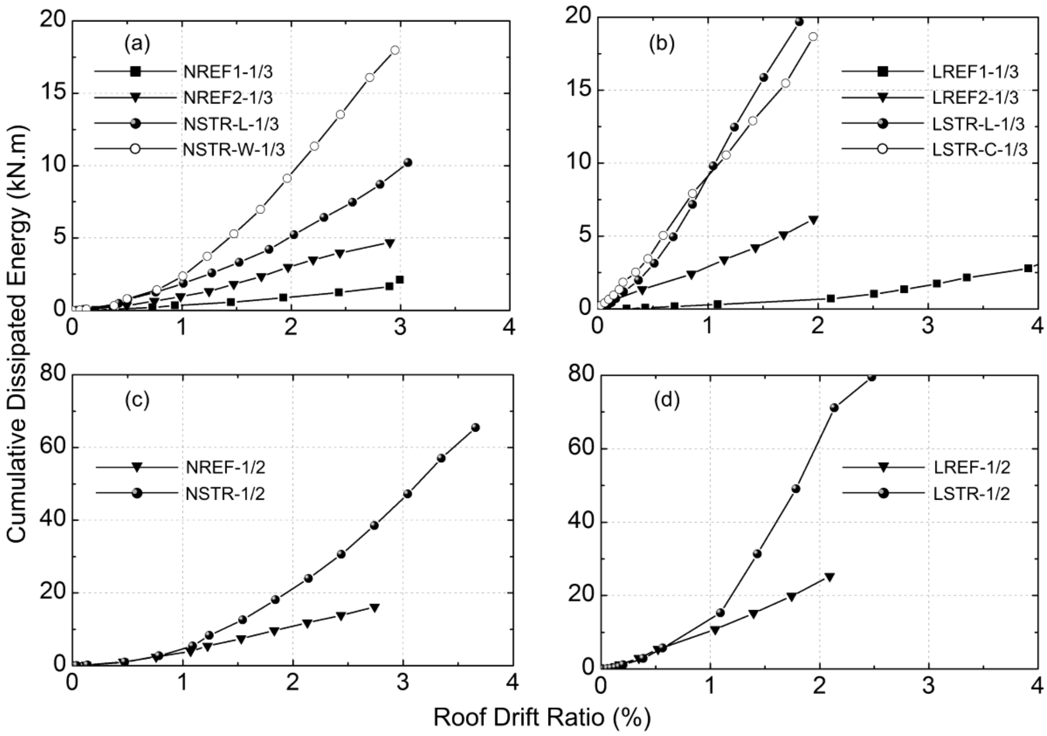

Figure 5. 7 Cumulative dissipated energy curves for (a) Group-I, Series-N; (b) Group-I, Series-L; (c) Group-II, Series-N; (d) Group-II, Series-L specimens

As seen in Figure 5.7, the strengthening implemented in Series-N of the first group (NSTR-L-1/3) again provided a significant amount of increase in the energy dissipation. Since the infill walls remained almost intact in this frame, this may substantially be related to the confinement of the lap-splice regions and beam-column joints where the formation of plastic hinges would be expected. Much further increment (i.e. about 75 percent in terms of total energy) could be achieved in specimen NSTR-W-1/3 compared to NSTR-L-1/3; although energy dissipation characteristics of these two frames were similar up to nearly 0.5 percent roof drift level. It may be concluded that the containment of plain bar slip by means of applied welding lead to a superior response also in terms of energy absorption capacity.

As observed in Figure 5.7, both strengthened specimens of Series-L in Group-I displayed a similar behavior in terms of dissipated energy. The increased lateral load capacity through an efficient utilization of the diagonal CFRP sheets (i.e. tension ties) in squat walls lead to an increment in the total dissipated energy more than three times, compared to specimen LREF2-1/3 (Table 5.3).

Table 5. 3 Total amounts of dissipated energy

Specimen	*Total Dissipated Energy, kN.m*	*Change in energy diss. compared to that of ref. frame with infills*
NREF1-1/3	2.11	0.45
NREF2-1/3	4.68	1.00
NSTR-L-1/3	10.21	2.18
NSTR-W-1/3	17.97	3.84
LREF1-1/3	3.43	0.56
LREF2-1/3	6.16	1.00
LSTR-L-1/3	19.68	3.19
LSTR-C-1/3	18.65	3.03
NREF-1/2	16.13	1.00
NSTR-1/2	65.49	4.06
LREF-1/2	25.22	1.00
LSTR-1/2	79.50	3.15

In both series of Group-II, the energy dissipation characteristics of the reference and strengthened frames were close during early drift levels (Figure 5.7). However, the energy dissipation curves of these specimens diverge progressively with the increasing drift ratio. This was most probably due to prevailing effects of CFRP reinforcements (diagonal fabrics on the HCT infill and lateral confinement at the column ends) on the response of strengthened specimens. The total energy dissipation capacities of specimens NSTR-1/2 and LSTR-1/2 were approximately four and three times that of reference frames in Series-N and Series-L, respectively. It should be noted that the larger scale of Group-II specimens engendered a considerable increase in the dissipated energy, which was around four times compared to companion specimens in Group-I (more than six times in case of NSTR-1/2 with respect to NSTR-L-1/3).

5.2.4 Drift Characteristics

5.2.4.1 Global Drift

The global lateral drift characteristics of the specimens were evaluated through an observation of the envelope curves shown in Figure 5.2. The most remarkable inference for Group-I specimens was that, except the two strengthened specimens in Series-N, all other frames displayed a behavior tending to a bare frame response at large displacement amplitudes. Specimen NSTR-L-1/3 experienced a sudden decrease in both strength and stiffness after the peak capacity. This loss of strength and stiffness may be associated to the large bond-slip deformations at the base of the first story columns. Eventually, at a load level corresponding to 60 percent of the ultimate load, the specimen continued to undergo large displacements without a new downfall in strength. In specimen NSTR-W-1/3, welding of the lapped reinforcement prevented the large bond-slip rotations, which engenders the most ductile response among all other frames. However, the load-displacement hysteretic curves of NSTR-W-1/3 displayed some pinching (Figure 5.1) which may be the result of partial welding of the lapped reinforcement. It should be reminded that only two of the four column longitudinal bars were welded in this frame. Similar conclusions can be deduced for Group-II specimens. All specimens, except strengthened frame in Series-N, experienced progressive strength degradation with increasing drift levels after the ultimate load level.

5.2.4.2 Inter-story Drift

The inter-story drift ratio can be defined as the relative difference of the displacements at the top and bottom of a story divided by the height of that story. Limiting inter-story drift is important in terms of decreasing non-structural/structural damage and controlling second order effects. Therefore, limit values are defined by different codes and technical reports. In ATC-40 (ATC, 1996), the story drift ratio limits are classified considering different performance levels; where taken as 2.0 percent for “Life Safety” level. ASCE/SEI Standard 41-06 (ASCE, 2007) defines allowable story drift ratios of infill walls in case of a relatively weak frame at “Life Safety” level as 0.4, 0.3 and 0.2 percent, corresponding to infill width to height ratios of 0.5, 1.0 and 2.0, respectively. In TEC 2007 (The Ministry of Public Works and Settlement, 2007), the inter-story drift ratio limit for the “Life Safety” level is defined as 0.35 percent in the case of reinforced infill walls having an aspect ratio between 0.5 and 2.0.

By a comparison of the inter-story drift ratio curves presented in Chapter 4, it may be stated that the first story drift ratios are more critical compared to those of second stories. Therefore, only the first story drift ratios are considered in this section. The first story drift ratio vs. base shear curves of the frames with infill walls are shown in Figure 5.8. The limiting drift ratios as proposed by ATC-40 and TEC are also shown on each figure. Besides the failure states of CFRP reinforcement are indicated on the graphs in strengthened frames.

In order to evaluate the effect of strengthening on the story drift characteristics of frames, the normalized first floor drift ratios corresponding to 15 percent decrease in the ultimate capacity ($0.85V_{max}$) are presented in Figure 5.9, individually for each sub-group. The normalization was performed with respect to the reference frames with infill walls in each sub-group.

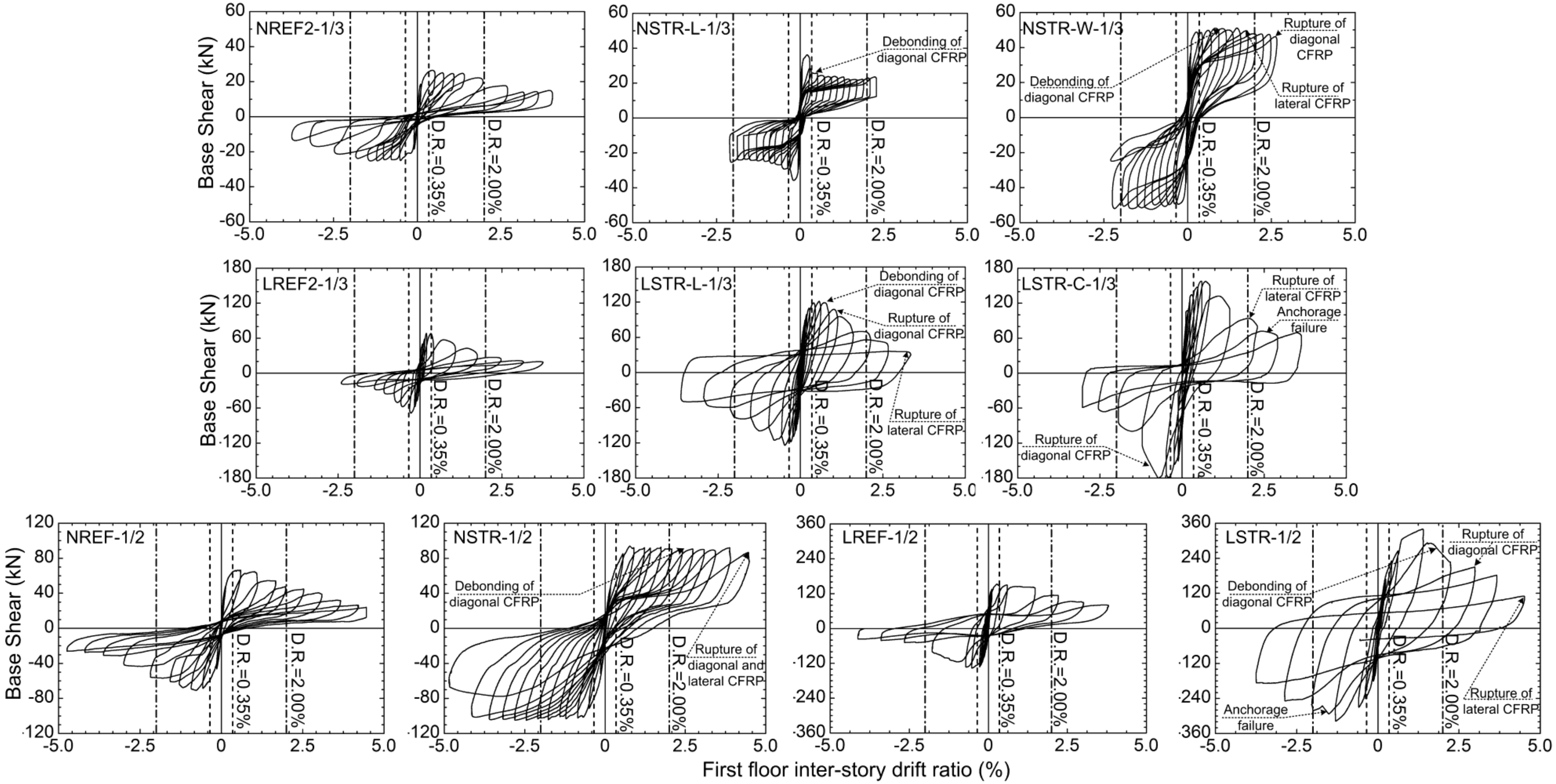

Figure 5. 8 The first floor drift ratio vs. base shear curves of frames with infills

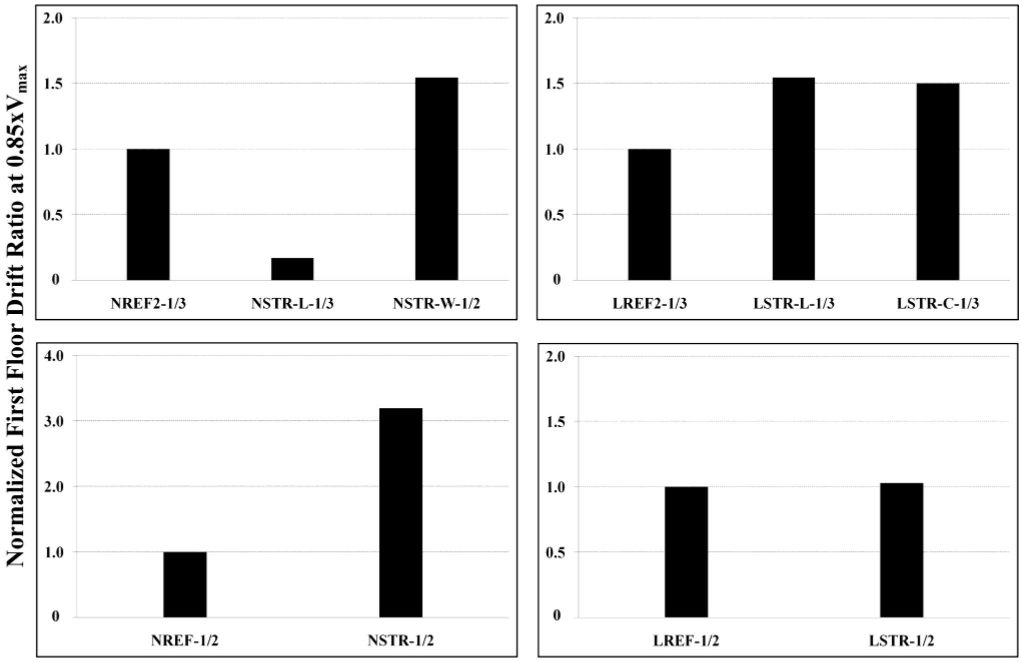

Figure 5. 9 The normalized first floor drift ratios of the frames corresponding to 85 percent of the ultimate capacity

As may be observed in Figure 5.8, the inter-story drift limit proposed by TEC for the reinforced infill walls remain at the vicinity of the ultimate capacity point. This characteristic limit value is assessed more thoroughly in the next chapter with the assistance of analytical results.

In ATC-40, it is stated that the lateral resistance of a building system should not degrade more than 20 percent of the maximum resistance to sustain its stability (ATC, 1996). This ratio was taken as 15 percent in order to be compatible with the ductility definition of Section 5.2.5. As shown in Figure 5.9, the normalized drift ratios of the frames at $0.85V_{max}$ refer to the increased story drift characteristics provided by strengthening, in general. The only exception was specimen NSTR-L-1/3, due to the reasons explained in the previous section. Besides, the enhancement in LSTR-1/2 may be neglected. As mentioned previously, this frame experienced a more abrupt strength reduction after the ultimate capacity had been attained. The significant anchor dowel failures which were observed during the test of this specimen may be the major reason of this reduction. The anchor dowel failures might be related to the poor workmanship. Therefore, it is emphasized that special care should be paid while implementing anchorages. Besides, increasing the number of anchor dowels would also be beneficial in terms of improving the post-elastic behavior of this frame.

5.2.5 Ductility

Ductility is defined as the ability of the structure to sustain deformations beyond the elastic limit without significant strength degradation which may lead to failure. In order to quantify ductility, the forward cycle envelope curves of the frame specimens (Figure 5.2) are idealized as bi-linear curves. This is achieved by using an iterative process that is based on equal area concept as shown in Figure 5.10 (Dimova and Negro, 2005). The elastic portion of the bi-linear curves is assumed to represent the secant stiffness of the specimens ($K_{ini,2}^{+}$) as explained in Section 5.2.2. The following horizontal portion, which represents the post-elastic response, proceeds up to $\Delta_{0.85}^{+}$ (i.e. the displacement level corresponding to the 15 percent decrease in the ultimate lateral load capacity, $0.85V_{max}^{+}$). This horizontal portion is leveled so as to result in approximately equal gained and lost areas with respect to the original curve up to $\Delta_{0.85}^{+}$. The yield point (i.e. yield displacement, Δ_y^{+} and yield load V_y^{+}) is assumed as the point joining the elastic and horizontal portions of the idealized curve. The ratio between the estimated values of $\Delta_{0.85}^{+}$ and Δ_y^{+} is defined as the ductility of the frame specimens. The resulting displacement and ductility values and, the change in ductility with respect to reference frame in each sub-group are presented in Table 5.4.

In Group-I Series-L, strengthening of the frame having lap splices (LSTR-L-1/3) did not increase the system ductility. However, the use of continuous longitudinal column reinforcement in addition to CFRP implementation in specimen LSTR-C-1/3 leads to nearly 60 percent increase in the ductility ratio when compared with LREF2-1/3 and LSTR-L-1/3. On the other hand, in Group-I Series-N, the ductility ratio of the strengthened specimen, NSTR-L-1/3, was only 35 percent of specimen

NREF2-1/3. The sudden drop in the lateral load capacity of NSTR-L-1/3 resulted in a relatively low level of $\Delta_{0.85}$, which seems to be the reason for the low ductility estimated for this specimen. Besides, partial welding of the lapped bars at the first story columns in specimen NSTR-W-1/3 increased the system ductility 91 percent compared to specimen NREF2-1/3.

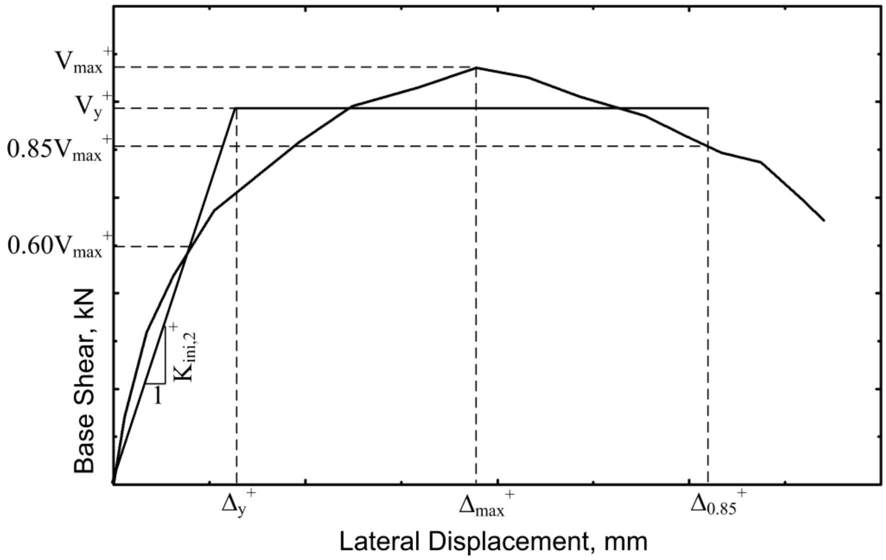

Figure 5. 10 Bi-linear approximation of the envelope curves

Table 5. 4 Yield point and ductility values of the frame specimens

Specimen	V_y, kN	Δ_y^+, mm	$\Delta_{0.85}^+$, mm	$\Delta_{0.85}^+/\Delta_y^+$ mm/mm	Change in Ductility
NREF1-1/3	8.7	5.8	56.8	9.8	0.73
NREF2-1/3	24.8	2.3	30.4	13.4	1.00
NSTR-L-1/3	35.2	2.0	9.3	4.8	0.36
NSTR-W-1/3	49.2	2.4	60.2	25.6	1.91
LREF1-1/3	12.0	13.1	59.5	4.5	0.57
LREF2-1/3	66.0	1.4	11.1	7.9	1.00
LSTR-L-1/3	110.3	2.1	15.6	7.4	0.94
LSTR-C-1/3	142.7	1.0	12.1	12.1	1.53
NREF-1/2	62.0	4.9	33.0	6.8	1.00
NSTR-1/2	89.0	9.5	120.0	12.7	1.86
LREF-1/2	144.0	3.6	34.0	9.4	1.00
LSTR-1/2	305.0	11.2	40.0	3.6	0.38

A comparison of infilled frames with bare specimens leads to a significant increase in the ductility with the contribution of infill walls (more distinctive in Series-L). In Group-II, the ductility of NSTR-1/2 was almost 1.86 times that of NREF-1/2 which may be attributed to the implemented strengthening. On the other hand, the abrupt degradation in strength which occurred after the ultimate capacity of LSTR-1/2 accompanied by the anchorage failures and debonding/rupturing of CFRP reinforcement resulted in a much lower ductility compared to LREF-1/2.

These results expose that the ductility, as being defined in this study, is not altered with the strengthening applied in non-ductile RC frames having lap-splice problems, compared to reference frames with infill walls. However, a measure of preventing the extreme bar slip deformations at these regions may result in the desired levels of ductile response. It should also be noted that this further supports the conclusion presented by Saatçioğlu (2006) as "the seismic retrofit strategy for non-ductile frame wall assemblies should be based on elastic design, unless individual frame members are retrofitted for improved deformability".

5.3. SCALE EFFECT

A structural model analysis should be utilized for the assessment of scale effect. The similitude relationships between the model (i.e. scaled structure) and prototype (i.e. actual structure) characteristics are defined in the structural model analysis. By means of these relationships, various response characteristics obtained by testing scaled models may be converted into prototype characteristics. In this study, such a conversion was provided for 1/3 and 1/2 scaled test specimens in terms of ultimate lateral strength and energy dissipation characteristics, which were concluded to be altered significantly in previous sections. Details of the structural model analysis are given in Appendix F. The resulting ultimate strength and total energy dissipation of the equivalent prototype structures corresponding to Group-I and Group-II specimens are presented in Table 5.5 for comparison purposes. Only the reference frames with infill walls and strengthened specimens having lapped longitudinal column bars are considered in this table.

Table 5. 5 Ultimate lateral load and dissipated energy of the prototype structures

Test Groups	Specimen	Ultimate lateral load of prototype structure, (kN)	Ultimate lateral load ratio between Group-II and Group-I	Dissipated energy of prototype structure, (kN.m)	Dissipated energy ratio between Group-II and Group-I
Group-I	NREF2-1/3	239.4	-	126.4	-
	NSTR-L-1/3	324.0	-	275.7	-
	LREF2-1/3	630.0	-	166.3	-
	LSTR-L-1/3	1098.0	-	531.4	-
Group-II	NREF-1/2	265.2	1.1	129.0	1.0
	NSTR-1/2	376.0	1.2	523.9	1.9
	LREF-1/2	609.6	1.0	201.8	1.2
	LSTR-1/2	1359.2	1.2	636.0	1.2

In both series, the ultimate lateral load capacity of 1/2 scaled strengthened specimens are 20 percent higher than the corresponding 1/3 scaled frames. The same ratio is valid for the total energy dissipation of the strengthened frames in Series-L. However, in Series-N, the energy dissipated by the strengthened frame in Group-II (i.e. NSTR-1/2) is approximately 90 percent higher than that of companion frame in Group-I (i.e. NSTR-L-1/3). The sudden load degradation after attaining the ultimate capacity of NSTR-L-1/3, which was not observed in NSTR-1/2 may be the major reason for this difference.

CHAPTER 6

NUMERICAL SIMULATIONS

6.1. GENERAL

In order to facilitate a design-oriented parametric study, a realistic numerical model of the RC infilled frames strengthened with the proposed methodology should be developed. In this chapter, the efforts for such a modeling are discussed and the consequent analytical results are validated by use of experimental response curves.

The constituent parts of the numerical model, such as employed constitutive material models, sectional characteristics and member properties are described in Section 6.2. Besides, the software platform and performed type of analysis are also introduced in the same section. The significant bond slip deformations likely to occur at the lap-splice regions required further treatment in terms of modeling these areas, as thoroughly explained in Section 6.3. The details of the models representing the strengthened/non-strengthened infill walls are explained in Section 6.4. In Section 6.5, the results of numerical simulations are presented through a comparison with the companion test results. Finally, a parametric study, which further investigates the effect of aspect ratio of infills, is performed in Section 6.6.

6.2. NUMERICAL MODELING

The numerical modeling and nonlinear static pushover analyses of the frame specimens were performed by using OpenSees Software platform (Mazzoni et al., 2007). The implemented structural model of the strengthened specimens is presented in Figure 6.1.

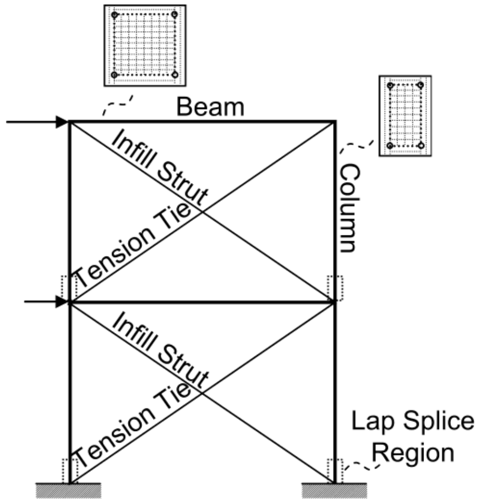

Figure 6. 1 Modeling of the strengthened specimens

RC members were modeled as nonlinear beam-column elements where five integration points were provided along the length of each member. The cross-sections of the members were converted into a number of discrete fibers of quadrilateral shape. The Hognestad (1951) and Modified Kent and Park (1971) concrete models were used for the unconfined and confined concrete sections, respectively. The typical uniaxial bi-linear steel model was employed for the longitudinal reinforcement. The strain hardening of the steel was ignored in the analyses. The material properties of the members as summarized previously in Table 3.3 in Chapter 3 were utilized for numerical simulations.

The first and second story weights of the frames were calculated by considering the regions bounded by half of the column lengths below and above the story level. The resulting nodal masses were distributed equally and assigned to the corresponding nodes at each story level. Besides the total axial load applied during the tests of the frames were also imposed equally as constant vertical loads at the second story nodes. Top story lateral displacements were used as the parameter that controls the pushover analyses. The reference lateral loads were defined at the story levels with the proportions simulating the load pattern applied during the tests (i.e. two thirds of the total lateral load goes to the upper story).

6.3. MODELING OF LAP-SPLICE REGIONS

The modeling of lap-splice regions of the columns is an important issue, since large bond-slip deformations generated at these regions have considerable effect on the overall response, especially in the case of Series-N specimens. The effective steel stress approach proposed by Binici and Mosalam (2007) was used in order to model the behavior of longitudinal reinforcement at the lap-splice regions. As the longitudinal reinforcement of the frames were constituted by plain bars, the confining effect of FRP and transverse reinforcement was ignored in the model. The model assumes a bond stress distribution having zero stress at the free ends of the longitudinal bars and uses force equilibrium of the bars under this distribution at any selected level along the lap length (Figure 6.2). The resulting equilibrium equation regarding the assumed bond stress distribution is given by,

$$\tau_m = \frac{\sigma_s d_b}{2\left(\frac{l_1^2+(L_s-l_1)^2}{L_s}\right)} \tag{6.1}$$

where τ_m is the maximum shear resistance along the splice length (L_s), l_1 is the distance from the selected point to one end of the spliced region, σ_s is the total steel stress (i.e. $\sigma_{s1}+\sigma_{s2}$) at the considered level, and d_b is the diameter of the spliced bars.

In this study, the level of equilibrium was selected to be mid-point of the lap-length which yields the minimum effective stress. A bond stress-slip relationship was further utilized in addition to the force equilibrium, as given by

$$\tau_m = \frac{\tau_{max} r(u/u_{max})}{r-1+(u/u_{max})^r} \tag{6.2}$$

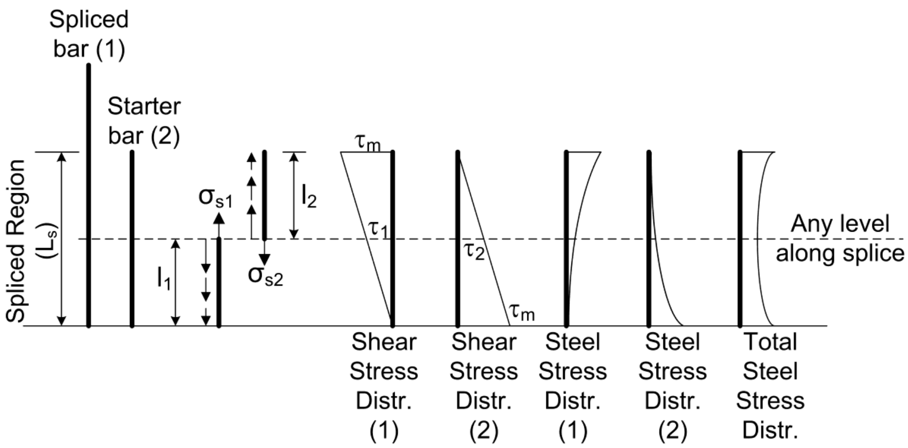

Figure 6. 2 Lap-splice model of longitudinal column bars (Binici and Mosalam, 2007)

where u is the splice slip and the definitions of other parameters are presented through Eqs. (6.3)-(6.6).

$$\tau_{max} = \tau^{'} + 1.4\sigma_3 \tag{6.3}$$

$$\tau' = 20\sqrt{f_c^{'}}/d_b \tag{6.4}$$

$$u_{max} = 0.25(1 + 75\,\sigma_3/f_c^{'}) \tag{6.5}$$

$$r = r_0 - 13\,\sigma_3/f_c^{'} \geq 1.1 \tag{6.6}$$

In Eqs. (6.3) to (6.6), σ_3 is the confining stress, which was assumed to be zero in order to ignore the confinement effect in case of plain bars. Besides, r_0, which is a constant parameter defined for steel grades, was assumed to be 1.5 for the analysis.

The two strain components of the steel bars (i.e. slip strain, ε_{ss}=u/L_s and elongation strain, ε_{se}) were determined by an iterative process which was utilized by use of Eqs. (6.1) and (6.2). After the strain corresponding to the direct elongation of the bars was computed, the effective steel stress was estimated by means of the constitutive steel model. The effective stress-strain models generated in this way for the spliced longitudinal column bars of Group-I and Group-II frames are shown in Figures 6.3.a and b, respectively. These model curves were approximated as bilinear curves and the yield strengths were found to be 170 and 145 MPa for Group-I and Group-II, respectively.

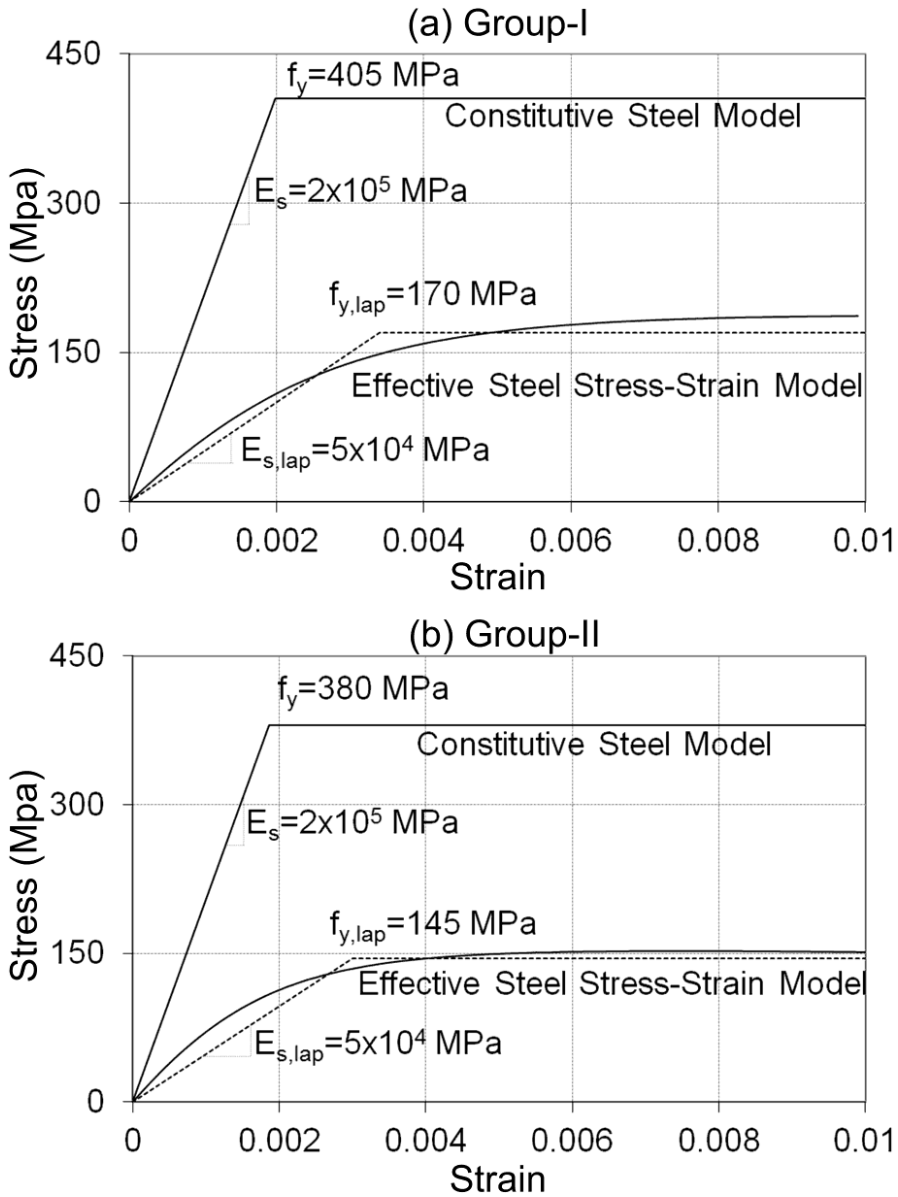

Figure 6. 3 Effective stress-strain model for lap slice regions of the columns

The resulting effective yield strength values of the lapped bars are confirmed by using the equation proposed by Cho and Pinchiera (2006) for estimating the capacity of the lapped bars that do not meet the development requirements of ACI 318-05 (ACI, 2005).

$$f_s = \left(\frac{l_b}{0.8 l_d^{ACI}}\right)^{2/3} f_y \tag{6.7}$$

where f_s is the yield capacity of lapped longitudinal bars, l_b is the provided lap-splice (development) length and l_d^{ACI} is the development length requirement of ACI 318-05 as given by Eq. (6.8).

$$l_d^{ACI} = \left(\frac{3}{40} \frac{f_y}{\sqrt{f_c'}} \frac{\Psi_t \Psi_e \Psi_s \lambda}{\left(\frac{c_b + K_{tr}}{d_b}\right)}\right) d_b \tag{6.8}$$

In Eq. (6.8), ψ_t, ψ_e and ψ_s are the factors used to modify the development length based on reinforcement location, size and coating, respectively. λ is the modification factor related to unit weight of concrete. c_b is the smaller of the distance from center of a bar to the nearest concrete surface or one-half center-to-center spacing of bars. Lastly, K_{tr} is defined as the transverse reinforcement index.

The upper bound of ψ_t ψ_e, which is given as 1.7, is considered in the calculations. ψ_s is taken as 0.8, that is defined for No. 6 (i.e. with a metric diameter of 19.05 mm) and smaller bars. The lower bound definition of λ is taken into account as 1.0. On the other hand $(c_b+K_{tr})/d_b$ component of Eq. (6.8), which is suggested as 1.5 for many construction cases, is assumed to be 1.0 to yield highest development length.

The resulting capacities of lapped bars in case of 8 and 12-mm diameter bars used in Group-I and Group-II test frames are calculated to be 141.8 and 146.6 MPa, respectively. These results are comparable with the effective yield stress values estimated previously. Different assumptions considered while using both approaches for simulating plain bar effect may be the main reason for slight difference between the results in the case of 8-mm diameter bars.

6.4. STRUT AND TIE MODELS

The macro compression strut and tension tie models proposed by Binici et al. (2007) were included in the numerical model to represent the response of masonry infills under compression and diagonal CFRP sheets under tension, respectively.

6.4.1 FRP Tie Model

A tri-linear stress-strain relationship is proposed by Binici et al. (2007) for the tensile response of infill walls reinforced by diagonal CFRP fabrics (Figure 6.4). It is assumed that FRP, plaster and infill wall contribute to the stiffness of tie. Therefore, the area of the tension tie is given by,

$$A_{tie} = w_f t_{tie} \tag{6.9}$$

In Eq. (6.9), w_f is the width of the diagonal FRP sheets and t_{tie} is defined as sum of the thicknesses of FRP, plaster and infill, as presented in the same order on the right hand side of Eq. (6.10).

$$t_{tie} = t_f + t_p + t_{in} \tag{6.10}$$

The cracking strength of the tension tie is defined by the two following equations,

$$f_{crt} = \frac{V_{crt}}{A_{tie}} \tag{6.11}$$

$$V_{crt} = f_{pt} w_f \left((t_{in} + t_p) + (E_f / E_m) t_f \right) \tag{6.12}$$

where f_{pt} is the tensile strength of the plaster, E_f and E_m are moduli of elasticity of FRP and mortar, respectively.

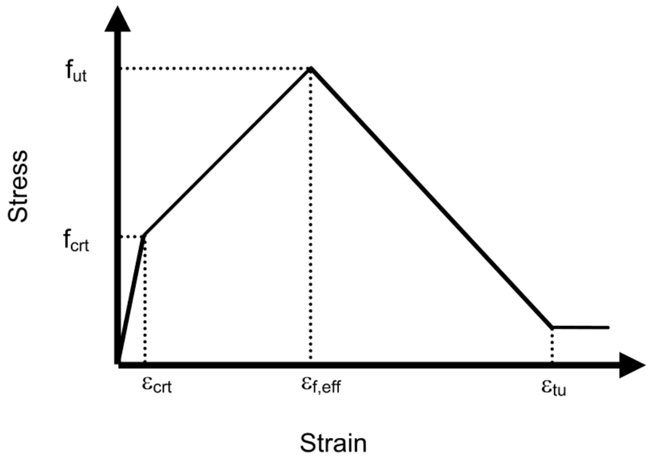

Figure 6. 4 Tension tie model for infill walls reinforced by diagonal FRP (Binici et al., 2007)

The ultimate tensile capacity and strength of the tie are defined by Eqs. (6.13) and (6.14), respectively.

$$V_{ut} = \varepsilon_{f,eff} w_f t_f E_f \tag{6.13}$$

$$f_{ut} = \frac{V_{ut}}{A_{tie}} \tag{6.14}$$

In Eq. (6.13), $\varepsilon_{f,eff}$ is the effective strain of FRP which depends on the type of failure (i.e. anchor failure or debonding of diagonal FRP). In the present study, the effective strain is assumed to be 0.002 corresponding to the anchor failure mode. The strain level stating the failure of FRP tie (ε_{tu}) is proposed to be three times the effective strain of FRP (i.e. 3x $\varepsilon_{f,eff}$=0.006).

6.4.2 Infill Strut Model

Two different equivalent strut models were utilized as proposed by Binici et al. (2007), for strengthened or non-strengthened infill walls. The infill walls of the non-strengthened frames were assumed to display a brittle response defined by a bilinear stress-strain curve (Figure 6.5.a). However, the infill walls strengthened by means of diagonal CFRP sheets were modeled by tri-linear model with a perfectly plastic plateau (Figure 6.5.b).

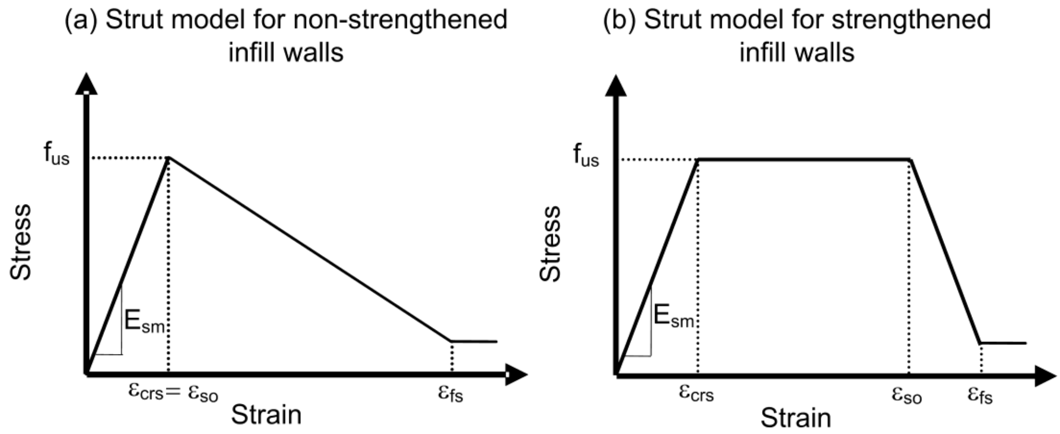

Figure 6. 5 Compression strut model for (a) non-strengthened and (b) strengthened infill walls (Binici et al., 2007)

The area of the compression strut, A_{str} is defined by,

$$A_{str} = t_{st} \times w_s \tag{6.15}$$

where t_{st} and w_s are the thickness and effective width of the equivalent diagonal strut, as designated through Eqs. (6.16) and (6.17), respectively.

$$t_{st} = t_p + t_{in} \tag{6.16}$$

$$w_s = \frac{(1-\alpha)\alpha h}{cos\theta} \tag{6.17}$$

In Eq. (6.17), h and θ are the height and inclination angle of the strut, respectively. On the other hand, α is a dimensionless parameter standing for the contact length between the frame and infill which is defined by,

$$\alpha = \sqrt{\frac{2(M_{pj}+0.2M_{pc})}{h^2 t_{st} f_{mc}}} \tag{6.18}$$

where M_{pj} represents the minimum of the moment capacities of column or beam, M_{pc} is the moment capacity of the column and f_{mc} is the compressive strength of infill plaster composite, which may be obtained by Eq. (6.23).

Based on the previous experimental observations, two failure modes, namely sliding shear and corner crushing are defined for infill walls. The minimum of the capacities corresponding to sliding shear (V_{ss}) or corner crushing (V_{cc}) failure modes is regarded as the ultimate capacity of the compressive strut (V_{us}).

$$V_{ss} = f_{mv} L t_{st} \tag{6.19}$$

$$V_{cc} = 250 t_{st} f_{mc} \tag{6.20}$$

$$V_{us} = \min(V_{ss}, V_{cc}) \tag{6.21}$$

In Eq. (6.19), L is the width of the infill wall and f_{mv} is the shear strength of the mortar bed joint. Eventually, the ultimate strength of strut may be computed by,

$$f_{us} = \frac{V_{us}}{A_{st}} \tag{6.22}$$

In their study, Binici et al. stated that the initial slope of stress-strain relationship (E_{sm}) and compressive strength of the infill plaster composite (f_{mc}) may be obtained from uniaxial compression tests of the plastered infill walls. However, the following equations are suggested for these parameters in the absence of experimental results.

$$f_{mc} = \frac{f_{in} t_{in} + f_m t_p}{t_{st}} \tag{6.23}$$

$$E_{sm} = \frac{E_{in}t_{in}+E_m t_p}{t_{st}} \tag{6.24}$$

In these equations, f_{in} and E_{in} are the compressive strength and modulus of elasticity of the infill unit, respectively and f_m is the compressive strength of the mortar. After determination of the initial slope (E_{sm}), the cracking strain of the strut (ε_{crs}) may be estimated. In the case of strengthened infill walls, a perfectly plastic plateau is defined after cracking strain up to a strain level defined as two times the effective strain of FRP (i.e. ε_{so}=2x$\varepsilon_{f,eff}$). A strength degradation is introduced in the model up to failure strain of the compression strut (ε_{fs}) which was assumed to be 0.01 for both strengthened and non-strengthened infill walls in this study.

6.4.3 Applied Strut and Tie Models

The dimensions, reinforcement details and material properties of the test specimens, which were necessary for modeling purposes were extracted from Sections 3.2.2 and 3.2.3. The tensile strength of the plaster was assumed to be 0.5 MPa for all specimens. In specimens having lap splices, the effective steel stress-strain relationships given in Figure 6.3 were applied for the material model of the longitudinal reinforcement at these regions. Since flexural capacities of the beams are higher compared to columns, only the moment capacities of the columns were considered in the strut model. The employed flexural capacities of the columns in Group-I and Group-II frames were estimated to be 3.8 and 12.0 kN.m, respectively.

The resulting stress-strain relationships of the strut and tie members of Group-I frames are presented in Figures 6.6 and 6.7, respectively. Those of Group-II specimens are shown in Figures 6.8 and 6.9, respectively. It should be noted that the tension tie model proposed by Binici et al. is independent of the aspect ratio of infill walls; therefore the same model was used for all the strengthened specimens in the same test group.

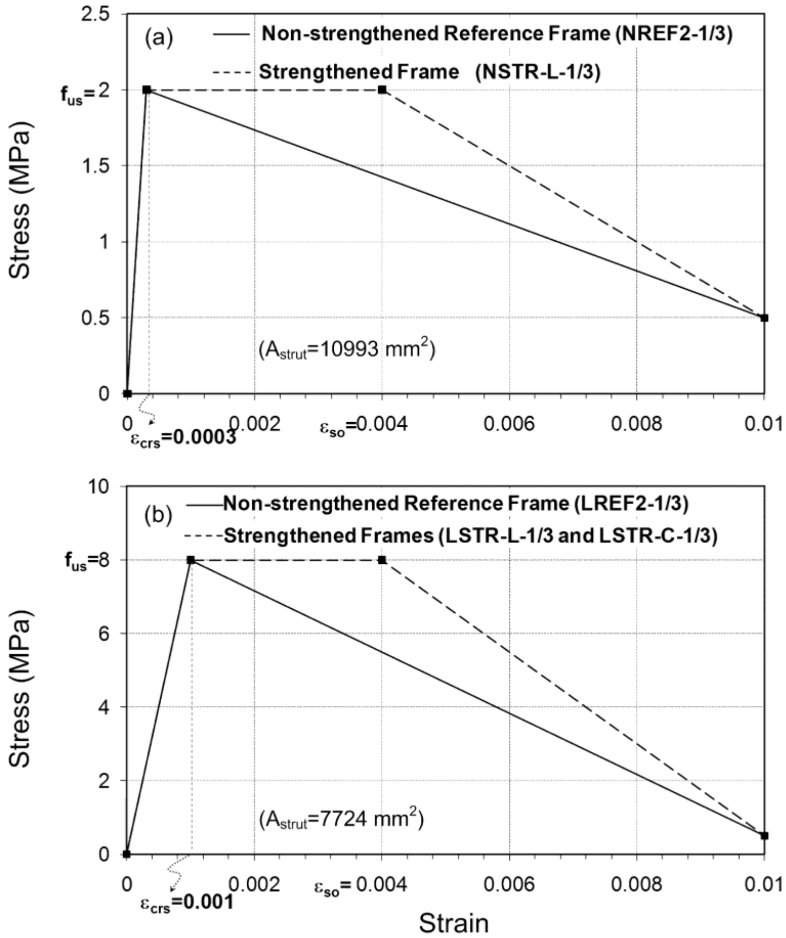

Figure 6. 6 Compression strut models for the strengthened/non-strengthened infill walls of (a) Series-N and (b) Series-L frames in Group-I

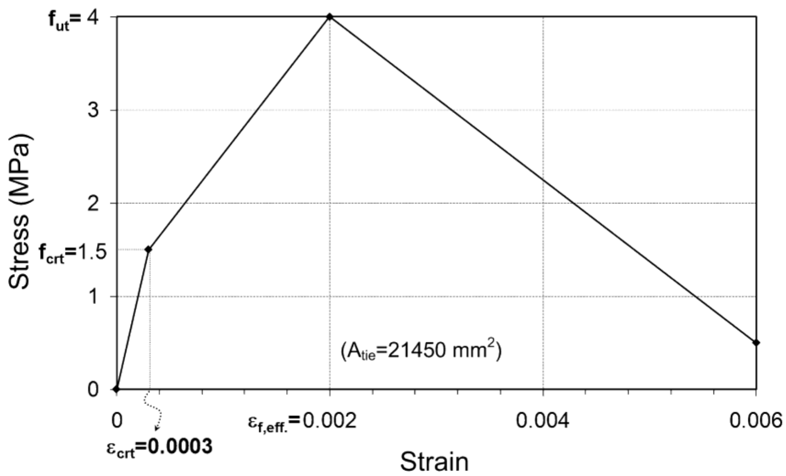

Figure 6. 7 Tension tie model for the diagonal CFRP sheets of the strengthened frames in Group-I

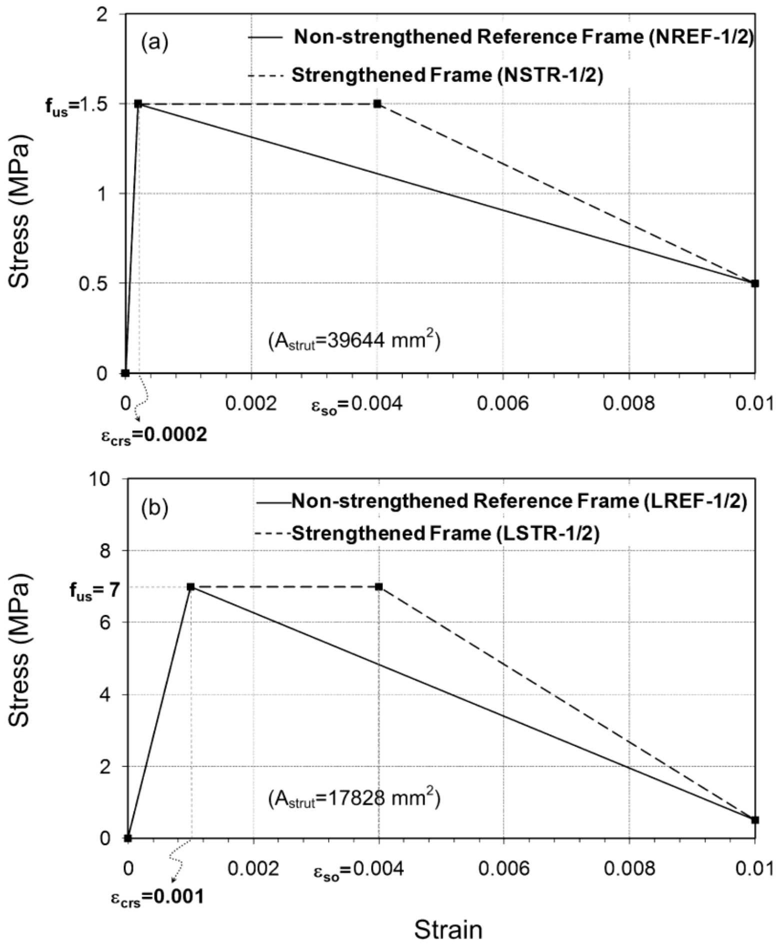

Figure 6. 8 Compression strut models for the strengthened/non-strengthened infill walls of (a) Series-N and (b) Series-L frames in Group-II

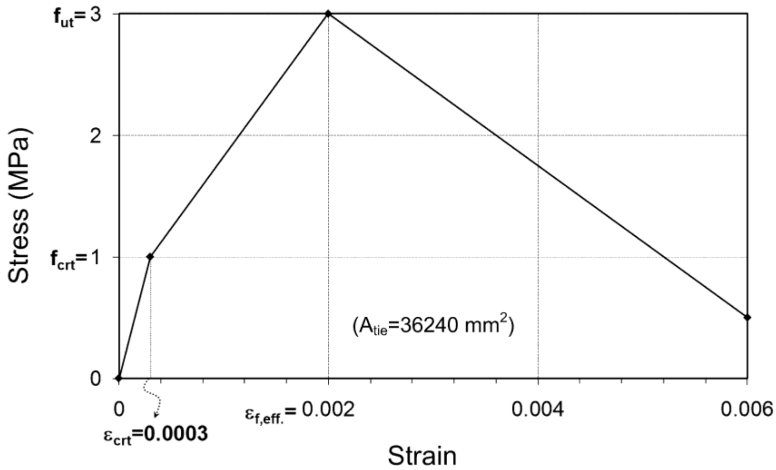

Figure 6. 9 Tension tie model for the diagonal CFRP sheets of the strengthened frames in Group-II

6.5. NUMERICAL RESULTS AND EXPERIMENTAL VALIDATION

The nonlinear static pushover analyses results of the generated models are presented in this section. These results are shown in Figures 6.10 and 6.11 as comparative to the experimental envelope curves of Group-I and Group-II specimens, respectively. All of the presented curves represent the base shear vs. second story lateral displacement response of the specimens. The inter-story drift ratio limit which is defined by TEC (The Ministry of Public Works and Settlement, 2007) for the life safety (L.S.) damage state of strengthened infill walls (i.e. 0.0035) is also provided on each graph. Furthermore, the limit values proposed by Binici et al. (2007) for the tensile strains of tie members corresponding to various damage levels are shown on the graphs. These strain limits are given as 0.003, 0.004 and 0.006 for the immediate occupancy (I.O.), life safety and collapse prevention (C.P.) levels, respectively. The limit values are obtained for the first story infill walls which may be regarded as more critical and correlative second story displacements are displayed on the graphs. The analytical and experimental values of the ultimate load and initial stiffness are presented in Table 6.1 together with their ratios for a better comparison.

The partial welding of the lapped bars in specimen NSTR-W-1/3 requires further treatment in terms of modeling the lap splice regions. Therefore, this specimen was excluded from the numerical study.

The ratios between the analytical and experimental ultimate lateral loads are in the range of 0.88-1.20 in Group-I and 0.73-1.11 in Group-II (Table 6.1). This shows that the lateral load capacity of the specimens could be successfully predicted in the analysis, especially in the case of 1/3 scaled frames. On the other hand, the stiffness was underestimated substantially in some specimens, such as frames with infill walls in Group-I Series-L.

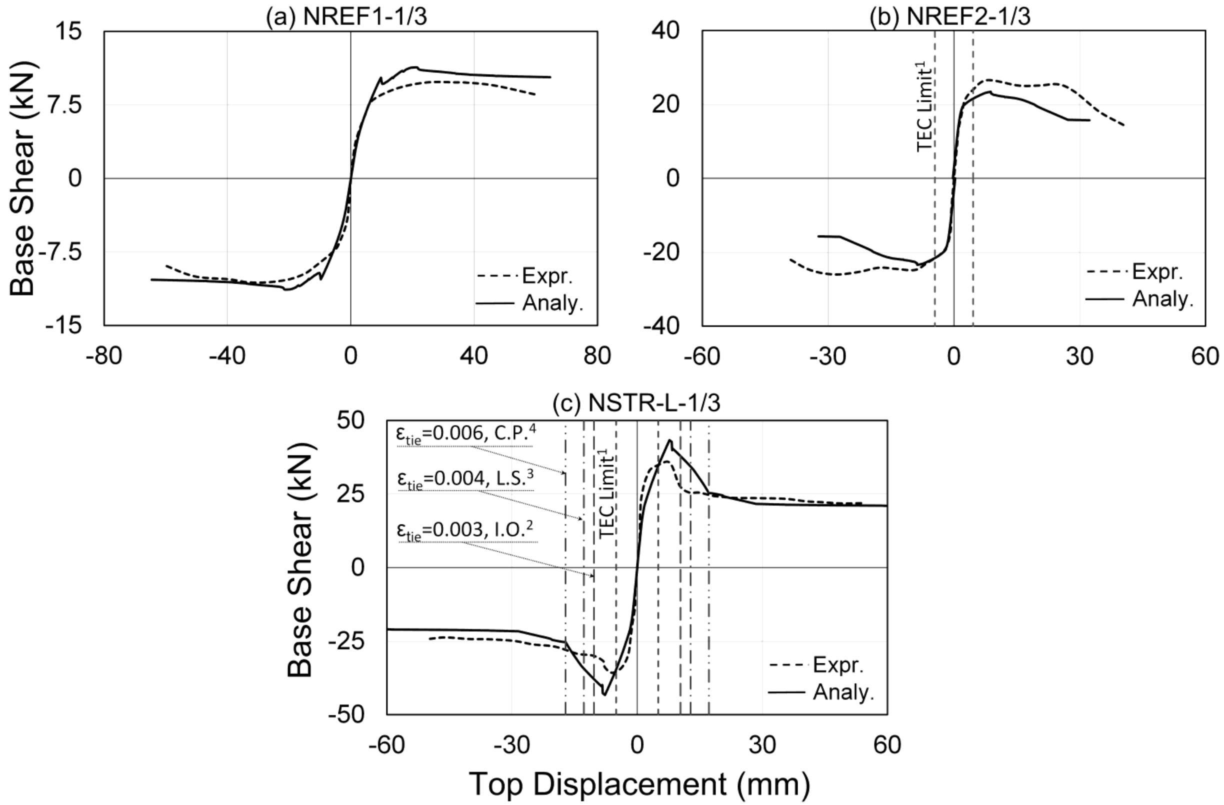

[1] Inter-story drift ratio limit for strengthened infill walls at life safety (L.S.) level defined by Turkish Earthquake Code (2007), D.R. =0.35%
[2] Strain limit for the tension tie (diagonal CFRP) at immediate occupancy (I.O.) level proposed by Binici et al. (ε_{tie}=0.003)
[3] Strain limit for the tension tie (diagonal CFRP) at life safety (L.S.) level proposed by Binici et al. (ε_{tie}=0.004)
[4] Strain limit for the tension tie (diagonal CFRP) at collapse prevention (C.P.) level proposed by Binici et al. (ε_{tie}=0.006)

Figure 6. 10 The analytical results comparative to the experimental envelope curves of specimens in Group-I

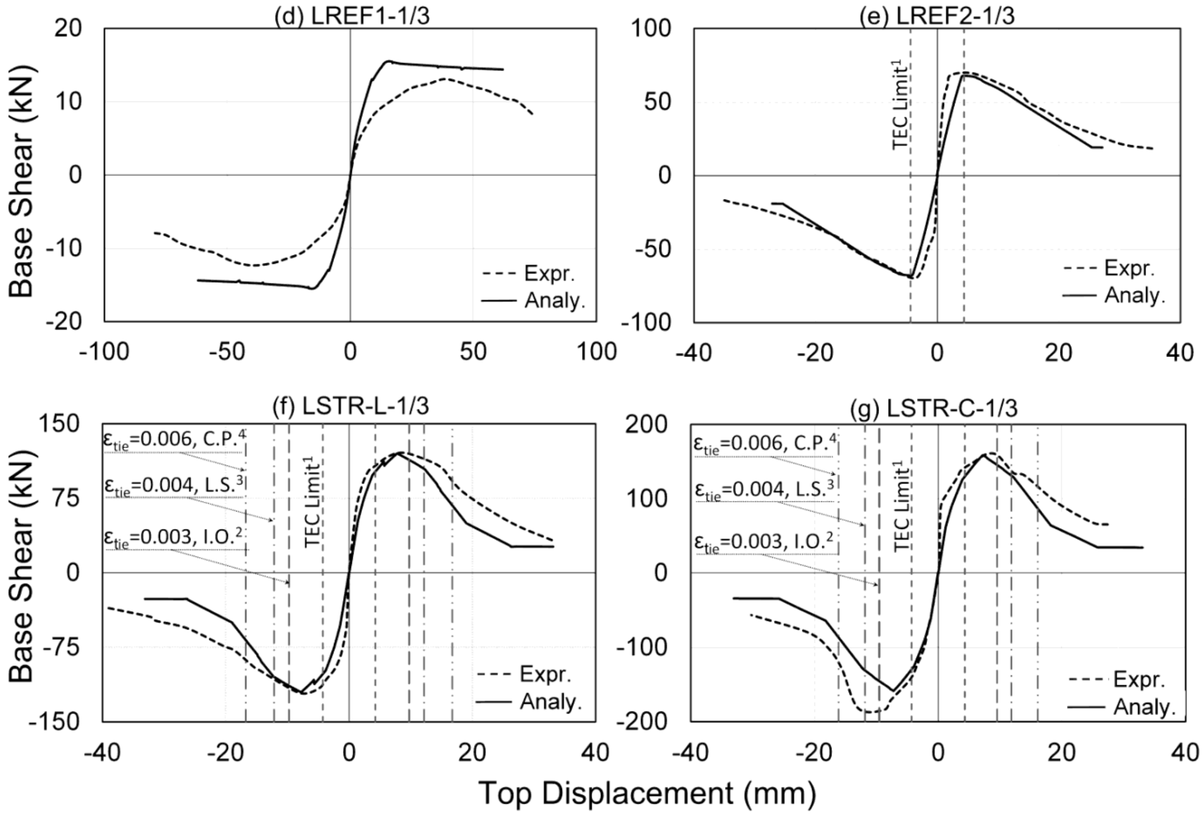

[1] Inter-story drift ratio limit for strengthened infill walls at life safety (L.S.) level defined by Turkish Earthquake Code (2007), D.R. =0.35%

[2] Strain limit for the tension tie (diagonal CFRP) at immediate occupancy (I.O.) level proposed by Binici et al. (ε_{tie}=0.003)

[3] Strain limit for the tension tie (diagonal CFRP) at life safety (L.S.) level proposed by Binici et al. (ε_{tie}=0.004)

[4] Strain limit for the tension tie (diagonal CFRP) at collapse prevention (C.P.) level proposed by Binici et al. (ε_{tie}=0.006)

Figure 6. 10 The analytical results comparative to the experimental envelope curves of specimens in Group-I (continued)

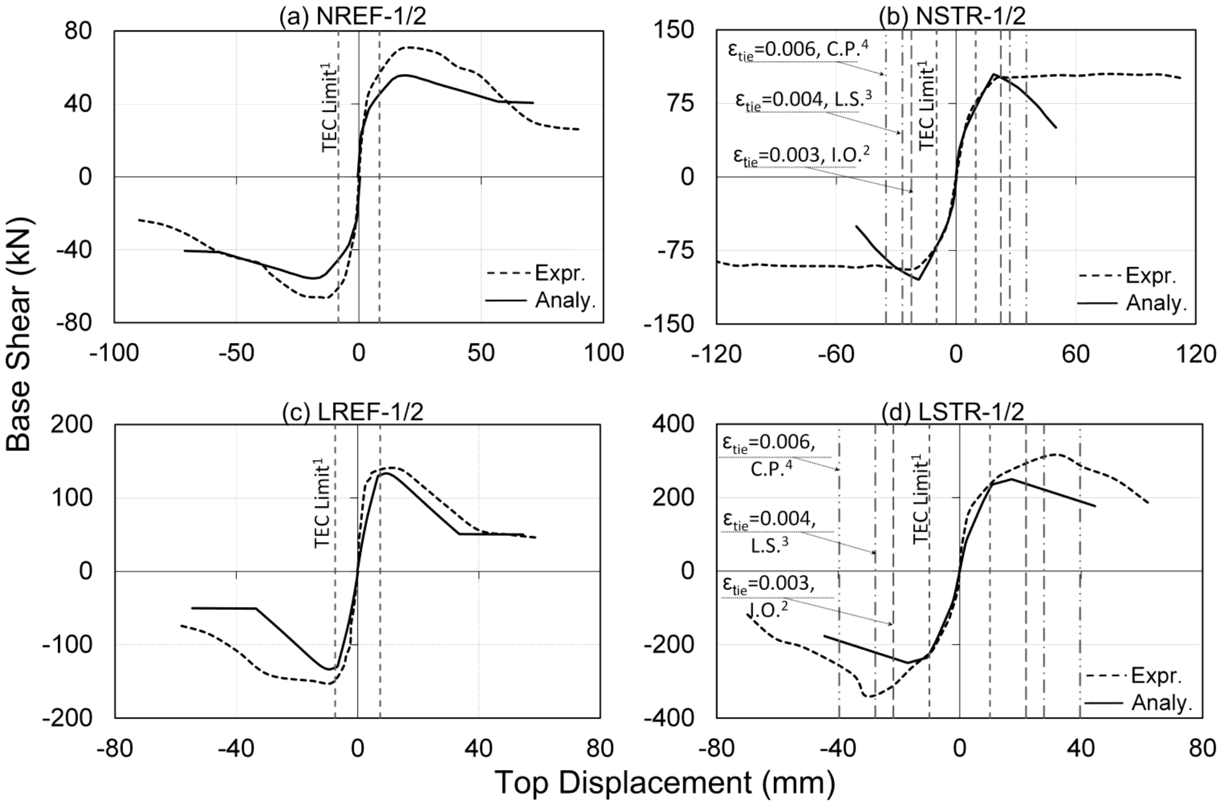

1 Inter-story drift ratio limit for strengthened infill walls at life safety (L.S.) level defined by Turkish Earthquake Code (2007), D.R.=0.35%
2 Strai%n limit for the tension tie (diagonal CFRP) at immediate occupancy (I.O.) level proposed by Binici et al. (ε_{tie}=0.003)
3 Strain limit for the tension tie (diagonal CFRP) at life safety (L.S.) level proposed by Binici et al. (ε_{tie}=0.004)
4 Strain limit for the tension tie (diagonal CFRP) at collapse prevention (C.P.) level proposed by Binici et al. (ε_{tie}=0.006)

Figure 6. 11 The analytical results comparative to the experimental envelope curves of specimens in Group-II

Table 6. 1 Comparison of experimental and analytical results

Specimen	***Ultimate Lateral Load (kN)***			***Initial Stiffness (kN/mm)***		
	Expr.	**Analy.**	**Analy./Expr.**	**Expr.**	**Analy.**	**Analy./Expr.**
NREF1-1/3	9.8	11.3	1.15	1.5	1.4	0.92
NREF2-1/3	26.6	23.3	0.88	10.9	11.0	1.01
NSTR-L-1/3	36.0	43.0	1.19	18.0	10.5	0.58
LREF1-1/3	12.8	15.4	1.20	0.9	1.8	1.90
LREF2-1/3	70.0	69.5	0.99	49.5	21.0	0.42
LSTR-L-1/3	122.0	120.0	0.98	52.5	30.0	0.57
LSTR-C-1/3	160.0	158.0	0.99	142.7	45.0	0.28
NREF-1/2	66.3	55.6	0.84	12.8	10.0	0.78
NSTR-1/2	94.0	104.4	1.11	9.4	8.3	0.88
LREF-1/2	152.4	133.4	0.88	39.7	22.5	0.57
LSTR-1/2	339.8	248.6	0.73	27.2	26.7	0.98

The analytical and experimental drift characteristics of the frames beyond the ultimate load level can be concluded to be in good aggrement in Group-I (Figure 6.10). The drift levels experienced by the strengthened frames in Group-II are underestimated by the numerical model (Figures 6.11.b and d), although this was not the case in reference frames with non-strengthened infills in the same group (Figures 6.11.a and c). At this point it should be remembered that the same effective FRP strain ($\varepsilon_{f,eff}$) was utilized for the tie models in both groups. As explained in Section 6.4, the effective FRP strain is the major parameter in terms of designating the post-elastic strain capacity of both strut and tie models. Therefore, in specimens NSTR-1/2 and LSTR-1/2, the FRP strain levels endured by the diagonal CFRP sheets, which might be higher than the assumed effective FRP strain may induce such a difference in the drift capacity.

All in all, with a comparison of the results presented in Figures 6.10 and 6.11, one may conclude that the employed model is capable of simulating the nonlinear monotonic response of RC infilled frames with the proposed strengthening scheme.

In majority of the specimens, the drift ratio limit values enforced by TEC for the life safety level remain in the elastic-plastic transition zone before the ultimate capacity level (Figures 6.10 and 6.11). Therefore this limit value may be regarded as conservative. On the other hand, the limit values proposed by Binici et al. seem to better represent the defined damage states of the considered frame specimens. This phenomenon can be better interpreted with further study of the results. For this purpose, the first floor inter-story drift ratios corresponding to the limiting damage states defined by Binici et al. are presented in Table 6.2 for the strengthened frames. The decreases in the lateral load capacity at each limit state as a percentage of the ultimate capacity are also provided in the same table.

Table 6. 2 First floor inter-story drift ratios at limit states defined by Binici et al.

Specimen	***ε_{tie}=0.003 (I.O.)***		***ε_{tie}=0.004 (L.S.)***		***ε_{tie}=0.006 (C.P.)***	
	1st Story Drift Ratio, %	***Decr. in load capacity, %***	***1st Story Drift Ratio, %***	***Decr. in load capacity, %***	***1st Story Drift Ratio, %***	***Decr. in load capacity, %***
NSTR-L-1/3	0.76	11	1.00	19	1.44	39
LSTR-L-1/3	0.98	5	1.30	12	1.95	42
LSTR-C-1/3	0.96	7	1.27	15	1.89	44
NSTR-1/2	0.90	3	1.17	7	1.69	20
LSTR-1/2	0.76	6	1.00	16	1.49	23

According to FEMA 356 (2000), the immediate occupancy (I.O.) damage level of reinforced masonry infill walls is defined as a state in which minor cracking may be observed without out-of-plane offsets. At the immediate occupancy level presented in Table 6.2, the first floor inter-story drift ratios were in the range of 0.76~0.98%. The average decrease in the ultimate load capacity was less than ten percent at that stage. The damage observed during the tests indicate minor cracks on the infill walls for almost all strengthened frames up to this level, after which the damage on the CFRP reinforcement initiated (Chapter 4.3).

The life safety level (L.S.) of the strengthened infill walls is defined as the damage state where extensive cracking is distributed throughout the wall and some isolated crushing is observed, especially at the corners (FEMA 356, 2000). At this state, the first floor inter-story drift ratios shown in Table 6.2 are higher than 1.00%, which means nearly three times that of suggested by TEC. Approximately 15 percent of the ultimate capacity was lost at this drift level. The specimens, obviously those in Series-L experienced damage as debonding of CFRP reinforcement at this level during the tests. This was followed by local masonry crushing in Series-L frames.

At the collapse prevention (C.P.) limit state, crushing, extensive cracking, damage at the corners and falling of some units may be expected on the reinforced infill walls according to FEMA 356 (2000). The first floor inter-story drift ratios of the frames were higher than 1.50% at this damage level, corresponding to approximately 35 percent decrease in the ultimate load capacity (Table 6.2). At this level, significant damage was observed in strengthened frames during the tests.

6.6. PARAMETRIC STUDY

A parametric study was performed in order to further understand the efficiency of applied strengthening method on varying aspect ratios of infill walls. The numerical models of 1/3 scaled frames were generated for this purpose, by referring the reasonably close predictions of the nonlinear response of Group-I specimens (as explained in the previous section). The generated models had identical properties except their varying infill aspect ratios and corresponding strut/tie models. The aspect ratios were chosen to be in a range not smaller than those in Series-L and not larger than those in Series-N test specimens. The effective FRP strain ($\varepsilon_{f,eff}$) was again assumed to be 0.002, as before. All of the analyzed frame models had one-bay and two-stories. The column height was identical at both stories of all frame models. The same column/beam cross-sectional dimensions and reinforcement layout were used as in Group-I specimens. The concrete compressive strength and modulus of elasticity were taken as 17 MPa and 27400 MPa, respectively, which were the average values of Group-I specimens. The material properties presented in Table 3.3 in Section 3.2.3 for the mortar, infill material and longitudinal reinforcements were so used in the analytical models. The frame specimens were assumed to have continuous longitudinal reinforcement at both stories.

Three models pertaining to a bare frame, a frame with non-strengthened infill walls and a strengthened frame were analyzed in each set having the same aspect ratio. The chosen aspect ratios and corresponding characteristic strain/stress values of the tie and strut models (Figures 6.4 and 6.5) are summarized in Table 6.3. The cross-sectional areas of the tie and strut in each set are also denoted in the same table. Since no such strut and tie models were used in the case of bare frames, these specimens are not included in Table 6.3.

The results of the nonlinear static pushover analyses for a total number of 21 frame models in seven different sets with different aspect ratios are presented in Figure 6.12. The ultimate strength and secant stiffness values of the frames are given in Table 6.4. The change in ultimate strength attained by the application of infill strut and further CFRP strengthening (i.e. addition of tension tie) with respect to the aspect ratio of the infill walls are shown in Figures 6.13.a and 6.13.b, respectively. The analogous variations of secant stiffness as a function of the aspect ratio are presented in Figures 6.13.c and 6.13.d. The results indicate that the substantial contribution of infill walls by increasing both strength and stiffness of RC frames tend to decrease with increased aspect ratio. This inference is compatible with the test results and observations which designate a more efficient strut formation in Series-L specimens compared to Series-N frames. The increase in ultimate strength ratio provided by the applied CFRP strengthening is in a range between 2 and 3 (Figure 6.13.b), which yields highest results in specimens with an aspect ratio of 0.8~1.2. In Figures 6.13.b and 6.13.d, it may be observed that the increase in ultimate strength is inversely proportional to the change in stiffness. In RC frames having infill walls with an aspect ratio in between 0.8~1.2, the superior increase in strength as a result of CFRP strengthening occurred with insignificant alteration in initial stiffness. This may result in increased displacement demands. However, it may also mean that in this range, the capacity increase can be provided without increasing the seismic demand.

Table 6. 3 The frame models used for parametric study

Aspect Ratio (h/w)	***Frame***	***Strut***					***Tie***					
		f_{us}, MPa	**ε_{crs}, mm/mm**	**ε_{so}, mm/mm**	**ε_{fs}, mm/mm**	**A_{st}, mm^2**	**f_{crt}, MPa**	**f_{ut}, MPa**	**ε_{crt}, mm/mm**	**$\varepsilon_{f,eff}$, mm/mm**	**ε_{tu}, mm/mm**	**A_{tie}, mm^2**
0.4	Infilled	8.3	0.0011	0.0011	0.01	7754	-	-	-	-	-	-
(h=750 mm, w=1875 mm)	Strength.	8.3	0.0011	0.004	0.01	7754	1	4	0.0003	0.002	0.006	21450
0.6	Infilled	5.1	0.0007	0.0007	0.01	8396	-	-	-	-	-	-
(h=750 mm, w=1250 mm)	Strength.	5.1	0.0007	0.004	0.01	8396	1	4	0.0003	0.002	0.006	21450
0.8	Infilled	3.5	0.0005	0.0005	0.01	9220	-	-	-	-	-	-
(h=750 mm, w=938 mm)	Strength.	3.5	0.0005	0.004	0.01	9220	1	4	0.0003	0.002	0.006	21450
1.0	Infilled	2.6	0.0003	0.0003	0.01	10182	-	-	-	-	-	-
(h=750 mm, w=750 mm)	Strength.	2.6	0.0003	0.004	0.01	10182	1	4	0.0003	0.002	0.006	21450
1.2	Infilled	1.9	0.0003	0.0003	0.01	11246	-	-	-	-	-	-
(h=750 mm, w=625 mm)	Strength.	1.9	0.0003	0.004	0.01	11246	1	4	0.0003	0.002	0.006	21450
1.4	Infilled	1.5	0.0002	0.0002	0.01	11246	-	-	-	-	-	-
(h=750 mm, w=536 mm)	Strength.	1.5	0.0002	0.004	0.01	11246	1	4	0.0003	0.002	0.006	21450
1.6	Infilled	1.2	0.0002	0.0002	0.01	13558	-	-	-	-	-	-
(h=750 mm, w=470 mm)	Strength.	1.2	0.0002	0.004	0.01	13558	1	4	0.0003	0.002	0.006	21450

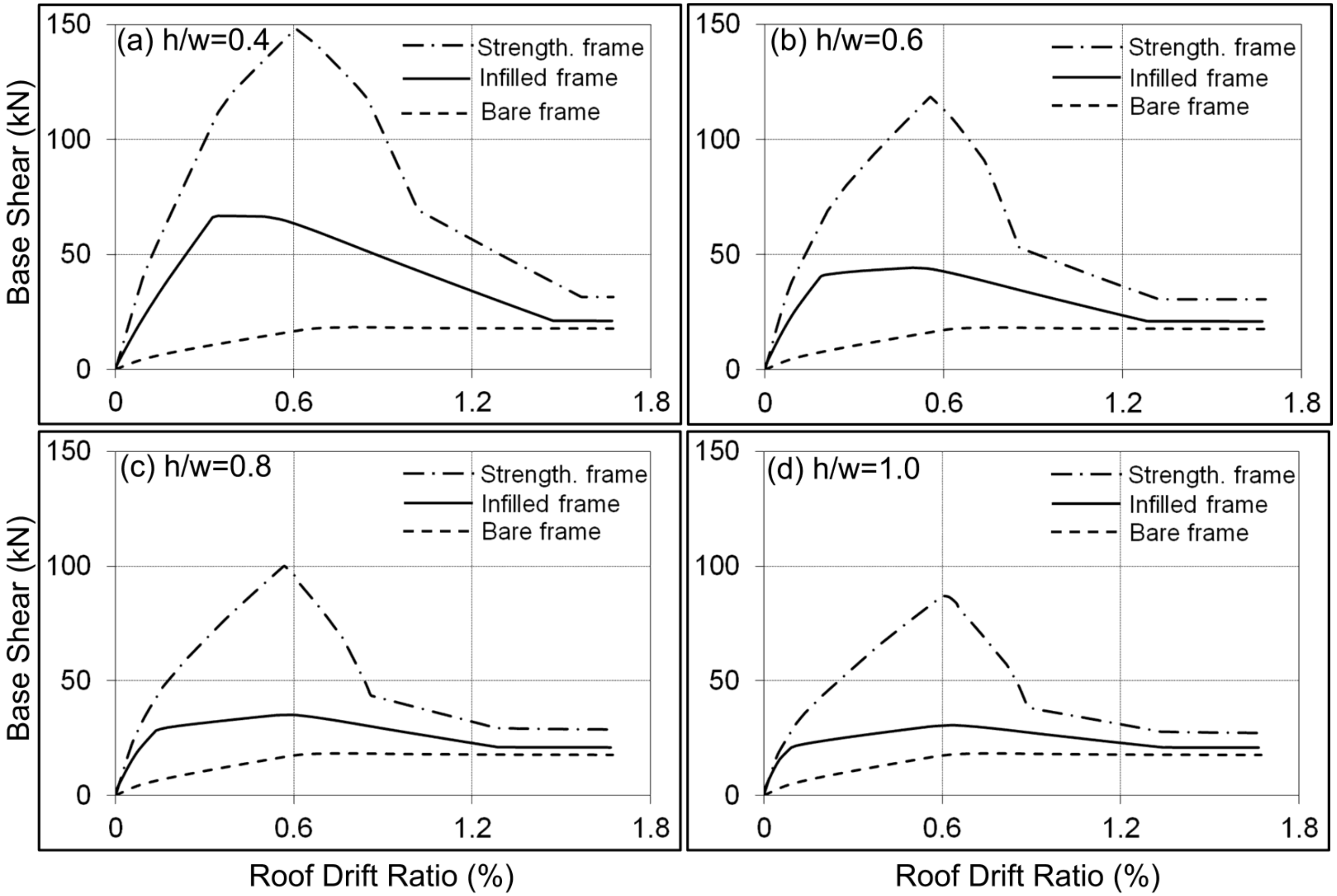

Figure 6. 12 The nonlinear static pushover analyses results of frame models having different aspect ratios

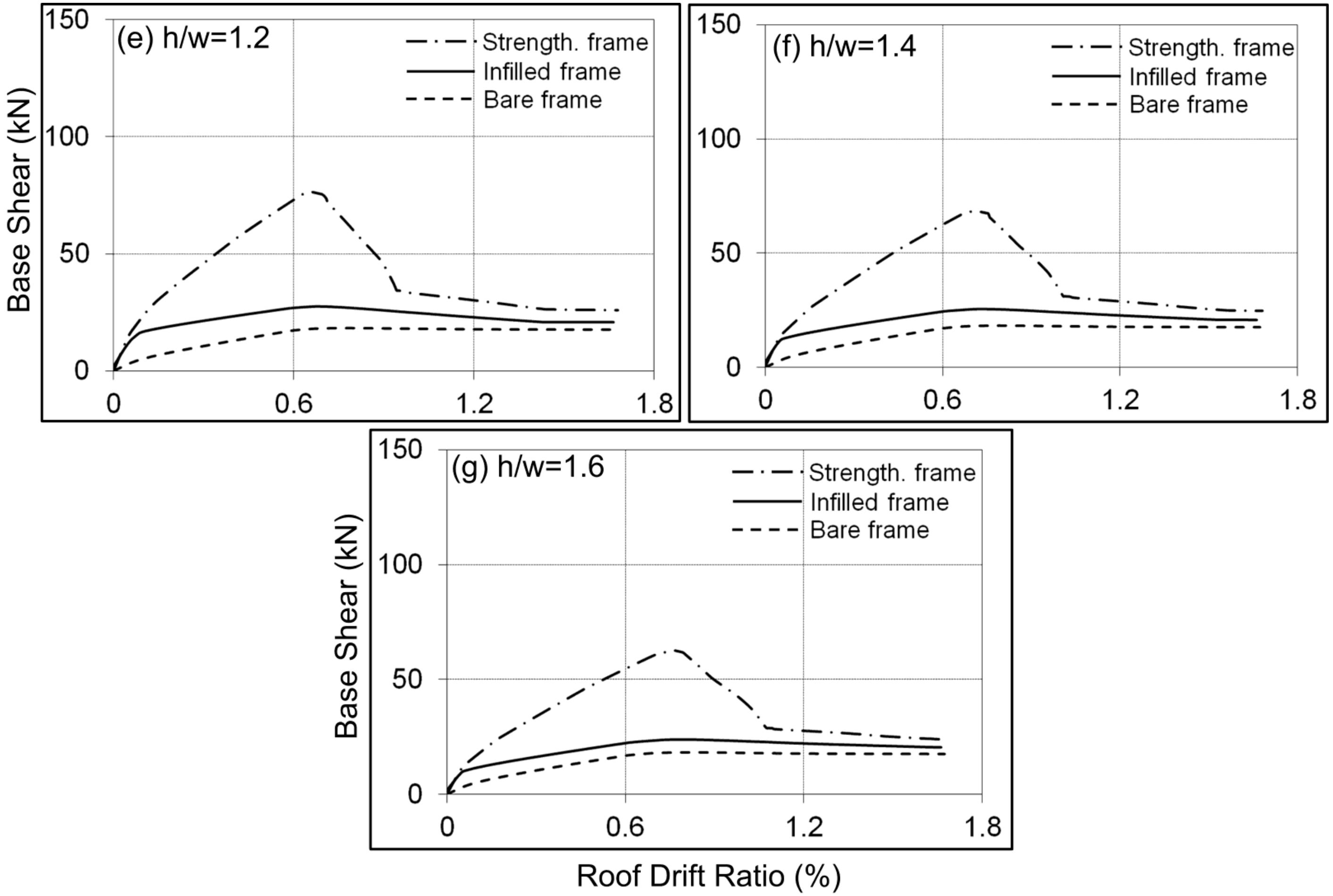

Figure 6. 12 The nonlinear static pushover analyses results of frame models having different aspect ratios (continued)

Table 6. 4 Ultimate strength and secant stiffness values of frame models

Aspect Ratio	***Strength***			***Secant Stiffness***		
	V_{bare} kN	**$V_{inf.}$ kN**	**$V_{str.}$ kN**	**K_{bare} kN/mm**	**$K_{inf.}$ kN/mm**	**$K_{str.}$ kN/mm**
0.4	18.36	66.83	148.16	1.84	12.75	20.00
0.6	18.33	44.32	118.50	2.00	14.50	18.60
0.8	18.30	35.11	100.00	2.00	14.30	14.25
1.0	18.30	30.62	87.00	2.00	14.60	11.10
1.2	18.30	27.49	76.52	2.00	10.40	8.90
1.4	18.30	25.50	68.60	2.00	5.75	7.30
1.6	18.25	23.84	62.64	2.00	4.00	6.26

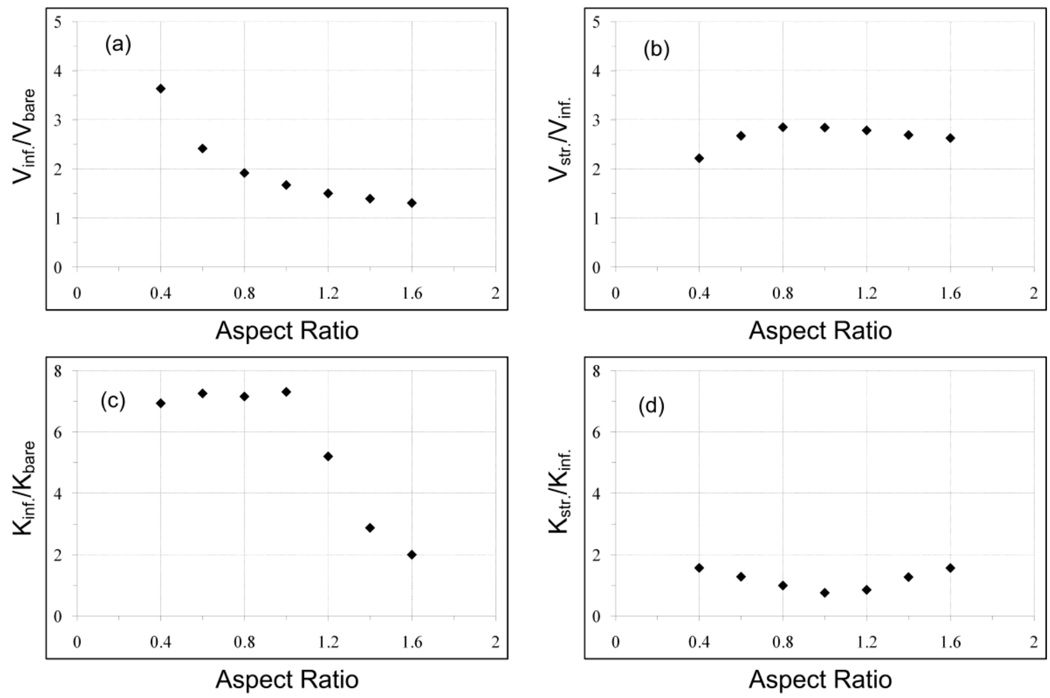

Figure 6. 13 The change in strength and stiffness increment due to infill wall application and strengthening with respect to aspect ratio of infills

CHAPTER 7

SUMMARY AND CONCLUSIONS

7.1. SUMMARY

This study mainly focused on conceiving the effects of different parameters on the performance of strengthening methodology which is based on upgrading existing HCT infill walls by means of CFRP fabrics. The main parameters of concern were the aspect ratio of infill walls and scale of the frame. The influence of insufficient development length of lapped plain bars was also investigated.

The tests of twelve frame specimens were performed in order to obtain the experimental data required for the assessment of aforementioned parameters. 1/3 and 1/2 scaled frame specimens were assembled in two major test groups, each having two sub-groups with varying infill aspect ratios. The frames were tested under reversed cyclic lateral loading. The columns were subjected to an axial load corresponding to ten percent of their axial capacity. The frame test results were evaluated in terms of strength, stiffness, ductility, energy dissipation and drift characteristics.

A numerical model of the frame specimens was generated and nonlinear static pushover analyses were performed by the aid of OpenSees software (Mazzoni et al., 2007). The non-strengthened and strengthened infill walls were modeled by equivalent strut and tie members. The lapped longitudinal reinforcement behavior was also simulated in the corresponding models. The experimental results were compared and verified with the analytical results with regard to ultimate strength, initial stiffness and global drift characteristics. The drift limit proposed by TEC for reinforced infill walls was assessed by a comparison with the limits suggested by Binici et al. (2007) for different damage states of CFRP applied HCT infill walls.

In the last stage, a parametric study was implemented which aims further investigation of the infill aspect ratio. The numerical models of 1/3 scaled frames having varied infill aspect ratios were constituted for this purpose. The analytical results of these frames provided notional information on the efficiency of applied strengthening in case of different practical aspect ratios.

7.2. CONCLUSIONS

The following conclusions can be summarized based on test results of RC frame specimens and pushover responses of the generated numerical models in this study.

- The test results have shown that the initial stiffness and strength of frames increased considerably with the addition of HCT infill walls, which may alter depending on the aspect ratio of infill. In squat frames with lower aspect ratio, the contribution of infill walls increase through efficient strut formations.

- Irrespective of the scale and aspect ratio, the base shear capacity of the frames enhanced significantly alone by the applied strengthening methodology. However, this was more prominent in squat (Series-L) frames of both test groups, as the diagonal CFRP tension ties could be utilized more efficiently in such frames. Besides the results point out a slightly higher base shear capacity improvement in the two series of Group-II specimens with a larger scale.

- The applied retrofitting alone did not alter stiffness of the frames substantially. The strengthening of infill walls and preventing significant damage on the infill shifted the failure mechanism; leading to higher bar slip deformations at the lap splice regions of the frames having lapped longitudinal plain bars, especially in the case of slender frames. Therefore, in frames having lapped longitudinal column bars at the floor levels with insufficient development length, this deficiency should be managed first for an ascendant overall rehabilitation.

- The use of continuous/welded column reinforcement in frames resulted in further enhancement in strength and lead to a higher initial stiffness compared to other specimens. This demonstrates the importance of solving the lap splice problem mentioned in the previous conclusion. However, it should be noted that welding should not be applied unless ability of the reinforcement for welding is assured.

- In Series-L frames, although the contribution of strengthened infill walls is more considerable, these squat specimens displayed strength deterioration after the ultimate capacity level. Also, specimen NSTR-L-1/3 in Series-N experienced such a sudden decrease in strength after the ultimate capacity which may be related to the extreme bond slip deformations developing at the lap-splice regions of the first story columns. Nevertheless, the strength decrement in NSTR-L-1/3 stabilized at a load level corresponding to 60 percent of the ultimate capacity and continued to undergo large displacements without a new down-fall in strength.

- The cyclic stiffness degradation of all specimens was precipitous up to ultimate lateral load capacity which became steady afterwards. In general, it may be stated that the effect of implemented rehabilitation by prevailing excessive damage on the infill resulted in far fewer stiffness degradation.

- The energy dissipation capacity of the frames enhanced significantly with the applied strengthening in all cases.

- The CFRP strengthening of infill walls increased the story drift capacities of the specimens, except specimen LSTR-1/2, which experienced the most abrupt strength deterioration amongst all other Series-L frames. The anchorage failures observed after the ultimate load level may be the major reason of this abrupt strength deterioration in LSTR-1/2.

- In Series-N specimens of both groups, ductility of the specimens were increased considerably with the applied strengthening in general. However, the strength deteriorations in Series-L frames precluded attaining such ductility levels.

- Tests have once more indicated that the use of CFRP wraps for the confinement of lap-splice regions is not an effective measure of insuring proper stress transfer between the lapped plain bars.

- The rehabilitation applied in specimen NSTR-W-1/3 by welding the lapped bars led to further improvements in the drift characteristics. The system ductility of the unreinforced HCT infill wall increased by nearly 100 percent by this implementation.

- In general, the system improvement provided by the CFRP retrofitting may be designated as superior in squat frames compared to more narrow specimens.

- In 1/2 scaled frames, the applied strengthening may be concluded to result in slightly higher improvements in terms of base shear capacity and dissipated energy, in comparison to 1/3 scaled specimens. This conclusion should not be generalized unless it is supported by further experiments and numerical studies with improved analytical models.

- The implemented analytical model may be regarded as successful in predicting the nonlinear monotonic response of RC infill frames strengthened with the proposed methodology, especially for the case of Group-I specimens. In Group-II, the post-peak drift characteristics of the strengthened frames were underestimated by the numerical model.

- Both analytical and experimental results indicated that CFRP reinforced infill walls may have capacity to experience higher drift ratios than the limit value proposed by TEC 2007 (i.e. 0.35 percent) without significant damage.

- The parametric study in terms of numerical simulations of frames similar to 1/3 scaled test specimens but with varying aspect ratios revealed that substantial contribution of infill walls alone tend to decrease with increased infill height/width ratios. Within the entire aspect ratio range investigated, the applied CFRP strengthening increased the base shear capacity considerably. However, the ultimate strength increment provided by CFRP strengthening yielded highest results for the aspect ratios in between 0.8 and 1.2. Moreover, as the results show, this strength enhancement could be attained without significant alteration of the initial stiffness of the frames.

- In the case of buildings which require system improvement without evacuation and when service delay of the building is a major concern, the strengthening methodology described herein may be one feasible alternative, as being a rapid and user friendly retrofitting approach.

7.3. RECOMMENDATIONS FOR FURTHER STUDY

The performed study may be extended with further studies in the following areas:

- The tests of 1/2 and 1/3 scaled two-dimensional planar frame specimens provided significant information on the efficiency of the proposed rehabilitation method. However a full scale planar frame or three-dimensional building strengthened by the proposed methodology may be tested with improved dynamic testing facilities.

- The numerical model suggested in this study may be enhanced to capture higher scale frame response more accurately in the post-elastic range. The effective FRP strain, $\varepsilon_{f,eff}$ is believed to be an important parameter in this respect.

REFERENCES

ACI, 2005, "Building Code Requirements for Structural Concrete (ACI 318-05) and Commentary (ACI 318R-05)", ACI 318-05, American Concrete Institute, Farmington Hills, MI, USA.

Altın S., 1990, "Strengthening of Reinforced Concrete Frames with Reinforced Concrete Infils", PhD Thesis, Middle East Technical University, Ankara, Turkey, 350 p.

Altın, S., Ersoy, U., 1992, "Hysteretic Response of Reinforced-Concrete Infilled Frames", Journal of Structural Eng., Volume 118, pp. 2133-2150.

Altın, S., Anıl, Ö., Kara, M. E., Kaya, M., 2008, "An Experimental Study on Strengthening of Masonry Infilled RC Frames using Diagonal CFRP Strips", Composites Part B: Engineering, Volume 39, pp. 680-693.

ASCE, 2007, "Seismic Rehabilitation of Existing Buildings", ASCE/SEI Standard 41-06, American Society of Civil Engineers, Reston, VA, USA.

ATC, 1996, "ATC-40 Seismic Evaluation and Retrofit of Concrete Buildings", Report No. SSC 96-01, Applied Technology Council, Redwood City, California, USA.

Bakis, C. E., Bank, L. C., Brown, V. L., Cosenza, E. et al., 2002, “Fiber-Reinforced Composites for Construction – State-of-the-Art Review”, Journal of Composites for Construction Volume 6, No. 2, pp. 73-87.

Baran M., 2005, “Precast Concrete Panel Reinforced Infill Walls for Seismic Strengthening of Reinforced Concrete Framed Structures”, PhD Thesis, Middle East Technical University, Ankara, Turkey, 265 p.

Bertero, V. and Brokken, S., 1983, “Infills in Seismic Resistant Building”, Journal of Structural Engineering, Volume 109, No. 6, June 1983, pp. 1337-1361.

Binici, B., Mosalam, K. M., 2007, “Analysis of Reinforced Concrete Columns Retrofitted with Fiber Reinforced Polymer Lamina”, Composites B: Engineering, Volume 38, pp. 265-276.

Binici, B., Özcebe, G. and Özçelik, R., 2007, “Analysis and Design of FRP Composites for Seismic Retrofit of Infill Walls in Reinforced Concrete Frames”, Composites Part B: Engineering, Volume 38, pp. 575-583.

Binici, B., Kobayashi, K., 2008, “Economical Seismic Retrofit Schemes for Vulnerable RC Buildings with Infill-Brick Wall Using New FRP Technologies”, The 14th World Conference on Earthquake Engineering, pp. 1-8.

Canbay, E., 2001, “Contribution of RC Infills to the Seismic Behavior of Structural Systems”, PhD Thesis, Middle East Technical University, Ankara.

Canbay, E., Ersoy, U. and Özcebe, G., 2003, “Contribution of Reinforced Concrete Infills to the Seismic Behavior of Structural Systems”, Structural Journal, ACI; 100(5):637-43.

Canbay, E., Ersoy, U., and Tankut, T., 2004, “A Three Component Force Transducer for Reinforced Concrete Structural Testing”, Engineering Structures, Volume 26, pp. 257-265.

CEB (Comite Euro-International du Beton), 1996, “RC Frames under Earthquake Loading – State of Art Report”, Thomas Telford Publications, Lausanne, Switzerland.

Cho, J. and Pincheira, J. A., 2006, “Inelastic Analysis of Reinforced Concrete Columns with Short Lap Splices Subjected to Reversed Cyclic Loads”, ACI Structural Journal, Volume 103, pp. 280-290.

Çamlı, Ü. S., 2005, “Anchorage Strength of Fiber Reinforced Polymers”, Master of Science Thesis, Middle East Technical University, Ankara, Turkey, 83 p.

Dimova, S. L. and Negro, P., 2005, “Seismic Assessment of an Industrial Frame Structure Designed According to Eurocodes. Part 2: Capacity and Vulnerability”, Engineering Structures, Volume 27, pp. 724-735.

Duvarcı M., 2003, “Seismic Strengthening of Reinforced Concrete Frames with Precast Concrete Panels”, Master of Science Thesis, Middle East Technical University, Ankara, Turkey, 93 p.

El-Dakhakhni, W. W., Hamid, A. A., and Elgaaly, M., 2004, “Seismic Retrofit of Masonry-Infilled Steel Frames Using GFRP”, ASCE Journal of Structural Engineering, Volume 130, No:9, pp. 1343-1352.

El-Sokkary, H. and Galal, K., 2009, “Analytical Investigation of the Seismic Performance of RC Frames Rehabilitated Using Different Rehabilitation Techniques”, Engineering Structures, Volume 31, September, pp. 1955-1966.

Erdem, İ., 2003, “Strengthening of Existing Reinforced Concrete Frames”, Master of Science Thesis, Middle East Technical University, Ankara, Turkey, 123 p.

Erdem , İ., Akyüz, U., Ersoy, U. and Özcebe, G., 2006, “An Experimental Study on Two Different Strengthening Techniques for RC Frames”, Engineering Structures, Volume 28, pp. 1843-1851.

Erduran E., 2002, “Behaviour of Brick Infilled Reinforced Concrete Frames Strengthened CFRP Reinforcement : Phase II”, Master of Science Thesis, Middle East Technical University, Ankara, Turkey, 94 p.

Erol, G., Demir, C., İlki, A., Yüksel, E. et al., 2006, “Effective Strengthening of RC Frames with and without Lap Splice Problems”, Proceedings of 8th International Conference on Earthquake Engineering, 19-21 April, San Francisco, California, USA.

Erol, G., Karadoğan, H. F., and Çılı, F., 2008, “Seismic Strengthening of Infilled RC Frames by CFRP”, Proceedings of 14th World Conference on Earthquake Engineering, 12-17 Oct., Beijing, China.

Ersoy, U., Uzsoy, Ş. Z., 1971, “The Behavior and Strength of Infilled Frames”, TUBITAK MAG-205 Report, Ankara, Turkey (in Turkish).

Ersoy, U., Özcebe, G., 2002, “Lessons from Recent Earthquakes in Turkey and Seismic Rehabilitation of Buildings”, ACI Special Publication, SP197-05, Volume 197, pp. 105-126.

Ersoy, U., Özcebe, G., Tankut, T., Akyüz, U., Erduran, E., and Erdem, İ., 2003, "Strengthening of Infilled Walls with CFRP Sheets", International Advanced Research Workshop, Seismic Assessment and Rehabilitation of Existing Buildings, İzmir, Turkey.

Ersoy, U., 2007, "Repair and Strengthening of Reinforced Concrete Buildings Research and Applications", Proceedings of 6th National Conference on Earthquake Engineering, 16-20 Oct., Istanbul, Turkey, pp. 207-216 (in Turkish).

Ersoy, U., 2009, "Seismic Rehabilitation of Reinforced Concrete Buildings", Earthquakes and Tsunamis, Geotechnical, Geological and Earthquake Engineering, Volume 11, pp. 7-20.

FEMA 356, 2000, Prestandard and Commentary for the Seismic Rehabilitation of Buildings, Federal Emergency Management Agency, Washington DC, USA.

Garevski, M., Hristovski, V., Talaganov, K., Stojmanovska, M., 2004, "Experimental Investigations of 1/3-Scale R/C Frame with Infill Walls Building Structures", Proceedings of the 13th World Conference on Earthquake Engineering, Paper No. 772, Vancouver B.C., Canada, August 1-6.

Hashemi, A. and Mosalam, K. M., 2006, "Shake Table Experiment on One-Story RC Structure with and without Masonry Infill", Advances in Earthquake Engineering for Urban Risk Reduction, NATO Science Series, Volume 66, pp. 411–426.

Hognestad, E., 1951, "A Study of Combined Bending and Axial Load in R.C. Members", University of Illinois Engineering Experiment Station, Bulletin No.339, November.

Jirsa, J. O., 2006, "Learning from Earthquakes to Improve Rehabilitation Guidelines for Reinforced Concrete Buildings", Advances in Earthquake Engineering for Urban Risk Reduction, NATO Science Series, Volume 66, pp. 209-227.

Jirsa, J. O. and Kim, I., 2009, "Use of CFRP to Strengthen Splices and Provide Continuity in Reinforced Concrete Structures", Earthquakes and Tsunamis, Geotechnical, Geological and Earthquake Engineering, Volume 11, pp. 21-34.

Kent, D. C. and Park, R., 1971, "Flexural Members with Confined Concrete", Journal of the Structural Division, ASCE, July, Volume 97 (ST7).

Keskin, R. S. O., 2002, "Behavior of Brick Infilled Reinforced Concrete Frames Strengthened by CFRP Reinforcement: Phase I", Master of Science Thesis, Middle East Technical University, Ankara, 140 p..

Kobayashi, K., 2007, "Innovative Application of FRP's to Seismic Retrofit of Brick-Infilled RC Frames", Proceedings of FRPRCS-8, University of Patras, Patras, Greece.

Marjani, F., 1997, "Behavior of Brick Infilled Reinforced Concrete Frames under Reversed Cyclic Loading", PhD Thesis, Middle East Technical University, Ankara.

Mazzoni, S., McKenna, F., Scott, M. H., Fenves, G. L., et al., 2007, "Open System for Earthquake Engineering Simulation User (OpenSees) Command-Language Manual", Version 2.0, University of California, Berkeley, California, (http://opensees.berkeley.edu./OpenSees/manuals/usermanual/) (last accessed on 07/03/2011)

Mehrabi, A. B., Shing, P. B., Schuller, M. P., and Noland, J. L., 1996, “Experimental Evaluation of Masonry-Infilled RC Frames”, Journal of Structural Engineering, Volume 122, No. 3, pp. 228-237.

Mertol H. C., 2002, “Carbon Fiber Reinforced Masonry Infilled Reinforced Concrete Frame Behaviour”, Master of Science Thesis, Middle East Technical University, Ankara, Turkey, 67 p.

Mohyeddin-Kermani, A., Goldsworthy, H. M., and Gad, E. F., 2008, “The Behaviour of RC Frames with Masonry Infill in Wenchuan Earthquake”, Proceedings of the Australian Earthquake Engineering Society Conference (AEES) 2008, Ballarat, Victoria, Australia, 21-23 November, Paper No:39.

Murty, C. V. R., Brzev, S., Faison, H., Comartin, C. D. et al., 2006, “AT RISK: The seismic performance of reinforced concrete frame buildings with masonry infill walls (First Edition)”, Earthquake Engineering Research Institute, Publication Number WHE-2006-03.

Nateghi-Elahi, F. and Dehghani, A., 2008, “Analytical and Numerical Study of RC Frames with URM Infilled Retrofitted by CFRP”, Proceedings of 14th World Conference on Earthquake Engineering, 12-17 Oct., Beijing, China.

Negro, P. and Verzeletti, G., 1996, “Effect of Infills on the Global Behaviour of R/C Frames: Energy Considerations from Pseudodynamic Tests”, Earthquake Engineering and Structural Dynamics, Volume 25, pp. 753-773.

Okuyucu, D. and Tankut, T., 2009, “Effect of Panel Concrete Strength on Seismic Performance of RC Frames Strengthened by Precast Concrete Panels”, WCCE-ECCE-TCCE Joint Conference: Earthquake and Tsunami, IMO Publication Nr.: E/09/03, Istanbul, Turkey.

Özcan, O., Binici, B. and Özcebe, G., 2008 "Improving Seismic Performance of Deficient Reinforced Concrete Columns Using Carbon Fiber-Reinforced Polymers", Engineering Structures, Volume 30, pp. 1632-1646.

Özcebe, G., Ersoy, U. Tankut, T., Akyüz, U., Erduran, E., 2004, "Rehabilitation of Existing Reinforced Concrete Structures Using CFRP Fabrics", 13th Conference on Earthquake Engineering, Vancouver B. C. Canada, August, Paper No:1393.

Özcebe, G., Sucuoğlu, H., Yücemen, M. S., and Yakut, A., 2006-a, "In Defence of Zeytinburnu," NATO Science Series IV: Earth and Environmental Sciences; Advances in Earthquake Engineering for Urban Risk Reduction, NATO Science Series, Volume 66, pp. 95–116.

Özcebe, G., Binici B., Ersoy, U., Tankut, T., Middle East Technical University, Ankara, Turkey; Özden, Ş., Kocaeli University, Turkey; Karadoğan, F., Yüksel, E., İlki, A., Istanbul Technical University, Turkey, 2006-b, "Analysis of infilled reinforced concrete frames strengthened with FRP's", Retrofitting of Concrete Structures by Externally Bonded FRP's, FIB, Technical Report, April, pp. 167-197.

Özden, Ş, Akgüzel, U., 2003, "Seismic Retrofit of Brick Infilled R/C Frames With Lap Splice Problems in Columns", Master of Science Thesis, Graduate Program in Civil Engineering, Bogazici University, Istanbul, 125 p.

Özdemir G., 2005, "Mechanical Properties of CFRP Anchorages", Master of Science Thesis, Middle East Technical University, Ankara, Turkey, 74 p.

Saatçioğlu, M., Serrato, F. and Foo, S., 2005, "Seismic Performance of Masonry Infill Walls Retrofitted with CFRP Sheets", ACI-SP230: 7th Int. Symp. on Fiber-Reinforced (FRP) Polymer Reinforcement for Concrete Structures, 341-354.

Saatçioğlu, M., 2006, “Seismic Risk Mitigation through Retrofitting Non-ductile Concrete Frame Systems”, Advances in Earthquake Engineering for Urban Risk Reduction, NATO Science Series, Volume 66, pp. 179-194.

Sonuvar, O., 2001 “Hysteretic Response of Reinforced Concrete Frames Repaired by Means of Reinforced Concrete Infills”, PhD Thesis, Middle East Technical University, Ankara.

Sonuvar, M. O., Özcebe, G., Ersoy, U., 2004, “Rehabilitation of Reinforced Concrete Frames with Reinforced Concrete Infills”, Structural Journal, ACI; July-August, 101(4):494-500.

Stafford Smith, B., 1967, “Methods for Predicting the Lateral Stiffness and Strength of Multi-Storey Infilled Frames”, Building Science, Volume 2, pp. 247-257.

Süsoy, M., 2004, “Seismic Strengthening of Masonry Infilled Reinforced Concrete Frames with Precast Concrete Panels”, Master of Science Thesis, Middle East Technical University, Ankara, 138 p.

The Ministry of Public Works and Settlement, 2007, “Turkish Code for Buildings in Seismic Zones”, 159p.

Triantafillou, T. C., 1998, “Strengthening of Masonry Structures Using Epoxy Bonded FRP Laminates”, ASCE J. Compos. For Constr., 2(2), pp. 96 104.

Üzümeri, Ş. M., Tankut, T., Özcebe, G., and Atımtay, E., 1999, “Assessment, Repair/Strengthening of Moderately Damaged Reinforced Concrete Buildings in Ceyhan Earthquake (1998)", Uğur Ersoy Symposium on Structural Engineering Proceedings, METU, Ankara, pp. 413-429.

Van Den Einde, L., Zhao, L., Seible, F., 2003, "Use of FRP Composites in Civil Structural Applications", Construction and Building Materials, Volume 17, September-October, pp. 389-403.

Yakut, A., 2004, "Reinforced Concrete Frame Construction", World Housing Encyclopedia, Summary Publication.

Yüksel E., İlki A., Erol G., Demir C., Karadoğan, H. F., 2006, "Seismic Retrofit of Infilled Reinforced Concrete Frames with CFRP Composites", Advances in Earthquake Engineering for Urban Risk Reduction, NATO Science Series, Vol. 66, pp. 285-300.

Yüksel, E., Özkaynak, H., Büyüköztürk, O., and Yalçın, C., 2009, "Performance of Alternative CFRP Retrofitting Schemes Used in Infilled RC Frames", Construction and Building Materials, Volume 24, pp. 596-609.

Zarnic, R. and Tomazevic, M., 1984, "An Experimentally Obtained Method for Evaluation of the Behaviour of Masonry Infilled R/C Frames", 9th World Conference on Earthquake Engineering, San Fransico, USA, Volume VI, pp. 863-870.

APPENDIX A

PANEL TESTS

A.1 Panel Test Specimens

A total number of ten square HCT panels having edge length of 700 mm and thickness of 75 mm (without plaster) were built-up using specially produced 1/3 scaled HCT's. The specimens were constructed in the horizontal position. Two specimens having identical properties were tested in five groups in order to ensure a sound assessment of the results. The specimens with their designations, corresponding properties and view on the test setup are shown in Table A.1. Two of the specimens (NP-1 and NP-2) were non-plastered panels. Plaster with a thickness of 10 mm was applied on both faces of the other two panels (P-1 and P-2), however no CFRP was implemented. These four panels constituted the reference specimens for assessing different strengthening configurations applied in the last six panels. The first set of strengthening was applied on specimens LD-1 and LD-2, where one layer of CFRP was implemented only in the diagonal direction of loading. In specimens PLD-1 and PLD-2, CFRP fabric was applied along the diagonal which was perpendicular to the loading direction. And lastly, both diagonal directions of the specimens CR-1 and CR-2 were strengthened using CFRP fabrics.

Table A. 1 Properties of the Panel Specimens

Specimens	Retrofitting	View
NP-1 NP-2	-	
P-1 P-2	-	
LD-1 LD-2	CFRP along the loading diagonal direction	
PLD-1 PLD-2	CFRP along the diagonal perpendicular to the loading direction	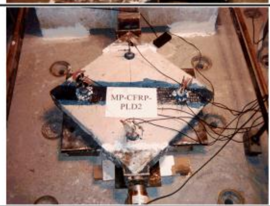
CR-1 CR-2	CFRP in both diagonal directions (i.e. Cross)	

A.2 Strengthening of Panels

Strengthening was provided through application of one layer of CFRP strips with constant width of 100 mm on both faces. In all specimens, CFRP sheets were bonded above the plastered surface. For strengthening, HCT panels were cautiously raised in the vertical position, in order to be able to use both faces of the specimens for CFRP application. Three holes with a diameter of 8 mm were drilled over the diagonals of the panels where CFRP sheets were planned to be bonded. An equal interval length (i.e. around 250 mm) was provided for the holes which would serve as sockets for anchor dowels.

The anchor dowels were used to fix the CFRP sheets on the panels and consequently, to delay or prevent early debonding of CFRP. Therefore, a monolithic behavior of the CFRP and panel was provided under the action of shear stresses. These dowels were prepared using CFRP strips having a width of 60 mm and height of 200 mm in the fiber direction.

The drilled holes were cleaned out of dust by the help of an air-compressor. The locations of CFRP sheets were marked on the specimens. The undercoat material of MBT-MBrace® Primer was applied over the marked areas. After dry-up of the undercoat, the chemical mortar (Concressive® 1406) was applied on the undercoats before the installation of CFRP reinforcement. In terms of basic principles, the installation of the CFRP on the HCT walls were the same as the strengthening process explained in Section 3.2.5. Also the anchor dowels were prepared and implemented in a similar manner as explained for Group-I specimens in Section 3.2.5 (i.e. Type-B dowels). The wet-lay-up process was followed where MBT-MBrace® Adesivo Saturant was used as adhesive. A panel specimen strengthened in only one diagonal direction is shown in Figure A.1.

A.3 Material Properties

The mix design of the joint mortar and plaster, as shown in Table A.2 was selected amongst different alternatives prepared prior to the preparation of specimens. In order to determine the compressive strength of the mortar and plaster, cylinder specimens with a diameter of 75 mm and a height of 150 mm were taken during the construction of the panels. Test results indicated that the average compressive strength of mortar and plaster were 12.1 and 9.3 MPa, respectively. Plaster was applied on both faces of the panels. The thickness of the plaster was 10 mm.

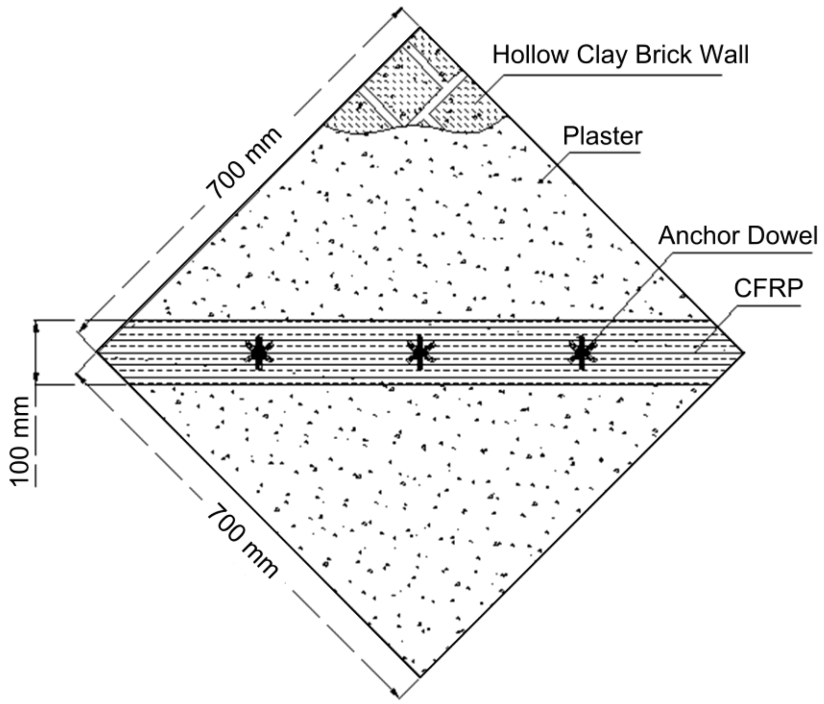

Figure A. 1 Panel Specimen strengthened in one diagonal direction only

Table A. 2 Mix proportions of mortar and plaster

Material	**Weight Proportions(%)**
0-3 Aggregate	65.3
Lime	10.6
Cement	10.6
Water	13.5
Total	100.0

The same HCTs which were used for the construction of infill walls in Group-I frames were also utilized for panel specimens. The geometrical and mechanical properties of these HCTs are presented in Section 3.2.3.3.

The CFRP material used for strengthening of the HCT panels was the same as used for frame specimens. In Section 3.2.5, it was stated that the CFRP was applied in conjunction with the chemicals; MBT-MBrace® Primer, Concressive® 1406 (putty) and MBT-MBrace® Adesivo Saturant (adhesive). The mechanical properties of the CFRP and these chemicals were presented in Section 3.2.3.4 in detail.

A.4 Test Setup and Instrumentation

The test setup was formed in between two heavy concrete blocks which were further encased by a steel frame, as shown in Figure A.2. The main function of these blocks was to support the setup by working as a reaction wall. Steel box profiles were situated between the concrete blocks and panels in the vertical position. Monotonic loading was applied throughout the test, up to the brittle failure of the specimens, by means of a manually controlled hydraulic jack. A load cell was located between the specimen and the jack in order to measure the level of applied load.

The specimens were placed over the marbles which were located on a greasy plate in order to minimize the friction. The corners of the specimens were inserted into triangular metal caps, which were filled with lime plaster to fill the gaps and provide a perfect bond between the cap and the corners of the panel. The applied load was transferred along the diagonals of the HCT panels through these caps over a width of 350 mm. The back of these metal caps was leaned to the steel box profile on one side and to the load cell and hydraulic jack on the other side. At the connection point between the metal cap and the load cell, a roller was nested into specially produced sockets on each side. By this way, any possible flexural out-of-plane actions were avoided and the applied loads could be transferred via diagonal compression.

The in-plane displacements in the two diagonal directions along a length of 580 mm and four directions parallel to the edges of the specimen along a length of 410 mm were monitored. So as to detect these displacements, six dial gauges were placed on the HCT panel in the directions as shown in Figure A.2. The dial gauges and the load cell were connected to a data acquisition system to collect the required data.

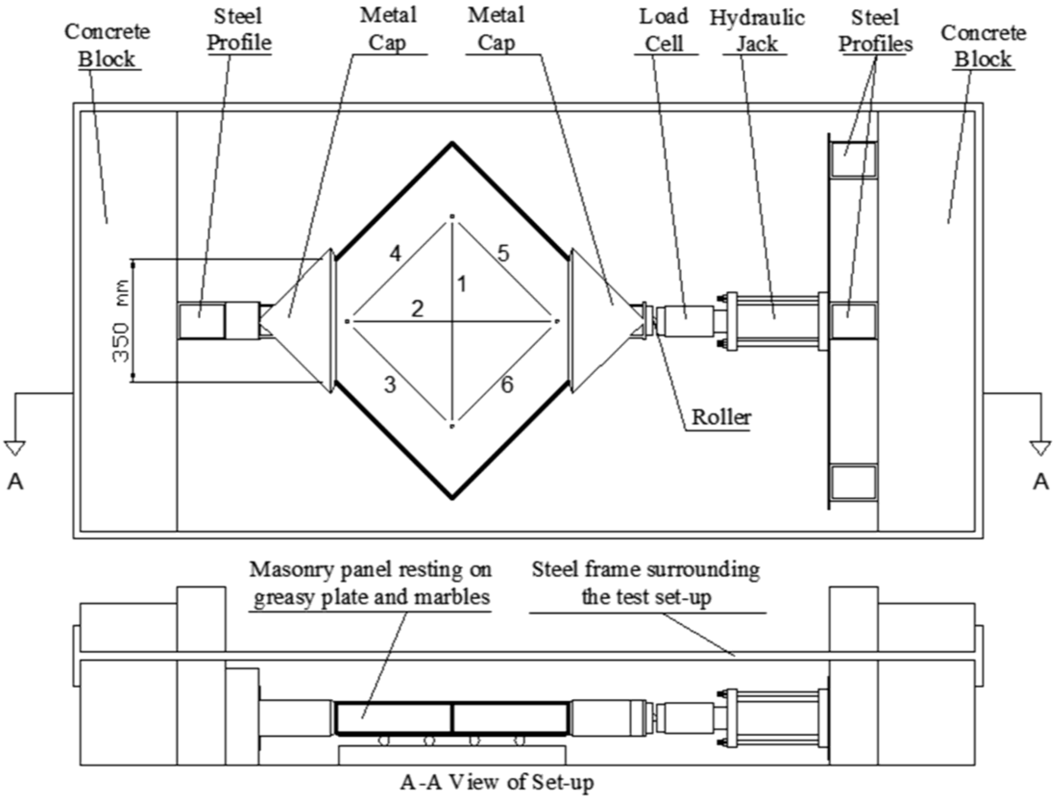

Figure A. 2 Test setup for panel specimens

A.5 Panel Test Results

Since two identical panel specimens were tested for reliability purposes, the results of these specimens are depicted as a group. Because of an error that occurred during the test of specimen PLD-1, the results of this panel are ignored and only those of PLD-2 are presented. The diagonal load vs. strains on both diagonal directions are plotted and shown for each panel specimen separately. The strain values in the compressive and tensile directions are calculated by dividing the displacements measured in directions "1" and "2" shown in Figure A.2 by the gauge length, respectively. The compressive displacements along the loading direction are marked as negative and the tensile displacements along the perpendicular direction as positive. The ultimate strength values experienced by the panel specimens are summarized in Table A.3.

Table A. 3 Panel Test Results

Specimen	*Ultimate Strength (kN)*	*Average Ultimate Strength (kN)*
NP-1	66.0	62.8
NP-2	59.5	
P-1	126.8	131.2
P-2	135.6	
LD-1	158.7	143.0
LD-2	127.3	
PLD-1	-	228.0
PLD-2	228.0	
CR-1	194.7	195.1
CR-2	195.4	

A.5.1 NP-1 and NP-2

Both NP-1 and NP-2 were reference panel specimens without a plaster. The average of the ultimate diagonal load experienced by the specimens was approximately 62.8 kN. The load vs. strain curves of the specimens are shown in Figure A.3. It can be seen that the behavior was quite brittle as expected. The failure of the specimens was in the form of diagonal splitting. As seen in Figure A.4, one major crack which formed almost along the loading direction engendered the failure. This major crack was partially chasing the bed joints (i.e. joint slipping) and cracking the HCT's.

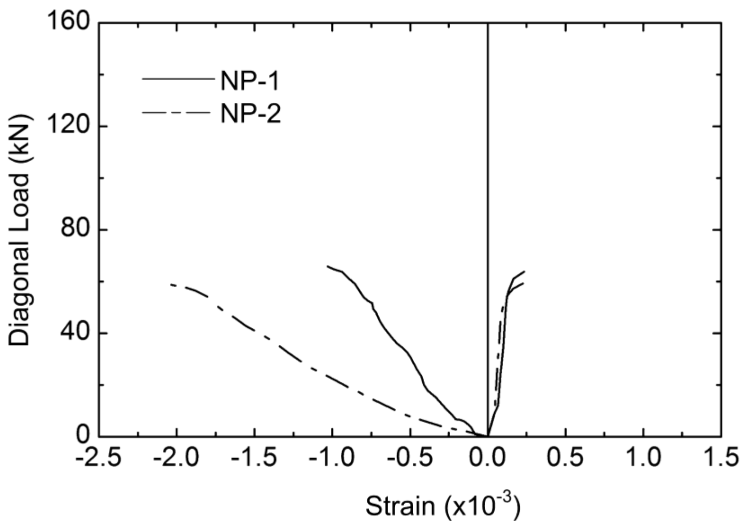

Figure A. 3 The diagonal load vs. strain curves of the panel specimens NP-1 and NP-2

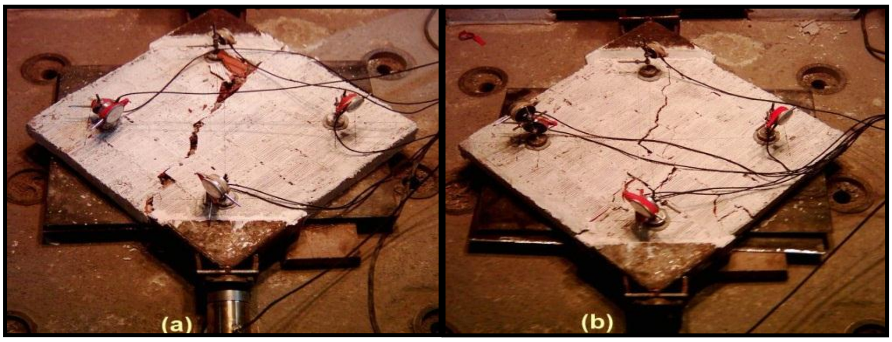

Figure A. 4 The view of the specimens, (a) NP-1 and (b) NP-2 after the test

A.5.2 P-1 and P-2

These panel specimens may also be regarded as reference specimens with a plaster applied on both faces. An average ultimate diagonal load of 131.2 kN was attained during the tests. This indicates a strength increase more than 100 percent by virtue of the applied plaster. Comparing the load vs. strain curves given in Figures A.3 and A.5, it can be concluded that the initial stiffness of the specimens were also increased considerably by the application of plaster. The failure was again triggered by diagonal splitting. However, especially in the case of P-2, the failure was more sudden and severe compared to previous two specimens. In specimen P-2, also local crushing of the panel was observed at the vicinity of the metal loading caps (Figure A.6).

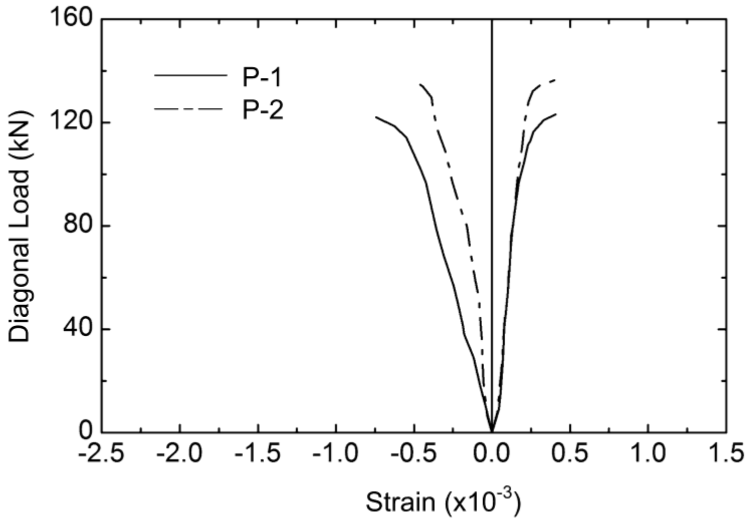

Figure A. 5 The diagonal load vs. strain curves of the panel specimens P-1 and P-2

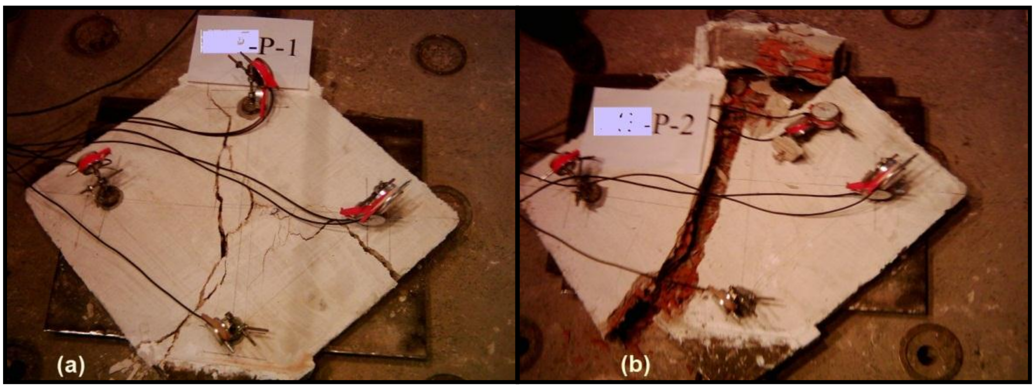

Figure A. 6 The view of the specimens, (a) P-1 and (b) P-2 after the test

A.5.3 LD-1 and LD-2

In specimens LD-1 and LD-2, the unidirectional CFRP sheet was implemented only in the loading direction along which the compression strut was expected to form. The average ultimate load capacity of the panels was 143.0 kN. This shows that laying CFRP fibers in the compression strut direction did not change the strength significantly. The diagonal load vs. strain curves of these specimens are presented in Figure A.7.

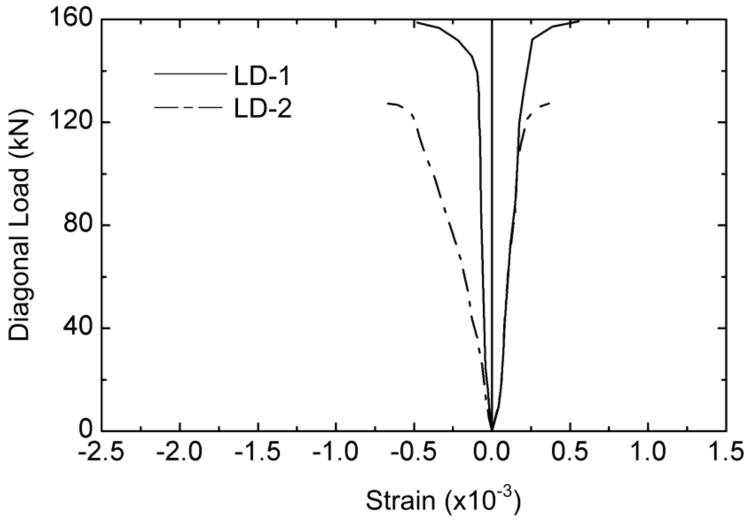

Figure A. 7 The diagonal load vs. strain curves of the panel specimens LD-1 and LD-2

Similar to the reference specimens, splitting along the loading diagonal caused failure of the specimens. The splitting was quite sudden, such as breaking into pieces. The popping noises were heard before failure which indicated debonding of the CFRP sheet. After breaking loose from the panel surface, the sheets experienced buckling under compression. Additionally, local crushing of the panel was observed at the vicinity of the loading caps close to hydraulic jack (Figure A.8).

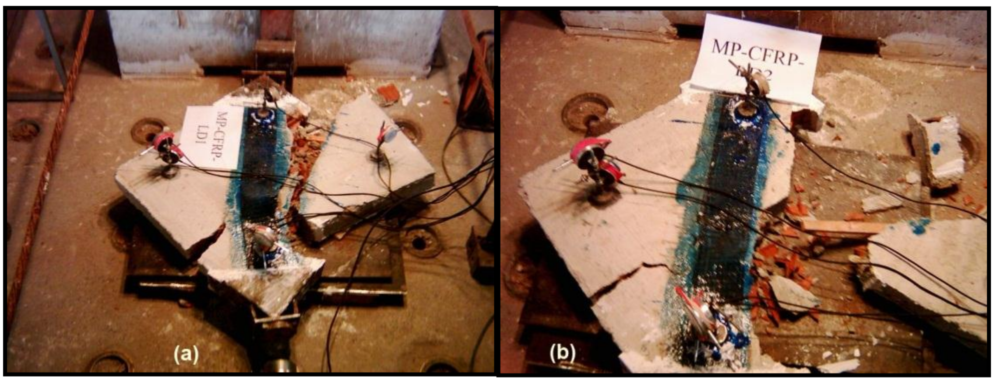

Figure A. 8 The view of the specimens, (a) LD-1 and (b) LD-2 after the test

A.5.4 PLD-2

In specimens PLD-1 and PLD-2, the unidirectional CFRP sheet was implemented only in the diagonal direction which was perpendicular to the loading direction. In other words, the CFRP fibers were aimed to be utilized under tensile stresses triggered by the volumetric expansion. As mentioned before, the results of PLD-1 are not considered here due to an error observed during the test. The diagonal load vs. strain curve of the specimen PLD-2 is shown in Figure A.9. The ultimate diagonal load was 228.0 kN. This is 1.74 times higher than the average load capacity of the plastered reference specimens. Therefore, it may be concluded that a significant increase in the load capacity of the HCT panels could be provided by applying CFRP along the direction of potential tensile stresses. The formation of the diagonal crack which caused failure was not as severe and sudden as the previous specimens. Only after the separation of the CFRP from the panel surface, the diagonal crack propagated. However, the applied CFRP sheets on both faces which were connected with anchor dowels were successful in limiting the diagonal crack width. On the other hand, the crushing of the corner of the panel was more severe under increased compressive loads, as shown Figure A.10.

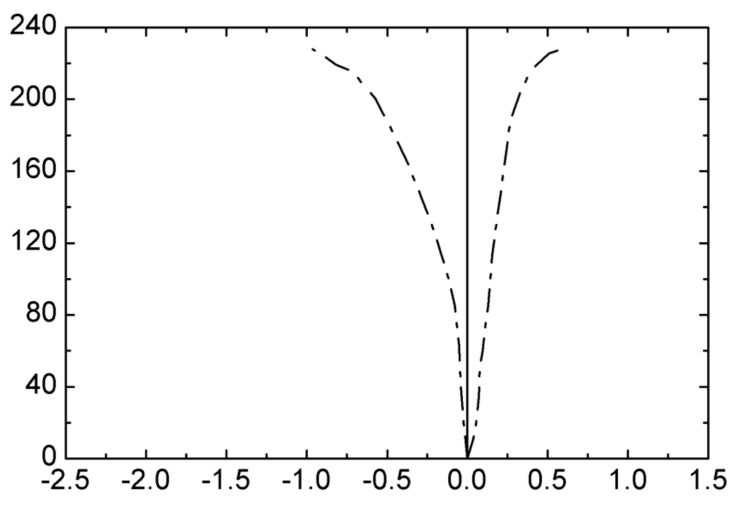

Figure A. 9 The diagonal load vs. strain curves of the panel specimen PLD-2

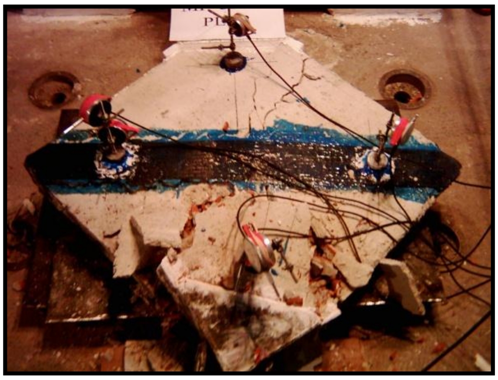

Figure A. 10 The view of the specimen PLD-2 after the test

A.5.5 CR-1 and CR-2

The CFRP reinforcement was applied along both diagonal directions of specimens CR-1 and CR-2. The ultimate lateral load experienced by the specimens was approximately 195 kN, which was slightly lower than that of specimen PLD-2. The diagonal load-strain responses of the specimens are presented in Figure A.11. The failure states of the specimens are illustrated with the pictures shown in Figure A.12.

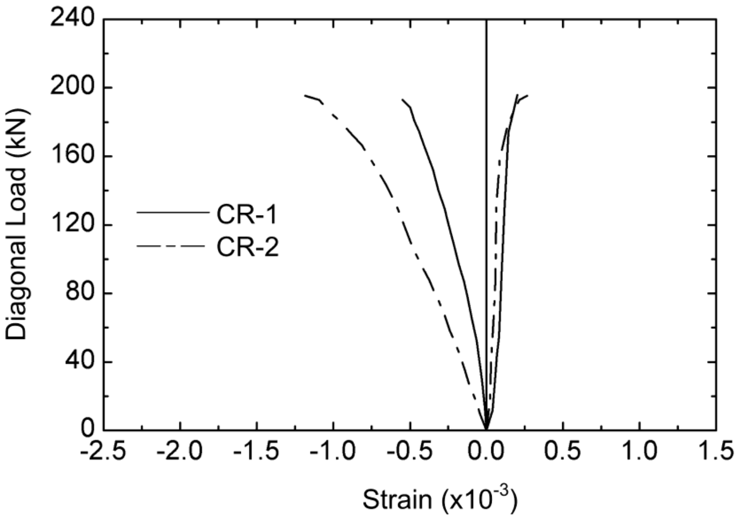

Figure A. 11 The diagonal load vs. strain curves of the panel specimens CR-1 and CR-2

In specimen CR-1, a behavior similar to panel PLD-2 was observed. The CFRP sheet exposed to tensile stresses delayed propagation of the diagonal crack until debonding took place. The CFRP reinforcement along the loading direction buckled under high compressive forces and the CFRP sheet under tensile stresses separated from the panel surface. The formation of diagonal crack on the panel was quite sudden after this stage. On the other hand, the specimen CR-2 was exposed to a drastic failure which caused bursting into pieces after separation of the diagonal CFRP sheets and failure of the anchor dowels (Figure A.12).

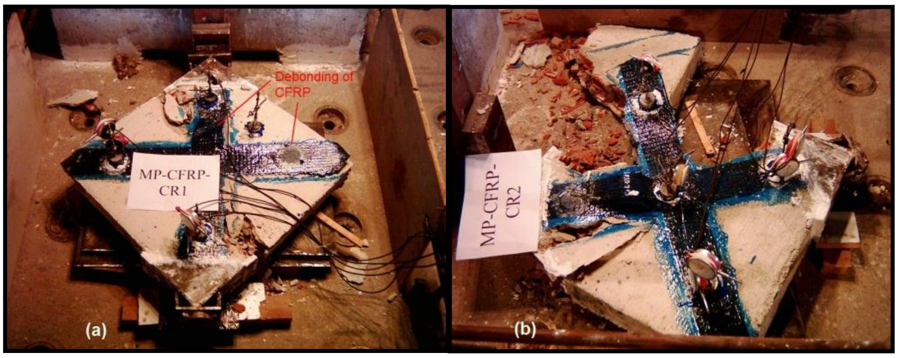

Figure A. 12 The view of the specimens, (a) CR-1 and (b) CR-2 after the test

A.6. Evaluation of Panel Test Results

The average ultimate diagonal loads of the identical panel specimens are shown in Table A.4 which also designates the ratio of these values to that of plaster applied reference panels (i.e. P-1 and P-2). The type of failure observed in each group of panels is given in the same table. Besides, the diagonal load-strain curves of one sample specimen from each group are presented in Figure A.13 for comparison purposes.

As indicated in Table A.4 and shown in Figure A.13, the increase in the load carrying capacity of the panels was more than two times by application of the plaster alone. Although similar type of failure was observed in both non-plastered and plastered panels, splitting was much more sudden for specimens with plaster. Besides, the slipping of HCT panel bed joints in non-plastered panels was not observed in other group of specimens. It may be concluded that, in the absence of plaster, the diagonal compressive force was transferred only through shear stresses along bed joints which may be regarded as weaker compared to brick units. The more uniform stress distribution which could be ensured by the plaster may be the reason of this difference and much higher load capacities.

Table A. 4 Comparison of the panel test results

Specimens	*Average Ult. Load, $P_{panel,ult}$ (kN)*	*Average Ult. Load Relative to Ref. Panels*	*Failure Type*
NP-1 and NP-2	62.8	0.48	Diagonal splitting by combined joint slipping and cracking of HCT units
P-1 and P-2 (ref.)	131.2	1.00	Diagonal splitting by cracking of HCT units (sudden)
LD-1 and LD-2	143.0	1.09	Diagonal splitting (sudden) and local crushing near loading caps
PLD-2	228.0	1.74	Diagonal splitting after debonding of CFRP and crushing near loading caps
CR-1 and CR-2	195.1	1.49	Diagonal splitting after debonding of CFRP and crushing near loading caps

By the application of CFRP fabric along the loading diagonal direction alone seems not to change both the behavior and load carrying capacity of the panels (Table A.4 and Figure A.13). After debonding of the CFRP which was exposed to high level of compressive strains, the HCT panel cracked suddenly along the loading diagonal. This lead to an explosive type of splitting in these specimens, which were not reinforced along tensile direction.

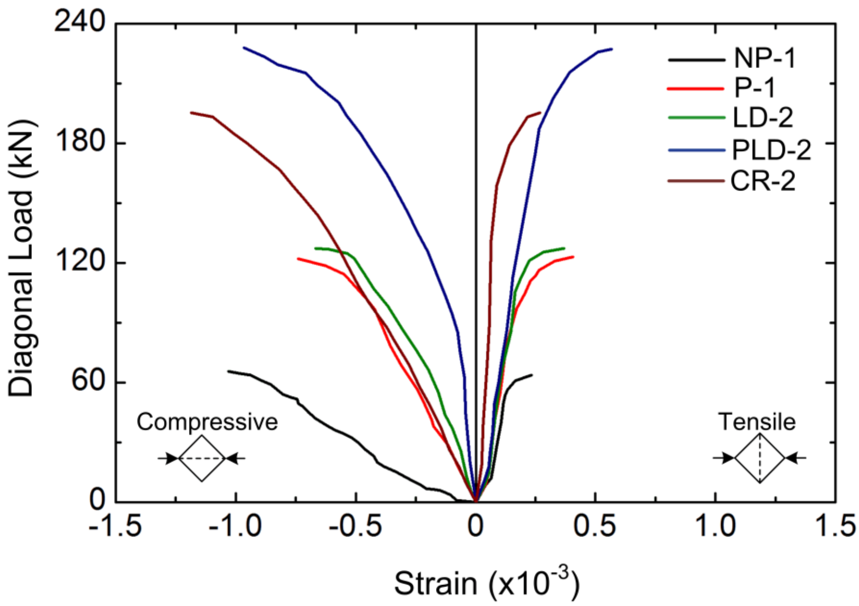

Figure A. 13 The diagonal load vs. strain curves of sample panel specimens

In specimens PLD-2, CR-1 and CR-2, the implementation of CFRP along the diagonal that was perpendicular to the loading diagonal direction provided considerable amount of increment in the load capacity. This increment was around 75 percent in PLD-2 and 50 percent in CR-1 and CR-2. In these panels, the CFRP fibers were utilized in tension and resisted against dilatation of panel up to significant level of load. At this level, straining of HCT panel in the tensile diagonal direction caused failure of anchor dowels, debonding of the fabric from the panel surface and terminated the contribution of CFRP in this direction. Consequently, the diagonal splitting took place suddenly together with corner crushing at the vicinity of loading caps.

APPENDIX B

STRAIN OF DIAGONAL CFRP SHEETS

As mentioned in Section 3.3.7 of Chapter 3, the straining of the diagonal CFRP sheets were monitored on different locations of the retrofitted frames. The highest strain values of the diagonal sheets were observed close to bottom corners of the first story walls, either at the back or front faces. The CFRP strain values only at one critical location for each frame are plotted against the applied base shear forces. And the corresponding hysteretic curves are shown in Figures B.1, B.2, B.3, B.4 and B.5 for specimens NSTR-L-1/3, LSTR-L-1/3, LSTR-C-1/3, NSTR-1/2 and LSTR-1/2, respectively.

As may be observed by a comparison of the maximum strain values experienced by the diagonal CFRP sheets of Series-N specimens with those of Series-L frames, the strain values are significantly higher in the case of squat frames in both groups. This further supports the previous inference about more decent utilization of CFRP sheets as tension ties in specimens with lower aspect ratio.

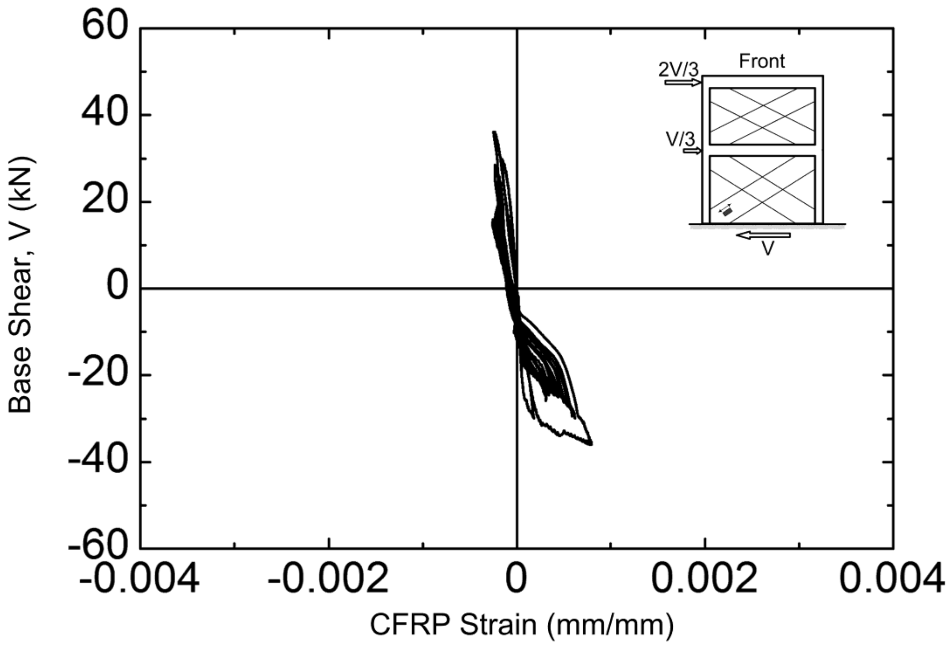

Figure B. 1 The applied base shear vs. strain at the bottom of diagonal CFRP strip on the front face of specimen NSTR-L-1/3

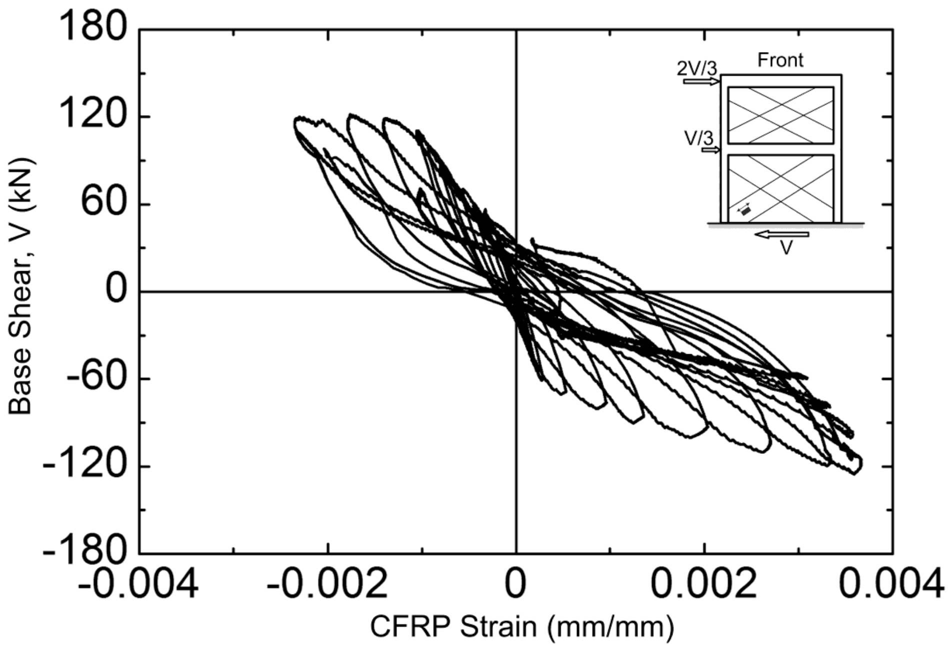

Figure B. 2 The applied base shear vs. strain at the bottom of diagonal CFRP strip on the front face of specimen LSTR-L-1/3

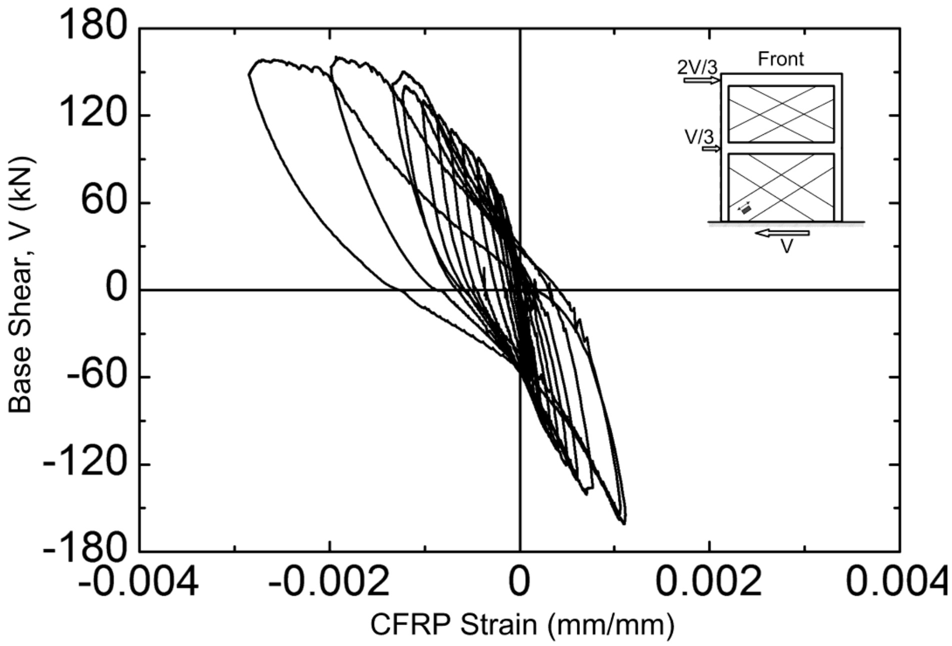

Figure B. 3 The applied base shear vs. strain at the bottom of diagonal CFRP strip on the front face of specimen LSTR-C-1/3

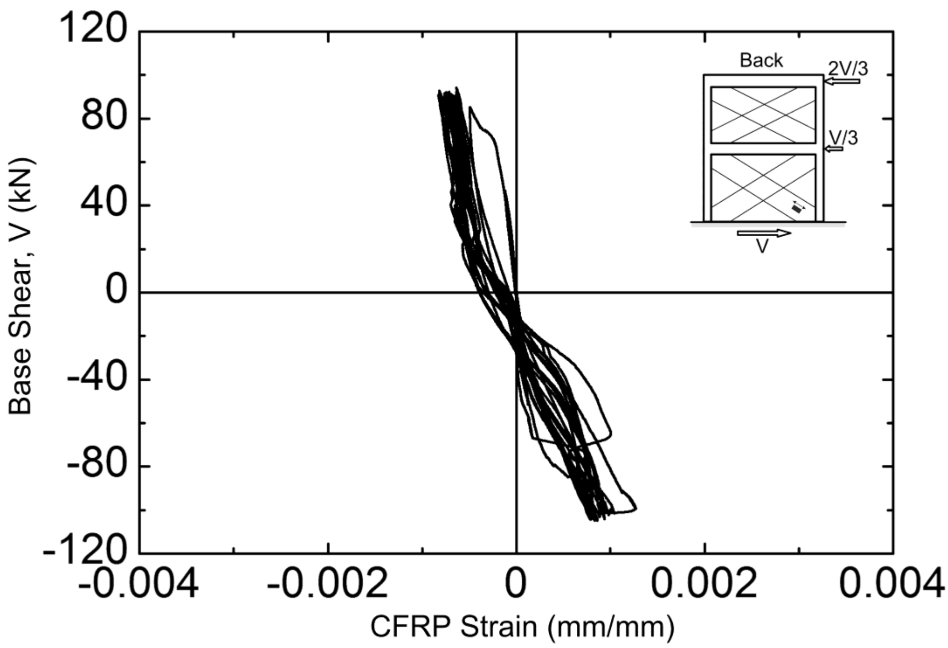

Figure B. 4 The applied base shear vs. strain at the bottom of diagonal CFRP strip on the back face of specimen NSTR-1/2

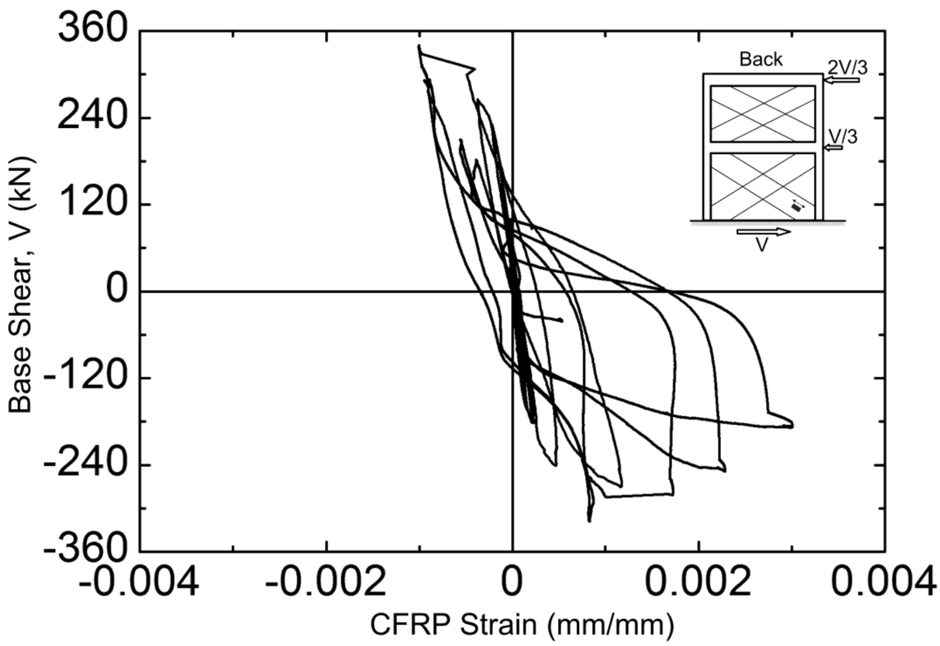

Figure B. 5 The applied base shear vs. strain at the bottom of diagonal CFRP strip on the back face of specimen LSTR-1/2

APPENDIX C

EVALUATION OF PANEL SHEAR DEFORMATIONS

In Section 3.3.7, it was mentioned that the deformations of both story infill panels were measured and monitored along the two diagonal directions in order to assess the shear deformations experienced by these infill walls. The shear deformation of the panels can be estimated through an idealization of the deformed body as shown in Figure C.1. Thus, the original rectangular shape "abde" having a height "h" (i.e. $|bd|=|ae|$) and width "w" (i.e. $|ad|=|be|$) is assumed to change into idealized parallelogram "a'b'd'e'" under applied shear. The original lengths along the first and second diagonal directions are defined as $l_1=|de|$ and $l_2=|ab|$, respectively. In the deformed body, these lengths are assumed to degrade into $l_1'=|d'e'|$ and $l_2'=|a'b'|$, defined by Eqns. C.1 and C.2, respectively.

$$l_1{}' = l_1 + \delta_1 \tag{C.1}$$

$$l_2{}' = l_2 + \delta_2 \tag{C.2}$$

where, δ_1 and δ_2 are deformations along the diagonal directions "de" and "ab", respectively.

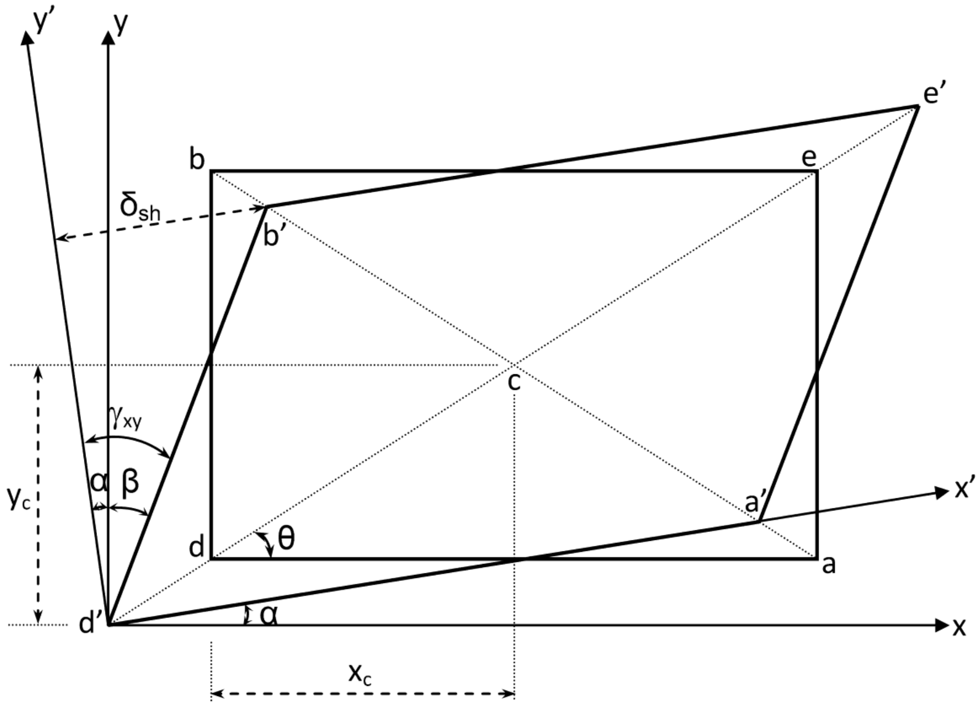

Figure C. 1 Idealized deformed shape of infill panel subjected to shear deformations

The coordinates of the geometric center of panel (i.e. point c) with respect to designated x and y axes are defined as x_c and y_c, respectively.

$$x_c = \frac{l_1}{2}\cos\theta \tag{C.3}$$

$$y_c = \frac{l_1}{2}\sin\theta \tag{C.4}$$

where, θ is the angle between the diagonal "de" and the horizontal axis.

$$\theta = \tan^{-1}(h/w) \tag{C.5}$$

Considering the coordinates of the geometric center of panel will remain the same after deformations take place, the x- and y-coordinates of the deformed corner points a' and b' may eventually be defined as follows.

$$x_{a'} = x_c + \frac{l_2'}{2}\sin\theta \tag{C.6}$$

$$y_{a'} = y_c - \frac{l_2'}{2}\cos\theta \tag{C.7}$$

$$x_{\mathrm{b}'} = x_c - \frac{l_2'}{2}\sin\theta \tag{C.8}$$

$$y_{\mathrm{b}'} = y_c + \frac{l_2'}{2}\cos\theta \tag{C.9}$$

The angular reduction of two orthogonal sides of the panel subjected to shearing strains (i.e. α and β) may be estimated through Eqns. C.10 and C.11, which are expanded using the above definitions.

$$\alpha = \tan^{-1}\left(\frac{y_{a'}}{x_{a'}}\right) = \tan^{-1}\left[\frac{(l_1+\delta_1)(h/w)-(l_2+\delta_2)}{(l_1+\delta_1)+(l_2+\delta_2)(h/w)}\right] \tag{C.10}$$

$$\beta = \tan^{-1}\left(\frac{y_{b'}}{x_{\mathrm{b}'}}\right) = \tan^{-1}\left[\frac{(l_1+\delta_1)-(l_2+\delta_2)(h/w)}{(l_1+\delta_1)(h/w)+(l_2+\delta_2)}\right] \tag{C.11}$$

The sum of the angles defined in Eqns. (C.10) and (C.11) yields the shearing strain of the panel, γ_{xy}.

$$\gamma_{xy} = \alpha + \beta \tag{C.12}$$

And in the last step, shear deformation of the panel, δ_{sh} can be estimated using Eqn. C.13 by referring the small angle assumption for γ_{xy}.

$$\delta_{sh} = \gamma_{xy} h \tag{C.13}$$

APPENDIX D

EVALUATION OF BASE ROTATIONS AND MOMENTS

The base rotation definition is adapted in this study in order to observe the effect of coupled elongation and shortening on each side of the frame on a single hysteretic curve. These curves provided some notable information for the effect of infill walls, applied retrofitting and existence of lapped longitudinal bars on the overall response. The base rotations (i.e. θ_b) are estimated by means of the readings of dial gauges situated at the bottom of frames, as shown in Figure D.1.

$$\theta_b = \frac{\delta_{D.G.\#1} - \delta_{D.G.\#2}}{l_{D.G.}} \tag{D.1}$$

In Eqn. D.1, $\delta_{D.G.\#1}$ ("+" or "-") and $\delta_{D.G.\#2}$ ("-" or "+") stand for the readings of the dial gages at the left and right ends of frame, respectively. And $l_{D.G.}$ is the distance between the dial gages. It should be noted that the dial gauge was placed 50 mm. from the outer column surface. The base moment is the overturning moment at the base of the frame originated by the applied lateral forces (Eqn. D.2). The second order moments are neglected in the calculations.

$$M_b = \frac{V}{3}\left(h_1 + \frac{h_b}{2}\right) + \frac{2V}{3}\left(h_1 + h_2 + \frac{3}{2}h_b\right) \tag{D.2}$$

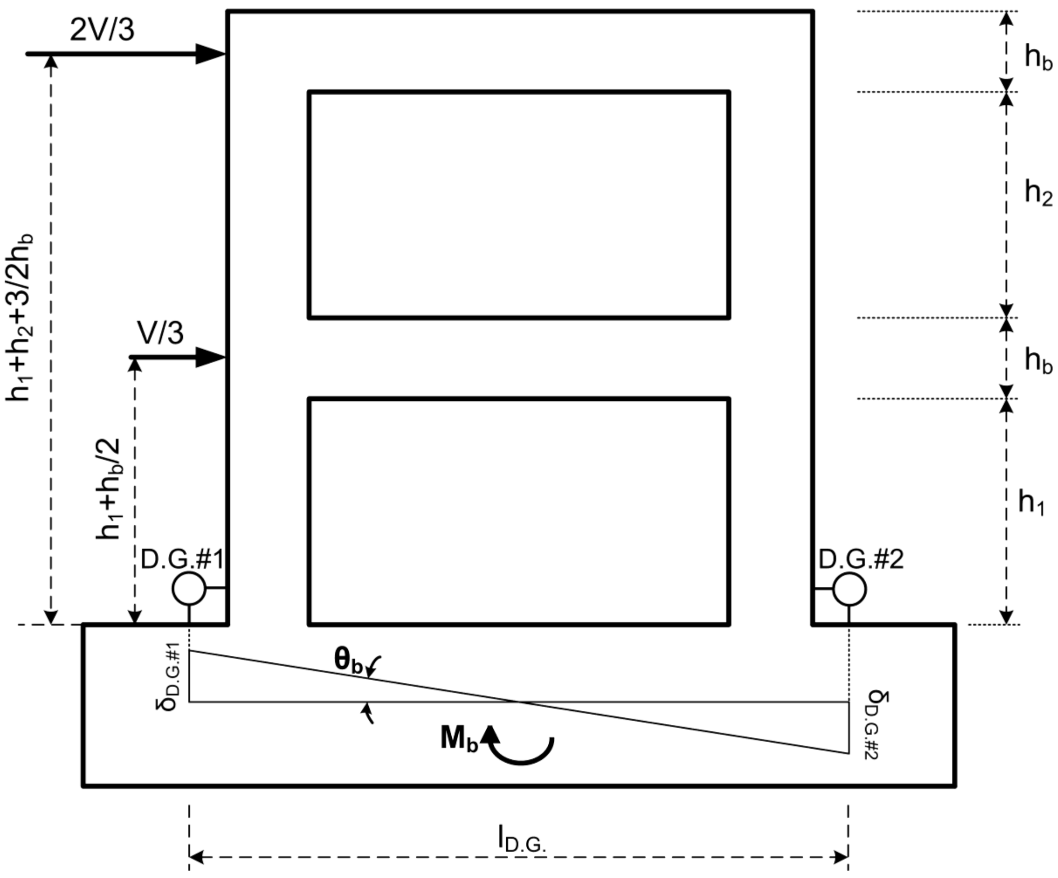

Figure D. 1 Frame base rotation and base moment

APPENDIX E

ILLUSTRATIONS OF DAMAGE PATTERNS

The damage experienced by the frame specimens, as also explained and shown through pictures in Chapter 4, are illustrated in Figures E.1 to E.12 in a more detailed manner.

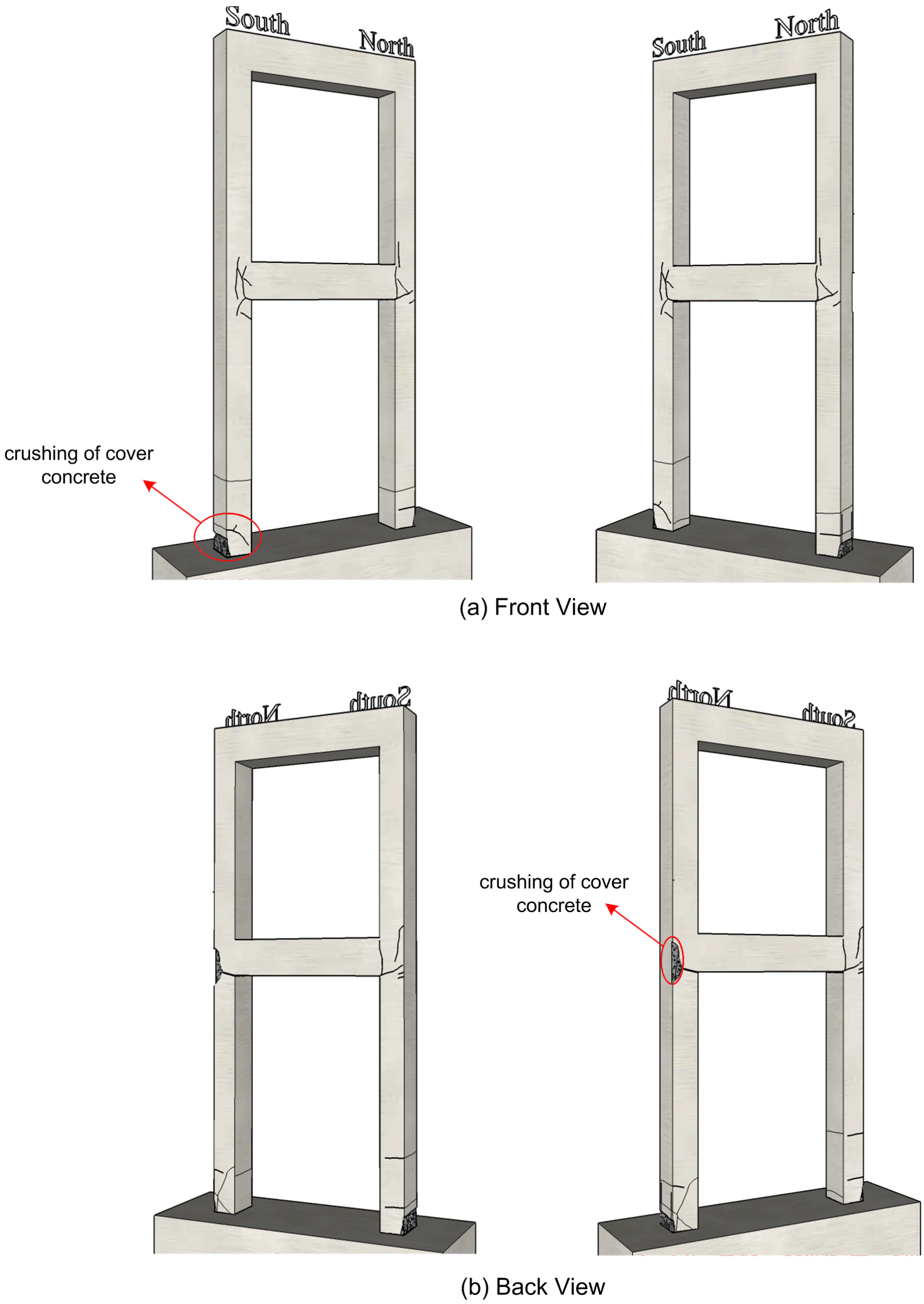

(a) Front View

(b) Back View

Figure E. 1 Illustration of the damage pattern for specimen NREF1-1/3

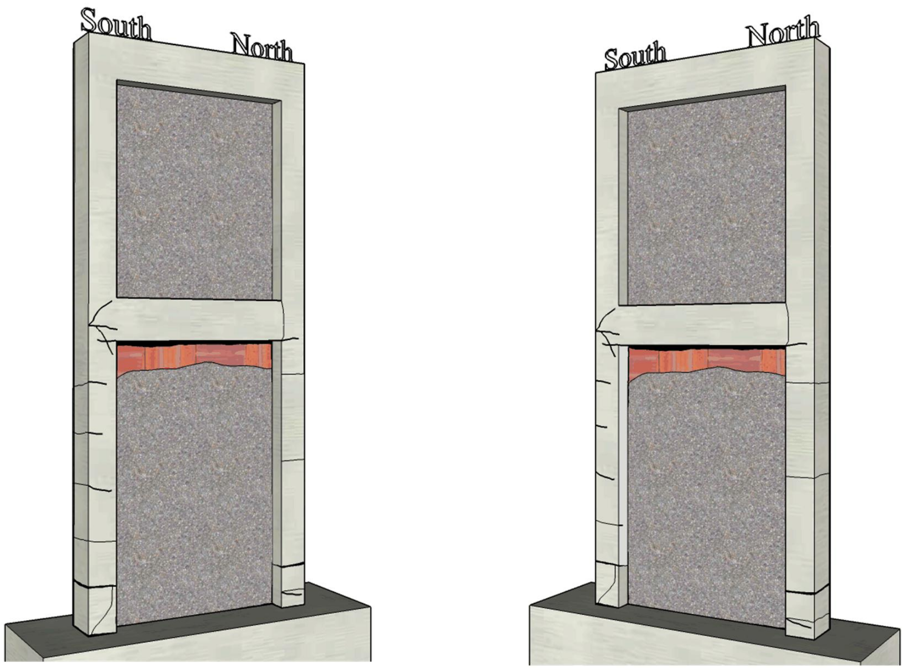

(a) Front View

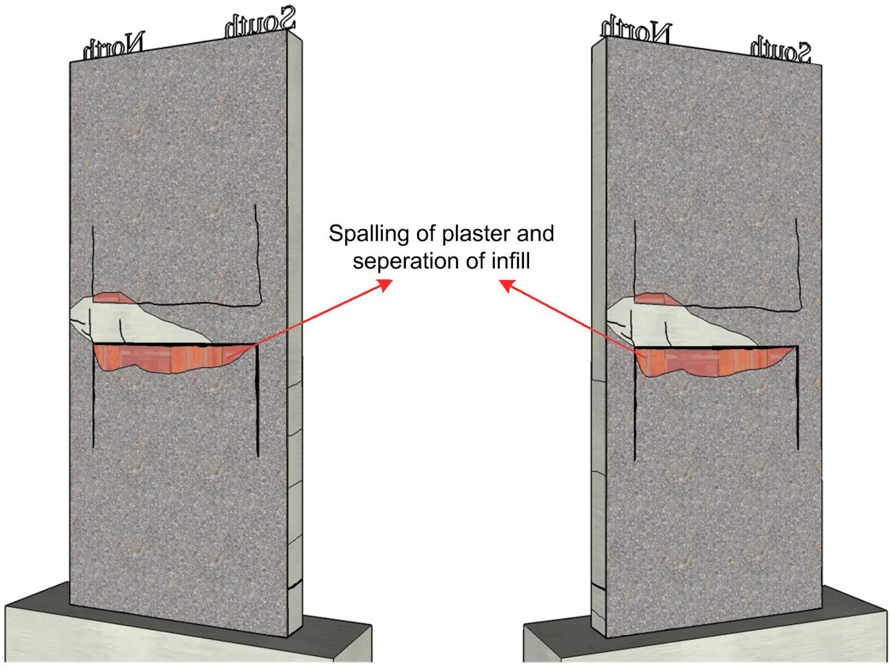

(b) Back View

Figure E. 2 Illustration of the damage pattern for specimen NREF2-1/3

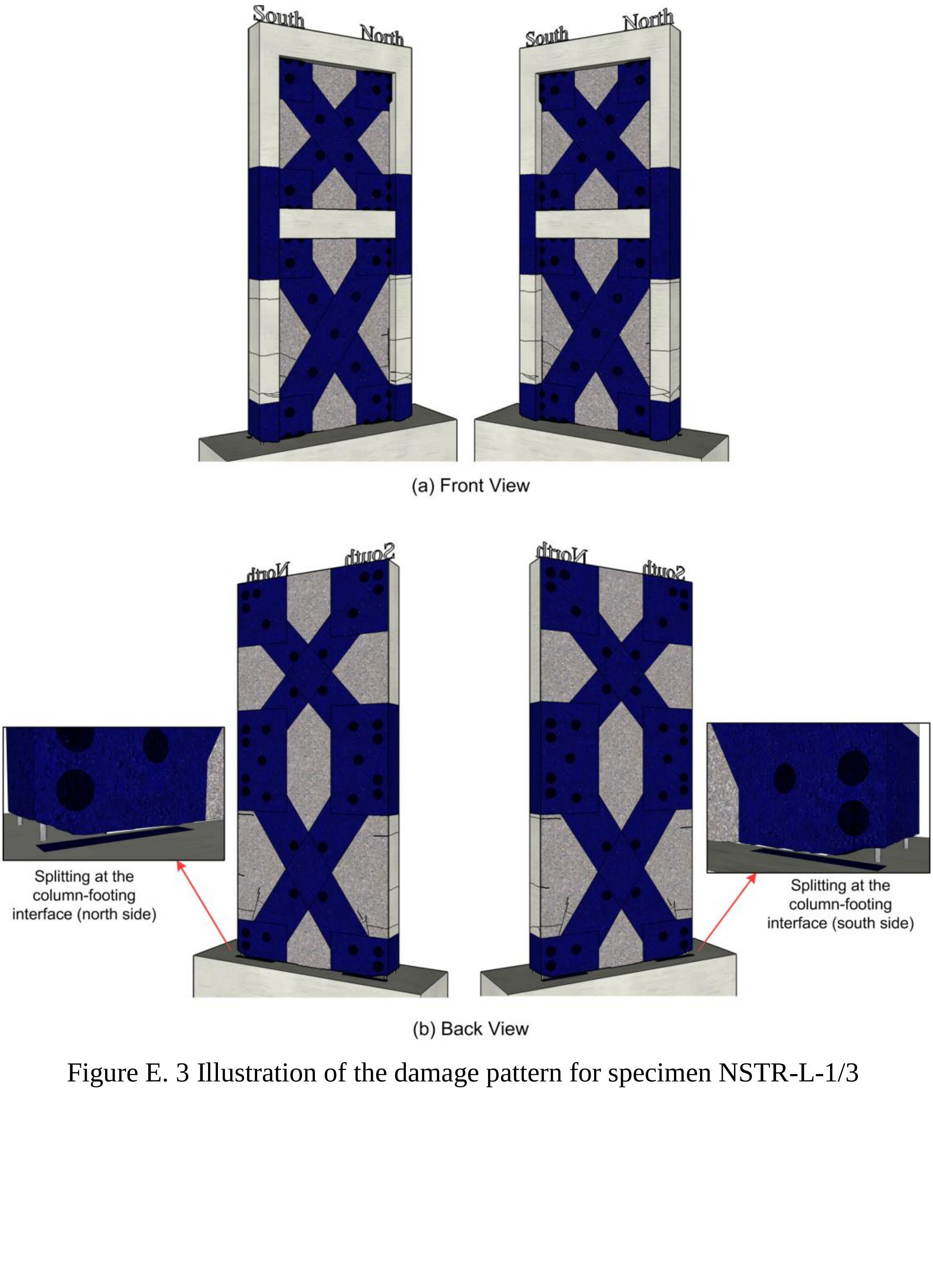

Figure E. 3 Illustration of the damage pattern for specimen NSTR-L-1/3

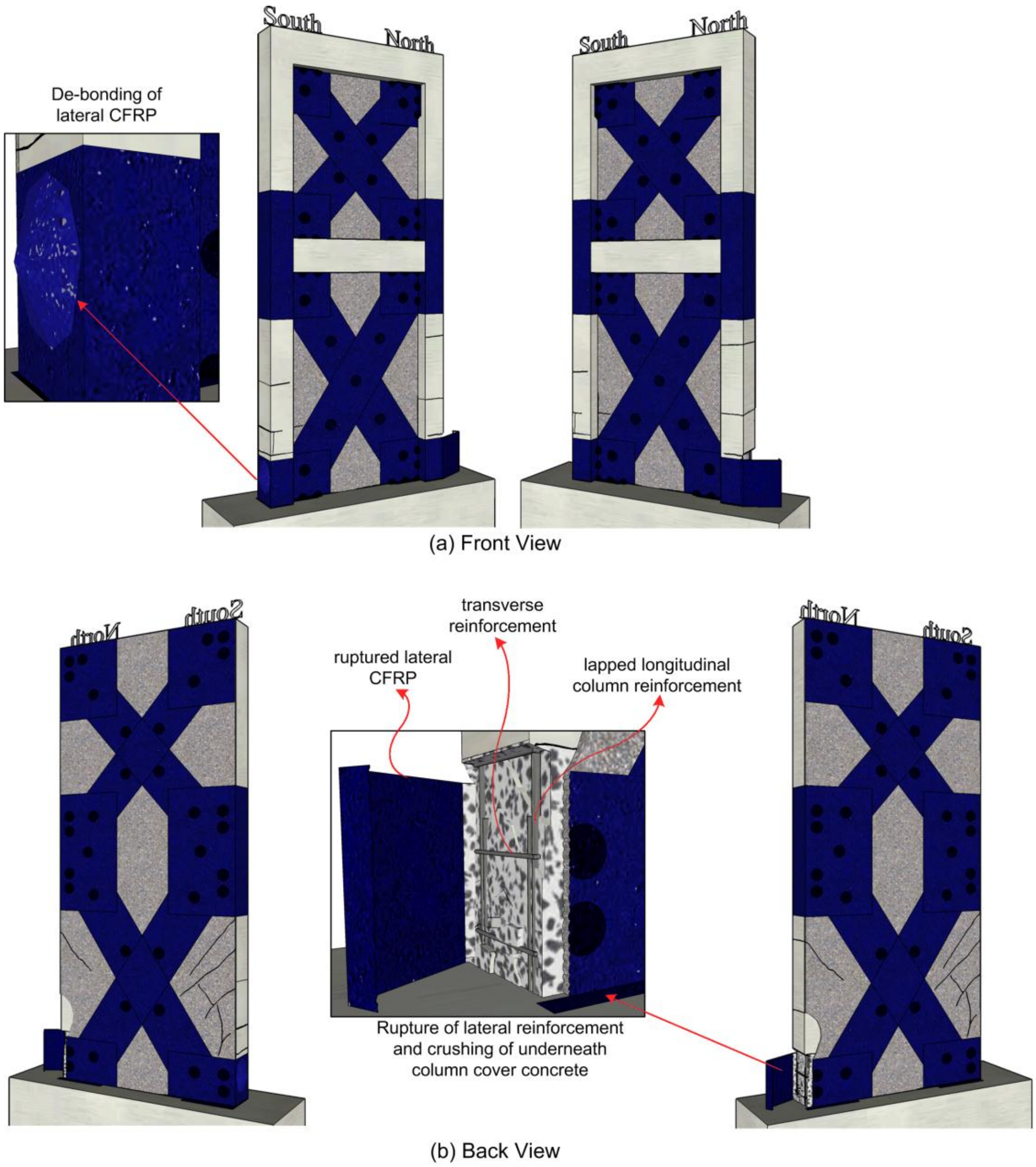

Figure E. 4 Illustration of the damage pattern for specimen NSTR-W-1/3

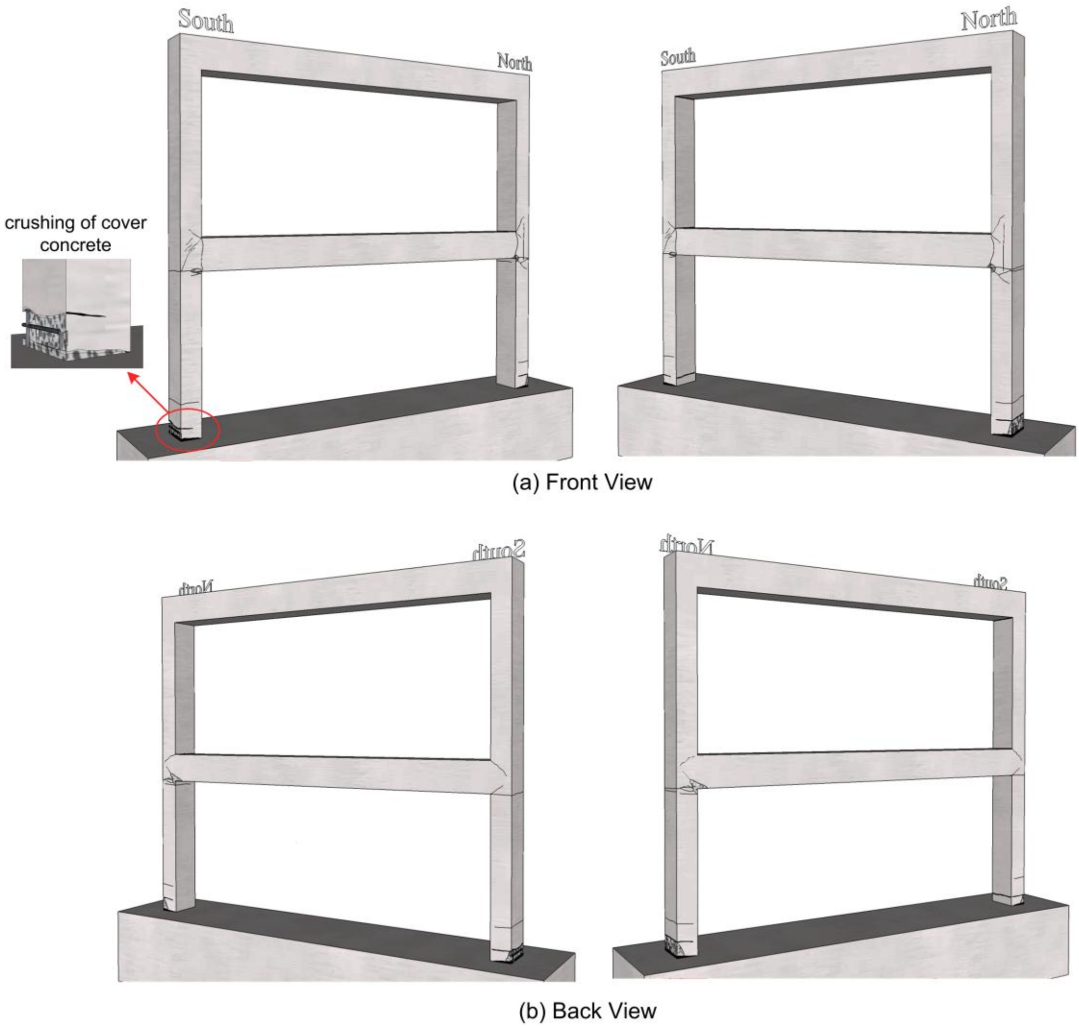

Figure E. 5 Illustration of the damage pattern for specimen LREF1-1/3

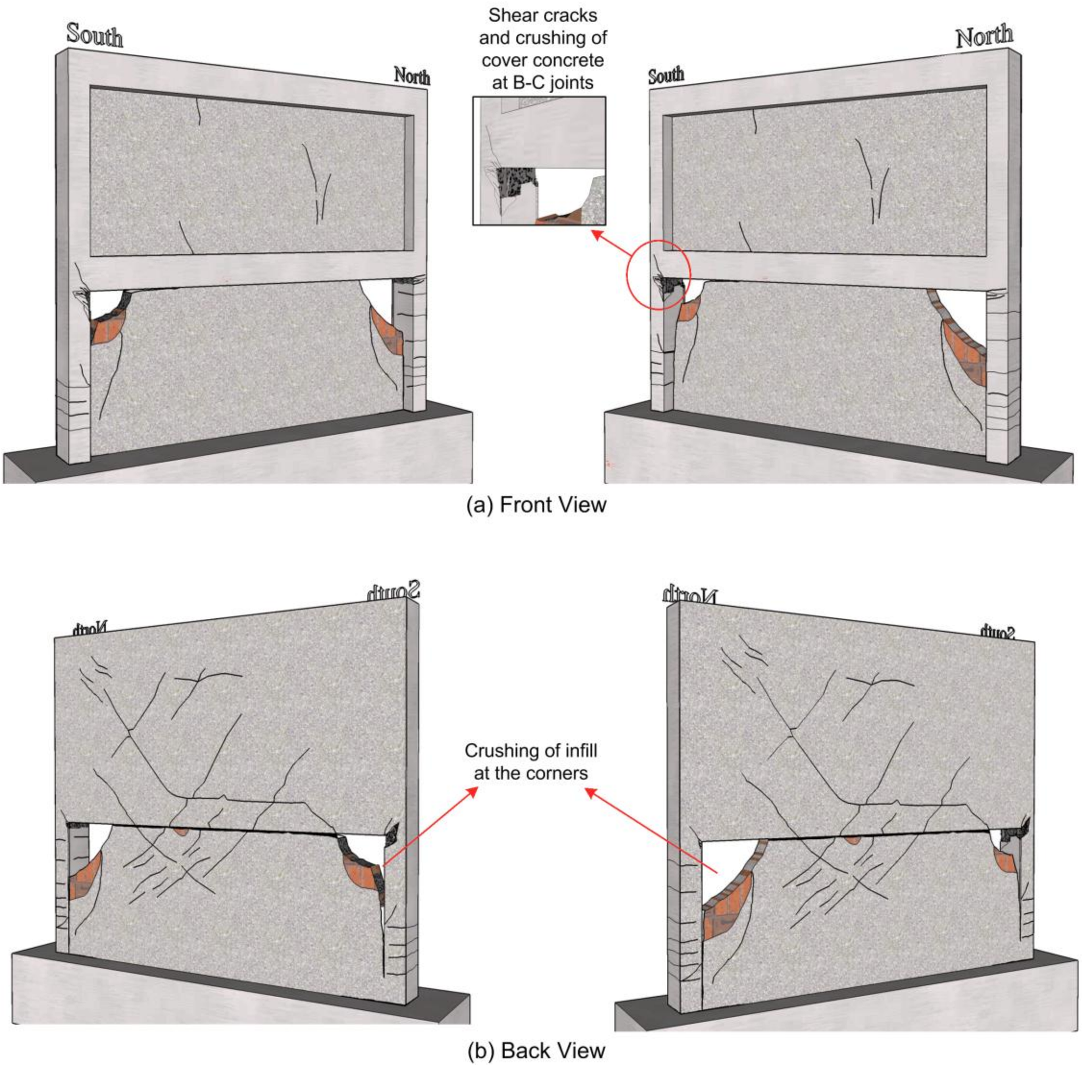

Figure E. 6 Illustration of the damage pattern for specimen LREF2-1/3

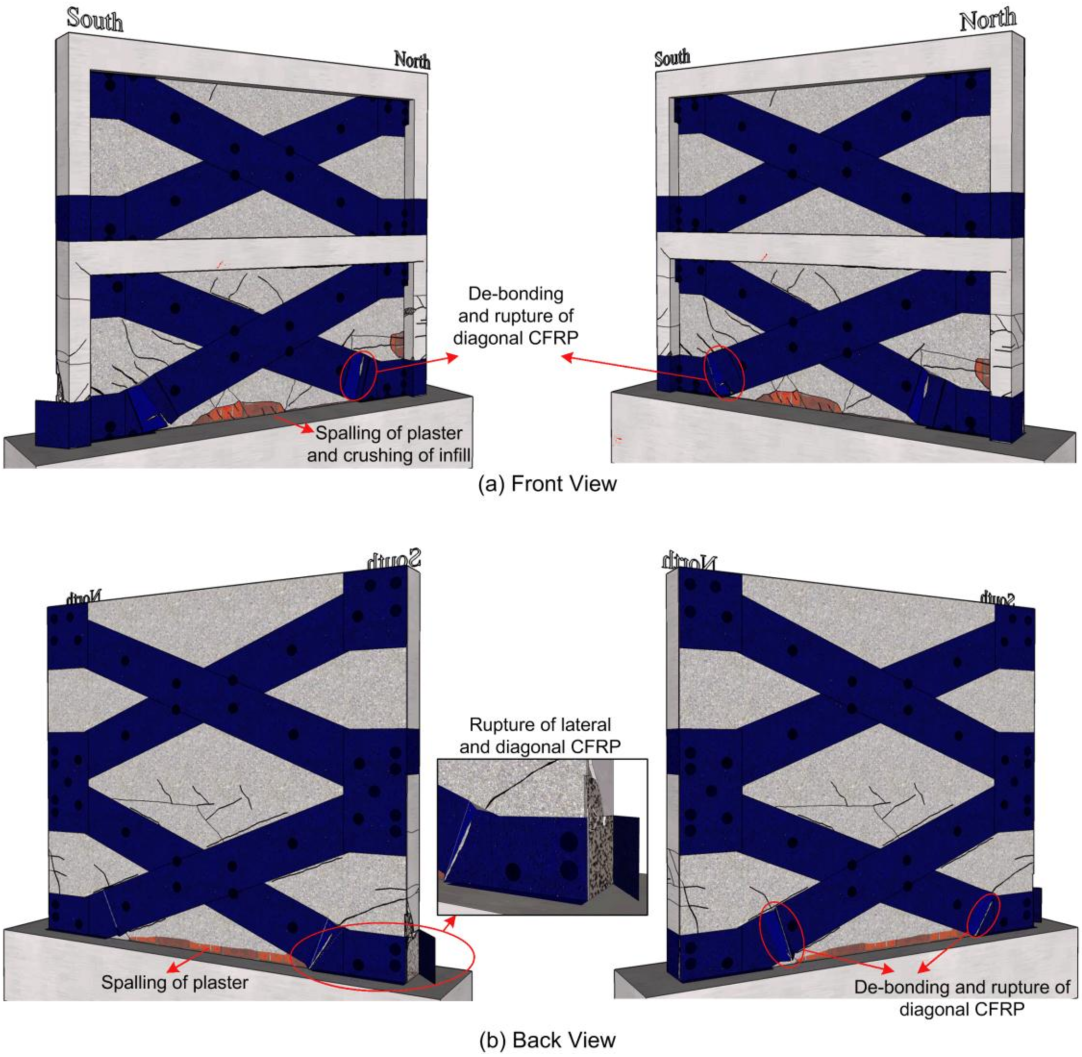

Figure E. 7 Illustration of the damage pattern for specimen LSTR-L-1/3

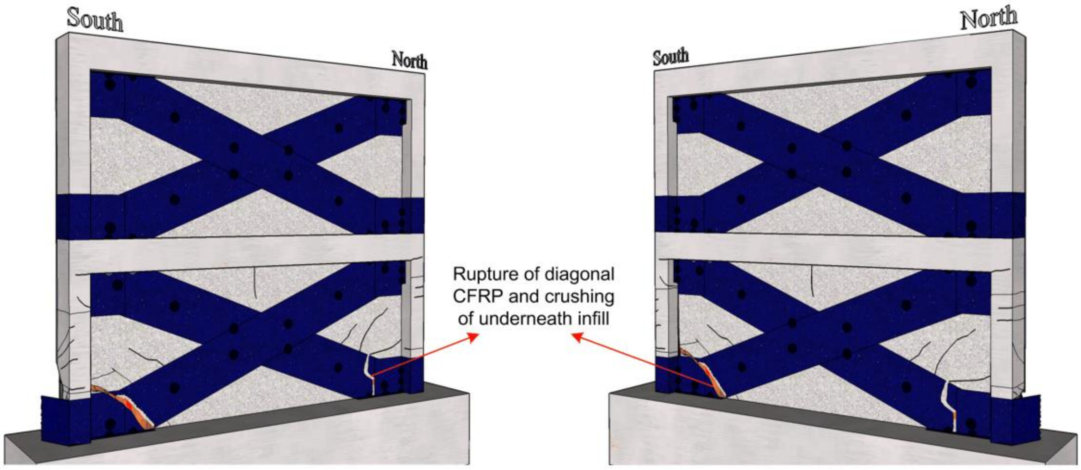

(a) Front View

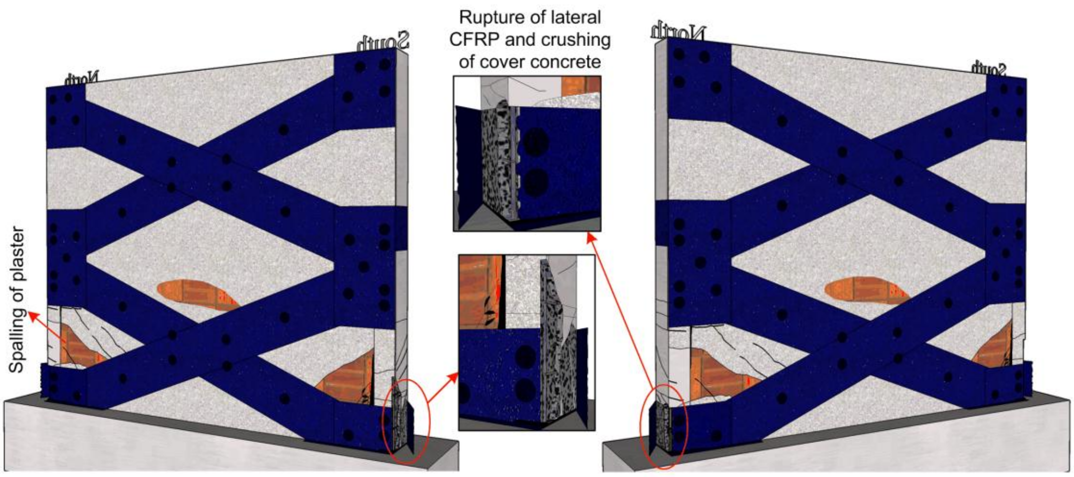

(b) Back View

Figure E. 8 Illustration of the damage pattern for specimen LSTR-C-1/3

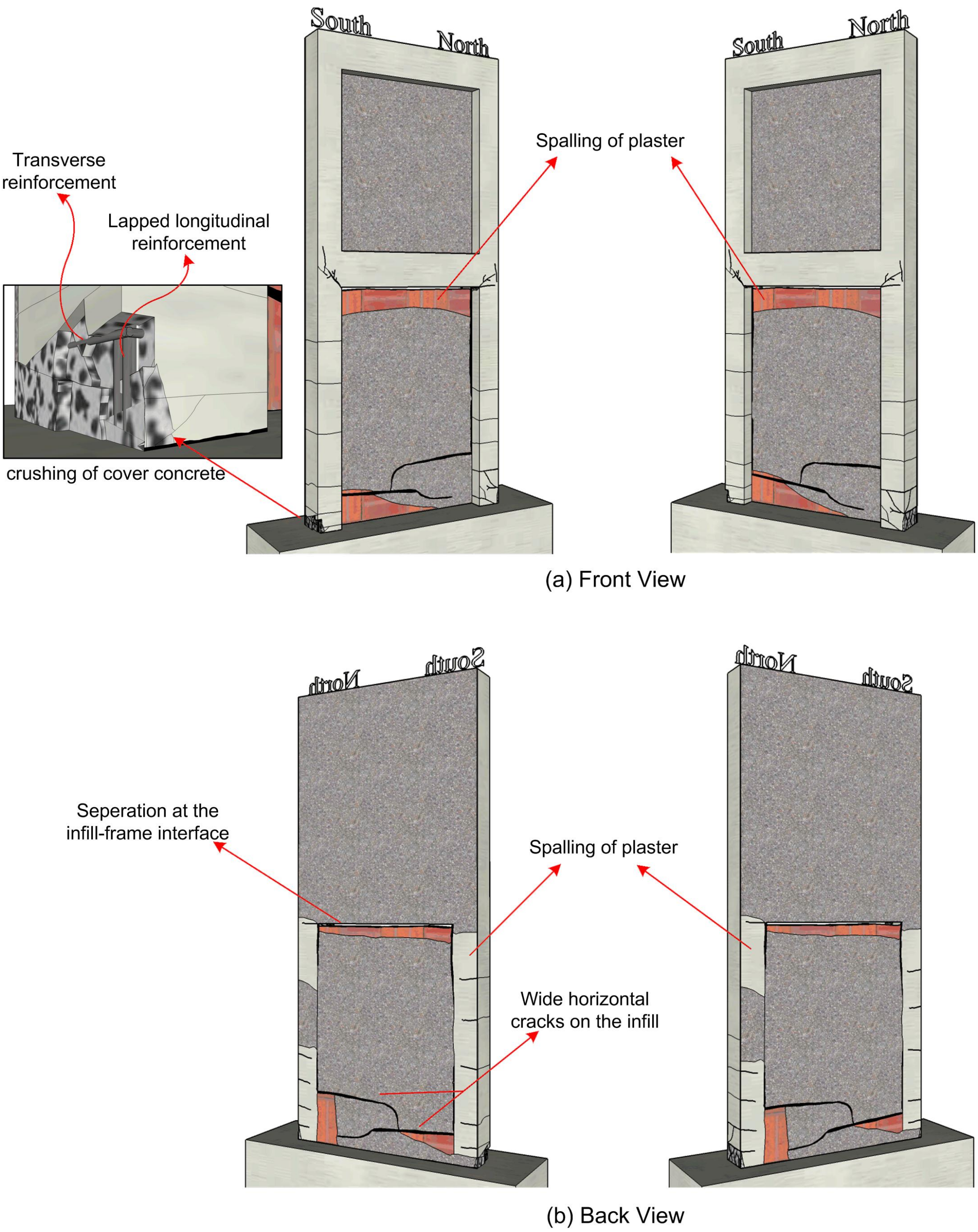

Figure E. 9 Illustration of the damage pattern for specimen NREF-1/2

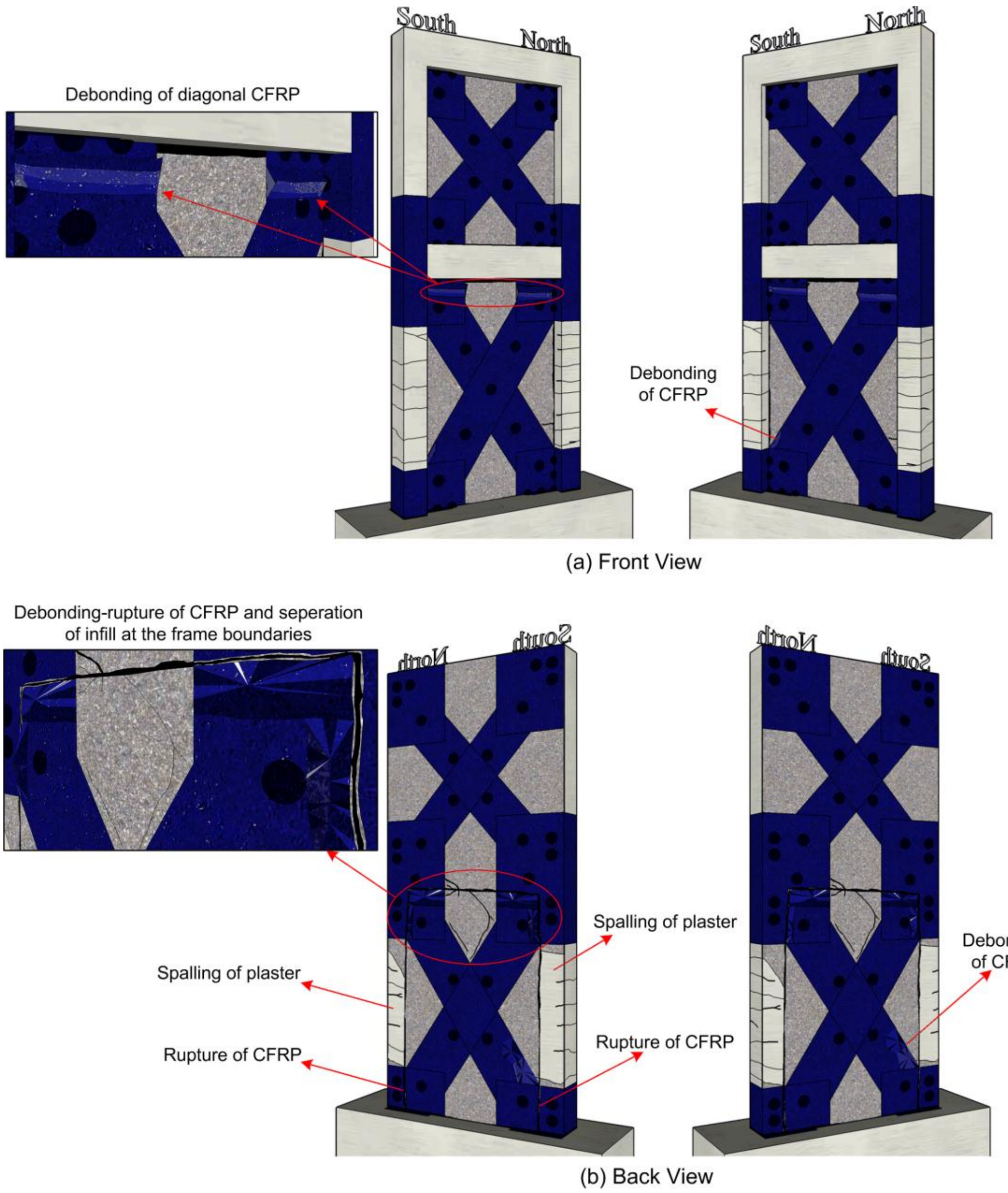

Figure E. 10 Illustration of the damage pattern for specimen NSTR-1/2

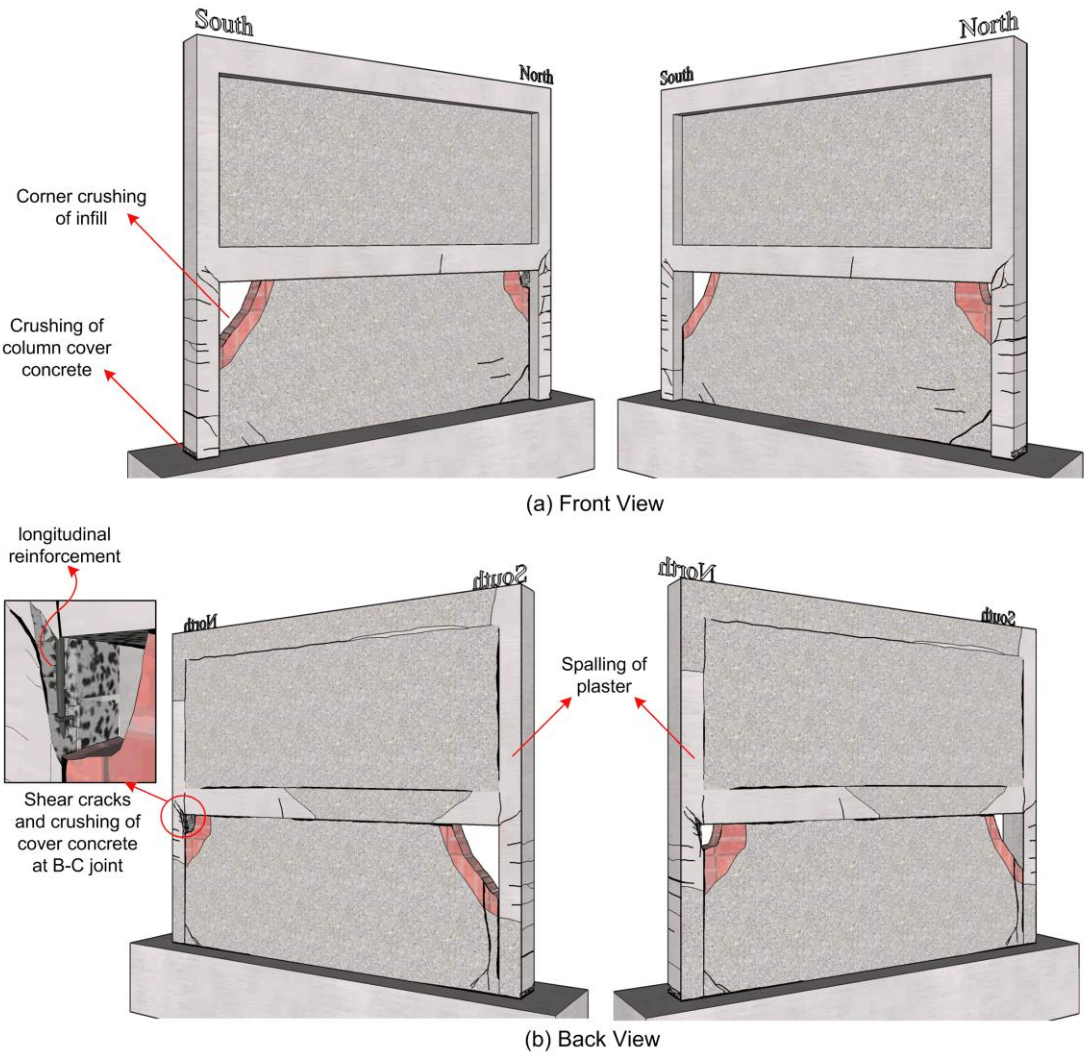

Figure E. 11 Illustration of the damage pattern for specimen LREF-1/2

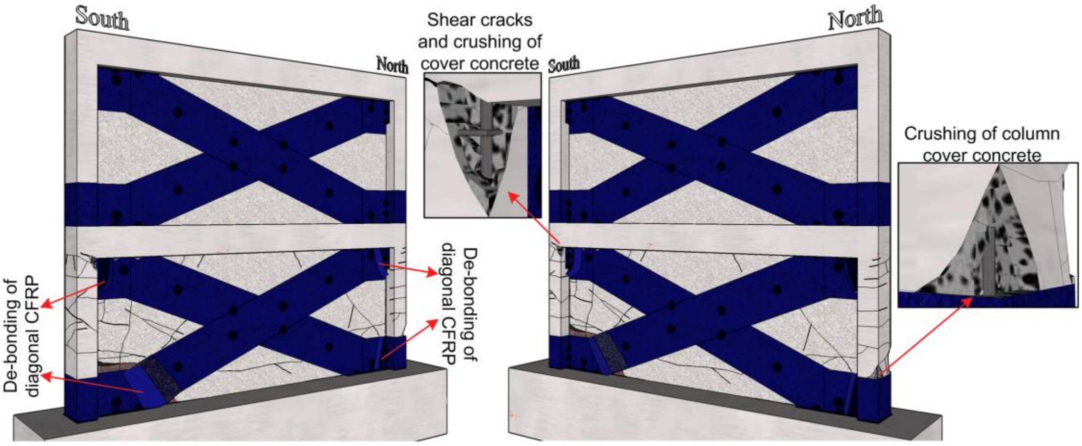

(a) Front View

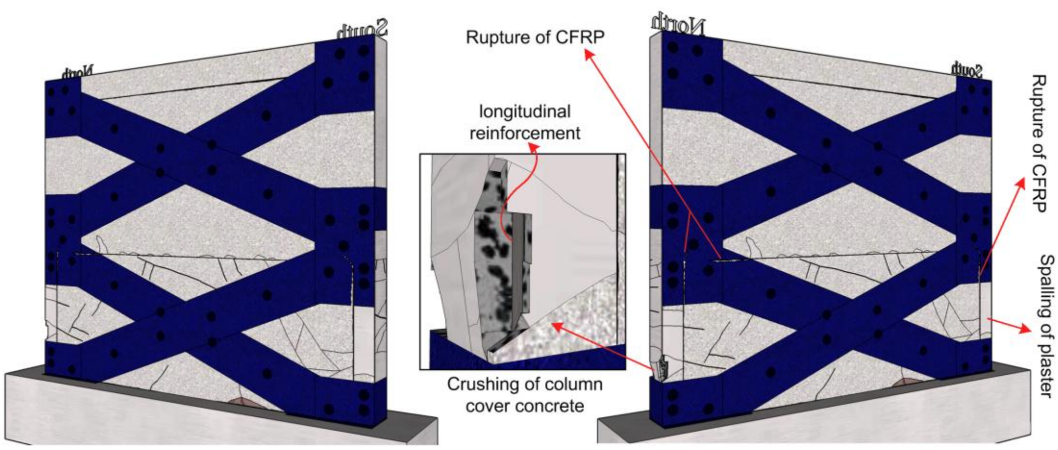

(b) Back View

Figure E. 12 Illustration of the damage pattern for specimen LSTR-1/2

APPENDIX F

STRUCTURAL MODEL ANALYSIS

A prototype may be defined as the structure where all scale factors are unity. The scaled models of these prototype structures can be obtained by means of various similarity relationships (i.e. similitude equations). These relationships are summarized below.

- Geometric similarity : $L_{model} = \lambda \times L_{prot.}$ (F.1)
- Kinematic similarity : $\delta_{model} = \mathrm{n} \times \delta_{prot.}$ (F.2)
- Static similarity : $\sigma_{model} = n \times \sigma_{prot.}$ (F.3)
- Material similarity : $E_{model} = \mathrm{s} \times E_{prot.}$ (F.4)

where, L, δ, σ and E represent length, displacement, stress and modulus of elasticity, respectively. The subscripts are used for the model and prototype structures as “model” and “prot.”. λ, n and s represent the similitude constants relating the model and prototype structures.

Besides, cross-sectional dimensions (a and b) and consequent cross-sectional area (A) of the model and prototype structures may be related by means of a similitude constant “ν” as follows.

$$a_{model} = \nu \times a_{prot.} \; and \; b_{model} = \nu \times b_{prot.} \tag{F.5}$$

$$A_{model} = \nu^2 \times A_{prot.} \tag{F.6}$$

If we take an axially loaded member as an example for simplicity, then we may derive similar similitude equations for applied force and dissipated energy. By using the conventional equations of mechanics and the defined similitude relationships, the axial displacements of the model and prototype structures may be given as in Eqs. (F.7) and (F.8).

$$\delta_{prot.} = \frac{F_{prot.} \times L_{prot.}}{E_{prot.} \times A_{prot.}} \tag{F.7}$$

$$\delta_{model} = \frac{\lambda}{s \times \nu^2} \frac{F_{model} \times L_{prot.}}{E_{prot.} \times A_{prot.}} \tag{F.8}$$

The similitude relationships for the applied force may be obtained by using Eqs (F.2), (F.7) and (F.8). This relationship is defined by Eq. (F.9), after assuming λ=n=ν and s=1 (i.e. same material used for both prototype and model).

$$F_{model} = \lambda^2 \times F_{prot.} \tag{F.9}$$

The dissipated energy is directly proportional to the applied force multiplied by the displacements. Therefore, the similitude relationship for the dissipated energy may be obtained as in Eq. (F.10).

$$DE_{model} = \lambda^3 \times DE_{prot.} \tag{F.10}$$

It should be noted that the same relationships may be obtained for the case of bending and shear instead of axial loading.

In this study λ is 1/3 and 1/2 for Group-I and Group-II specimens, respectively. Eventually, the similitude relationships of the applied force and dissipated energy may be presented as follows for Group-I and Group-II.

$$F_{prot.} = 9 \times F_{model} \; and \; DE_{prot.} = 27 \times DE_{model} \quad \ldots\text{(Group-I)} \tag{F.11}$$

$$F_{prot.} = 4 \times F_{model} \; and \; DE_{prot.} = 8 \times DE_{model} \quad \ldots\text{(Group-II)} \tag{F.12}$$

CURRICULUM VITAE

PERSONAL INFORMATION

Name	: Emre AKIN
Birth Date	: 10/05/1978
Birth Place	: Silifke / Mersin
Citizenship	: Republic of Turkey
Phone	: +90 (312) 2105474
Fax	: +90 (312) 2101193
e-mail	: emreakin78@gmail.com

EDUCATION

2002 - 2010	Ph.D., Civil Engineering, METU	(CGPA: 3.54/4.00)
1997 - 2001	BS, Civil Engineering, Çukurova Univ.	(CGPA: 3.43/4.00)
1989 - 1996	İçel Anatolian High School	

EMPLOYMENT RECORD

2002 - 2010: Research Assistant, Dept. of Civil Eng., METU

SCIENTIFIC PUBLICATIONS

International Conference Proceedings

1 Özcebe G., **Akın E.**, 2007**,** "Strengthening of Brick Infilled R/C Frames with CFRP Reinforcement", 9th Canadian Conference on Earthquake Engineering, Ottawa, Ontario, Canada.

2 **Akın E.**, Özcebe G., Ersoy U., 2007**,** "Strengthening of Brick Infilled RC Frames with CFRP Sheets", International Workshop on Measures for the Prevention of Total Collapse of Existing Low-Rise Structures, Istanbul, Turkey.

3 **Akın E.**, Özcebe G., 2008**,** "Strengthening of Brick Infilled RC Frames Using CFRP", 8th International Congress on Advances in Civil Engineering, Famagusta, North Cyprus.

International Book Chapters

1 **Akın E.**, Özcebe G., Ersoy U., 2009**,** "Strengthening of Brick Infilled Reinforced Concrete (RC) Frames with Carbon Fiber Reinforced Polymers (CFRP) Sheets", Seismic Risk Assessment and Retrofitting-Geotechnical, Geological and Earthquake Engineering, Vol. 10, pp 367-386.